AFOSR-TR- 85-0560

AD-A158 291

Rocket Propulsion
Research Meeting

DTIC
ELECTE
AUG 21 1985

1985 AFOSR/AFRPL Chemical Rocket Research Meeting

18-21 March 1985

DTIC FILE COPY

Abstracts and Agenda

Includes Abstracts of AFOSR Sponsored Research on Diagnostics of Reacting Flow

Lancaster, California

Approved for public release;
distribution unlimited.

20000814104

85 8 21 162

UNCLASSIFIED

SECURITY CLASSIFICATION OF THIS PAGE

REPORT DOCUMENTATION PAGE

1a. REPORT SECURITY CLASSIFICATION Unclassified	1b. RESTRICTIVE MARKINGS
2a. SECURITY CLASSIFICATION AUTHORITY	3. DISTRIBUTION/AVAILABILITY OF REPORT Approved for Public Release; Distribution Unlimited.
2b. DECLASSIFICATION/DOWNGRADING SCHEDULE	
4. PERFORMING ORGANIZATION REPORT NUMBER(S)	5. MONITORING ORGANIZATION REPORT NUMBER(S) AFOSR-TR- 85-0560
6a. NAME OF PERFORMING ORGANIZATION AIR FORCE OFFICE OF SCIENTIFIC RESEARCH 6b. OFFICE SYMBOL (If applicable) NA	7a. NAME OF MONITORING ORGANIZATION AFOSR/NA
6c. ADDRESS (City, State and ZIP Code) BOLLING AFB DC 20332-6448	7b. ADDRESS (City, State and ZIP Code) BOLLING AFB DC 20332-6448
8a. NAME OF FUNDING/SPONSORING ORGANIZATION 8b. OFFICE SYMBOL (If applicable)	9. PROCUREMENT INSTRUMENT IDENTIFICATION NUMBER IN-HOUSE
8c. ADDRESS (City, State and ZIP Code)	10. SOURCE OF FUNDING NOS. PROGRAM ELEMENT NO.: 61102F PROJECT NO.: 2308 TASK NO.: A1, A3, M1 / M2, M3 / 2307; 2303 / M1; M1 WORK UNIT NO.
11. TITLE (Include Security Classification) AFOSR/AFRPL Chemical ROCKET RESEARCH MEETING - 1985	
12. PERSONAL AUTHOR(S) /EDITOR(S) LEONARD H CAVENY ANTHONY MATUSZKO WAYNE E ROE *	
13a. TYPE OF REPORT INTERIM 13b. TIME COVERED FROM MAR 84 TO FEB 85	14. DATE OF REPORT (Yr., Mo., Day) 1985, February 15. PAGE COUNT
16. SUPPLEMENTARY NOTATION *Air Force Rocket Propulsion Laboratory Edwards AFB CA 93534	

17. COSATI CODES			18. SUBJECT TERMS (Continue on reverse if necessary and identify by block number)	
FIELD	GROUP	SUB. GR.		
			ROCKETS	PROPELLANTS
			COMBUSTION	CHEMICAL KINETICS
			ENERGETIC MATERIALS	THERMAL PROPERTIES

19. ABSTRACT (Continue on reverse if necessary and identify by block number)

This document contains expanded abstracts from the Air Force basic research program on rocket propulsion. The document contains the agenda for the Rocket Research Meeting held at Lancaster, CA on 18-21 March 1985. Major topics include: energetic material combustion; metal combustion; diagnostics of reacting flow; chemical kinetics; thermal properties; Propellant synthesis of new ingredients; combustion stability; acoustic interaction plumes; beamed energy; solar propulsion; and electrical propulsion.

20. DISTRIBUTION/AVAILABILITY OF ABSTRACT UNCLASSIFIED/UNLIMITED ☒ SAME AS RPT. ☐ DTIC USERS ☐	21. ABSTRACT SECURITY CLASSIFICATION UNCLASSIFIED
22a. NAME OF RESPONSIBLE INDIVIDUAL LEONARD H CAVENY	22b. TELEPHONE NUMBER (Include Area Code) (202) 767-4937 22c. OFFICE SYMBOL AFOSR/NA

DD FORM 1473, 83 APR EDITION OF 1 JAN 73 IS OBSOLETE.

UNCLASSIFIED

SECURITY CLASSIFICATION OF THIS PAGE

18. SUBJECT TERMS (Cont)

EXHAUST PLUMES
COMBUSTION STABILITY
ACOUSTICS
STRUCTURAL MECHANICS
LASER HEATING
ELECTRIC PROPULSION
BEAMED ENERGY

Table of Contents

Form 1473 i

Table of Contents iii

Preface iv

Agenda Summary v

Agenda

Abstracts: Energetic Materials

Abstracts: Rocket Research

Abstracts: Diagnostics of Reacting Flow

Appendix 1 Propulsion Research Goals

Index to Abstracts, Investigators, and Presentations

Accession For
NTIS GRA&I ☒
DTIC TAB ☐
Unannounced ☐
Justification
By
Distribution/
Availability
A-1

COPY INSPECTED

PREFACE

This booklet serves dual purposes: (1) provides a status report on the Air Force's basic research program on both chemical and nonconventional rocket propulsion and (2) is the program for the contractors' meeting on rocket research.

Most of the abstracts follow a specific format. The text begins with a short statement of relevant scientific questions addressed by the research, followed by an explanation of the scientific approach. A statement of the uniqueness of each approach was solicited from the investigators. The major portion of the text describes the results obtained during the last twelve months. The abstracts should describe two figures: Figure 1 illustrates the main (or a representative) feature of the scientific approach and Figure 2 presents a primary accomplishment.

Hard copies of the vugraph material and collateral information are in file folders (one for each presentation) on a table at the rear of the meeting room.

Since the research on metal combustion and structural mechanics have had adequate national forums in recent months, that research will be presented in the March 1986 Rocket Research Meeting. The abstracts on metal combustion research are included in this booklet.

The research on advanced diagnostics of reacting flow is the subject of a separate meeting which is held every other year. The next meeting is scheduled for Spring 1986. The abstracts on that research are included in a special section of this booklet.

A primary objective of the meeting and this booklet is to encourage the participants to interpret the technological barriers and to consider new research approaches. Since a 25 to 30 percent annual turn-over is built into the program, each year opportunities exist for new research approaches and for new principal investigators. Several of the presentations provide introductions to some of the barriers and technological challenges. Prospective principal investigators should not feel constrained by these presentations and are encouraged to look beyond the identified items. The location of the meeting (i.e., near organizations interested in the research) promotes interchanges among the investigators and those responsible for Air Force programs. Accordingly, many of the participants will be able to provide specific information on Air Force requirements. Questions concerning the meeting can be directed to either:

Leonard H. Caveny
AFOSR/NA
Bolling AFB
Washington, DC 20332-6448
Phn: (202) 767-4937
Autovon: 297-4937

or

Wayne E. Roe
AFRPL/XRX
Edwards AFB, CA 93534
Phn: (805) 277-5206
Autovon: 350-5206

1985 AFOSR/AFRPL ROCKET RESEARCH MEETING

Antelope Valley Inn Lancaster, CA 93534

MONDAY (AM)
18 March 1985

0730 Registration

Session Chairman: Anthony Matuszko, AFOSR/NC

Topic: New Syntheses and Synthetic Methods

TIME	NUM.	
0800	1	ELECTROLYTIC PREPARATION OF NOVEL AZIDODINITRO COMPOUNDS. Milton B. Frankel and James F. Weber, Rocketdyne Division, Rockwell International, Canoga Park, CA
0830	2	SYNTHESIS OF DIFLUOROAMINOXY-, DIFLUOROAMINO-, OR FLUORODIAZONIUM CONTAINING MATERIALS. Jean'ne M. Shreeve, University of Idaho, Moscow, ID
0900	3	SYNTHESIS OF NEW POLYNITROPOLYHEDRANES. Alan P. Marchand, Suresh C. Suri, and D. Sivakumar Reddy, North Texas State University, Denton, TX
0930	4	SYNTHESIS OF HIGH NITROGEN CONTENT HETEROCYCLIC NITRAMINES AND ENERGETIC MATERIAL PLASTICIZERS. Rodney L. Willer and James A. Hartwell, Morton-Thiokol Inc., Elkton, MD (New Start)
0945		Break
1015	5	SYNTHESIS AND REACTIVITY OF UNSATURATED METAL NITROGEN COMPLEXES. William C. Trogler, Joseph H. Osborne, and Mary Maciejewski, University of California at San Diego, La Jolla, CA
1045	6	SYNTHESIS AND CHEMISTRY OF POLYNITROALKANES AND POLYNITROOLEFINS. Clifford D. Bedford and Robert J. Schmitt, SRI International, Menlo Park, CA
1115	7	NEW SYNTHETIC TECHNIQUES FOR ADVANCED PROPELLANT INGREDIENTS; SELECTIVE TRANSFORMATIONS AND NEW STRUCTURE. Robert D. Chapman, Scott A. Schaekelford, and John L. Andreshak, AFRPL
1145		Lunch (Reconvene at 1300)

MONDAY (PM)
18 March 1985

Session Chairman: Frank Roberto, AFRPL/MKP

Topic: New Syntheses and Synthetic Methods (continued)

TIME	NUM.	
1300	8	FLUOROPOLYAZIDOESTERS AS ENERGETIC POLYMERS. Robert M. Moriarty, University of Illinois at Chicago, Chicago, IL (New Start)
1315	9	NEW ENERGETIC POLYMERS AS BINDERS FOR PROPELLANTS. Moatafa A. H. Talukder and Stanley D. Morse, University of Dayton Research Institute, Dayton, OH
1345	10	ENERGETIC FLUOROCARBONS. Carl J. Schack and Karl O. Christe, Rocketdyne, Canoga Park, CA (New Start)

Topic: Reaction Mechanisms and Decomposition

TIME	NUM.	
1415	-	INVITED: ENERGETIC MATERIALS SYNTHESIS RESEARCH SPONSORED BY ONR. Richard S. Miller, Office of Naval Research, Arlington, VA
1445	11	CONTROL OF THE URETHANE CURE REACTION WITH SOLID, BLOCKED ISOCYANATES. William H. Graham, J. B. Canterberry, Inella G. Shepard, Jerrell W. Blanks. Morton Thiokol/Huntsville Division, Huntsville, AL
1530	12	PHYSICAL AND CHEMICAL CONSEQUENCES OF ANTIAROMATICITY IN THE BORACYCLOPENTADIENE SYSTEM. John J. Eisch, Sinpei Kozima, and James E. Galle, State University of New York at Binghamton, NY (New Start)
1545	13	HIGH ENERGY MOLECULES OF HIGH SYMMETRY. William S. Anderson, Chemical Systems Division/United Technologies Corporation, San Jose, CA (New Start)
1600	14	STRUCTURE-DECOMPOSITION RELATIONSHIPS IN NEWER ENERGETIC MATERIALS. Thomas B. Brill and Yoshio Oyumi, University of Delaware, Newark, DE
1630	15	DEUTERIUM ISOTOPE EFFECTS IN RDX DECOMPOSITION AND COMBUSTION PROCESSES. Scott A. Schackelford, Stephen L. Rodgers, and Michael B. Coolidge, AFRPL/LJLR; Robert E. Aakins, Morton Thiokol Corporation, Huntsville, AL
1700		ADJOURN SESSION
1700		Discussion Symposia (Snacks ,soft drinks, cash bar) - Antelope Valley Inn

1985 AFOSR/AFRPL ROCKET RESEARCH MEETING

Antelope Valley Inn Lancaster, CA 93534

TUESDAY (AM)
19 March 1985

0730 Registration

Session Chairman: Julian Tishkoff, AFOSR/NA

Topic: Combustion

TIME	NUM.	
0800	16	FLAME MECHANISMS AND FLAME INHIBITION. Jay D. Eversole and David P. Weaver, AFRPL
0830	17	SUPPRESSION OF AFTERBURNING IN SOLID ROCKET PLUMES BY POTASSIUM SALTS. Eugene Miller, University of Nevada Reno, Reno, NV
0900	18	CHEMICAL KINETICS OF NITRAMINE PROPELLANT COMBUSTION. Melvyn C. Branch, University of Colorado, Bolder, CO
0930	19	COMBUSTION OF HYDROGEN AND HYDROCARBONS IN FLUORINE. Myron J. Kaufman, Emory University, Atlanta, GA (New Start)
1000		Break
1030	20	ANALYSIS OF HETEROGENEOUS DIFFUSION FLAME STABILIZATION. Warren C. Strahle and Jechiel I. Jagoda, Georgia Institute of Technology, Atlanta, GA
1045	21	EXPERIMENTAL INVESTIGATION OF HETEROGENEOUS FLAME STABILIZATION. Warren C. Strahle and Jechiel I. Jagoda, Georgia Institute of Technology, Atlanta, GA
1100	22	HIGH PRESSURE SOLID PROPELLANT COMBUSTION ZONE STRUCTURE FROM ANALYSIS OF HYDROXYL RADICAL CHEMILUMINESCENCE. David P. Weaver, Tim Edwards, Susan Hulsizer, and David H. Campbell, AFRPL and University of Dayton
1120	23	EVALUATION OF HMX PROPELLANT CHEMISTRY FROM RAMAN SPECIES AND TEMPERATURE MEASUREMENTS. David H. Campbell, Tim Edwards, David P. Weaver, and Susan Hulsizer, AFRPL and University of Dayton
1140	24	APPLICATION OF MOLECULAR KINETIC MODELS TO THE PREDICTION OF BACKFLOW CONTAMINATION. David P. Weaver and David H. Campbell, AFRPL and University of Dayton
-	25	*EVALUATION AND COMPILATION OF THE THERMODYNAMIC PROPERTIES OF HIGH TEMPERATURE SPECIES. Malcolm W. Chase, The Dow Chemical Company, Midland, MI
-	26	*CRITICAL EVALUATION OF HIGH TEMPERATURE CHEMICAL KINETIC DATA. Norman Cohen and Karl Westberg, Aerospace Corporation, Los Angeles, CA
1200		Lunch (Reconvene at 1300)

*Abstract only, no presentation.

TUESDAY (PM)
19 March 1985

Session Chairman: Robert C. Corley, AFRPL/DYC

Topic: Combustion (continued)

TIME	NUM.	
1300	27	AZIDE DECOMPOSITION AND COMBUSTION. Joseph E. Flanagan, Dean O. Woolery, and Wallace W. Thompson, Rocketdyne Division; Rockwell International, Canoga Park, CA
1315	28	STABILITY OF RDX, AP AND BTTN NEAR ROOM TEMPERATURE. Douglas B. Olson and Robert J. Gill, AeroChem Research Laboratories, Inc, Princeton, NJ
1345	-	INVITED: COMBUSTION OF ENERGETIC MATERIALS AT THE SANDIA COMBUSTION RESEARCH FACILITY. Sheridan Johnston, Sandia National Laboratories, Livermore, CA
-	29	*FUEL-RICH SOLID PROPELLANT BORON COMBUSTION. Merrill K. King and James J. Komar, Atlantic Research Corporation, Alexandria, VA
-	30	*GROWTH BEHAVIOR IN A COMPOSITE PROPELLANT WITH STRAIN GRADIENTS. C. T. Liu, AFRPL
-	31	*CRACK GROWTH BEHAVIOR IN A COMPOSITE PROPELLANT WITH STRAIN GRADIENTS. C. T. Liu, AFRPL
	32	*HIGH RESOLUTION MOVIES OF PROPELLANT DEFLAGRATION. Roger J. Becker, Paul F. Luehrmann, and Janet L. Laird, University of Dayton Research Institute, Dayton, OH
-	33	*WIDE DISTRIBUTION PROPELLANTS. Robert A. Frederick, Jr. and John R. Osborn, Purdue University, West Lafayette, IN

. . . continued on next page.

*Abstract only, no presentation.

TUESDAY (PM) (Continued)
19 March 1985

Session Chairman: Robert C. Corley, AFRPL/DYC

Topic: Combustion Instability

TIME	NUM.	
1415	34	COUPLING BETWEEN VELOCITY OSCILLATIONS AND SOLID PROPELLANT COMBUSTION. Robert S. Brown, A. M. Blackner, Paul G Willoughby, and Roger Dunlap, United Technologies/Chemical Systems Division, San Jose, CA
1445	35	FLAME-ACOUSTIC WAVE INTERACTION DURING AXIAL SOLID ROCKET INSTABILITIES. Ben T. Zinn, Brady R. Daniel, Jechiel J. Jagoda, and Uday Hedge, Georgia Institute of Technology, Atlanta, GA
1515		Break
1530	36	MECHANISMS OF ACOUSTIC SUPPRESSION. Merrill W. Beckstead and Richard L. Raun, Brigham Young University, Provo, UT
1600	37	FLOWFIELD EFFECTS ON COMBUSTION INSTABILITY. T. J. Chung, University of Alabama/Huntsville, Huntsville, AL
1630	38	ROCKET MOTOR FLOW TURNING LOSSES. Alan S. Hersh, Hersh Acoustical Engineering, Chatsworth, CA
1700	-	OVERVIEW OF AFRPL PLANS IN COMBUSTION. Robert C. Corley, AFRPL
1715		OPEN DISCUSSION
		ADJOURN
1725		Discussion Symposia (Snacks ,soft drinks, cash bar) - Antelope Valley Inn

Abstract only, no presentation.

1985 AFOSR/AFRPL ROCKET RESEARCH MEETING

Antelope Valley Inn Lancaster, CA 93534

WEDNESDAY (AM)
20 March 1985

0730 Registration

Session Chairman: Leonard H. Caveny, AFOSR/NA

Topic: General

TIME	NUM.	
0800		Announcements
0805	-	WELCOME: Don A. Hart, Director, AFRPL/CC
0815	-	OVERVIEW: AIR FORCE ROCKET PROPULSION. Richard R. Weiss, Chief Scientist, AFRPL
0915	38	OVERVIEW: AFOSR INTERESTS IN ROCKET PROPULSION. Leonard H. Caveny, AFOSR/NA
0930	-	OVERVIEW: AFRPL RESEARCH INTERESTS IN ROCKET PROPULSION. Wayne E. Ace, AFRPL/XRX
0945		Break
1015	-	ADVANCED DIAGNOSTICS OF REACTING FLOWS. Ronald K. Hanson, Stanford University, Stanford, CA
1100	39	INTERACTION OF MULTI-DIMENSIONAL MEAN AND ACOUSTIC FIELDS IN SOLID ROCKET COMBUSTION CHAMBERS. Joseph D. Baum and Jay N. Levine, AFRPL/DYCR
1130	-	INVITED: TRANSATMOSPHERIC PROPULSION. Leik N. Myrabo, Rensselaer Polytechnic Institute, Troy, NY
1200		Lunch (Reconvene at 1300)

WEDNESDAY (PM)
20 March 1985

Session Chairman: Capt. William Sowell, AFRPL/LKCS

Topic: Beamed and Solar Energy to Flowing Media

TIME	NUM.	
1300	40	LASER THERMAL PROPULSION. Dennis R. Keefer, Carroll Peters, Herbert Crowder, and Richard Welle. University of Tennessee Space Institute, Tullahoma, TN
1330	41	ANALYTICAL MODELING OF STRONG RADIATION GAS-DYNAMIC INTERACTION. Charles L. Merkle, The Pennsylvania State University, University Park, PA
1400	42	EXPERIMENTAL STUDIES OF LASER-SUSTAINED ARGON PLASMAS FOR CW LASER PROPULSION APPLICATIONS. Herman Krier and Jyoti Mazumder, University of Illinois at Urbana-Champaign, Urbana, IL
1430	43	LINEAR AND SATURATED ABSORPTION OF LASER RADIATION IN HEATED GASES. Robert H. Krech, Lawren M. Cowles, George E. Caledonia, David I. Rosen, Physical Sciences Inc., Andover, MA
1500		Break
1515	44	ENERGY DEPOSITION OF PULSED ONE MICRON LASER RADIATION IN H_2 AND AR. David I. Rosen and Nelson H. Kemp, Physical Sciences Inc, Andover, MA
1545	45	ADVANCED ENERGY CONVERSION CONCEPT FOR MICROWAVE BEAMED-ENERGY PROPULSION. Leik N. Myrabo, Rensselaer Polytechnic Institute, Troy, NY (New Start)
1615		ADJOURN SESSION
1615-1645		ADMINISTRATIVE MEETING (FOR AFOSR CONTRACTORS ONLY)
1615		Discussion Symposia (Snacks ,soft drinks, cash bar) - Antelope Valley Inn
1800		WORKING SESSION: SHUTTLE BASED ELECTRICAL PROPULSION AND PLASMA FLOW EXPERIMENTS. (Open agenda)

Abstract only, no presentation.

THURSDAY (AM)
21 March 1985

0730 Registration

Session Chairman: Robert J. Vondra, AFRPL/LKCJ

Topic: Electromagnetic Acceleration of Plasmas

TIME	NUM.	
-	46	*BASIC PROCESSES IN PLASMA PROPULSION. Herbert O. Schrade, Institut fur Raumfahrtantriebe der Universitat Stuttgart.
0800	47	PERFORMANCE-LIMITING FACTORS IN MPD THRUSTERS. Manuel Martinez-Sanchez, Daniel Heimerdinger, Mark Chanty and David Melanson, Massachusetts Institute of Technology, Cambridge, MA
0830	48	EROSION AND ONSET MECHANISMS IN MAGNETOPLASMADYNAMIC THRUSTERS. John L. Lawless, Carnegie-Mellon University, Pittsburgh, Pa
0900	49	CATHODE OPERATION IN A 50KW SUBSCALE MPD THRUSTER TEST BED. David Q. King, Jet Propulsion Laboratory, Pasadena, CA
0930	50	MAGNETICALLY CONTAINED ELECTROTHERMAL THRUSTERS. George R. Seikel, SeiTec, Inc., Cleveland, OH (New Start)
1000		Break
1030	51	PLASMA-GAS INTERACTION STUDIES IN A HYBRID PLUME PLASMA ROCKET. Franklin R. Chang, NASA Johnson Space Flight Center, Houston, TX Warren A. Krueger, Ted F. Yang, and Jay L. Fisher, Massachusetts Institute of Technology, Cambridge, MA (New Start)
1045	52	A TANDEM MIRROR PLASMA SOURCE FOR HYBRID PLUME PLASMA STUDIES. Ted F. Yang, Ron H. Miller, Kevin W. Wenzel, Warren A. Krueger, and Franklin R. Chang, MIT, Cambridge, MA (New Start)
1100	53	COUPLING BETWEEN GAS DYNAMICS AND MICROWAVE ENERGY ABSORPTION. Michael M. Micci, Pennsylvania State University, University Park, PA (New Start)
1115	54	PULSED INDUCTIVE ENERGY TRANSFER. Peter P. Mongeau and Douglas P. Hart, Electromagnetic Launch Research, Inc., Cambridge, MA
1145	55	LASER DIAGNOSTICS FOR ELECTRIC FIELD MEASUREMENTS. Roger J. Becker, Blair A. Barbour, and Allen T. Buswell, University of Dayton Research Institute, Dayton, OH (New Start)
1200		Lunch (Reconvene at 1300)

THURSDAY (PM)
21 March 1985

Session Chairman: Frank Mead, AFRPL/LKCS

Topic: Energy Conversion

TIME	NUM.	
1300	56	OPTICAL TECHNIQUE TO MEASURE ELECTRODE EROSION. James D. Trolinger and David F. Schaack, Spectron Development Laboratories, Inc., Costa Mesa, CA (New Start)
1315	57	VARIABLE FIELD EFFECTS FOR THE ROTATING FLUIDIZED BED REACTOR. Owen C. Jones, Jr., Rensselaer Polytechnic Institute, Troy, NY
1345	58	EFFECT OF INTERFACIAL PHENOMENA ON CONTACT LINE HEAT TRANSFER Peter C. Wayner, Jr., Rensselaer Polytechnic Institute, Troy, NY (New Start)
1415	59	UNIFIED STUDY OF PLASMA-SURFACE INTERACTIONS FOR SPACE POWER AND PROPULSION. Peter J. Turchi, Craig N. Boyer, John F. Davis, and Joseph Norwood, Jr., R D Associates, Washington Research Laboratory, Alexandria, VA
-	60	*CLOSE-SPACE, HIGH TEMPERATURE KNUDSEN FLOW. John B. McVey, Rasor Associates, Inc., Sunnyvale, CA
1445		ADJOURN MEETING

*Abstract only, no presentation.

Topic: Diagnostics of Reacting Flow

61 TWO-PHOTON DETECTION TECHNIQUES FOR ATOMIC FLUORINE. William K. Bischel, SRI International, Menlo Park, CA

62 COHERENT OPTICAL TRANSIENT SPECTROSCOPY IN FLAMES. John W. Daily, University of California, Berkeley, CA

63 DEVELOPMENT OF VELOCITY MEASUREMENT TECHNIQUE BY PULSED LASER DOPPLER ANEMOMETRY. B. C. R. Ewan and J. Swithenbank, University of Sheffield, Sheffield, GB

64 QUANTITATIVE FLOW VISUALIZATION. Ronald K. Hanson, Stanford University, Stanford, CA

65 OPTICAL PROCESSING AND PHASE CONJUGATION. Lambertus Hesselink, Stanford University, Stanford, CA

66 STRATEGY FOR ADVANCED SENSING AND CONTROL OF COMBUSTION. Mark L. Nagurka, Juan I. Ramos, and W. A. Sirignano, Carnegie-Mellon University, Pittsburgh, PA

67 1-D LASER DOPPLER INSTRUMENTATION. Holger T. Sommer, Carnegie-Mellon University, Pittsburgh, PA

68 RESONANT CARS DETECTION OF OH RADICALS. James F. Verdieck, United Technologies Research Center, East Hartford, CT.

69 SPRAY CHARACTERIZATION USING PHASE ANGLE DETECTION. William D. Bachalo, Aerometrics, Inc., Mountain View, CA

70 LASER EMISSION AND COHERENT RAMAN SCATTERING FROM INDIVIDUAL FLOWING DROPLETS. Richard K. Chang, Marshall B. Long, and Roman Kuc, Yale University, New Haven, CT

71 SIZE AND SHAPE CHARACTERIZATION OF INDIVIDUAL FLOWING DROPLETS BY LASER LIGHT SCATTERING. Richard K. Chang, B. T. Chu, and Marshall B. Long, Yale University, New Haven, CT

72 SPRAY CHARACTERIZATION WITH A NONINTRUSIVE OPTICAL SINGLE PARTICLE COUNTER. Cecil F. Hess, Spectron Development Laboratories, Inc., Costa Mesa, CA

73 INTELLIGENT LASER DIFFRACTION INSTRUMENTATION FOR PARTICLE SIZE ANALYSIS. E. Dan Hirleman and Joseph I. Koo, Arizona State University, Tempe, AZ

74 APPLICATION OF ATOMIC FLUORESCENCE TO MEASUREMENT OF COMBUSTION TEMPERATURES IN SOLID PROPELLANTS. Larry P. Goss and Arthur A. Smith, Systems Research Laboratories, Inc., Dayton, OH

75 REAL-TIME, TWO-DIMENSIONAL FUEL SPRAY VISUALIZATION. Lynn A. Melton, University of Texas at Dallas, Richardson, TX; James F. Verdieck, United Technologies Research Center, East Hartford, CT

76 SINGLE PARTICLE SIZING BY MEASUREMENT OF BROWNIAN MOTION. Alan C. Stanton, Aerodyne Research, Inc., Billerica, MA, and Wai K. Cheng, Massachusetts Institute of Technology, Cambridge, MA

ELECTROLYTIC PREPARATION OF NOVEL AZIDODINITRO COMPOUNDS

Milton B. Frankel and James F. Weber

Rockwell International Corporation
Rocketdyne Division
Canoga Park, CA 91304

Future higher performance propellants will require new classes of more energetic ingredients. Polynitro- and azido-alkyl compounds either have been or are being evaluated for this purpose. Highly substituted geminal dinitro compounds [e.g., $R\text{-}C(NO_2)_2X$, where $X=NO_2, CH_3, F$] are of particular interest, and substitution of an azido group ($X=N_3$) will further enhance the energetics of such compounds. This results from the fact that the azide group contributes ~80 Kcal/mole to the compound without decreasing the O/C ratio.

The preparation of compounds containing the azidodinitromethyl group, for example, presents a challenging problem. Prior studies conducted by C. L. Wright on the electrochemical azidization of nitro compounds have only afforded 1,1,1-azidodinitro-ethane and -propane. On the other hand, only the former compound has been synthesized in low yield and purity by standard chemical synthetic techniques.

The present program is directed toward investigating the experimental variables which influence the electrochemical azidization of nitro organics, and extending this basic knowledge to the synthesis of compounds having potential value as propellant ingredients. Cyclic voltammetry is being used to determine the oxidation potentials of the various reactants, the course of the half reactions (i.e., reversibility), pH and temperature dependence, and solvent/electrolyte effects. To date, these electroanalytical studies have shown that the voltammetric peak potentials of the azide ion and dinitro carbanions, containing various other functional groups, fall within a range of 290 mv. Furthermore, it has been determined that the anodic oxidations are irreversible and relatively insensitive to pH (6 to 11) and temperature (10 to 50C). For those cases wherein the anodic peak potential difference between the azide ion and dinitro carbanion is ~150 mv, simultaneous oxidation of both anions occur as desired. For those reactant pairs which exhibit greater differences in peak potentials, the apparent preferred reaction is one involving a step-wise oxidation-addition-oxidation pathway leading to the formation of diazidonitro-substituted compounds.

The above studies have led to the synthesis of 1,1,1-azidodinitroethane in improved yields of 30 to 40% at both platinum and graphite anodes. In addition, azidodinitromethyl-substituted esters and alcohols have been synthesized by this technique albeit in low (<20%) yields.

SCIENTIFIC APPROACH

- ELECTROCHEMICAL SYNTHESIS OF ENERGETIC $RC(NO_2)_2N_3$ COMPOUNDS
  - CONDUCT CYCLIC VOLTAMMETRIC STUDIES ON $RC(NO_2)_2^-$ AND N_3^- IONS
    - EXPERIMENTAL VARIABLES
      - SOLVENT
      - TEMPERATURE
      - pH
      - ELECTRODE MATERIAL
  - PERFORM ELECTROSYNTHESIS OF MODEL $RC(NO_2)_2N_3$ MATERIALS
    - OPTIMIZE
      - REACTANT CONCENTRATIONS
      - CURRENT DENSITY
      - CELL DESIGN
  - EXTEND BASIC ELECTROCHEMICAL TECHNOLOGY TO CANDIDATE PROPELLANT INGREDIENTS

ACCOMPLISHMENTS

- ESTABLISH IRREVERSIBILITY AND pH/TEMPERATURE INDEPENDENCE OF ANODIC REACTIONS

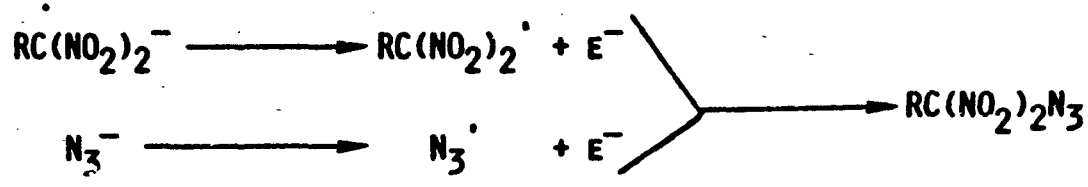

- IMPROVED ON REPORTED YIELD OF $CH_3C(NO_2)_2N_3$ TO 30-40%

- DEMONSTRATED NON-INTERFERENCE OF VARIOUS FUNCTIONAL GROUPS ON THE ELECTROCHEMICAL REACTION

  $C_2H_5O_2CCH_2CH_2C(NO_2)_2N_3$ $CH_3CO_2CH_2CH_2CH_2C(NO_2)_2N_3$

  $CH_3CO_2CH_2CH_2C(NO_2)_2N_3$ $HOCH_2CH_2CH_2C(NO_2)_2N_3$

- DIAZIDONITRO COMPOUNDS PRODUCED WHERE THE OXIDATION POTENTIAL OF THE CARBANION IS 250 MV GREATER THAN AZIDES

  $CH_3OCH_2C(N_3)_2NO_2$ $N{\equiv}CCH_2C(N_3)_2NO_2$

SYNTHESIS OF DIFLUORAMINOXY-, DIFLUORAMINO- or FLUORODIAZONIUM-CONTAINING MATERIALS

Jean'ne M. Shreeve

University of Idaho
Moscow, Idaho 83843

Future rocket propulsion advances require new stable high energy materials. The research is concerned with the synthesis of stable, highly oxidizing compounds which may contain, but are not limited to, nitrogen-fluorine bonds and the subsequent investigation of their physical and chemical properties.

Several routes to these compound types have been examined or are presently under investigation.

(a) The Lewis acid catalyzed introduction of $-ONF_2$ into F-olefins and functionalized F-olefins via reactions of NF_3O.

(b) In situ generation of an active fluorinating reagent through the interaction of NF_3O with NO.

(c) Development of a versatile, inexpensive, mild fluorination technique.

(d) Deoxygenation of N-fluoroazoxy compounds to fluorodiazonium compounds, $R_fN{=}NF$.

(e) Syntheses of $R_fN{=}NR$ compounds where R is an effective leaving group that can be displaced by fluorine.

(f) Michaelis-Arbuzov rearrangements which involve sulfur as the central atom.

(g) Novel reactions at the sulfur-fluorine bond in various substituted fluorosulfates.

Trifluoramine oxide (NF_3O) has been found to react rapidly with nitric oxide to give nitrosyl fluoride (FNO). A free radical reaction involving the known difluoronitryl ($F_2NO\cdot$) radical is proposed as a plausible mechanism. This reaction has been used as an *in situ* source of nitrosyl fluoride to synthesize the previously unknown nitroso compounds $R_f(CF_3)CFNO$ (R_f = n-C_5F_{11}, SF_5, OC_2F_5).

The perfluoronitrosocycloalkanes, heptafluoronitrosocyclobutane and nonafluoronitrosocyclopentane, are convenient precursors to a family of new perfluorocycloalkyl(aryl)diazenes. With aniline and *o*-aminobenzamide, $\overline{CF_2(CF_2)_xCFN{=}NC(CH)_4CH}$ and $\overline{CF_2(CF_2)_xCFN{=}NC(CH)_4CC(O)NH_2}$ (x = 2,3) are formed. Additionally, heptafluoronitrosocyclobutane gives $\overline{CF_2(CF_2)_2CFN{=}NCCFCFCHCFCF}$ and $\overline{CF_2(CF_2)_2CFN{=}NC(CH)_4CNH_2}$ with 2,3,5,6-tetrafluoroaniline and *o*-phenylenediamine.

NEW FLUORINE-TRANSFER REAGENT

COF_2

PROPERTIES

- STABLE TO HEAT, SHOCK
- B. P. -83°C
- REACTIVE AT 25°C OR ABOVE
- VERSATILE
- SYNTHESIZED WITHOUT USE OF FLUORINE

APPLICATIONS

- OXIDATIVE FLUORINATION
- REPLACE C-H, P-H, N-H, B-H WITH C-F, P-F, N-F, B-F
- CONVERT M=O BONDS TO MF_2

ACCOMPLISHMENTS

- IN SITU GENERATION OF FNO

$$2NO + NF_3O \longrightarrow 3\ ONF \quad (100\%)$$

$$N_2O_4 + KF \xrightarrow{S} ONF + KNO_3 \quad (100\%)$$

$$ONCL + KF \xrightarrow{S} ONF + KCL \quad (100\%)$$

- FLUORINATION UNDER MILD CONDITIONS

$$(RO)_2P(O)H + COF_2 \xrightarrow[S]{B} (RO)_2P(O)F + CO + B\cdot HF$$

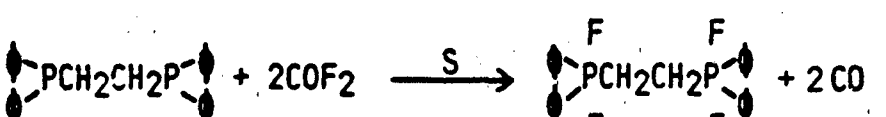

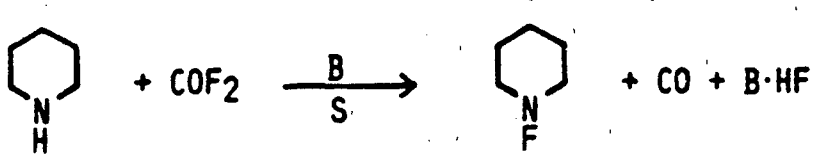

$$\phi_3CH + COF_2 \xrightarrow[S]{B} \phi_3CF + CO + B\cdot HF$$

- MICHAELIS-ARBUZOV REARRANGEMENTS

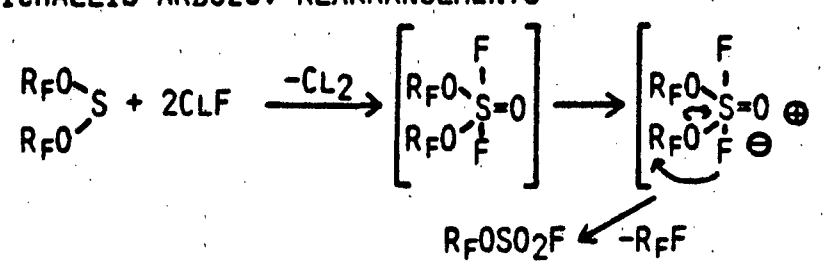

SYNTHESIS OF NEW POLYNITROPOLYHEDRANES

Alan P. Marchand*, Suresh C. Suri, and D. Sivakumar Reddy
Department of Chemistry, North Texas State University
NTSU Station, Box 5068, Denton, Texas 76203-5068

Our research program centers on the synthesis of polynitropolycyclic compounds. These compounds belong to a new class of explosives and propellants. However, relatively few polynitropolycyclic compounds have thus far been reported.

Our approach to the synthesis of these compounds involves first constructing highly functionalized (X-substituted) polycyclic "cage" systems; the individual substituents, X, are converted subsequently into nitro groups. Typical methodology, illustrated for the synthesis of polynitro-1,3-bishomocubanes, is outlined in Figure 1. In this approach, the substituted polycyclic framework is constructed via a combination of thermal and photochemical cycloadditions; the substituent groups, generally cage ketone carbonyl groups or pendant carboxylic ester, acid, or phenyl functionalities, can then be converted subsequently into nitro groups. This approach has the distinct advantage that increasing number of nitro groups are introduced sequentially into the cage molecule. Thus, the cumulative effects of increasing nitro-substitution upon product stability, upon relative ease of product-forming reactions, and upon explosive performance can be gauged in a gradual and orderly fashion.

Using the general approach described above, we have recently completed the syntheses of a trinitro- and a tetranitro-1,3-bishomocubane in thirteen and ten stereo-controlled steps, respectively (Figure 2). Efforts to synthesize an octanitro-1,3-bishomocubane and a hexanitro-trishomocubane are underway currently in our laboratory.

Typical approach to the synthesis of polynitropolyhedranes as illustrated for the synthesis of polynitro-1,3-bishomocubanes.

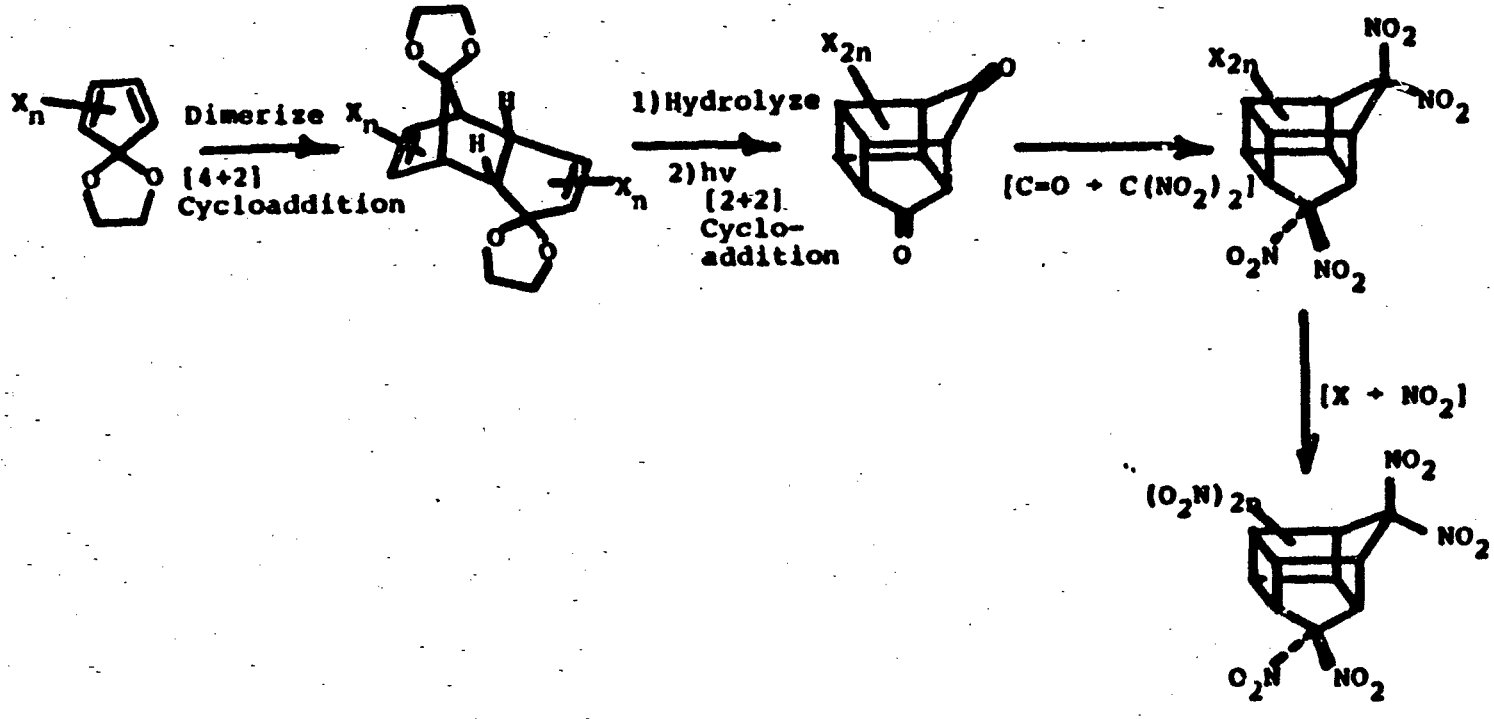

FIGURE 1

Synthesis of 2,5,8-Trinitropentacyclo[5.3.0.0^{2,6}.0^{3,10}.0^{4,8}]decane

Alan P. Marchand* and Suresh Chandra Suri

Department of Chemistry, North Texas State University, Box 5068, Denton, Texas 76203

J. Org. Chem. 49, 2041-2043 (1984).

Scheme I

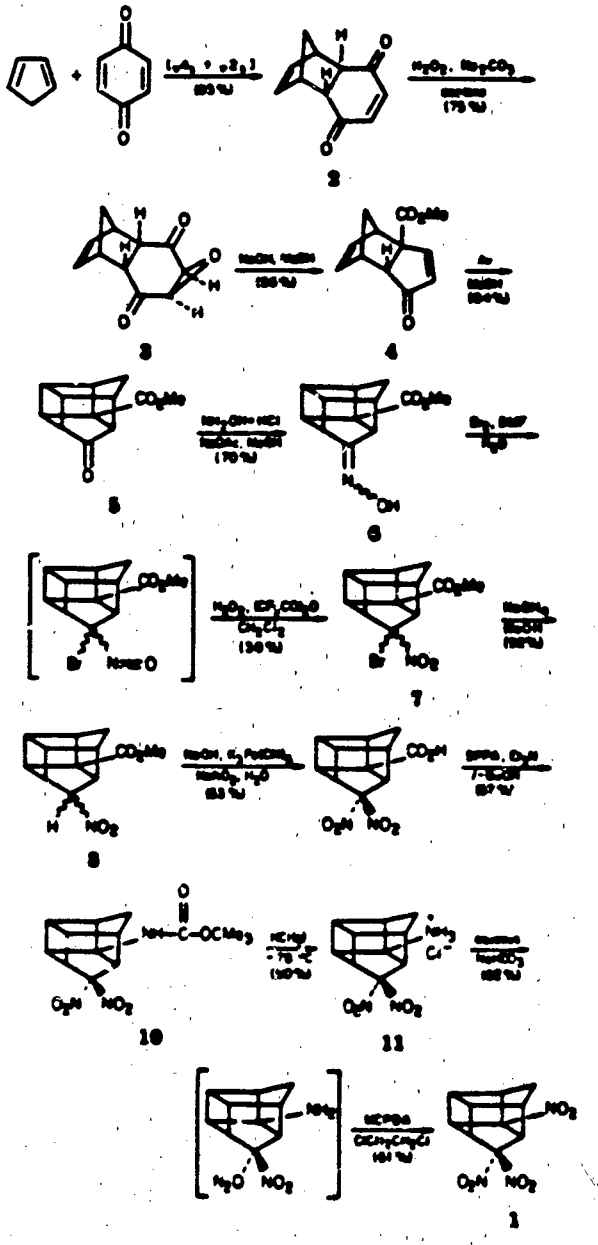

Synthesis of 5,5,9,9-Tetranitropentacyclo[5.3.0.0^{2,6}.0^{3,10}.0^{4,8}]decane

Alan P. Marchand* and D. Sivakumar Reddy

Department of Chemistry, North Texas State University, NTSU Station, Denton, Texas 76203

J. Org. Chem., 49, 4078-4080 (1984).

Scheme I

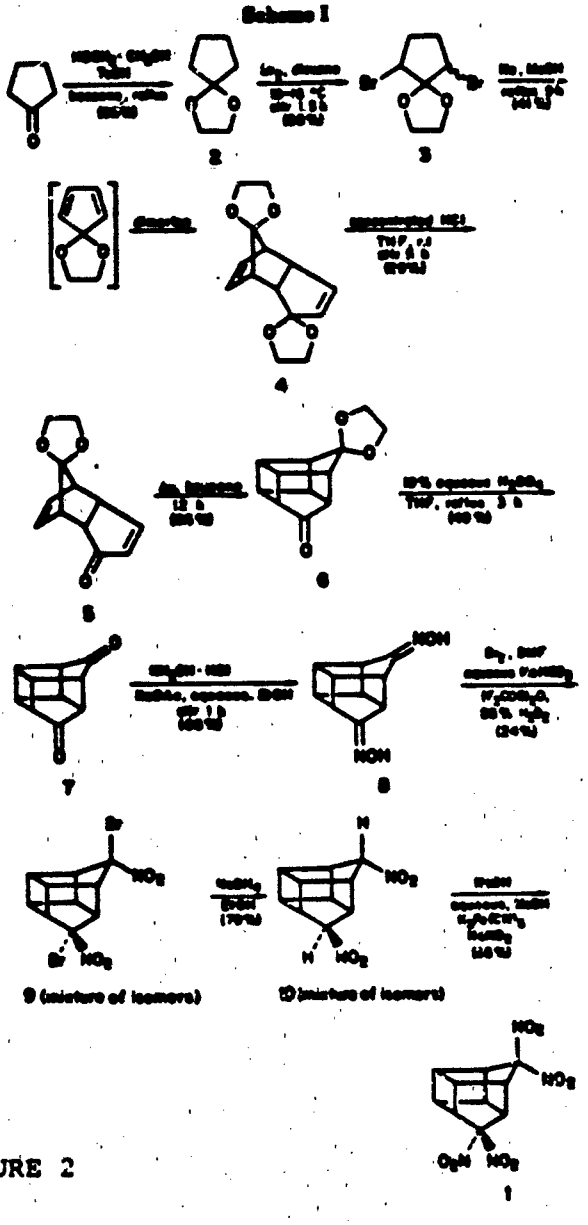

FIGURE 2

Synthesis of High Nitrogen Content Heterocyclic Nitramines and Energetic Internal Plasticizers

Dr. Rodney L. Willer and Dr. James A. Hartwell
Morton Thiokol, Inc.
Elkton Division
Elkton, Maryland 21921-0214

A considerable need exists for energetic materials which are denser and more energetic than 1,3,5,7-tetranitro-1,3,5,7-tetrazocine (HMX) and are thermally and hydrolytically stable. These dense, energetic materials are needed as ingredients for advanced explosives and propellant formulations that would exceed the performance of current formulations and allow future weapons systems to meet projected performance requirements. Most of the effort in this area has focused on two classes of compounds, the polynitro caged hydrocarbons, typified by octanitrocubane, and the caged nitramine compounds, typified by compounds such as hexanitrohexaazaadamantane and hexanitrohexaazawurtzitane. Some progress has been made with both types of compounds.

There are other classes of compounds that might also have the desired energy and density and that might be easier to synthesize. The basic requirements for high energy in a compound are a high-nitrogen content, a high-positive heat of formation, and a close to stoichiometric oxygen balance for the formation of CO and H_2O. The main requirement for high density is highly symmetric structures that incorporate as many rings as possible. Our approach to the design of molecules is to combine high-nitrogen-content heterocyclic rings such as furazan, furoxan, and tetrazole rings with nitramine groups in polycyclic structures. Our reasoning for this approach is that both groups are known to have positive heats of formation and low-molar-volume increments and combining them in polycyclic structures further maximizes the density and minimizes the amount of carbon atoms needed to hold the components together. This in turn allows for a desirable oxygen balance.

In Figure 1 are drawn some of our current target molecules which were designed by these criteria along with their predicted densities and predicted specific impulses. In Figure 2 are drawn two compounds which were designed by these criteria and then subsequently synthesized. A summary of the predicted and measured properties of these compounds is included.

We are also initiating a basic research program into type 3 internal plasticizers (IP's) and energetic internal plasticizers (EIP's). The ethylene glycol malonate (EGM) prepolymer system has been chosen as our model system because of its great synthetic flexability. Hydroxy-terminated EGM prepolymers with varying percentage of straight chain alkyl groups (12, 14, 16, 18 & 20 carbon atoms) attached to the malonate moiety will be synthesized. These prepolymers will be cured into gumstocks using isocyanate cure agents. The physical and mechanical properties of the gumstocks will be determined in order to determine the optimum length and percent incorporation for the side chains for improvement of the low temperature properties of the gumstocks. An attempt to replace the non-energetic side chains with energetic side chains of comparable length will then be made.

CURRENT TARGET MOLECULES

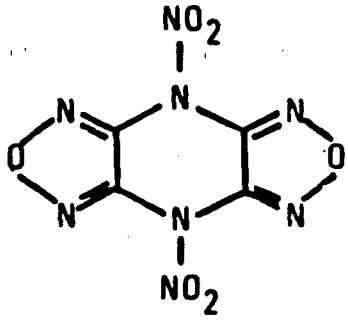

d = 2.00
I_{SP} = 278

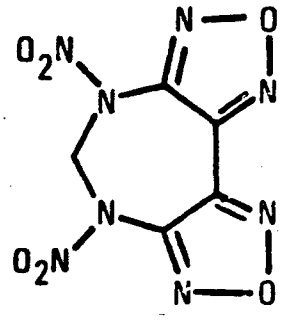

d = 1.91
I_{SP} = 272

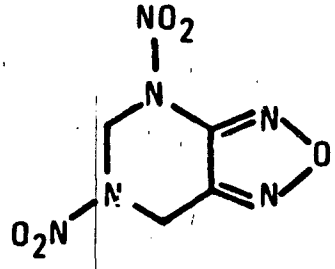

d = 1.83
I_{SP} = 256

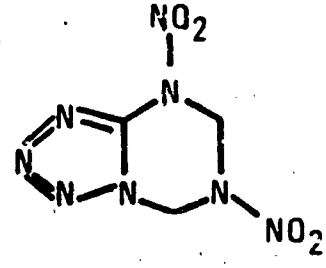

d = 1.83
I_{SP} = 256

FIGURE 1

COMPOUNDS PREVIOUSLY SYNTHESIZED

FURAZANO-FUSED NITRAMINES

SA14438(2)

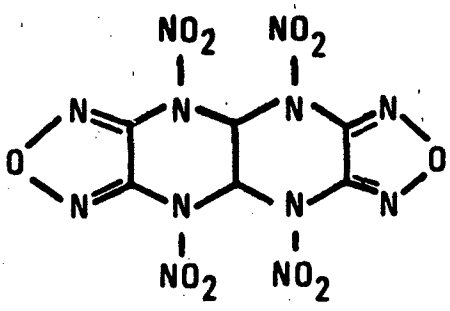

CL-15

d = 2.00 g/CC
I_{SP} = 275

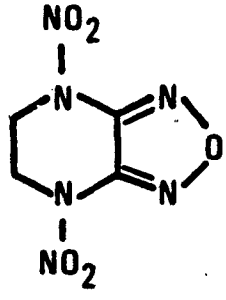

DNFP (CL-7.5)

d = 1.83 g/CC
I_{SP} = 256

PREDICTED AND MEASURED PHYSICAL PROPERTIES OF CL-15 AND DNFP

	CL-15		DNFP	
	Predicted	Measured	Predicted	Measured
Density , g/cc	2.00	2.00	1.82	1.83
Detonation pressure , kbar	4.37	4.19*	3.58	3.25*
Detonation velocity , mm/ μsec	9.57	9.43*	8.72	8.53*

*Calculated from measured density and heat of formation by the Kamlet Short Method.

FIGURE 2

Synthesis and Reactivity of Unsaturated Metal Nitrogen Complexes.

William C. Trogler, Joseph H. Osborne, and Mary Maciejewski
Department of Chemistry, D-006
University of California, San Diego
La Jolla, California 92093

Reactions between organic azides, N_3R (R = CH_3, C_6H_5, 2,6-$(CH_3)_2C_6H_3$, o-biphenyl, $SiMe_3$, $SiPh_3$, CPh_3, and neopentyl) and $(\eta\text{-}C_5Me_5)_2V$ lead to (Figure 1) either $(\eta\text{-}C_5Me_5)_2VNR$ or $(\eta\text{-}C_5Me_5)_2VN_3$. Mechanisms for the mode of reactivity will be presented. The nitrene complexes exhibit one unpaired electron according to bulk magnetic susceptibility measurements. At room temperature EPR spectra are observed that reveal both vanadium and nitrogen hyperfine splitting. The three dimensional structure of $(\eta\text{-}C_5Me_5)_2VN[2,6\text{-}(CH_3)_2C_6H_3]$ has been established, in collaboration with Dr. A. Rheingold of the University of Delaware, by X-ray crystallography (Figure 2) and the complex exhibits a linear V-N-R group. The unsymmetrical energetic tetrazene, Ph(PhC(O))N-N=N-(PhC(O))Ph, has been prepared in 4 steps from phenylhydrazine and its reactivity with metal reagents has been examined. Group I or II metal alkyls fragment the tetrazene to PhN_3 and $NH_2[C(O)Ph]$ while complexes form with transition metal carbonyls. Recent chemistry obtained with unsaturated nitrogen complexes, that are derived from monosubstituted hydrazines will be discussed.

Figure 1: Reactions Between $(\eta\text{-}C_5Me_5)_2V$ and Organic Azides.

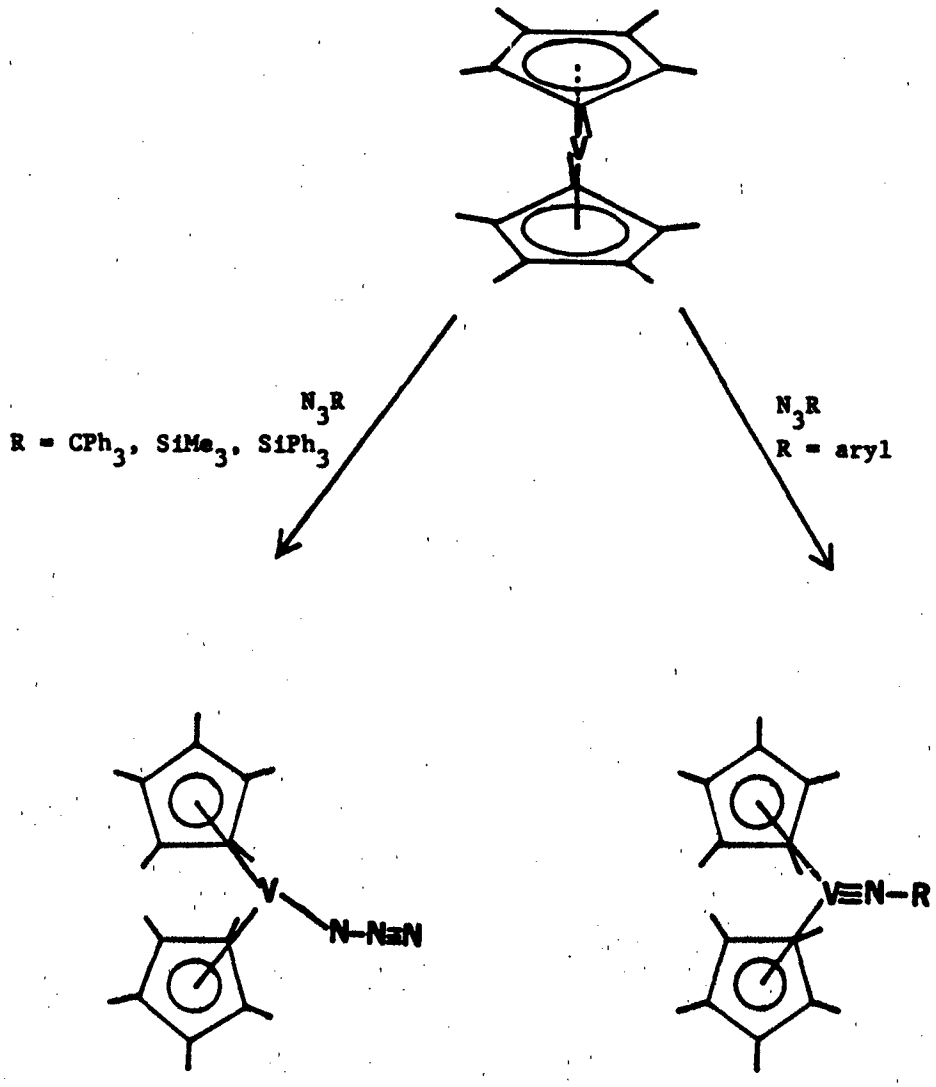

Figure 2: Molecular Structure of $(\eta\text{-}C_5(CH_3)_5)_2VN[2,6\text{-}(CH_3)C_6H_3]$ as Determined by Single Crystal X-ray Diffraction. Only the Nonhydrogen Atoms are Shown.

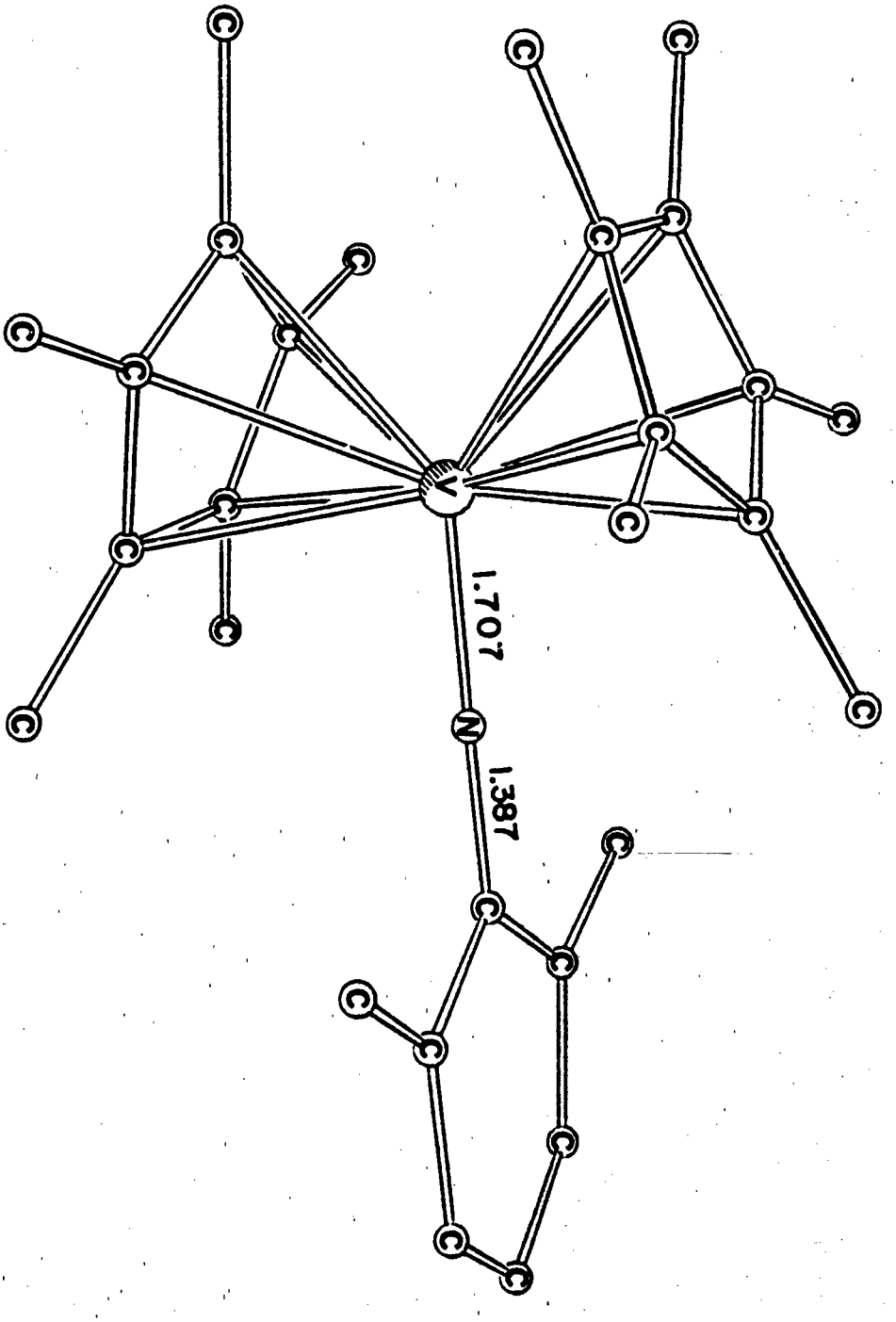

SYNTHESIS AND CHEMISTRY OF POLYNITROALKANES AND POLYNITROOLEFINS

Contract: F49620-83-K-0028

Clifford Bedford and Robert J. Schmitt
SRI International
Energetic Materials Program
333 Ravenswood Avenue
Menlo Park, CA 94025

Research programs in energetic materials synthesis and mechanisms have been hampered by the lack of general methods for synthesizing geminal dinitroalkenes and non-acidic methods for nitramine synthesis. Efforts to identify and overcome these research barriers have thus far been directed toward special situations and have met with only limited success.

The objectives of this research program have been to develop new methods for the introduction of nitro groups on olefins and amines. We have recently begun the study of new non-acidic methods of amine nitration. This work utilizes the synthetic capabilities of trimethylsilyl (TMS) protecting/leaving groups. The TMS group significantly enhances the solubility of amines in aprotic solvents while providing a specific site for attack for the nitrating agents. These protecting groups can be displaced from amines and potentially olefins by reaction with tetranitromethane, NO_2Cl, or NO_2F. This unique application of silane chemistry utilizes the formation of a very strong TMS-Halogen bond as the principle driving force.

We have explored the scope and limitations of our newly discovered nitrodealumination reaction. While this reaction has proven effective in the preparation of a few nitroolefins, the overall scope of the reaction is rather narrow, limiting its synthetic value for nitroolefin synthesis.

Studies on the synthesis of nitroquinodimethanes have been initiated. The goal of this work is the synthesis and characterization of novel pi-electron acceptors. Success will lead to a better understanding of the chemistry of polynitro compounds and to the design of a new class of organic solids having useful electrical properties.

The work to date is summarized below:

- We have developed a new nitrodesilylation reaction utilizing trimethylsilyl groups as protecting/leaving groups in non-acidic amine nitration/nitrosations.
- We discussed our completed work on the new nitrodealumination reaction.
- We have initiated the synthesis and characterization of tetranitroquinodimethane.
- We have initiated a study of the reactions of nitryl fluoride with TMS-alkenes and TMS-alkynes.

NEW SYNTHETIC METHODS FOR NITRO COMPOUND SYNTHESIS

- **NEW NON-ACIDIC AMINE NITRATION**

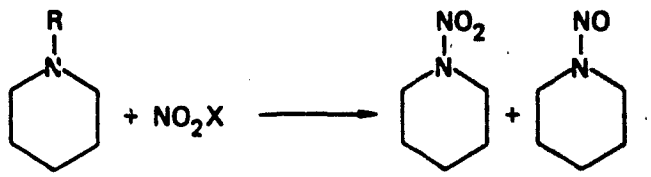

R = H, $Si(CH_3)_3$

X = F, Cℓ, $C(NO_2)_3$

- **NITRODEALUMINATION FOR NITROOLEFIN SYNTHESIS**

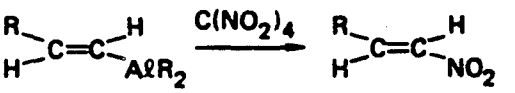

41% Yield

- **TETRANITROQUINODIMETHANE SYNTHESIS**

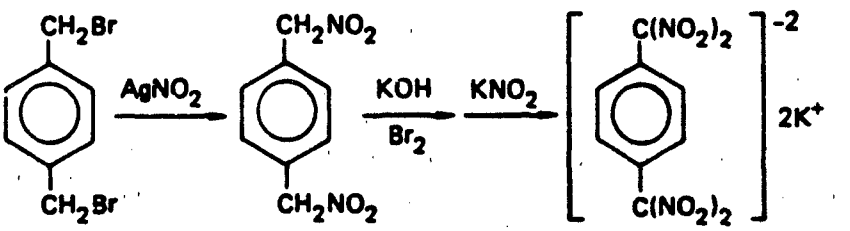

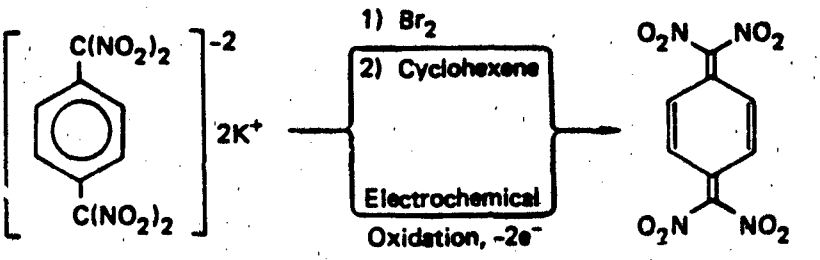

JA-6770-20

NON-ACID NITRAMINE/NITROSAMINE SYNTHESIS

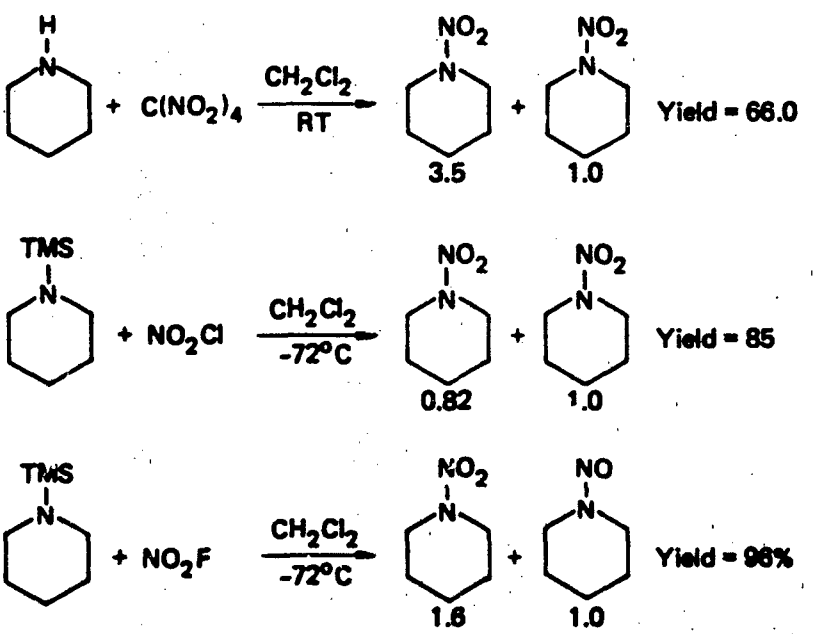

Advantages

- Non-acidic -- No amine degradation by acid
- TMS Group enhances amine solubility in Aprotic solvents
- Strong driving force for replacement of Amine-TMS bond

JA-6770-19

NEW SYNTHETIC TECHNIQUES FOR ADVANCED PROPELLANT INGREDIENTS: SELECTIVE TRANSFORMATIONS AND NEW STRUCTURES

Robert D. Chapman, Scott A. Shackelford,
John L. Andreshak

Air Force Rocket Propulsion Laboratory
Edwards AFB, CA 93523

New chemical transformations and methods are being investigated which potentially lead to energetic target compounds with new and novel molecular structures, or which improve synthetic routes to known compounds that are currently expensive propellant luxuries. Three of four scheduled research tasks are in progress.

Task 1 Nucleophilic substitutions of alkyl bromides with silver triflate were conducted to form precursor triflate ester compounds for conversion into key energetic ingredients. Triflate ester intermediates provide a facile and selective pathway to energetic compounds not available by direct synthetic routes. The scope and limitations of this triflate ester synthesis have not been investigated systematically, especially with dihaloalkanes. The α,ω-dibromoalkanes react much more rapidly with silver triflate than do corresponding monobromoalkanes, and unlike the monobromides, dibromoalkanes resist unwanted isomerization to 2° triflate products in CCl_4 solvent. This behavior is explained by an SN_1-type reaction where intramolecular Br anchimeric assistance occurs in bromoalkyl monotriflate product formation, followed by intramolecular anchimeric stabilization by the triflate group during alkylditriflate product formation. There is also a greater tendency to form the ditriflate product as chain length increases in the α,ω-dibromoalkanes up through 1,5-dibromopentane where this effect plateaus. Higher reaction temperatures render the intermediate triflate product unstable; decomposition with polymerization then occurs in CCl_4 solvent and aromatic alkylation results in benzene solvent. A manuscript has been prepared for Journal of Organic Chemistry.

Task 2 The reaction of alkenes, alkyl carbonyls, or organometallic compounds with energetic triflate esters could permit selective, direct syntheses of energetic alkanes or alkenes in which an overall anti-Markownikov introduction of energetic groups is desired. Preliminary reactions between fluorodinitroethyl triflate and carbonyl compounds imply low-yield formation of energetic α,β-unsaturated ethers. Reactions between nitronium triflate and organolithium compounds tentatively show promise as a selective non-acidic nitration technique, and studies of such systems are continuing.

Task 3 Collaborative AFRPL/Pt Loma College (D. F. Shellhamer) studies are being conducted with alkene methoxyfluorination reactions using methanolic XeF_2 suspensions. Elucidation of this mechanism could permit an exclusive regioselective control which produces the anti-Markovnikov ether adduct. Substitution of energetic alcohols for methanol could directly produce stable, partially fluorinated energetic ethers rather than undesirable acetal-type products. Reactions with norbornene produced different fluoromethoxynorbornane isomers identified as those where the methoxy moiety exclusively added first when catalyzed by BF_3. New isomers occurred with HF catalysis in which the F atom added first. This is consistent with our initially proposed reaction mechanism in which effecting methoxy addition first produces the desired anti-Markownikov product. A manuscript has been submitted to J. Org. Chem. Studies are underway with the energetic fluorodinitroethanol substrate.

APPROACH

Task I: Reactions of triflate salts for selective intermediate syntheses

- $RCH_2Br + AgOTf \xrightarrow{-AgBr} RCH_2OTf$
- $CH_2=C(R)-Br + AgOTf \xrightarrow{-AgBr} CH_2=C(R)-OTf$

  then conversion: $RCH_2OTf + EngOH \longrightarrow RCH_2OEng$ (Eng = energetic substituent, e.g., polynitroalkyl)

Task II: Reactions of energetic triflates (including nitronium triflate)

- 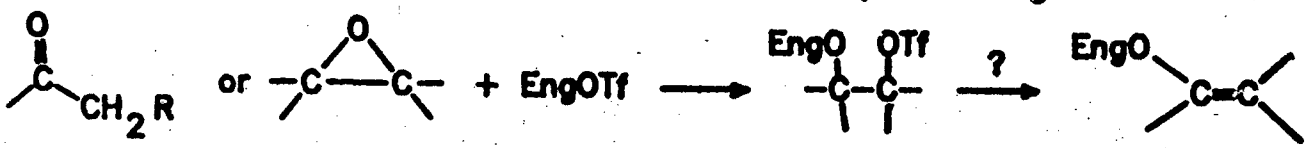 (ketone or epoxide + EngOTf → EngO, OTf intermediate → ? → EngO-C=C)
- $M^+R^- + NO_2{}^+OTf^- \xrightarrow{-M^+OTf^-} NO_2R$ (selective, non-acidic nitration)

  R = alkyl, alkenyl

Task III: Selective fluorination by xenon difluoride

- 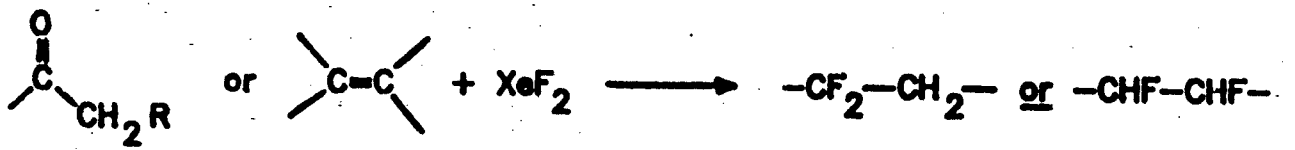 + $XeF_2 \longrightarrow -CF_2-CH_2-$ or $-CHF-CHF-$

  Chemical catalysis ⟶ ionic reaction mechanism
  Light initiation ⟶ radical reaction mechanism
  } different fluoride products

- $ROCH=CH_2 + XeF_2 \xrightarrow{EngOH} ROCH(F)-CH_2(OEng)$ + ~~$ROCH(OEng)-CH_2F$~~ { hydrolytically unstable acetal product

  −OEng 1st addition −F 1st addition

RESULTS

Task I

- $Br(CH_2)_4H + AgOTf \xrightarrow[CCl_4\ (RT)]{t_{1/2} = 76.5\ h} TfO(CH_2)_4H + CH_3\overset{OTf}{C}HCH_2CH_2-H$ (rearrangement)

- $Br(CH_2)_4Br + AgOTf \xrightarrow[CCl_4\ (RT)]{t_{1/2} = 0.95\ h} TfO(CH_2)_4Br \xrightarrow[AgOTf/CCl_4]{t_{1/2} = 267\ h} TfO(CH_2)_4OTf$ (no rearrangement)

- $Br(CH_2)_nBr + AgOTf \longrightarrow \underset{1}{TfO(CH_2)_nBr} + \underset{2}{TfO(CH_2)_nOTf}$ [2]/[1] ↑ as n ↑

Task II (Preliminary)

- $CH_3C(O)C(O)CH_3 + CF(NO_2)_2CH_2OTf \xrightarrow{Bu'_2PY} CH_2=\overset{(FDNE)O}{C}-\overset{O(FDNE)}{C}=CH_2$ (?)

- $NO_2^+OTf^- + \underset{(xs)}{n\text{-BuLi}} \xrightarrow{hexane} \left[\begin{matrix}H\\C_3H_7\end{matrix}\!\!>C=NO_2\right]^- Li^+$

Task III

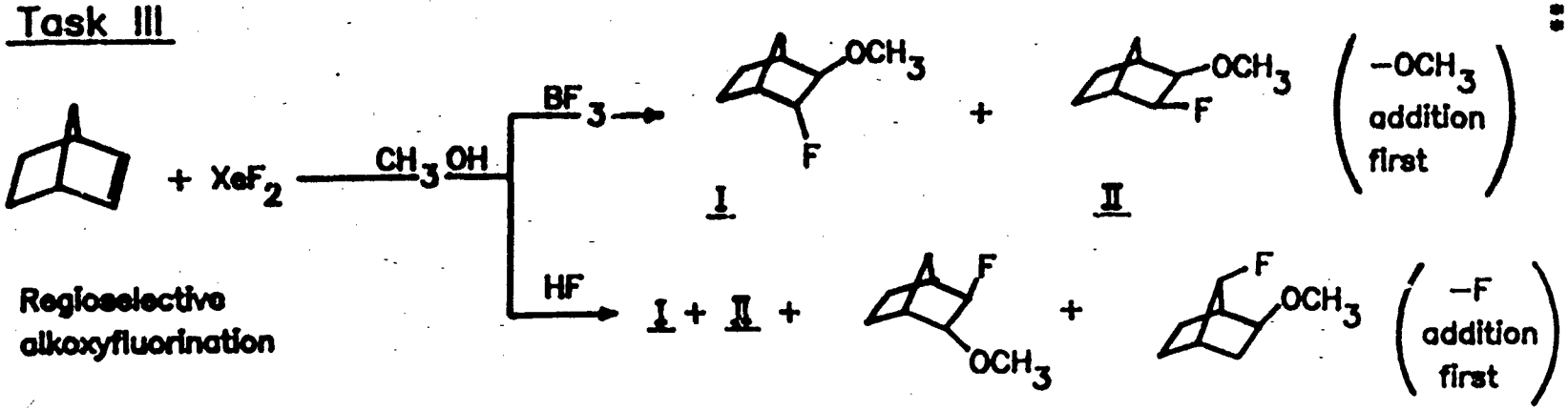

FLUOROPOLYAZIDO-ESTERS AS ENERGETIC POLYMERS

Robert M. Moriarty

University of Illinois at Chicago
Department of Chemistry
Chicago, Il 60680

The objective of our work is to introduce the energy rich azido group into a fluorine containing polymer. The monomeric compound which we will synthesize are fluoroazido-ketenes (1 and 2):

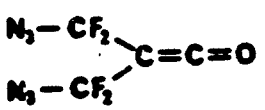

1

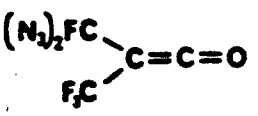

2

The polymerization of 1 and 2 depends upon the spontaneous reaction of the highly reactive α-lactone formed by oxygen atom transfer (O_3 or C_6H_5IO) to the ketene:

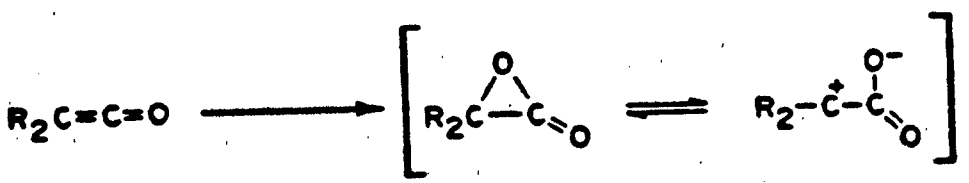

MW = 6483 for

R = C_6H_5

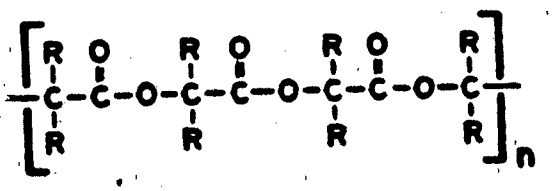

In a second approach to fluoroazidopolymers, the copolymerization of the intermediary α-lactones will be carried out in the presence of azido co-monomers:

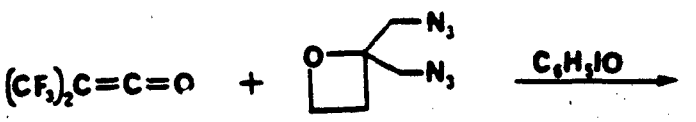

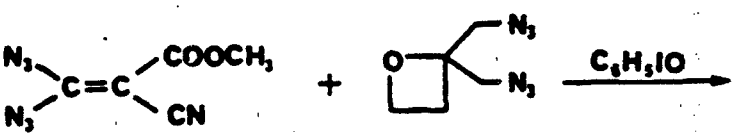

Syntheses of the relevant compounds will be presented.

NEW ENERGETIC POLYMERS AS BINDERS FOR PROPELLANTS

Mostafa A.H. Talukder and Stanley D. Morse
Air Force Rocket Propulsion Laboratory
Edwards AFB, CA 93523

(University of Dayton Research Institute)

New polymeric syntheses and chain modification techniques are being investigated to obtain improved mechanical properties of known energetic binders, new energetic prepolymer and binder systems, and correlations of polymerice chemical structure to physical/mechanical properties. Its approach centers on new energetic polymer syntheses via cationic polymerization or by synthetic modifications of known polymers. Two tasks are active.

Task 1 seeks to improve the physical and mechanical properties of known energetic polyether polymers derived from glycidyl-substituted monomers. The modified copolymerization technique, successfully demonstrated with the PECH polymer will be used to prepare modified energetic prepolymers to maximize stress, strain, and modulus properties. Epibromohydrin polymerizations were conducted to assess the PEBH modified polymer as viable precursor for the aforementioned energetic binder materials. It has been shown that an epibromohydrin polymer can be formed that will react with NaN_3 or $AgNO_3$ in displacement reactions. The reaction rates are faster than for the same reactions with polyepichlorohydrin.

Task 2 will seek to obtain a hydroxy-containing poly-dinitropropyl vinyl ether polymer suitable for propellant urethane curing procedures. The dinitropropyl vinyl ether monomer is obtained in a high-yield one-step synthesis and has successfully been polymerized into an energetic non-hydroxyterminated binder for pressed HMX explosive fills. Its inherent superior thermochemical stability, coupled with its excellent hydrolytic stability and chemical compatibility at elevated temperatures with HMX, makes it a very attractive energetic binder candidate for minimum smoke propellants.

Task 3 addresses the polymerization of any new energetic monomer structures. Polymerization reactions will be conducted to characterize new energetic polymer structure, functionality, and physial properties.

Task 4 employs polymerization syntheses and techniques which provide structurally controlled polymer backbones for correlation investigations of structure and physical/mechanical properties. Unlike Task 1 which seeks to optimize the physical and mechanical properties of energetic polymer via individual synthetic modification procedures, Task 4 seeks to modify only the energetic pendant substituent on an identically synthesized polymer backbone structure. Any differences in mechanical or physical properties of energetic polymer samples will be caused solely by the $-N_3$,- ONO_2, or $-OCH_2CF(NO_2)_2$ groups themselves. Because of the ease with which a pendant triflate group could be displaced by energetic but weak nucleophiles ($-N_3$, - ONO_2,-OFDNE), glycidyl triflate monomer was synthesized from the reaction of epibromohydrin and silver triflate. The method was limited to low yield of the product. However a modified synthesis and isolation technique has been developed to increase the yield and improve the purity of the material.

It is to be noted here that the research work of the project was postponed for about 7 months in Jan 1984 because of the absence of research personnel.

APPROACH

Task I + IV: Modification and synthesis of glycidyl polymers

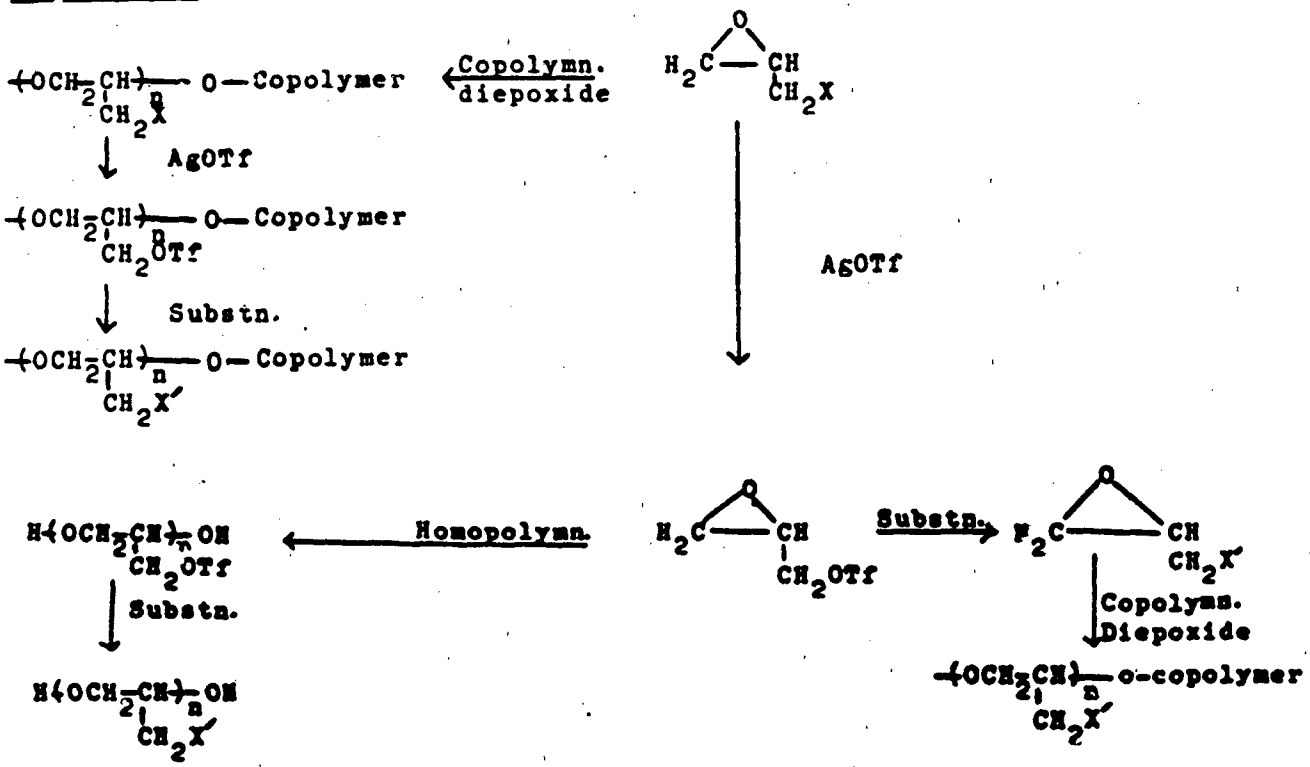

Task II: Poly-DNPVE modification

CH_2=CH-ODNP $\xrightarrow{\text{Polymerize}}$ HO—(CH—CH)$_n$—OH (ODNP)

DNP = $-CH_2C(NO_2)_2CH_3$

Task III: New energetic prepolymer structures

Syntheses via novel monomers: H(OCH(CH$_2$X′)CH(CH$_2$X′))$_n$OH, H(OCH$_2$CH(NX′$_2$))$_n$OH

X= Cl, Br, I
X′=-N_3, -ONO_2, -$OCH_2CF(NO_2)_2$
OTf=-OSO_2CF_3

RESULTS

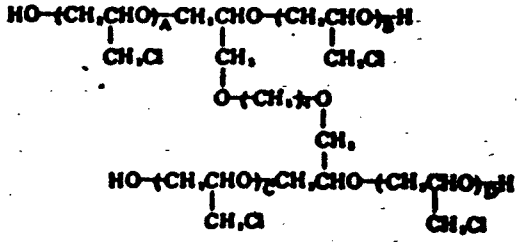

Obtained: Modified PECH with increased molecular weight prepared. Elastomers obtained from modified PECH showed low elongation and high modulus.

Expected: Energetic crosslinked copolymers with improved mechanical properties.

(Expected)

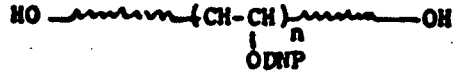

Thermally stable, nitramine-compatible energetic polymer for minimum smoke applications.

(Expected)

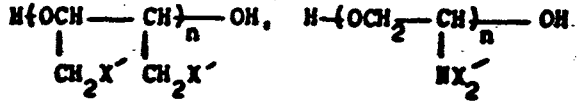

New energetic polymer structures/improved energetics.

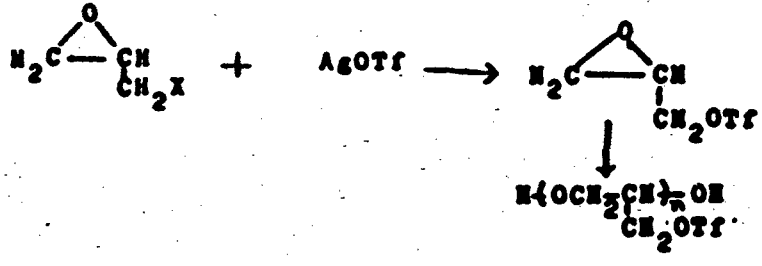

Obtained: Glycidyl triflate monomer as an intermediate in the preparation of different energetic prepolymers has been successfully synthesized. A modified synthesis and isolation technique has been developed to increase the yield and improve the purity of the product. Glycidyl triflate polymer obtained will be used to prepare different energetic prepolymers for structure- property correlation study.

Expected: Predictable property variations from energetic substituent changes.

X= Cl, Br, I
X'= $-N_3$, $-ONO_2$, $-OCH_2CF(NO_2)_2$
OTf= $-OSO_2CF_3$

ENERGETIC FLUOROCARBONS

Carl J. Schack and Karl O. Christe
Rocketdyne Division of Rockwell International
Canoga Park, California 91304

The purpose of this program is the development of general methods for the synthesis of energetic fluorocarbons and their conversion to olefins and epoxides suitable for the preparation of polyether-type energetic binders. Fluorocarbons with energetic substituents offer the potential advantages of high energy, high thermal stability high density, and also low sensitivity. This program is in its initial stages.

The technical approach involves the synthesis and characterization of new transfer agents such as XeY_2 and R_3SiY [where $Y=N_3$, ClO_3, CF_2NO_2, and $CF(NO_2)_2$], $B(N_3)_3$, N_3SO_3F, and NO_2N_3. As part of the characterization of these novel compounds, their addition to unsaturated functions and/or displacement of reactive halogens from fluorocarbons will be investigated as means for the preparation of new energetic fluorocarbons.

Applications of XeF_2 as a highly reactive fluorinating agent for organic substrates are well known. Similarly, it was shown in our laboratories that $Xe(OTeF_5)_2$ is efficient in transferring TeF_5O groups to unsaturated fluorocarbons. Consequently, the proposed XeY_2 transfer agents are promising reactants for analogous transfers of energetic groups. Displacement reactions in fluorocarbons, which involve fluorine, should be possible by suitable activating molecular environments such as adjacent C=C, C=O, or C=N functions. Substrates incorporating these features will be employed with formation of the favorable byproducts Me_3SiF and MSO_3F serving as driving forces for the reactions.

For energetic binders, the most desirable type of polymeric chain is a polyether due to its good thermal stability, flexibility, glass transition point, and load bearing capability. To synthesize these ethers, energetic fluoroolefins and their corresponding epoxides will be prepared in part using the new transfer agents and alternatel by other known reactions. In addition to the strong focus on azides and nitro compounds, work in this area will also include SF_5O- derivatives. It should be remembered that the weak S-F bonds make that group an oxidizing substituent. Epoxidation of the olefins will be conducted with an emphasis on the highly successful technique of Kolenko using NaOCl in aprotic solvents. The synthesis effort on the energetic epoxides will be "capped" by converting them to low molecular weight polymers. These will be homopolymers in order to minimize complications.

APPROACHES

Proposed syntheses of new transfer agents

$$XeF_2 + 2XN_3 \xrightarrow{\text{solv.}} Xe(N_3)_2 + 2XF \quad (X=H,Cl,Br,I,Na,Me_3Si)$$

$$Me_3SiCl + HR_x \longrightarrow Me_3SiR_x + HCl \quad (R_x=CF_2NO_2,\ CF(NO_2)_2)$$

$$S_2O_6F_2 + MN_3 \longrightarrow N_3SO_3F + M^+SO_3F^-$$

$$NO_2BF_4 + MN_3 \xrightarrow[-10°]{\text{solv.}} NO_2N_3 + M^+BF_4^- \quad (M=Li,Na,K)$$

Use of transfer agents for the introduction of energetic groups

$$\geq C{=}C\leq + Xe(N_3)_2 \longrightarrow N_3{-}\overset{|}{C}{-}\overset{|}{C}{-}N_3 + Xe \text{ (innocuous byproduct)}$$

$$CF_2{=}CFCF{=}CF_2 + Xe(N_3)_2 \longrightarrow N_3CF_2CF(N_3)CF{=}CF_2 \text{ or } N_3CF_2CF{=}CFCF_2N_3 + Xe$$

Olefins suitable for epoxidation and polymerization

$$CF_3N{=}CF_2 + Me_3SiN_3 \xrightarrow{-Me_3SiF} CF_3N{=}CFN_3 \overset{?}{\rightleftharpoons}$$

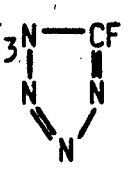

Ring formation stabilizes azido compound

$$CF_2{=}CF_2 + N_3SO_3F \longrightarrow N_3CF_2CF_2OSO_2F$$

Fluorosulfate is a reactive functionality

$$CF_3CN + N_3SO_3F \xrightarrow[-MSO_3F]{MF} CF_3CF{=}NN_3 \overset{?}{\rightleftharpoons}$$

APPROACHES

Synthesis of energetic monomers and their polymerization

$$CF_2{=}CF_2 + MN_3 \xrightarrow{solv.} CF_2{=}CFN_3 + MF \quad (M{=}Na, Me_3Si)$$

$$CF_2{=}CFH + SF_5OCl \longrightarrow SF_5OCFHCF_2Cl \xrightarrow[-HCl]{KOH} SF_5OCF{=}CF_2$$

$$CF_2{=}CFY + NaOCl \xrightarrow{solv.} CF_2\text{—}O\text{—}CFY$$

(Y = energetic group)

$$YCF_2CF\text{—}O\text{—}CF_2 \xrightarrow[R_fCFO]{F^-} R_fCF_2O\text{—}\left[CF_3Y\ \text{|}\ CFCF_2O\right]_n\text{—}C(CF_2Y)\text{—}C(=O)F$$

CONTROL OF THE URETHANE CURE REACTION WITH SOLID, BLOCKED ISOCYANATES

William H. Graham, JB Canterberry
Inella G. Shepard, Jerrell W. Blanks
Morton Thiokol/Huntsville Division
Huntsville, Alabama 35807

This program addresses the problem of controlling the cure kinetics of the isocyanate/hydroxyl reaction and the formation of polyurethanes. Successful completion of the program would provide unprecidented control of the reaction; the goal would be to demonstrate an infinite potlife below a "trigger" temperature and a rapid, but controllable, cure above that temperature. More generally, the approach addresses the question of differences in reactivities of molecules in solution and in the solid state. Although the system selected for study involves polyurethane cure chemistry, successful demonstration of the concept would imply that other solid state compounds could be used in triggering desired reactions only above their melt temperature, thus providing temperature sensitive on-off control of chemical reactions.

The materials which are envisioned as providing the desired potlife/cure profile for the polyurethane cure reaction are solid, blocked difunctional isocyanates which melt at temperatures slightly above a convenient processing temperature but below the desired cure temperature. As the temperature is raised above the melting point, the blocked isocyanate melts and dissociates to a soluble, difunctional isocyanate. If the insoluble, solid blocked isocyanate is evenly distributed in a difunctional alcohol prepolymer, a cure reaction will take place just above the melting point, but not below that temperature. After melting and dissociation of the blocked isocyanate into the reactive, free isocyanate, the latter material must be soluble in and diffuse readily and evenly into the binder phase where it can undergo the polyurethane-producing cure reaction. The relationship of molecular structure, melting temperature, solubility in binder, and particle size of the blocked isocyanate will be determined as it relates to polyurethane cure chemistry. The process is illustrated in Figure 1.

The results obtained using a carbon-filled gumstock of hydroxyl terminated polybutadiene (HTPB) and the solid blocked isocyanate of o-nitrophenol and 2,4-toluenediisocyanate (TDI) provide experimental evidence of the validity of the concept. It was shown that at 77°C (170°F) no cure reaction occurred, while at 121°C (250°F), the melting point of the blocked isocyanate, a cure reaction proceeded smoothly (see Figure 2). Infrared evidence for the unblocking reaction taking place only after melting is also shown. The isocyanate bond at ambient and 77°C (170°F) reflects the presence of the single unblocked isocyanate; the carbamate carbonyl band is a strong peak, but this is greatly reduced at 123°C (253°F) and the isocyanate peak is much stronger as the blocked isocyanate has dissociated back to TDI/and o-nitrophenol.

HTPB was added to the blocked isocyanate (TDI/o-nitrophenol) immediately after it was prepared and before crystallization occurred. This allows one hydroxyl on HTPB to react with the remaining free isocyanate group and kept the binder homogeneous. In this case, the cure took place readily at 77°C (170°F). From these experiments, we conclude that the crystalline nature of the blocked isocyanate inhibits its dissociation well beyond its normal dissociation temperature and allows it to occur only at or near its melting point.

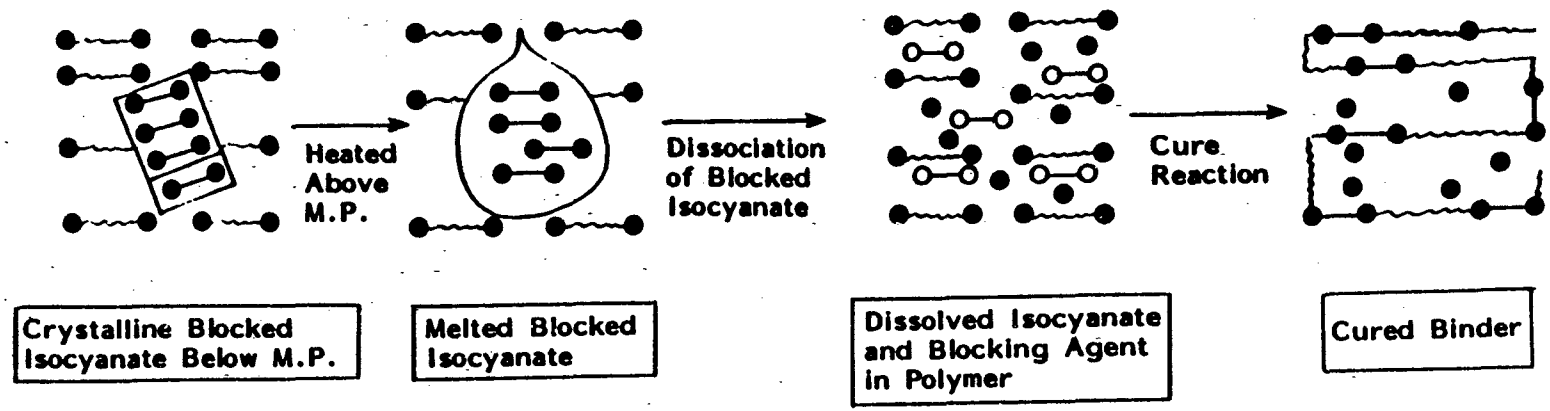

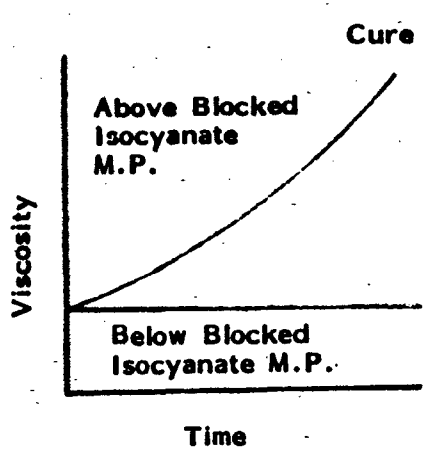

- Synthesis of Blocked Isocyanates (●—●) From Phenol (●) and Diisocyanate (○—○)
- Compile Catalog of Blocked Isocyanate Melting Points (M.P.)
- Relationship of Molecular Structure, Melting Temperature, Binder Solubility, and Particle Size of Blocked Isocyanate
- Cure Profile in Hydroxyl Functional Polymers (●~~~●)
- Catalysis of Cure Reaction

Figure 1. Control of the Urethane Cure Reaction With Solid Blocked Isocyanates.

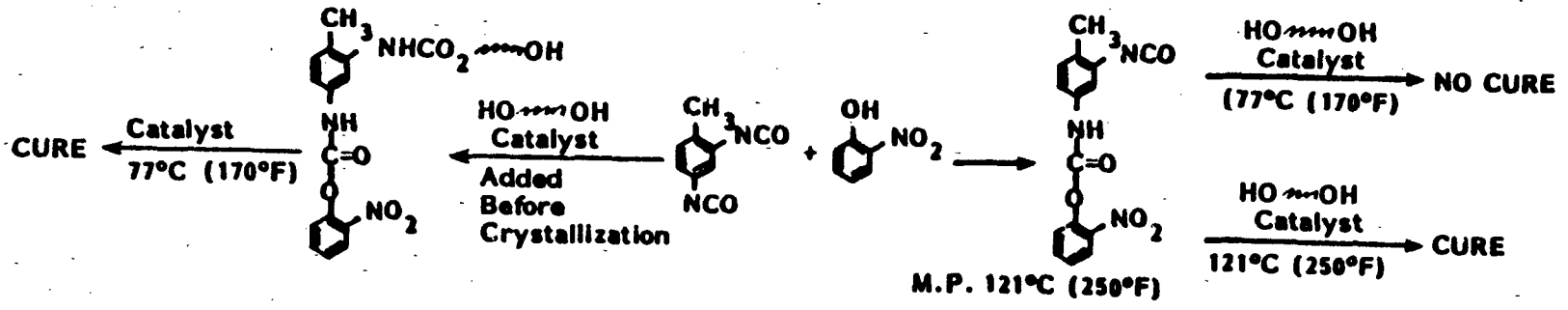

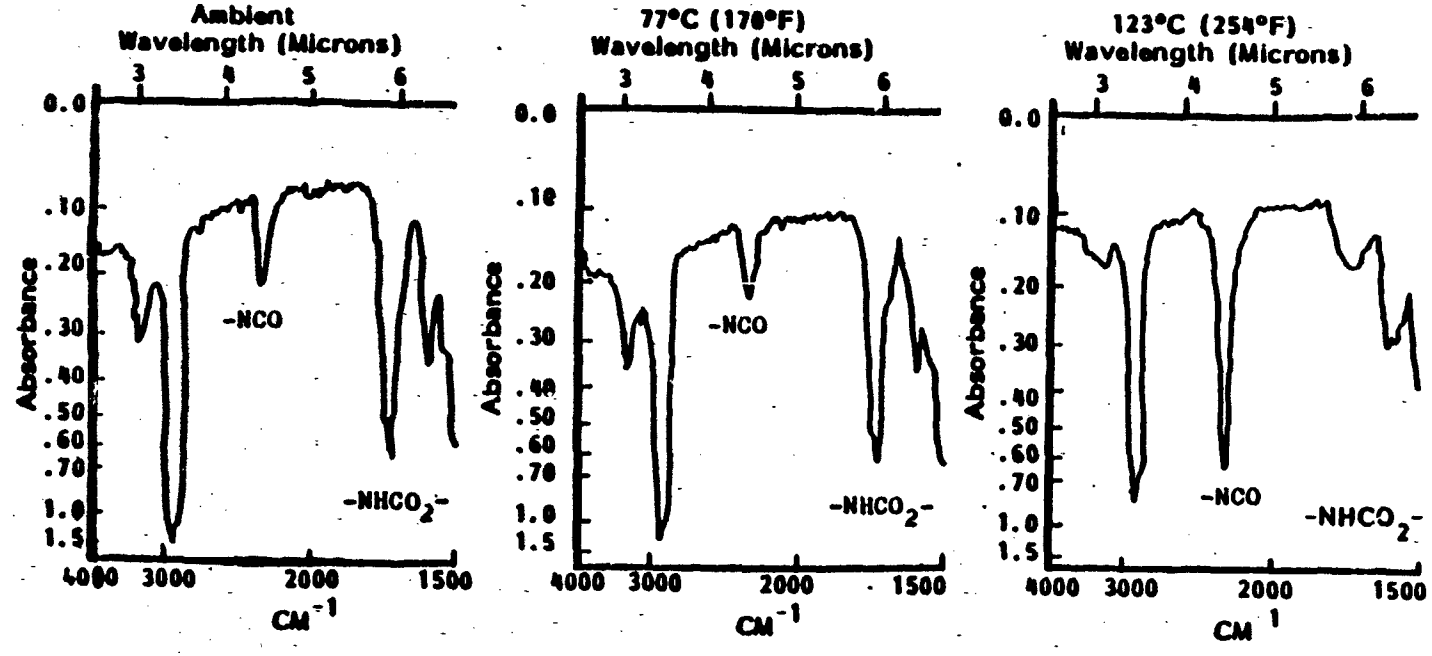

Figure 2. Polyurethane Cure Control With Blocked Isocyanates.

PHYSICAL AND CHEMICAL CONSEQUENCES OF ANTIAROMATICITY IN THE BORACYCLOPENTADIENE SYSTEM

John J. Eisch, Sinpei Kozima and James E. Galle
Department of Chemistry
The State University of New York at Binghamton
Binghamton, New York 13901

The mode of chemical bonding between boron atoms and clusters of carbon atoms should have a fundamental importance in determining the macroscopic physical and chemical properties of the resulting organoboron compounds. The stability of the boron-carbon bond is the basis for the use of organoboranes as a route to superior refractory materials, such as the boron carbides. By contrast, the lability or chemical reactivity of the boron-carbon bond in other organoboranes is the basis for the use of these compounds as rocket propellants. Because of the intimate connection between chemical bonding in organoboranes and their macroscopic chemical properties, we have sought to learn how pi-bonding between boron and carbon centers influences the reactivity of the boron center towards oxidants, protolyzing agents and Lewis bases.

Our initial approach, as depicted in Figure 1, has been to enclose a boron and an array of carbon atoms in an unsaturated ring. The cyclic systems of prime interest have been the boracyclopropene ring(A), the boracyclopentadiene ring(B) and the boracycloheptatriene ring(C). Syntheses of these rings have involved: 1) the photochemical rearrangement of the diphenyl(phenylethynyl)borane-pyridine complex to A; 2) the exchange between the corresponding stannole and the organoboron dihalide for B; and 3) the thermal reaction between B and an alkyne for C. According to Hueckel MO theory, supplemental pi-electron delocalization should cause A and C to be stabilized, while B should be antiaromatic and hence destabilized. As is summarized in Figure 2, pentaphenylboracyclopentadiene(D) manifests a heightened ease of oxidation, protolysis and Lewis complexation, compared with analogous reactions of A and C.

The insights into the synthesis and structural characteristics of these boron heterocycles, as gained in our studies thus far, will be brought to bear on exploring ways for the preparation of boron-carbon clusters containing more than one boron atom in the cluster. From a structural standpoint, what will be of unusual interest will be to determine at what ratio of boron-to-carbon atoms the planar structure displayed by the boron rings A-C will be changed for the electron-deficient structure characteristic of the carboranes. Since structure appears to be the fundamental determinant for chemical reactivity, the structure-reactivity insights gained from these studies should aid our predicting which structural types should exhibit unusual chemical reactivity in general, and oxidizability as a rocket propellant, in particular. Analogously, stabilizing trends identified by these studies may prove of great use in choosing the best precursors for the preparation of modified boron carbides. All such potential applications of organoboranes are rooted in the same fundamental problem that we take as our challenge: a thorough understanding of the nature and gradations of boron-carbon chemical bonding.

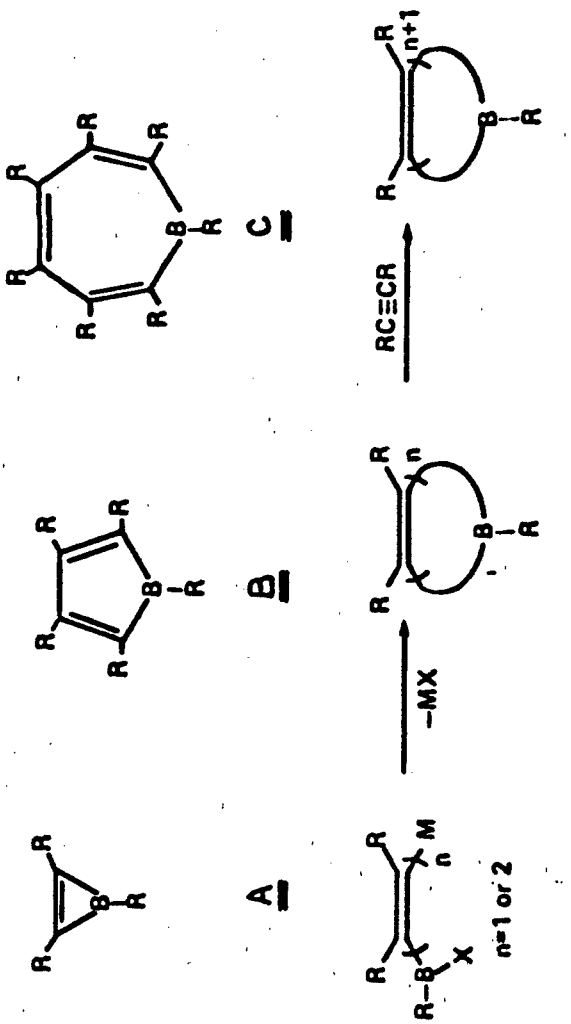

Figure 1: The Boracyclopolyenes and Their Preparative Interrelationship

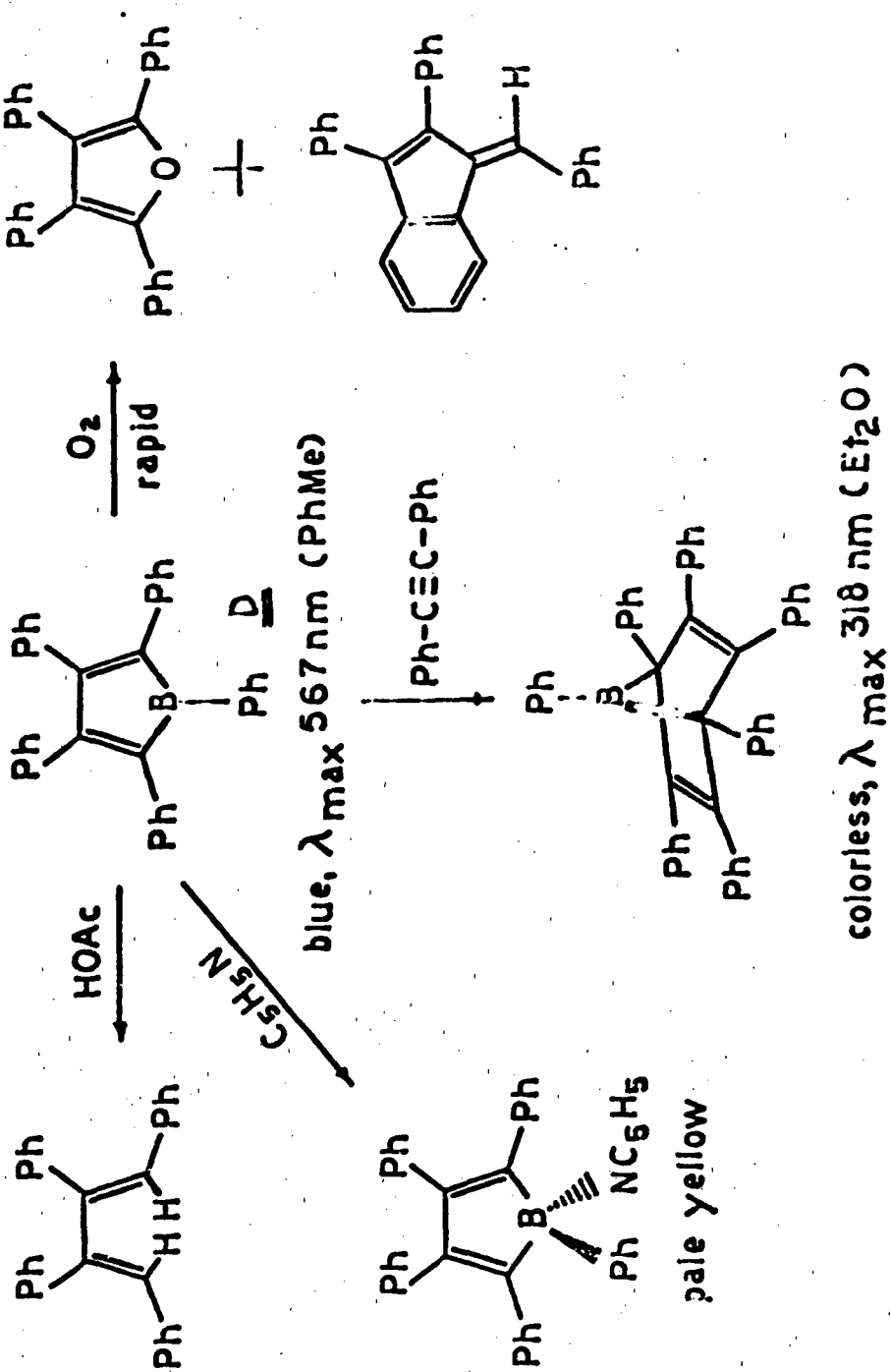

Figure 2: The Heightened Reactivity of Pentaphenylboracyclopentadiene in Oxidation, Protolysis, Diels-Alder Addition and Lewis-base Complexation

High Energy Molecules of High Symmetry

William S. Anderson
Chemical Systems Division
United Technologies Corporation
San Jose, CA 95150-0015

A series of symmetrical, fully hydroxyl-substituted organic materials is to be prepared and then converted to new, oxygen-rich, high-energy derivatives. The densities, crystal structures and heats of formation of these derivatives will be determined and observed values will be compared with predictions. The expected outcome is a better understanding of the relationship between chemical structure, density, oxidizing power and heat of formation in high-energy molecules.

Structures of the starting materials chosen are shown in the figure attached. We hope to be able to convert these per(hydroxy) carbons into amine nitrates or perchlorates, hydrazine nitrates or perchlorates, nitro ketals, oximes, nitro compounds or other oxygen-rich derivatives.

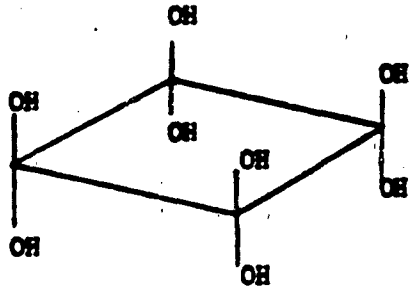

Octahydroxycyclobutane

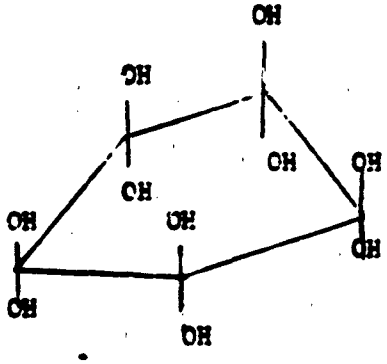

Leuconic acid

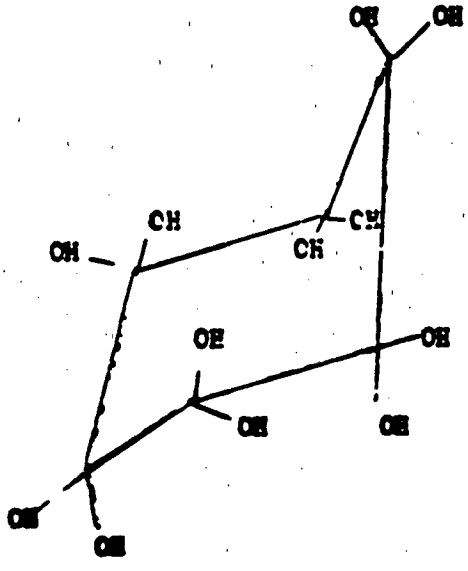

• $2H_2O$ Triquinoyl hydrate

Figure 1. Some cyclic per(hydroxy)carbone

Structure-Decomposition Relationships in Newer Energetic Materials

Thomas B. Brill and Yoshio Oyumi
Department of Chemistry
University of Delaware
Newark, DE 19716

Insufficient information exists to discuss the relationship between the molecular structure and the chemical reactivity of energetic materials. Toward remedying this deficiency, we are determining the molecular structures and decomposition mechanisms of a wide range of new "research-type" nitramines and other energetic materials prepared by our own synthesis program and from efforts at Rocketdyne, Morton-Thiokol, UT/CSD, SRI, and NSWC. The first of these studies has recently appeared.[1] X-Ray crystallography is being used for quantitative structure determination, FT-IR spectroscopy at high pressure and with high heating rates and thermal methods are employed for the decomposition studies, and solid-state NMR and NQR spectroscopy is used for analyzing the molecular motion as a function of temperature. The advantage of bringing many techniques to bear on the problem is that a multifaceted understanding of the thermal behavior of an energetic material can be achieved. The results should benefit synthetic chemists and propellant researchers by showing the effects on the physical properties and product formation resulting from specific molecular modifications. Also, a larger framework for understanding nitramine decomposition in relation to other energetic materials will result from this work.

The structure and thermolysis mechanism of pentaerythrityltetramine nitrate, $[C(CH_2NH_3)_4](NO_3)_4$, PTTN, has been completed (see accomplishment figure). HNO_3 appears to be the external oxidizing agent that attacks the otherwise stable cation. A study of the structure and molecular motion of 1,3,3,5-tetranitrohexahydropyrimidine (DNNC) and 1,3,3,5,7,7-hexanitro-1,5-diazacyclooctane, HNDZ, has been completed and shows the importance of torsional oscillations within the $C(NO_2)_2$ group. In situ thermolysis studies of HMX, RDX, several nitrosamines, HNDZ and DNNC have been completed as a function of external pressure (0.05-1000 psi) and heating rate (20-210 K sec^{-1}). The results from HMX and RDX reveal the presence of HONO as an initial product, that NO_2 is a major initial product whose concentration rapidly decreases owing to secondary reactions, that NO is a very minor initial product whose concentration rapidly increases in direct proportion to the loss of NO_2. The principal effect of pressure is to alter the rate of diffusion of the gases and, in this way, the secondary reaction rates. Comparisons of these results to those of nitrosamines and aliphatic nitro compounds have been made.

[1]T. B. Brill, R. J. Karpowicz, T. M. Haller, A. L. Rheingold, "A Structural and Fourier Transform Infrared Spectroscopy Characterization of the Thermal Decomposition of 1-(azidomethyl)-3,5,7-trinitro-1,3,5,7-tetrazacyclooctane," J. Phys. Chem. 1984, 88, 4138.

Approach: Structure and Decomposition Mechanisms of Energetic Materials

Structure Determination

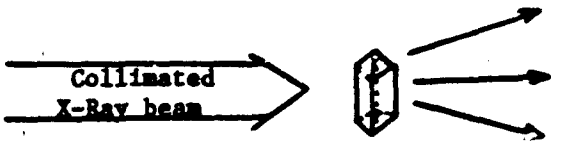

Analysis of diffraction pattern leads to the structure of the constituent molecules.

Crystal of energetic material

Thermolysis Studies of Energetic Molecule AB

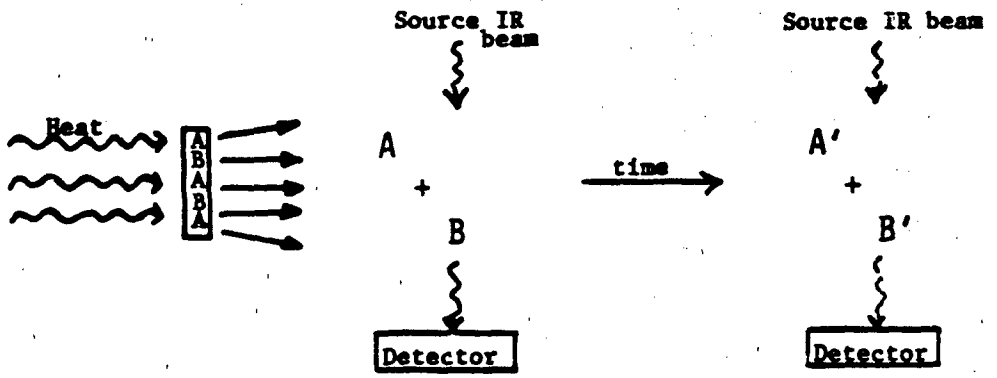

Solid phase sample of molecule AB heated at 200 K sec^{-1}.

Complete IR spectra for fragments A + B obtained immediately as they appear (<1 sec). Some initial transient species can be observed. Also the sequence of product formation is evident.

Spectra monitored for several seconds while A and B rearrange and react to produce A' and B'. Permits a description of the time-dependence of the gas phase products.

Objective: Correlate the structural details with the products of thermolysis to obtain the thermolysis mechanism.

An Accomplishment: The Thermolysis Mechanism of PTTN

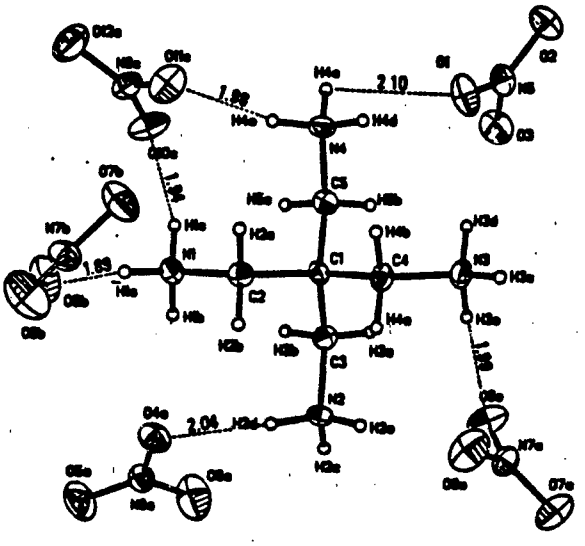

Molecular structure determinatio shows that strong N-H···O hydrogen bonding exists between the cation and the NO_3^- anion and is responsible for lattice cohesion. PTTN exhibits no phase transitions up to its decomposition point.

Decomposition Studies

Time-sequence infrared spectra show the following thermolysis mechanism of PTTN at a heating rate of 50 K sec^{-1}:

Initial Step (N-H bond rupture)

$$-NH_3^+(s) + NO_3^-(s) \longrightarrow -NH_{2(s)} + HNO_3 \text{ (adsorbed and desorbed)}$$
$$\text{(transient)}$$

Another Early Step

(a) Atmospheric pressure (C-N bond rupture)

$$-CH_2-NH_3^+(s) \xrightarrow{\Delta} -CH_2^+(s) + NH_{3(g)}$$

(b) >200 psig (C-N bond retention)

$$-CH_2-NH_3^+(s) \xrightarrow{\Delta} HCN_{(g)} + HNCO_{(g)}$$

Later Reactions (>3 sec)

$$HNO_3 \text{ oxidation of residue} \longrightarrow CO_{2(g)} + H_2O_{(g)} + NO_{x(g)}$$

Conclusion: PTTN decomposes by the production of HNO_3 which then acts as a reactant attacking the otherwise stable cation of PTTN. The oxidation of the cation occurs from the exterior inward.

Deuterium Isotope Effects in RDX Decomposition and Combustion Processes

Scott A Shackelford, Stephen L. Rodgers, Michael B. Coolidge
AF Rocket Propulsion Laboratory (AFSC)
Edwards AFB CA 93523

Robert E. Askins
Morton Thiokol, Inc./Huntsville Division
Huntsville AL 35807

The mechanisms of the decomposition and combustion processes of nitramines have been the subject of numerous research efforts because of their application as oxidizers in propellants and explosives. The understanding of these mechanisms and in particular the overall rate determining step, would aid in attempts to tailor the burn rates of nitramine propellants. In an attempt to elucidate this slowest step, the deuterium isotope effect has been used in the investigation of the mechanisms of thermal decomposition and combustion of RDX.

The deuterium isotope effect is increasingly being used in the investigation of energetic materials because it provides a way to sort out the overall rate determining step from amongst the many parallel chemical and physical processes occurring during a decomposition or combustion event. Since the isotope effect is only seen when the rate determining step of the mechanism involves the isotopically labeled substituent it provides an unique method of determining what part of the molecule is involved in the reactions controlling the rate of the overall decomposition or combustion process. The investigation of HMX thermal decomposition and combustion processes using the deuterium isotope effect has been reported earlier. This report concerns the continuation of that work with RDX.

The thermal decomposition of RDX was examined using isothermal differential scanning calorimetery at a temperature range of 505K-510K. At this temperature range RDX obeys first order kinetics and shows a primary deuterium isotope effect (2.1 at 505K and 1.7 at 510K). This isotope effect would suggest that the rate limiting step in the decomposition of RDX is C-H bond rupture. Under the experimental conditions employed, the thermal decomposition occurs solely in the liquid phase with RDX. By the time the DSC has equilibrated, the decomposition has already started and the DSC trace is seen as a slow decay. No induction phase can be seen with RDX.

The combustion experiments were performed in a window bomb with the burn rates measured by high speed photography. If the assumption is made that the burn rate data is directly proportional to the kinetic rate constants and that all the other factors influencing burn rate remain the same for both the deuterated and hydrogenated materials then an isotope effect can be derived from a ratio of the RDX burn rate to RDX-d6 burn rate. The isotope effects thus obtained are 1.46 at 1000 psi and 1.37 at 500 psi. At the high temperature limit an isotope effect of 1.35 or greater can be considered to be a primary effect. So it may be seen that the isotope effect observed in the RDX combustion is a primary isotope effect which would mean that the overall rate controlling step of RDX combustion involves the rupture of the carbon-hydrogen bond.

The deuterium isotope effect has been used to examine both the slow decomposition and fast combustion processes of RDX. In both cases it has been seen that a primary deuterium isotope effect has been observed indicating that carbon-hydrogen bond rupture is the overall rate controlling step in each process.

APPROACH

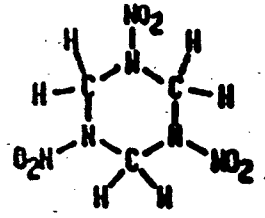

RDX

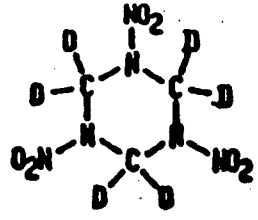

RDX-d_6

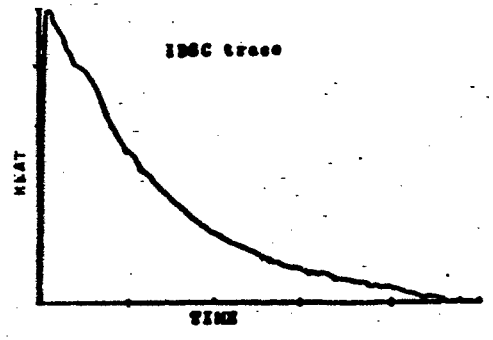

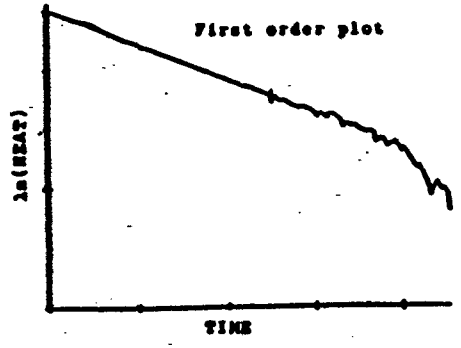

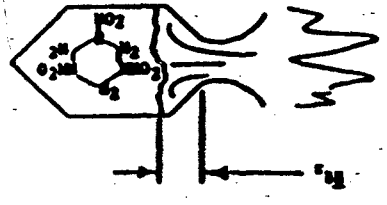

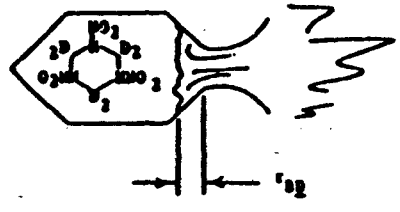

DEUTERIUM ISOTOPE EFFECT

*Results only from isotop substitution

DECOMPOSITION

*DIE derived from rate co:

k_H/k_D

COMBUSTION

*DIE derived from burning rates

r_{BH}/r_{BD}

RESULTS

■ THERMAL DECOMPOSITION

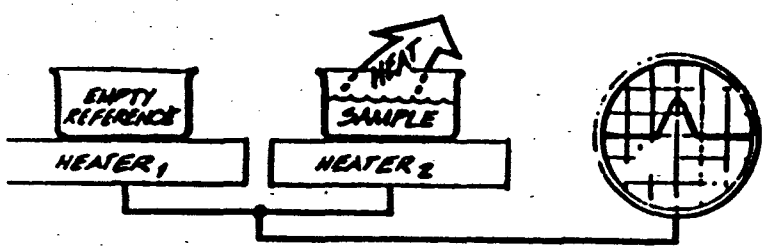

	505K	510K	
ISOTOPE EFFECT	2.1	1.7	(+/-.2)

- PRIMARY ISOTOPE EFFECT OBSERVED
- RATE OF DECOMPOSITION CONTROLLED BY C-H BOND RUPTURE

■ COMBUSTION

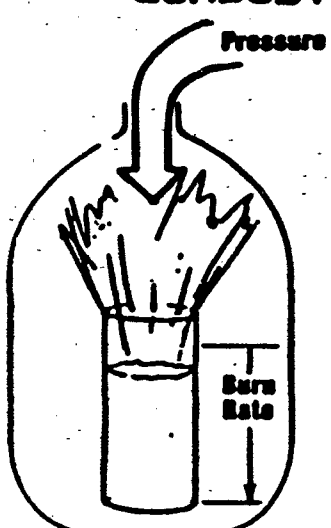

	500 PSIG	1000 PSIG	
ISOTOPE EFFECT	1.4	1.5	(+/-.2)

- PRIMARY ISOTOPE EFFECT OBSERVED
- RATE OF COMBUSTION CONTROLLED BY C-H BOND RUPTURE

■BOTH RESULTS CONSISTENT WITH HMX RESULTS

FLAME MECHANISMS AND FLAME INHIBITION

J.D. EVERSOLE
UNIVERSITY OF DAYTON RESEARCH INSTITUTE, AFRPL
D.P. WEAVER
AIR FORCE ROCKET PROPULSION LABORATORY
EDWARDS AFB, CALIFORNIA 93523

This project is concerned with the definition and understanding of detailed chemical mechanisms in flames. Of special interest are gas-phase mechanisms responsible for, or contributing to, the suppression of afterburning in rocket plumes. An effort has been made to approach the problem of determining flame chemistry with a balance between experimental data collection and theoretical flame modelling. The over-all concept has been kept simple to gain as much specificity in the results as possible. Data from a laminar, premixed flat-flame burner is modelled using a detailed reaction, one-dimensional laminar flame computer program. Experimental data is obtained primarily by non-intrusive, optical diagnostic techniques. Most of the uniqueness of this approach lies in the integration of many separate aspects of the general problem.

A versatile burner facility has been constructed which incorporates motorized, three-dimensional burner positioning and sub-atmospheric flame operation. The burner chamber is connected to a large capacity vacuum pump external to the laboratory via a 10 cm diam. stainless steel line and a flexible welded bellows which allows the chamber up to 16 cm of vertical travel. The burner can be easily dissembled for modification of the burner surface or diameter. Hydrogen/oxygen, methane/oxygen, and methane/nitrous oxide flames have been run with different amounts of dilution with nitrogen. Optical diagnostics for the flame primarily consists of laser induced fluorescence (LIF) for OH species concentrations, and vibrational Raman scattering which provides temperature and some major species concentration data. An effort has been made to obtain these two types of data simultaneously with the same UV laser pump beam.

Axial profiles of temperature and concentrations through the flame zone are then compared to theoretical calculations generated by computer for the same initial conditions. For the flame inhibition work, the "unknown" is the chemical mechanism for the suppressant species. Different hypothetical reaction schemes can be either eliminated or distinguished by comparison of the computed profiles to the experimental data over a wide range of initial conditions. Most of the effort so far has been connected with hydrogen bromide inhibitor in H2/O2 flames. Of primary interest is the use of potassium as an inhibitor, and efforts have been made to construct a burner arrangement to introduce the potassium directly as an atomic vapor.

FIGURE 1. The experimental arrangement of the flat flame burner with the suppressant injector and laser diagnostics is schematically illustrated. Spatial maps (primarily z-axis) of temperature and species concentration are obtained from optical diagnostic data (Raman scattering, LIF, and atomic absorption) by translating the burner. Representative spectra (N_2 vibrational Raman) taken at different axial locations in the flame are illustrated at the top of the figure. Reduced data (in this case temperature) will then be compared to calculated flame profiles using a detailed chemistry, one-dimensional flame model (solid line of graph).

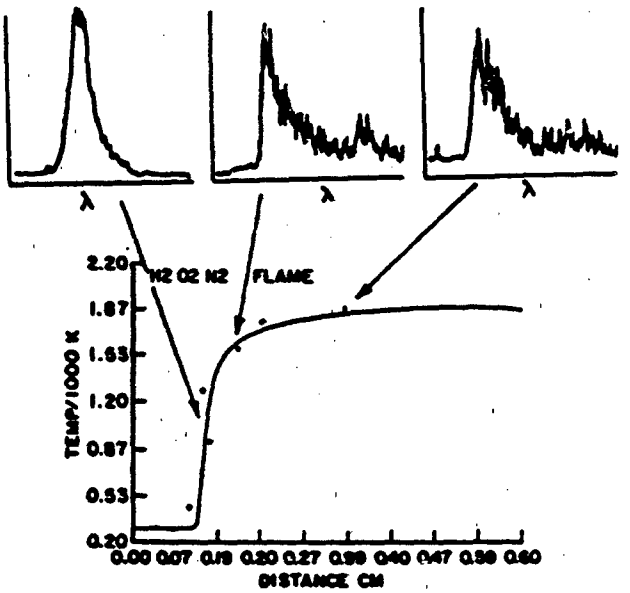

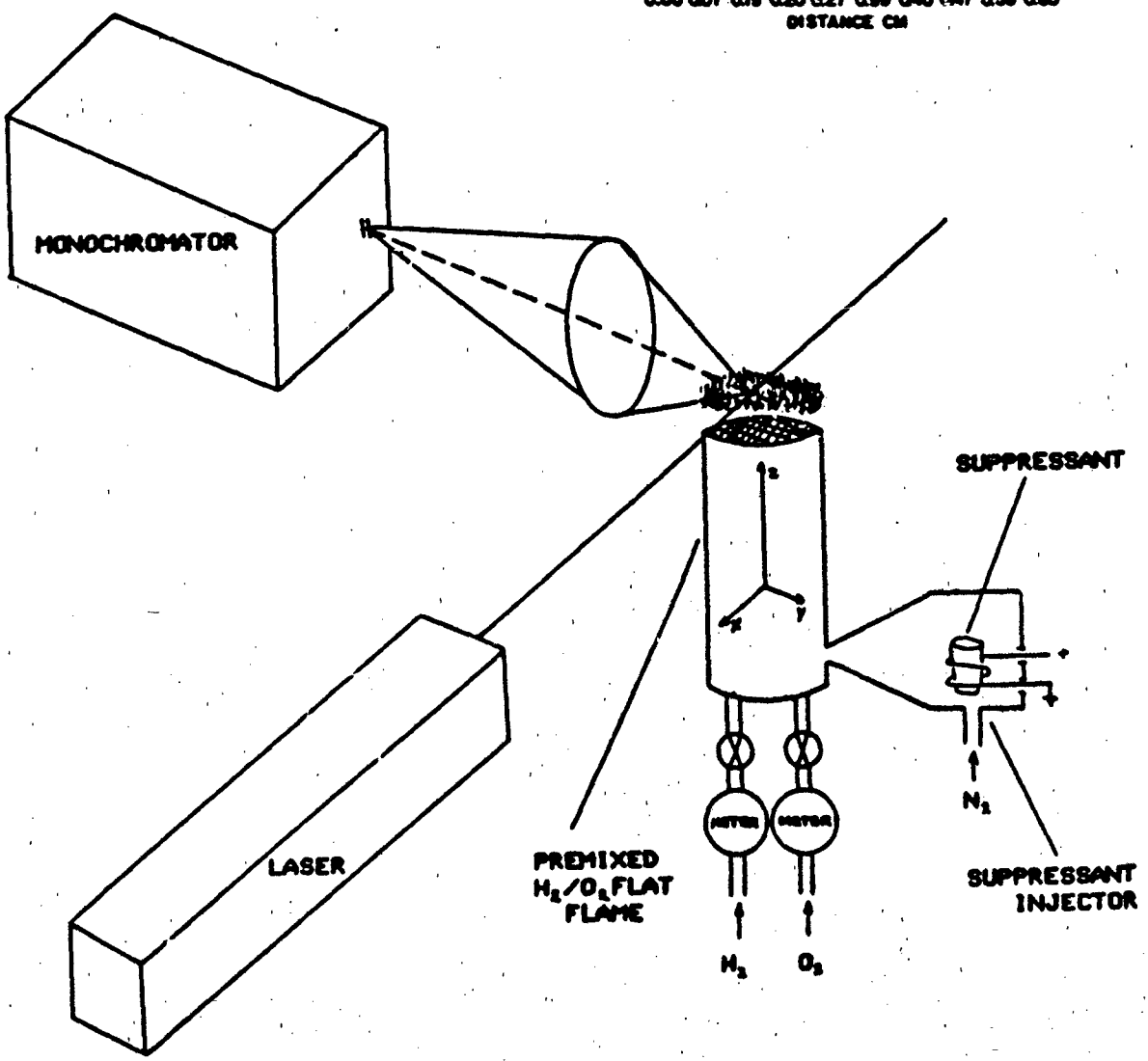

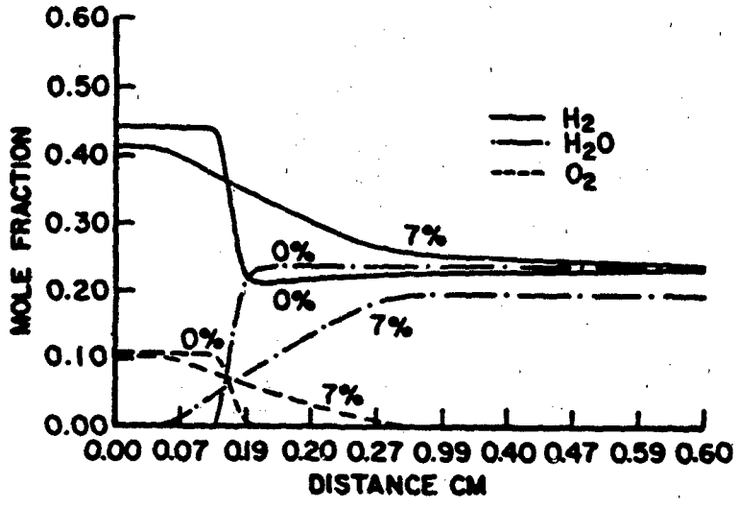

POSSIBLE REACTIONS

1. $K + O_2 + M \leftrightarrow KO_2 + M$
2. $KO_2 + OH \leftrightarrow KOH + O_2$
3. $KOH + OH \leftrightarrow H_2O + KO$
4. $K + OH + M \leftrightarrow KOH + M$
5. $K + H_2O \leftrightarrow KOH + H$
6. $KO_2 + H \leftrightarrow KO + OH$
7. $K + OH \leftrightarrow KO + H$

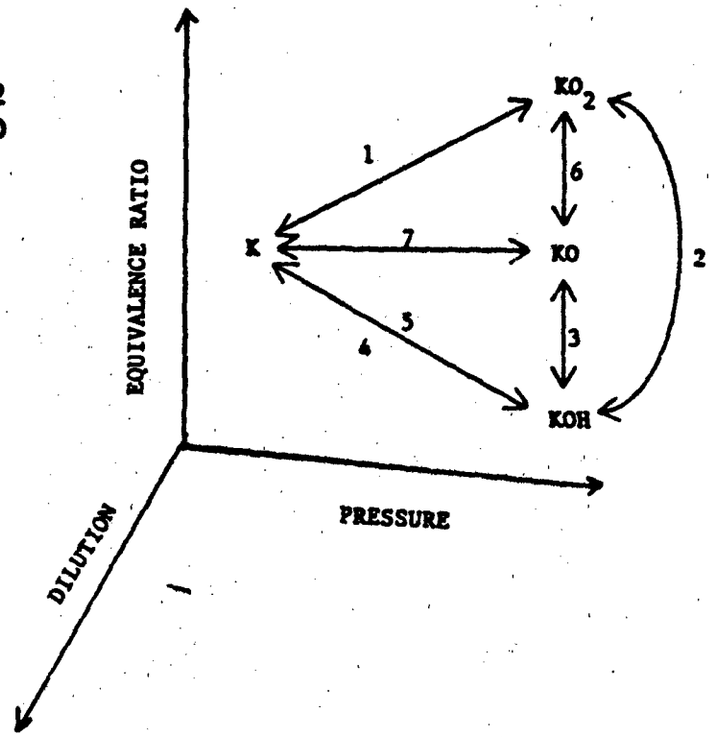

FIGURE 2. Flame inhibition (suppression) is indicated by the reduction of the laminar flame speed, and by the expansion of the flame zone as shown in the top graph of flame species concentration profiles calculated with and without the addition of 7% potassium. The detailed comparison of such profiles as a function of equivalence ratio, total pressure, and dilution (temperature) can reveal which reaction pathways become dominant under different conditions thereby defining the chemical mechanisms.

THE SUPPRESSION OF AFTERBURNING IN SOLID ROCKET PLUMES BY POTASSIUM SALTS

EUGENE MILLER
MACKAY SCHOOL OF MINES, CHEM & MET ENG'G DEPT.
UNIVERSITY OF NEVADA, RENO, NV 89557

The Services have increasingly emphasized the development and use of low signature tactical solid rocket motors. Visible primary and secondary smoke have been largely eliminated by the removal of ammonium perchlorate oxidizer and most of the aluminum powder and ballistic modifiers from the propellant formulation - the so called min-smoke propellants. The exhaust gases from min-smoke propellants however contain significant concentrations of hydrogen and carbon monoxide which when mixed with ambient air afterburn to water and carbon dioxide producing visible flash and increased infrared radiation. This research is directed towrd preventing or at least inhibiting the signatures due to afterburning.

Potassium salts inhibit the reactions of hydrogen and carbon monoxide. KNO_3 and K_2SO_4 have been added to propellant charges at a level of 1 - 3 wt pct to suppress gun muzzle flash and rocket plume afterburning. The mechanism by which the potassium salts inhibit is controversial, but it probably involves K, KOH and possibly KO_2 breaking the chain reactions involving H and OH radicals in the combustion of H_2 and CO.

The effects of K, KOH and KO_2 on the afterburning reactions are being studied by introducing them individually into an opposed jet flat diffusion flame of H_2-CO-O_2-N_2 and scanning the flame in small increments by infrared spectroscopy. A vaporizer-burner has been built permitting the vaporization of potassium and its salts prior to entering the the flame. The emission spectra from the flame is detected by means of a modified absorption spectrophotometer and an optical scanning system. It has been found that elemental potassium reduces the infrared radiation for rich and lean hydrogen flames but has a smaller effect on stoichiometric mixtures. KOH in a hydrogen flame inhibits the preflame reactions but actually increases the infrared radiation at levels below that required to prevent combustion totally. K therefore appears to be a more effective inhibitor than KOH as used in these experiments settling perhaps the disagreement that has arisen in the literature concerning the efficacy of inhibition by potassium in hydrogen flames. CO was not used in these experiments because reaction between H_2 and CO produced carbon in the salt vaporizer. The formation of carbon probably also occurs in the rocket plume increasing the infrared signature.

MIN-SMOKE SOLID ROCKET PLUME AFTERBURNING:

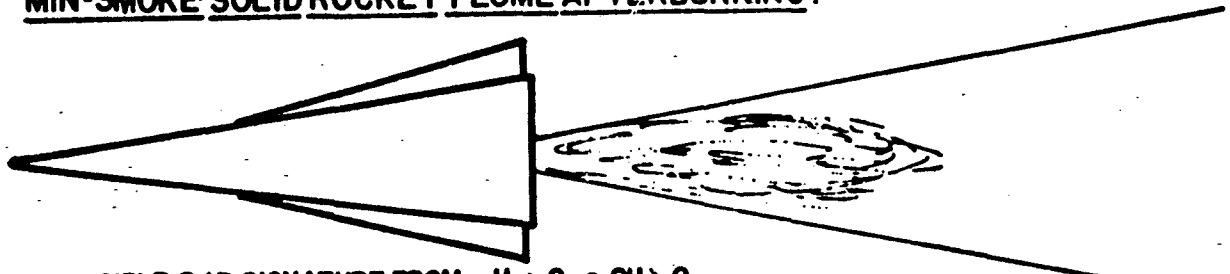

VISIBLE & IR SIGNATURE FROM

$$H + O_2 = OH + O$$
$$H + OH + M = H_2O + M^*$$
$$CO + OH = CO_2 + H$$
$$\overline{H_2 + CO + O_2 = CO_2 + H_2O}$$

SUPPRESS w/ KNO_3 or K_2SO_4 ADDITIVES

?
$$K + OH + M = KOH + M^*$$
$$KOH + H = H_2O + K$$

or

?
$$KNO_3 = K_2O + NO_2$$
$$K_2O + H_2O = 2KOH$$
$$KOH + OH \text{ or } = H_2O$$

?
$$K + O_2 + M = KO_2 + M^*$$
$$KO_2 + OH = KOH + O_2$$
$$KOH + OH = H_2O + KO$$

GOALS

- ESTABLISH MECHANISM & CONDITIONS REQ'D FOR SUPPRESSION
- DEFINE AS FUNCTION OF SPECIES, CONCENTRATION, F/O & T

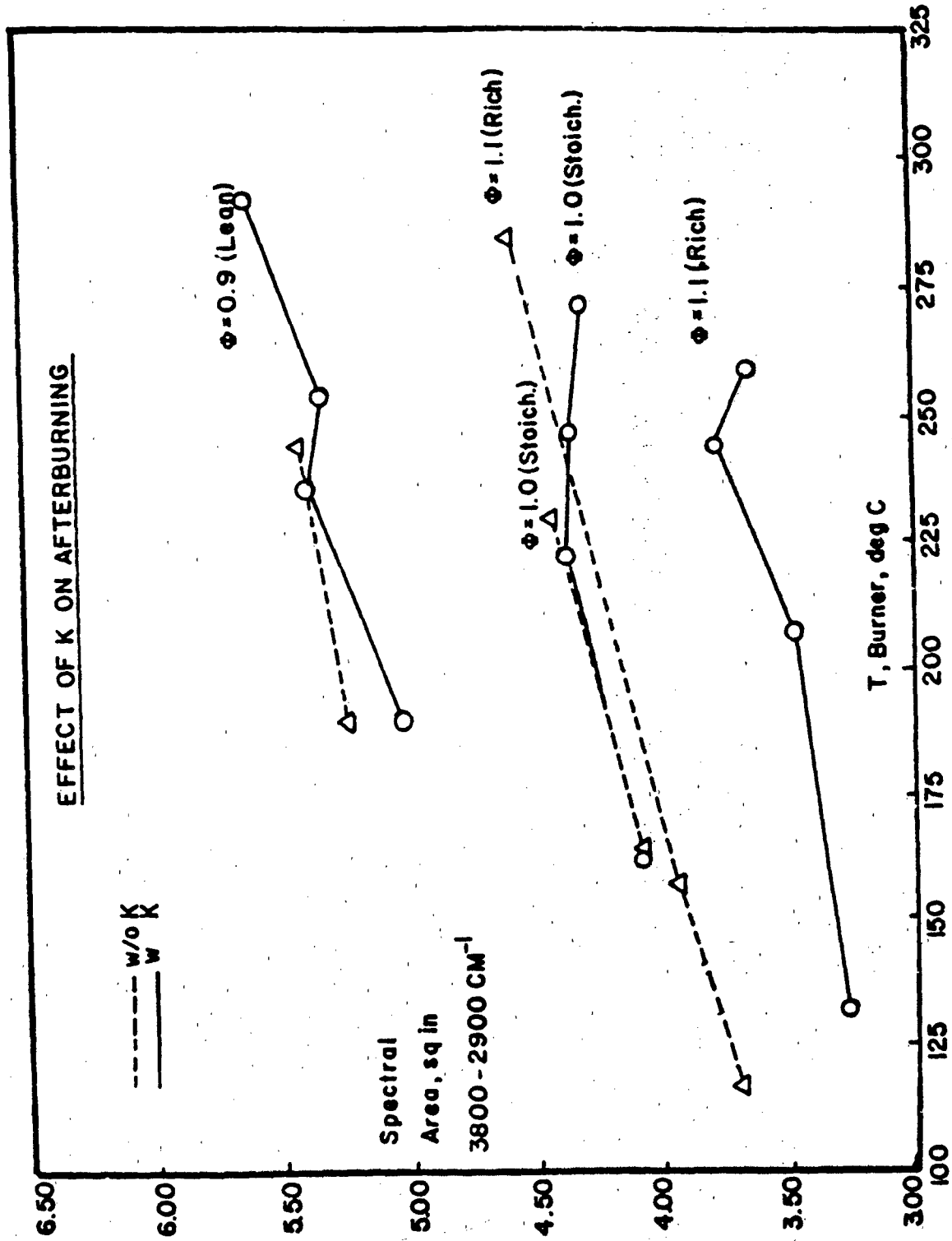
EFFECT OF K ON AFTERBURNING
w/o K
w K
Spectral
Area, sq in
3800-2900 CM⁻¹
T, Burner, deg C
Φ=0.9 (Lean)
Φ=1.0 (Stoich.)
Φ=1.1 (Rich)
Φ=1.0 (Stoich.)
Φ=1.1 (Rich)
6.50
6.00
5.50
5.00
4.50
4.00
3.50
3.00
100
125
150
175
200
225
250
275
300
325

CHEMICAL KINETICS OF NITRAMINE PROPELLANT COMBUSTION

Melvyn C. Branch
Mechanical Engineering Department
University of Colorado
Boulder, CO 80309

The objective of the studies reported here is to provide insight into the chemistry of reactions of gas phase species of importance in the combustion of nitramine propellants. Flame studies and associated chemical kinetic modeling of the gas reactions are being used to evaluate critical reaction paths and energetics and their influence on burn rate. The calculations thus far have identified a mechanism for the rapid reaction between CH_2O and NO_2 in the "fizz" zone at the propellant surface. A slower reaction was suggested for the "preparation" and "flame" zones standing off the surface which was supported by the exothermic reduction of NO. Both of these results provide a chemical kinetic mechanism to explain previous qualitative suggestions about the nature of the gas reactions of nitramines. The calculations also indicate that gas reactions may affect the reported product distributions in studies of nitramines. Finally, a mechanism for the modification of the reaction rate by NH_3 donors was outlined.

There are currently very limited experimental data available for detailed comparison to the results of the chemical kinetic modeling. We have begun low pressure flame studies of $CH_2O/NO_2/N_2O$ mixtures in order to identify reactant, intermediate and product species profiles for comparison to a kinetic model of the flame. Addition of NH_3 to the flame gases will also indicate the feasibility of burn rate control by NH_2 donors. The flame species composition measurements are by probe sampling and gas chromatography for stable species and by laser absorption and laser induced fluorescence for unstable species.

Recent evidence also suggests that the reaction between HCN and NO_2 may be of major importance in nitramine combustion. As a step in evaluation of this process, we have investigated the kinetic mechanism for conversion of HCN to NO and N_2 in low pressure H_2/O_2 flames doped with HCN. The experimental results showed good agreement to complete flame structure calculations based on a reaction mechanism developed almost solely from direct measurements of rate coefficients reported in the literature.

Research supported by the Air Force Office of Scientific Research under Grant AFOSR-84-0006.

SIGNIFICANT GAS PHASE REACTIONS

INITIATION

$$N_2O + M \longrightarrow N_2 + O + M$$

$$CH_2O + O \longrightarrow HCO + OH$$

PROPAGATION

$$HCO + M \longrightarrow CO + H + M$$

$$CH_2O + H \longrightarrow HCO + H_2 + 27 \text{ Kcal/mole}$$

$$N_2O + H \longrightarrow N_2 + OH$$

$$NO_2 + H \longrightarrow NO + OH + 28 \text{ Kcal/mole}$$

SECOND STAGE

$$CO + OH \longrightarrow CO_2 + H + 26 \text{ Kcal/mole}$$

$$NO + H \longrightarrow N + OH$$

$$NO + N \longrightarrow N_2 + O$$

$$H_2 + OH \longrightarrow H_2O + H + 16 \text{ Kcal/mole}$$

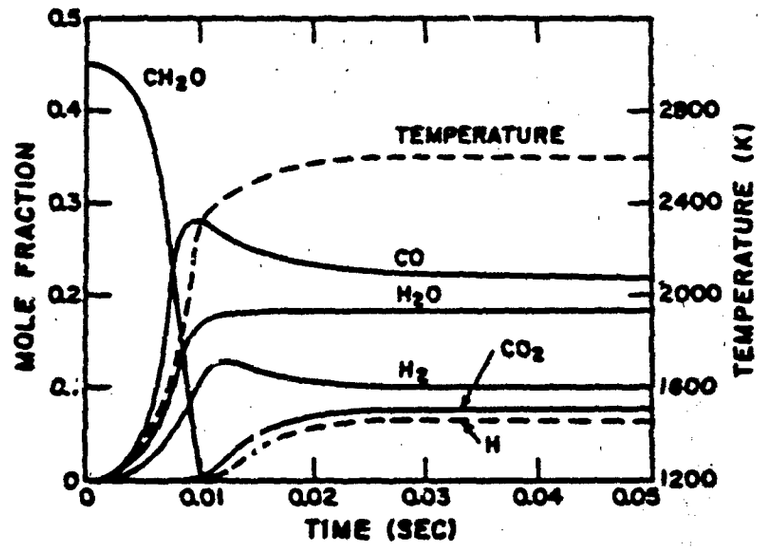

(a)

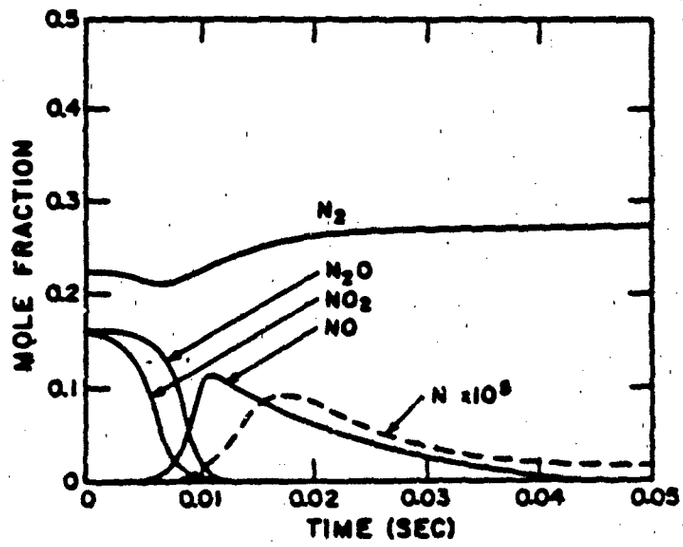

(b)

Figure 2. Calculated reaction profiles of the decomposition products of EDX at 40 atm. The initial mixture is $XCH_2O + NO_2 + H_2O + 3/2\ N_2$. A rapid first stage reaction is shown which ends at 0.01 sec followed by a second stage reaction. Carbon and hydrogen species are given in (a) and nitrogen species in (b).

Combustion of Hydrogen and Hydrocarbons in Fluorine

Myron Kaufman
Chemistry Department, Emory University
Atlanta, GA 30322

Because of the extreme exothermicity of many fluorine reactions, fluorine and fluorine-containing molecules have often been proposed and occasionally employed as oxidizers in high-performance developmental propulsion systems. Mechanistically, however, fluorine-supported combustion is not as well understood as oxygen-supported combustion. In fact, due to hard-to-remove O_2 impurity in commercial F_2, it is often difficult to even identify unique aspects of fluorine combustion. Some phenomena observed in both oxygen and fluorine combustion are listed in Figure 1, along with their generally accepted mechanisms in O_2 flames and some conjectures as to their possible mechanism in F_2 flames. In the current work, ionization and luminescence in the combustion of H_2 and hydrocarbons with F_2 will be investigated, and special precautions will be taken to study these phenomena in the absence of O_2 impurity. In addition, rate constants and branching ratios of several reactions key to understanding fluorine combustion will be measured. These include $F + HO_2$, important for understanding O_2-retardation of fluorine combustion and $F + CF_2H$, a prototype for assessing the prominence of atom displacement reactions in F_2-hydrocarbon combustion. Both optical and mass spectrometry will be employed in these kinetics studies. Our mass spectrometer is a unique instrument, employing an inhomogeneous magnetic field to direct only paramagnetic components of the sampled molecular beam into the ionizer, thus allowing atoms and free radicals to be monitored with little interference from stable molecules.

In this program we will study both atomic and molecular flames. Low-pressure premixed F_2 flames are studied in a stainless-steel burner assembly equipped with CaF_2 windows to spectroscopically monitor luminescence and movable Langmuir probes to measure the spacial variation of ionization. For most of our studies, the premixed flames will be diluted with He or Ar. However, when undiluted flames are burned in this apparatus, we have observed the interesting behavior illustrated in Figure 2 for the F_2-CH_4 flame. Over a range of relative concentrations, including stoichiometric mixtures, this flame burns as short pulses of duration ca. 1 msec and frequencies of 1 to 10 Hz. This behavior is explained as due to flashback resulting from the high burning velocity of these flames, followed by spontaneous reignition when the hypergolic mixture is replenished to its ignition limit.

O_2 Combustion	Phenomena	F_2 Combustion
$CH + O \rightarrow CHO^+ + e$	ionization	$CH^* + CH \rightarrow C_2H_2^+ + e$
$C_2 + OH \rightarrow CO + CH^*$	CH emission	$CH_3 + F_2 \rightarrow CH^* + 2HF$
uncertain	C_2 emission	$C + CH \rightarrow C_2^* + H$
complicated	soot formation	$CH_4 \xrightarrow{F} CH_3 \xrightarrow{F} CH_2 \xrightarrow{F} CH \xrightarrow{F} C$
$H + O_2 + m \rightarrow HO_2 + m$	O_2 quenching	$H + O_2 + m \rightarrow HO_2 + m$
$H + HO_2 \rightarrow H_2 + O_2$		$F + HO_2 \rightarrow HF + O_2$

Figure 1. Speculations on the Mechanism of Flame Phenomena

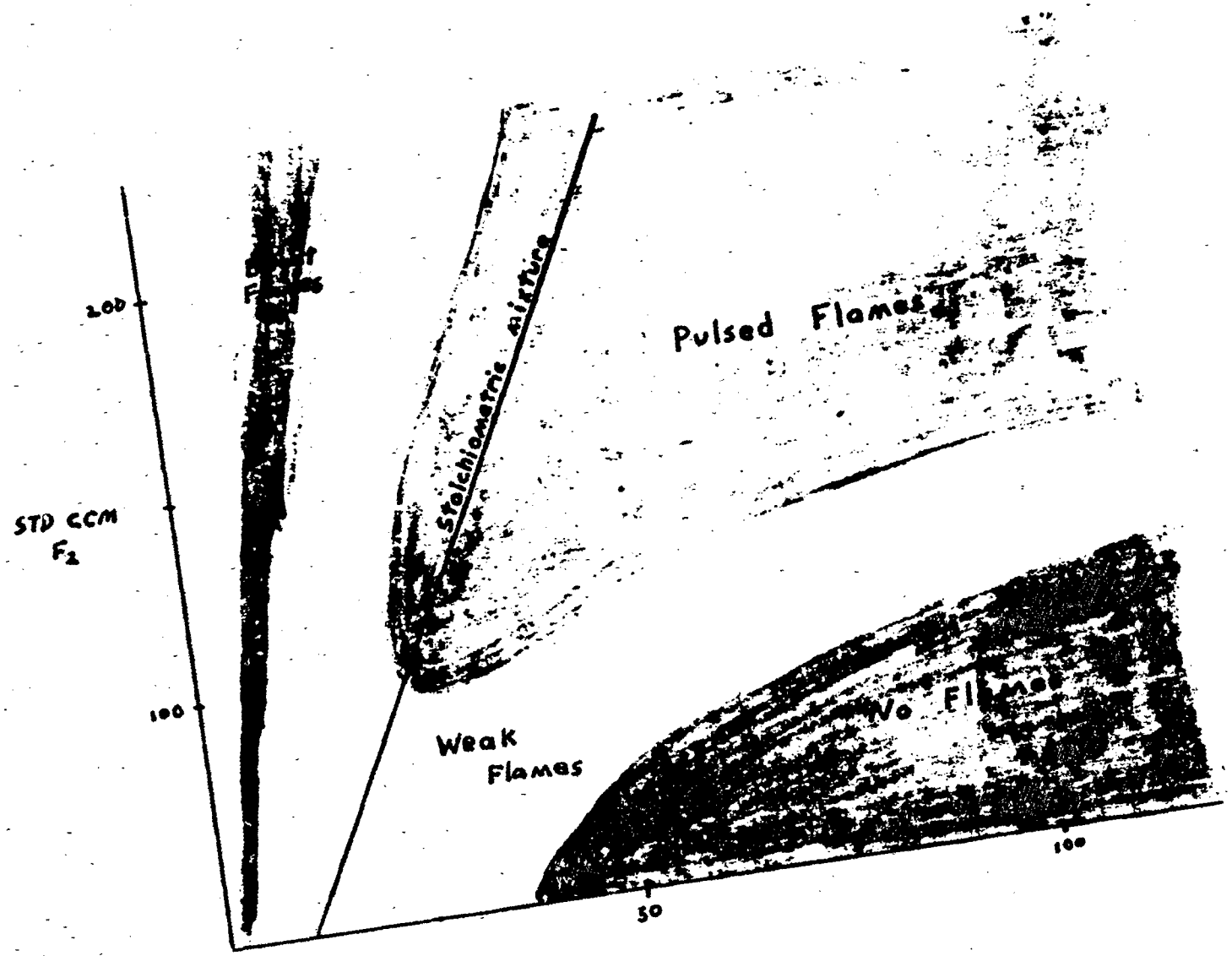

Figure 2. Steady and Pulsed CH_4 - F_2 Flames

ANALYSIS OF HETEROGENEOUS DIFFUSION FLAME STABILIZATION

Warren C. Strahle and Jechiel I. Jagoda

Georgia Institute of Technology/School of Aerospace Engineering
Atlanta, Georgia 30322

The ability to calculate complex turbulent reacting flows is in a state of development. The flow investigated here presents a unique challenge to the state-of-the-art. The flow is a fully turbulent two dimensional flow over a backward facing step with wall-blowing of a combustible from the floor behind the step. It is a model for the flowfield in the flame stabilization region of a solid fueled ramjet. The analytical approach has been with a k-ε method gradually being improved and modified as one progresses through various stages of complexity - from no-blowing cold flow to foreign gas injection in cold flow and then to the full combustion case. A parallel experimental program either validates the analysis or suggests modifications.

Figure 1 shows some typical technical issues on the overall program and includes some of the analytical issues. Excellent agreement (with one modification of standard analysis) has been found between the theory and experiment for the cold-flow, non bleed case. Current concern conceptually, however, with standard methods of applying boundary conditions are leading to further modifications.

Figure 2 shows calculated streamline plots and CO_2 mass fraction profiles for the case of cold CO_2 bleed. A secondary recirculation zone has been predicted and also found experimentally. The concern is, insofar as flame stabilization is concerned, the severe dimunition of massive recirculation as blowing increases. This is also revealed in the CO_2 profiles where a flat recirculation dominant profile gives way to a diffusion dominated profile as blowing increases. Detailed checks on velocity data show good agreement with the analysis. Comparison with mass fraction data await further experimentation.

Figure 1. Typical technical issues.

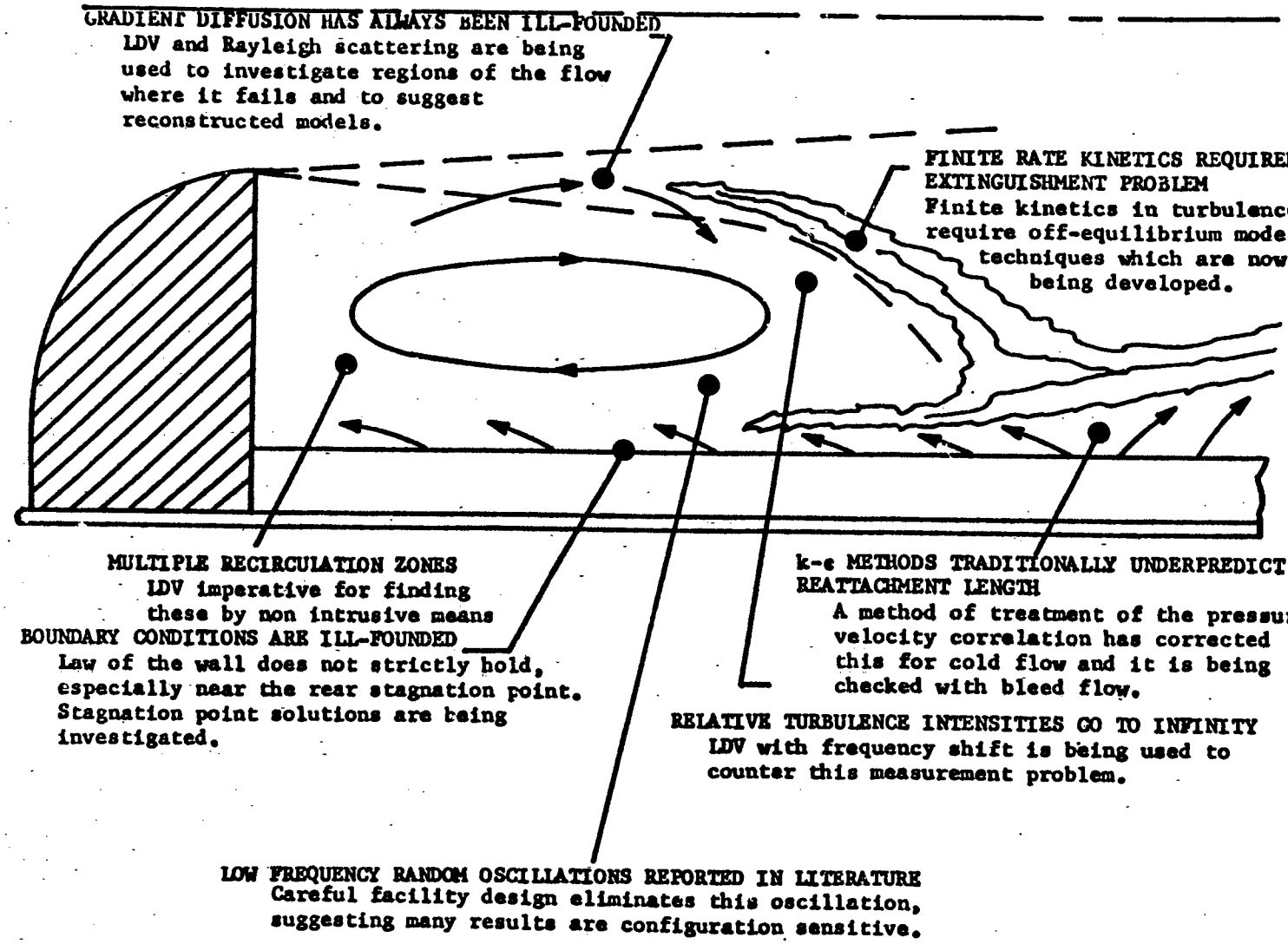

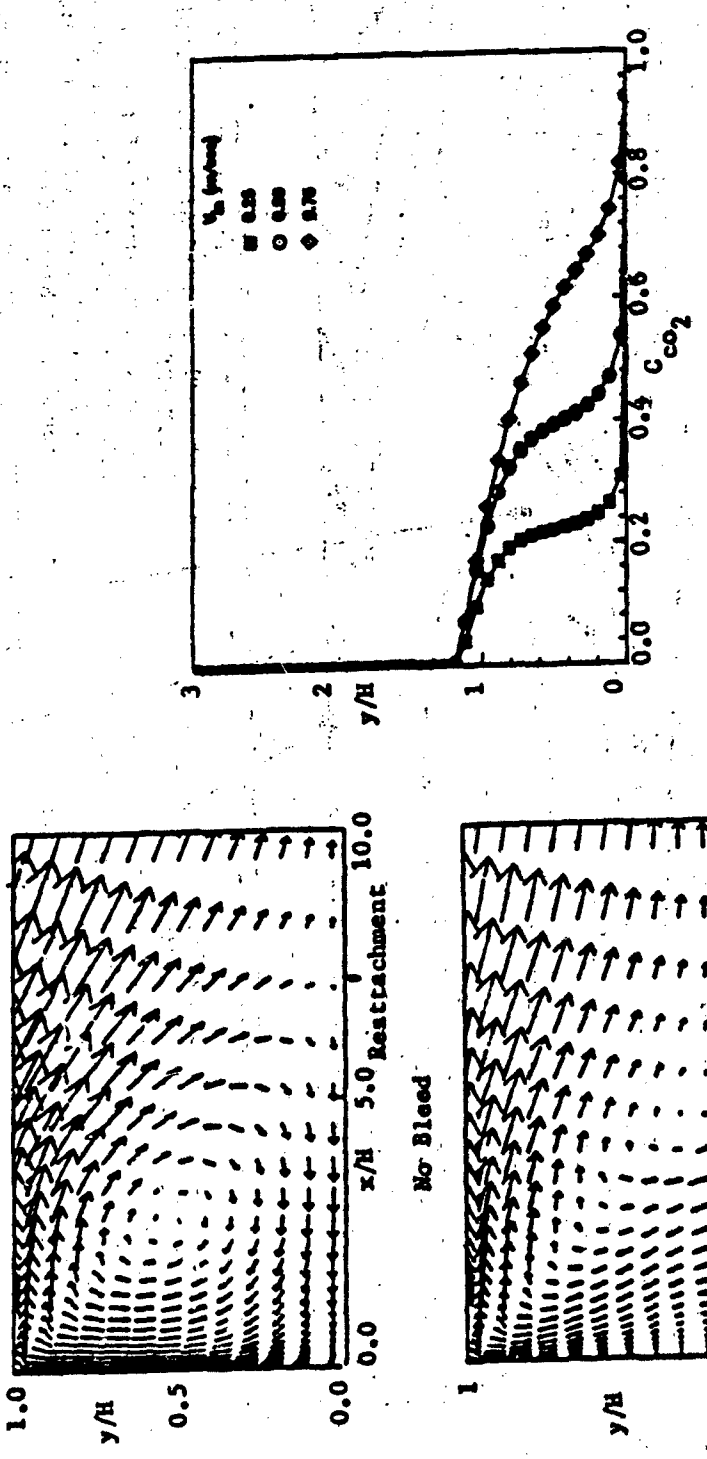

Figure 2. The effect on streamlines and injectant concentration of blowing at the wall.

EXPERIMENTAL INVESTIGATION OF HETEROGENEOUS FLAME STABILIZATION

Jechiel I. Jagoda and Warren C. Strahle

School of Aerospace Engineering
Georgia Institute of Technology
Atlanta, GA 30332

Solid fueled ramjets (SFRJ), as other ramjet types, require flame anchoring at the head of the combustion region. This is frequently provided by a recirculation zone behind a backward facing step as shown in Fig. 1. Flame stabilization can only be achieved in regions of relatively low flow velocities (such that the flow velocity does not exceed the burning velocity) and high turbulence and thus high Reynolds stresses resulting in mixing of the main and bleed flow (such that the local fuel air mixtures lie within the limits of flammability). In this project the SFRJ is simulated by a flow over a backward facing step with a secondary flow entering the recirculation region through a porous floor. The flow properties are determined using a 2-component LDV system. Bleed gas concentrations are measured, simultaneously, using Rayleigh scattering for the cold flow and spontaneous Raman for concentration and temperature measurements in flows with combustion. Although simultaneous LDV-Rayleigh or Raman measurements are currently being carried out for the simpler configuration of jet like flames, this is the first time the combined techniques are applied to the more complex and practical problems of flame stabilization behind a backward facing step.

The experimental efforts are divided into three steps:

(1) LDV measurements in the main flow over the step without bleed,

(2) LDV and concentration measurements for cold main plus bleed flows and

(3) LDV, concentration and temperature measurements in flows with combustion.

To date velocity measurements have been completed in cold flows with no bleed and two bleed gas velocities. Rayleigh measurements in the cold flow are underway.

The experimental results indicate that the bleed flow has a limited effect on the flow profiles except very close to the step where a secondary recirculation zone appears with blowing (Fig. 2). In the recirculation zone, the locations of maximum normal stresses in both the u and v directions are moved slightly away from the porous wall by the bleed flow, as are those of maximum shear stress. In regions of lower shear stress blowing has the effect of slightly increasing the measured shear stresses. The length of the recirculation zone, however, is only slightly shortened by the bleed flow, if at all. All measurements agree reasonably well with the analytical results reported separately.

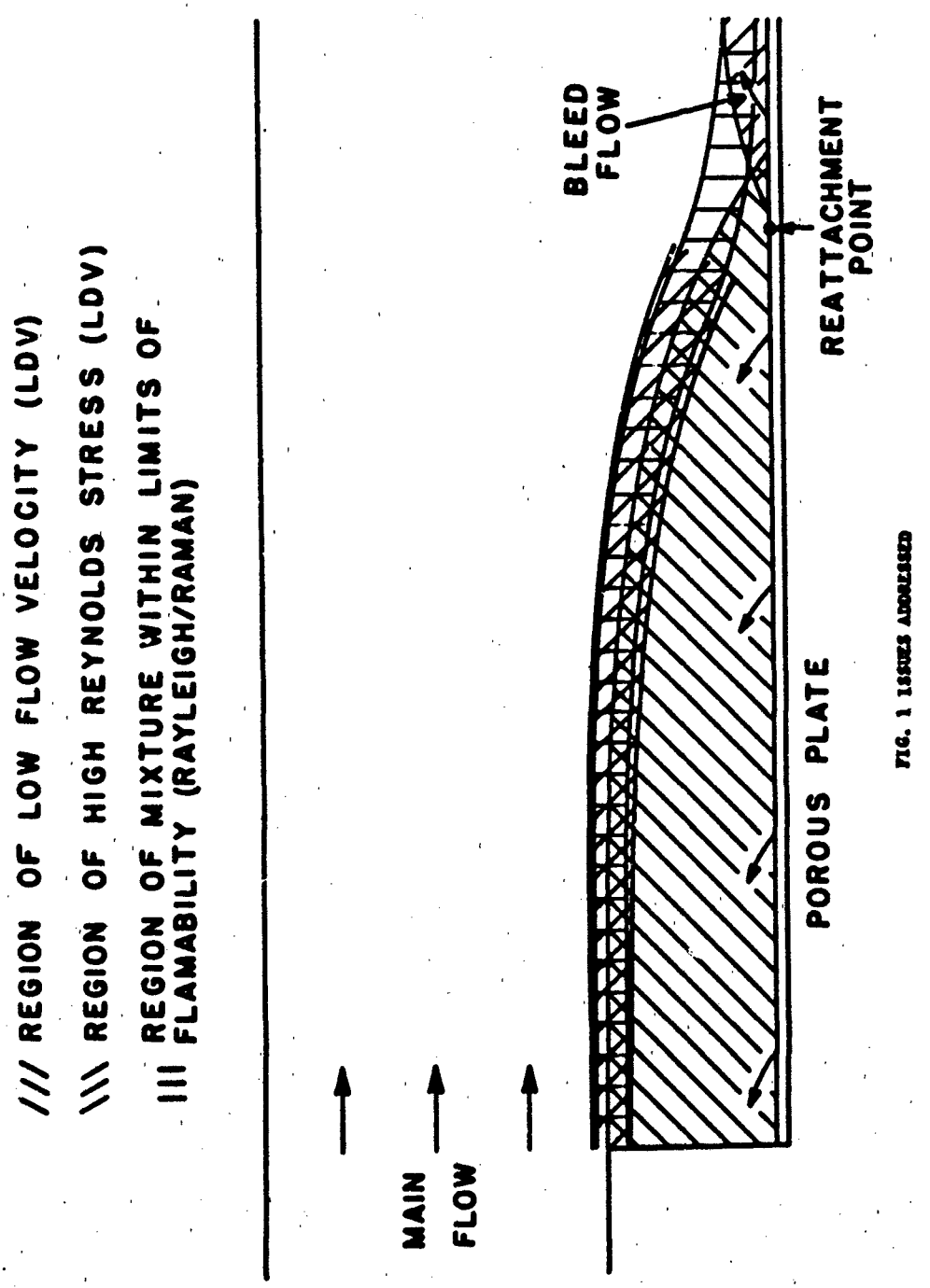

FIG. 1 ISSUES ADDRESSED

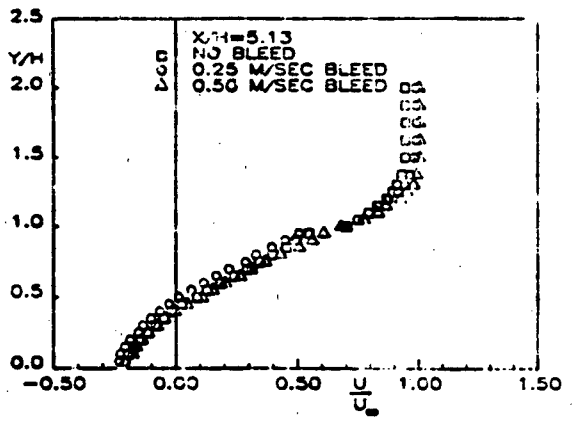

Mean streamwise velocity profiles through the recirculation region for three bleed conditions.

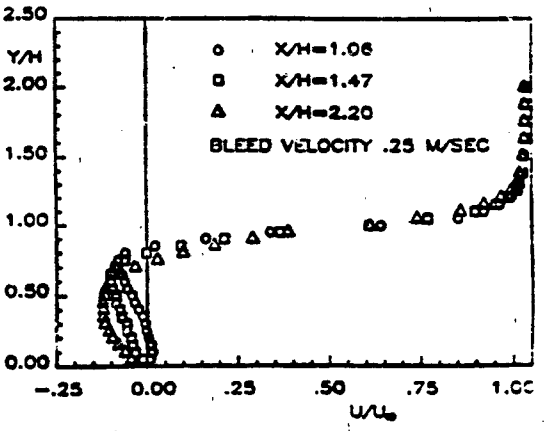

Mean streamwise velocity profiles at three downstream locations near the step with bleed flow indicating the existance of a secondary recirculation zone near the step.

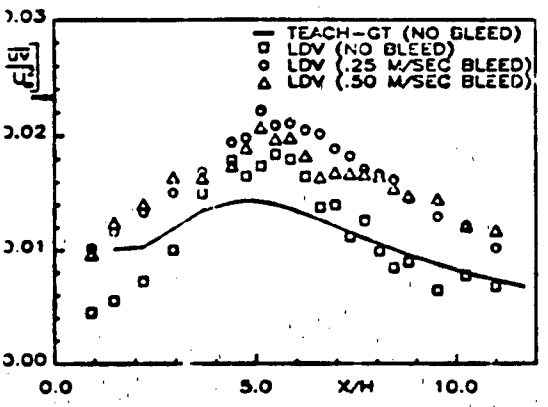

Maximum shear stress distributions in the downstream direction for three bleed conditions.

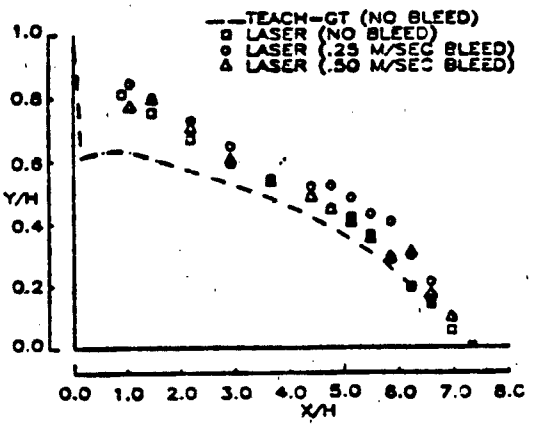

Extent of recirculation zone as defined by zero mean velocity in the downstream direction.

All spatial dimensions normalized by step height.
All velocities normalized by velocity upstream of step.

Fig. 2. Typical Results

HIGH PRESSURE SOLID PROPELLANT COMBUSTION ZONE STRUCTURE FROM ANALYSIS OF HYDROXYL RADICAL CHEMILUMINESCENCE

David H. Campbell, Susan Hulsizer,
Tim Edwards and David P. Weaver
University of Dayton Research Institute and AFRPL
Edwards AFB, CA 93523

The goal of this program is to utilize non-intrusive optical combustion diagnostic techniques to examine the important chemical processes in solid propellant combustion. To simulate the temperatures, pressures, and high heating rates encountered in the combustion environment of solid rocket propellants as closely as possible, optical diagnostic measurements are made by burning strands of propellant in a nitrogen-purged combustion bomb equipped with sapphire windows for optical access. A servo-positioning system keeps the burning surface of the propellant at a constant height relative to the optical system, and provides spatially precise measurements with respect to the surface. The system is capable of operating at pressures up to 1000 PSI.

The results presented in this paper concern the analysis of the natural chemiluminescence originating from the hydroxyl (OH) radical in the flame above burning ammonium perchlorate (AP) composite propellant. An attempt has been made to analyze quantitatively the semi-resolved (~.13 nm) OH emission spectra in the 304.0 to 316.0 nm spectral range to obtain a measure of the rotational temperature and vibrational population distribution of this molecule. At present, the chemical kinetic data base is insufficient to relate the final internal energy state distribution of OH to the specific reaction pathways which produce this molecule in specific rotational-vibrational states. Nonetheless, information about the overall flame zone structure and reaction processes can be deduced from the results.

The issue of flame height and reaction zones is important to the solid propellant combustion modeler because the location of these zones is an indication of the chemistry (and thus, the heat release) that is occuring above the propellant surface. Recent models for AP composite propellant combustion generally model the reactions in the primary (oxidizer and binder) diffusion flame and in the monopropellant flames as occurring within a distance of perhaps 50 μm from the propellant surface, and model any final flame (CO oxidation or NO reduction) as occurring within approximately 100-500 m of the surface at the elevated pressures within the normal rocket operating regime.

Basically, the data reduction technique consists of an iterative scheme to match the experimental spectra to synthetically generated spectra using rotational temperature and vibrational population distribution in the OH upper electronic state as variables. A sample match is shown in Figure 1. Emission spectra were obtained for a series of pressures and distances above the surface of an AP based composite propellant. The rotational temperatures determined from these spectra are shown in Figure 2. If the highly exothermic $CH + O2 \rightarrow CO + OH^*$ reaction is the primary source of excited OH molecules, then the results show that primary reaction zone chemistry occurs at distances much greater than would be expected from current solid propellant combustion models.

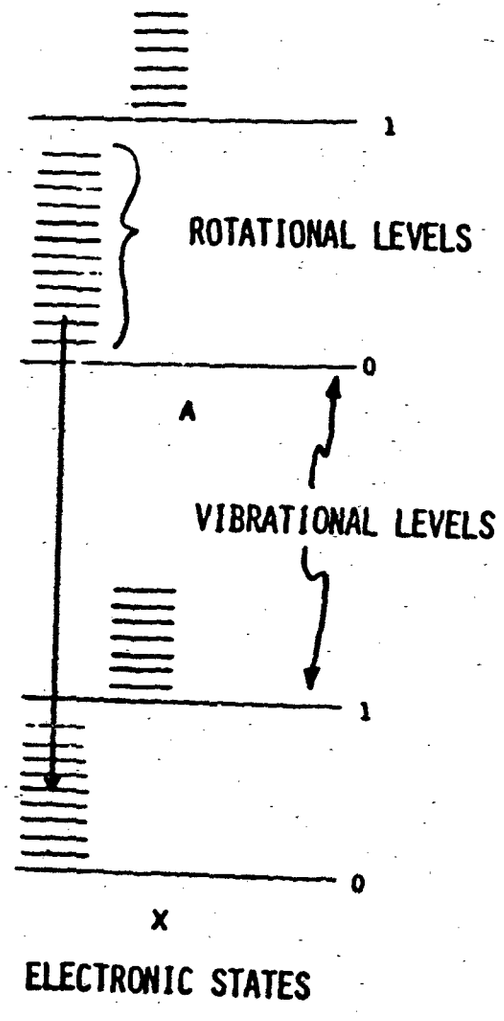

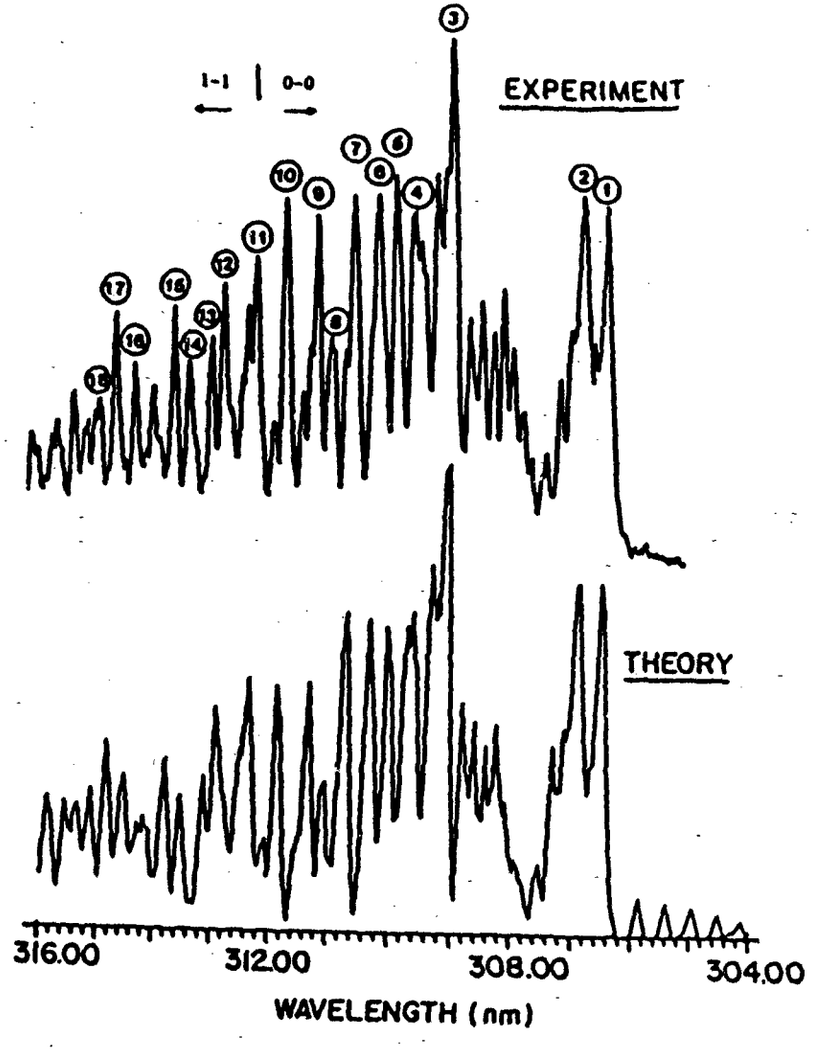

Figure 1: Comparison of experimental OH spectra and a synthetic spectra calculated using T_R=2350 K and N_{v_1}/N_{v_2}=0.66. Positions of the 18 peaks used to find the best fit rotational temperature and vibrational population are also shown.

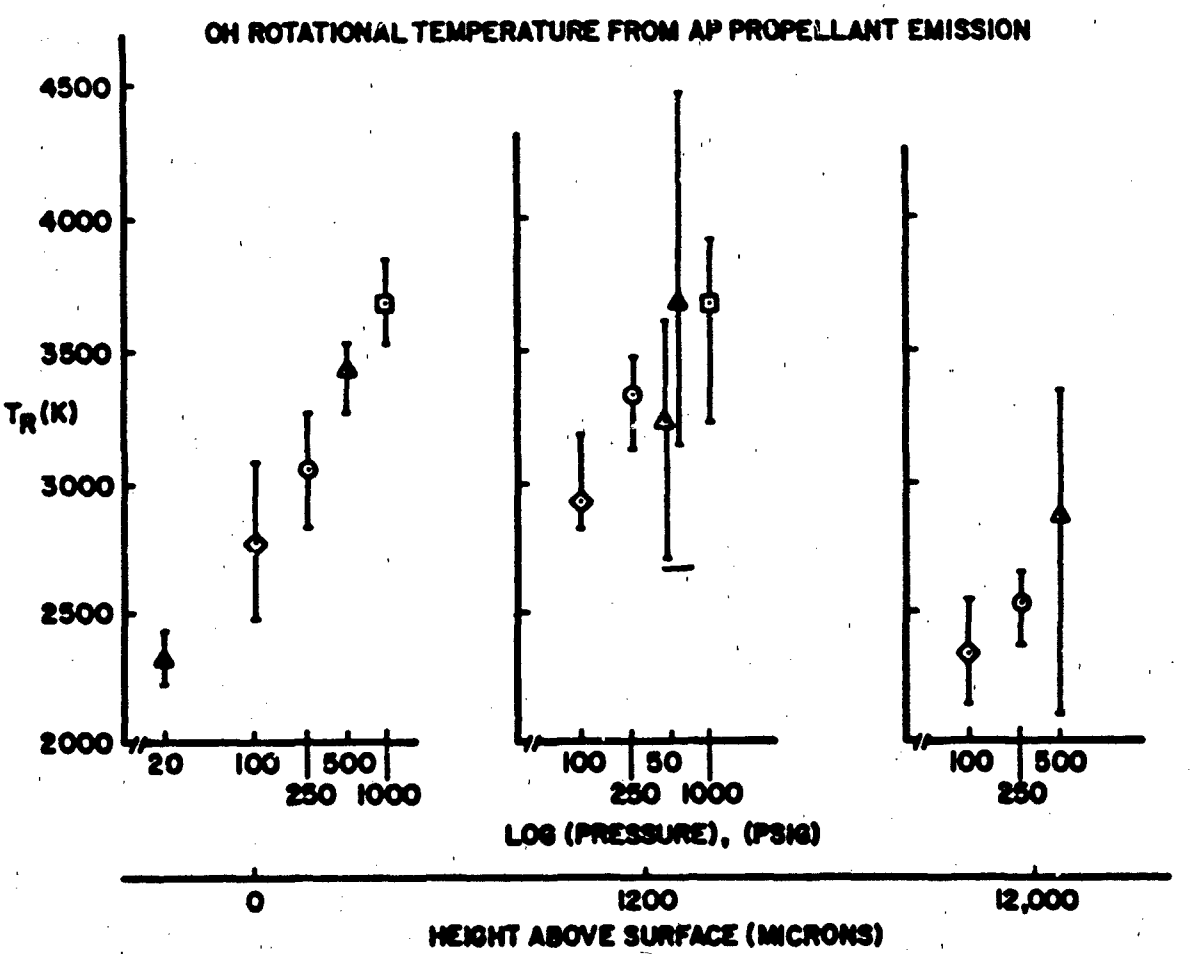

Figure 2: AP propellant OH emission analysis results - rotational temperature variation (v'=0).

Evaluation of HMX Propellant Chemistry From Raman and Laser Induced Fluorescence Species and Temperature Measurements

David P. Weaver and Tim Edwards
Air Force Rocket Propulsion Laboratory
Edwards AFB, California 93523-5000
Susan Hulsizer and David Campbell
University of Dayton Research Institute
Edwards AFB, California 93523-5000

The ability to accurately anticipate the behavior of burning solid rocket motor propellants is highly dependent on specific knowledge of the kinetic mechanisms and heat transfer properties of the reacting species near the surface of the burning propellant. With the developement of modern laser diagnostic techniques, the possibility of determining spatially specific species concentrations and temperatures related to the distance (e.g. the reaction time) from the burning propellant surface has emerged. The goal of the present is to gather such experimental information and to construct from it kinetic pathways in a laboratory propellant flame and to correlate their dependence on propellant composition. Such specific chemical information could then be related to known macroscopic properties of the solid propellant such as burning rate.

A schematic representation of the experimental arrangement for this measurement is given in Figure 1. Here the source radiation is injected into the propellant sample chamber and the resulting scattered radiation collected and focused onto the entrance slit of a dispersive spectroscopic element. A variety of optical techniques for obtaining species number density and temperature are employed including spontaneous Raman scattering, coherent anti-Stokes Raman scattering(CARS), laser-induced fluorescence(LIF) and Rayleigh scattering. Major species such as N2, O2, NO, NO2, H2, CO, and CO2 are monitored with Raman and Rayleigh techniques and combustion intermediates and flame radicals such as OH, CH, CN, and NH are determined using Raman scattering.

Initial efforts are being directed toward acquired temperature and concentration profiles through the flame zones near the surface of the burning solid propellant. Both low and high pressure studies on propellant flames are underway in an effort to identify reactant, intermediate, and product species values and to compare these results with simple kinetic models of known hydrocarbon reactions. Correlation of this data with propellant compositional variation will allow an overall quantitative assessment of the role of specific gas-phase kinetics in solid propellant combustion.

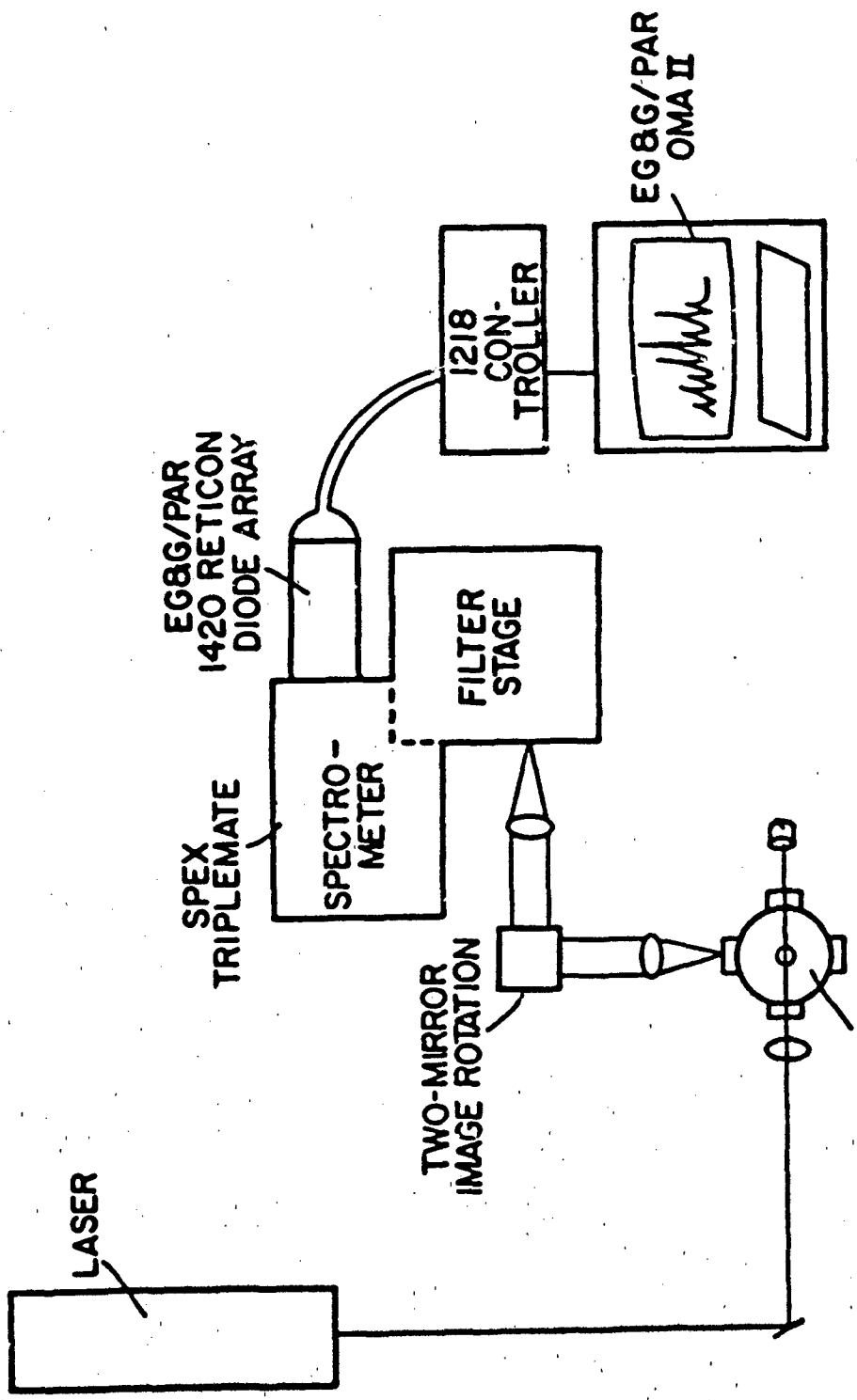

FIGURE 1: EXPERIMENTAL ARRANGEMENT FOR LASER-INDUCED FLUORESCENCE AND RAMAN SCATTERING STUDIES OF SOLID PROPELLANT FLAMES

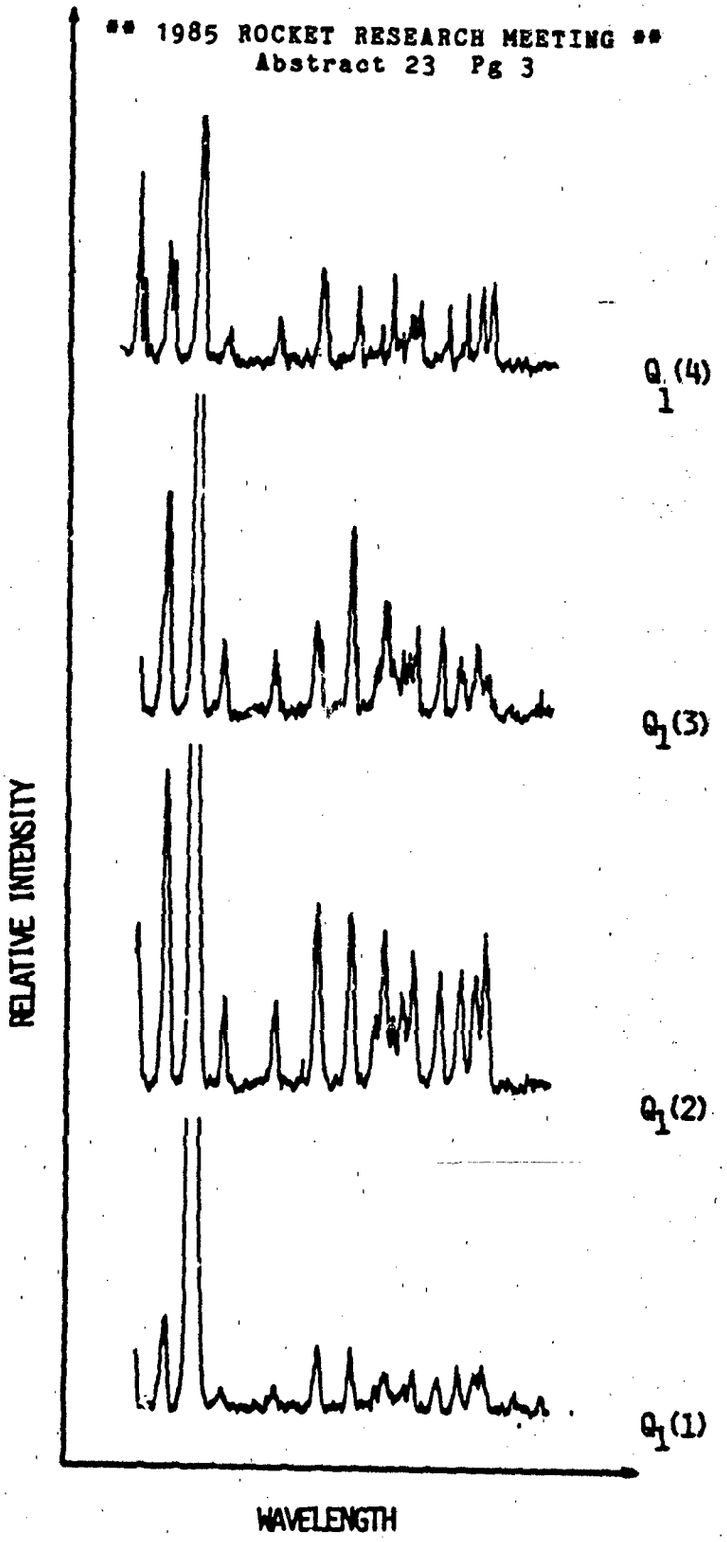

FIGURE 2. TYPICAL LASER-INDUCED FLUORESCENCE SPECTRA OF OH FOR EACH OF FIVE DIFFERENT EXICATION TRANSITIONS. THE SPECTRA SHOW UNDERPOPULATION OF ALL STATES OTHER THAN THAT BEING PUMPED BY THE LASER SOURCE

APPLICATION OF MOLECULAR KINETICS MODELS TO THE PREDICTION OF BACKFLOW CONTAMINATION

David H. Campbell and David P. Weaver
Univ. of Dayton Research Institute and AFRPL
Edwards AFB, CA 93523

The goal of this research project is to obtain a fundamental understanding of the basic physical mechanisms producing the unanticipated high level of backflow contamination observed upstream of the nozzle exit plane of spacecraft rocket nozzles and control thrusters. Information on the internal energy state population distributions, gas species number densities, flow velocities, and degree of condensation near the exit plane of a nozzle will provide the basis for more accurate modeling of the expansion flow inside the nozzle and around the nozzle lip. Such information is critical to the accurate prediction of contamination levels of sensitive spacecraft surfaces.

At present no vacuum expansion flow model exists that accurately predicts observed backflow mass flux levels since these models fail to account for some of the important physical mechanisms which occur in the flow, such as non-equilibrium gas dynamics and condensation. Monte-Carlo models for vacuum plume flows, for example, have been shown to miss experimentally measured backflow mass flux levels by an order of magnitude or more (Figure 1). Clearly, a more accurate collisional model must be determined before the models will be useful for the prediction of backflow contamination.

Vibrational and rotational internal energy state populations, translational mode temperature, gas species number densities, and condensed species densities are being acquired in laboratory scale vacuum expansion flows for diatomic and triatomic gas species using non-intrusive laser spectroscopic techniques. A map of these parameters near the nozzle lip will be used to correlate the degree of non-equilibrium and the degree of condensation with the velocity field and gas number density. The relative importance of these processes to the flux into the backflow region can then be determined.

The expected form of the experimental data and its utility is illustrated in Figure 2. An observation of the distribution of population in the vibrational state levels near the nozzle lip is compared to the mass flux for various angles. Two cases are shown in Figure 2: low nozzle stagnation pressure and high stagnation pressure. At the lower pressure the gas experiences significant vibrational decoupling from the rotational and translational modes as it expands. This produces a higher population in the vibrational levels than would occur if the vibrational state cooled along with the translational modes of the molecule. This in turn increases the total elastic scattering cross section of the gas and thus produces significant scattering of molecules into the backflow region. At higher stagnation pressures the density of the gas will be higher at any given point in the flow and consequently the vibrational state does not decouple from the translational mode until much later in the expansion process, at which point the vibrational state has cooled considerably. This produces a much lower population in the upper vibrational levels and a lower total elastic scattering cross section. The flux into the backflow will then be reduced due to a lower rate of scattering into that region of the flow.

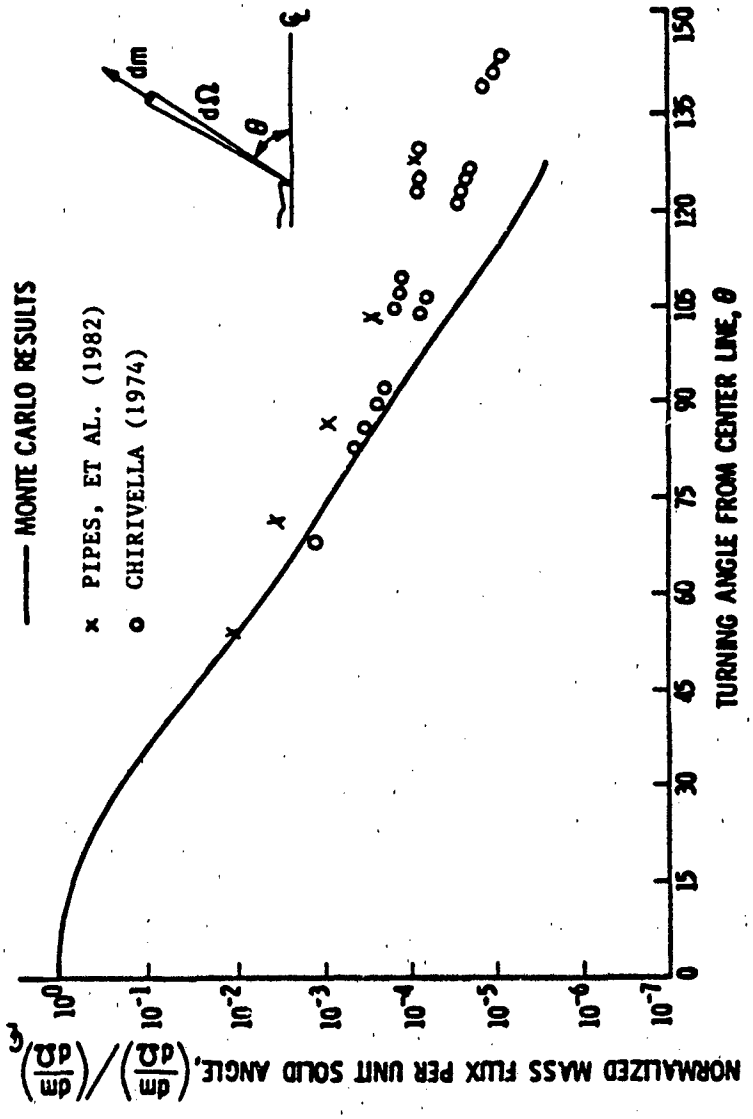

Figure 1: Comparison of theoretical Monte-Carlo backflow prediction with experimental mass flux measurements (pure N_2 flow).

(a) Low P_o

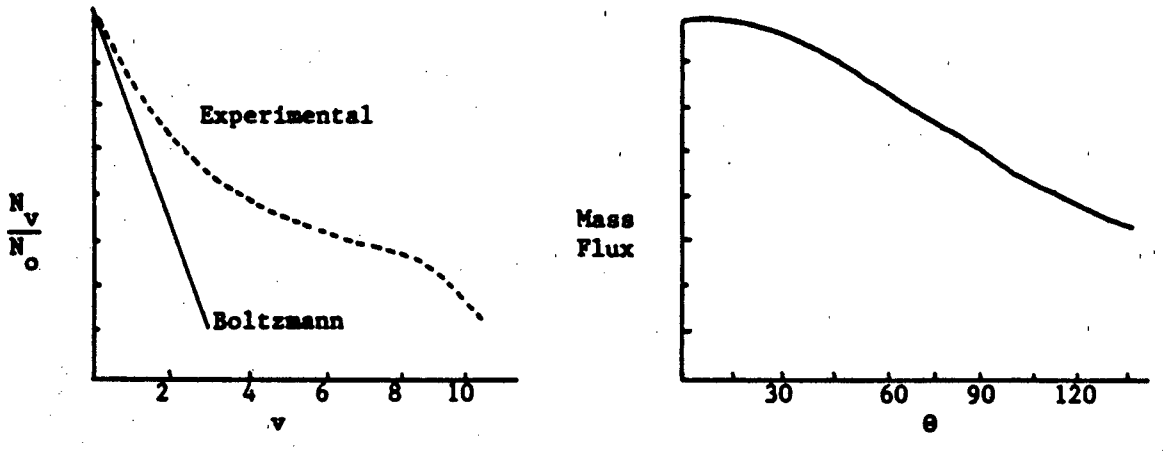

(b) High P_o

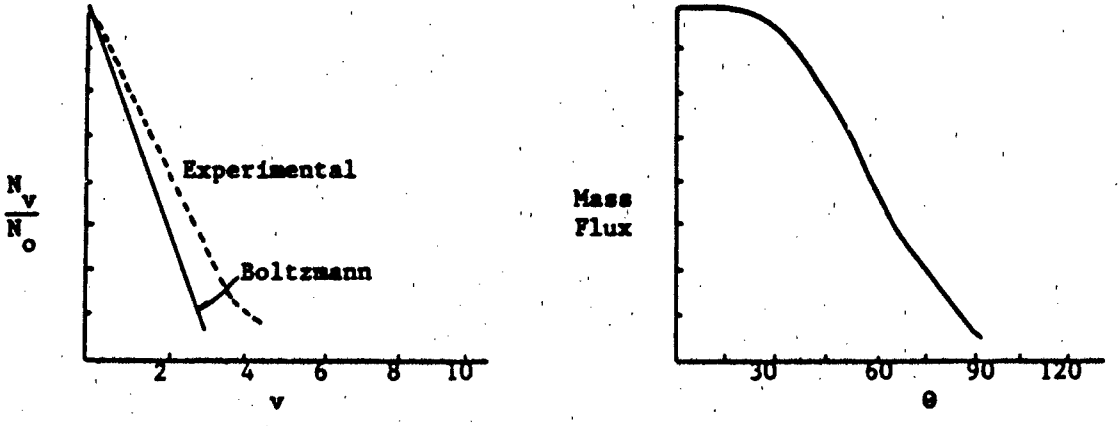

Figure 2: Expected Use of Experimental Data

EVALUATION AND COMPILATION OF THE THERMODYNAMIC PROPERTIES OF HIGH TEMPERATURE SPECIES

Malcolm W. Chase
The Dow Chemical Company
Thermal Lab
Midland, Michigan 48674

The JANAF Thermochemical Tables are a set of self-consistent thermodynamic data. These tables result from critically reviewing all literature sources, evaluating the accuracy and precision of the experimental data/theoretical calculations, calculating temperature-dependent thermodynamic functions, and publishing thermochemical tables for use in the Air Force community. During 1985, the JANAF Thermochemical Tables (3rd edition) will be published as a supplement to the Journal of Physical and Chemical Reference Data (a hard-bound book in two parts).

The past years contract involved the re-examination of the five alkaline earth metals, their dimers, oxides, hydroxides, halides, carbonates, sulfides, and sulfates. Bibliographies, data graphs, and data summaries were generated for 80 species; this will result in approximately 200 single- and multi-phase thermochemical tables. The examination of experimental/theoretical data for a given species by itself may not be sufficient to indicate potential problems whereas the examination of families of species often reveals interesting problems and discrepancies. For example, three of the five alkaline earth metals are not well characterized thermodynamically. This study revealed problems with the calcium data. To resolve this problem, two laboratories in the U.S. are currently measuring the low temperature heat capacities and high temperature enthalpy of calcium. In addition, the simultaneous study of the 20 alkaline earth dihalides yields a large framework in which more reliable decisions can be made as to the validity of the available data as well as guide better estimates for missing data; i.e. portions of the $CaCl_2$ data is questionable.

The quality of the tabulation is often temperature-dependent and is a compromise between the quality and extent of the available data and the calculational procedures used to generate the thermochemcal tables. The calculational procedures are always being re-evaluated in light of the extensive data available in some areas. For example, the thermal functions for monatomic and diatomic gases are being re-examined to determine the effect and reasonableness of new theories. Figure 1 shows the current Cp value for the alkali metal dimers recommended by the JANAF staff. Figure 2 shows the dependence of the calculated heat capacity values for $Li_2(g)$ on some calculational pathways. Discussions are in progress as to the "proper" mode of calculation.

The successful application of these tables depends on the user being aware of the uncertainties in the numerical values and the possible physical and chemical phenomena peculiar to the species of interest. Current effort directed towards preparing annotated bibliographies, data graphs, and data summaries is intended as an additional aid to the users in judging the effects of the uncertainties on the end results.

ALKALI METAL DIMERS

HEAT CAPACITY VERSUS TEMPERATURE

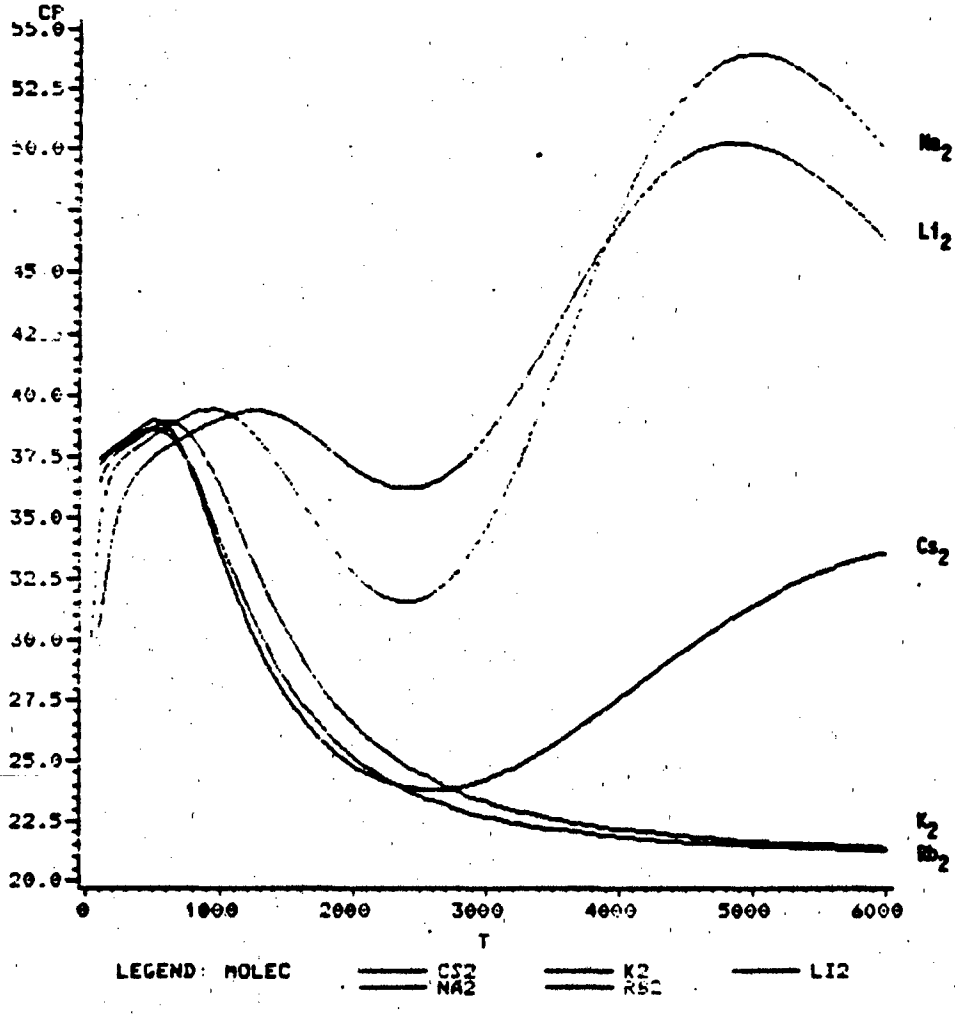

Figure 1

EVALUATION AND COMPILATION OF THE THERMODYNAMIC PROPERTIES OF HIGH TEMPERATURE SPECIES

Malcolm W. Chase
The Dow Chemical Company
Thermal Lab
Midland, Michigan 48674

The JANAF Thermochemical Tables are a set of self-consistent thermodynamic data. These tables result from critically reviewing all literature sources, evaluating the accuracy and precision of the experimental data/theoretical calculations, calculating temperature-dependent thermodynamic functions, and publishing thermochemical tables for use in the Air Force community. During 1985, the JANAF Thermochemical Tables (3rd edition) will be published as a supplement to the Journal of Physical and Chemical Reference Data (a hard-bound book in two parts).

The past years contract involved the re-examination of the five alkaline earth metals, their dimers, oxides, hydroxides, halides, carbonates, sulfides, and sulfates. Bibliographies, data graphs, and data summaries were generated for 80 species; this will result in approximately 200 single- and multi-phase thermochemical tables. The examination of experimental/theoretical data for a given species by itself may not be sufficient to indicate potential problems whereas the examination of families of species often reveals interesting problems and discrepancies. For example, three of the five alkaline earth metals are not well characterized thermodynamically. This study revealed problems with the calcium data. To resolve this problem, two laboratories in the U.S. are currently measuring the low temperature heat capacities and high temperature enthalpy of calcium. In addition, the simultaneous study of the 20 alkaline earth dihalides yields a large framework in which more reliable decisions can be made as to the validity of the available data as well as guide better estimates for missing data; i.e. portions of the $CaCl_2$ data is questionable.

The quality of the tabulation is often temperature-dependent and is a compromise between the quality and extent of the available data and the calculational procedures used to generate the thermochemcal tables. The calculational procedures are always being re-evaluated in light of the extensive data available in some areas. For example, the thermal functions for monatomic and diatomic gases are being re-examined to determine the effect and reasonableness of new theories. Figure 1 shows the current Cp value for the alkali metal dimers recommended by the JANAF staff. Figure 2 shows the dependence of the calculated heat capacity values for $Li_2(g)$ on some calculational pathways. Discussions are in progress as to the "proper" mode of calculation.

The successful application of these tables depends on the user being aware of the uncertainties in the numerical values and the possible physical and chemical phenomena peculiar to the species of interest. Current effort directed towards preparing annotated bibliographies, data graphs, and data summaries is intended as an additional aid to the users in judging the effects of the uncertainties on the end results.

ALKALI METAL DIMERS

HEAT CAPACITY VERSUS TEMPERATURE

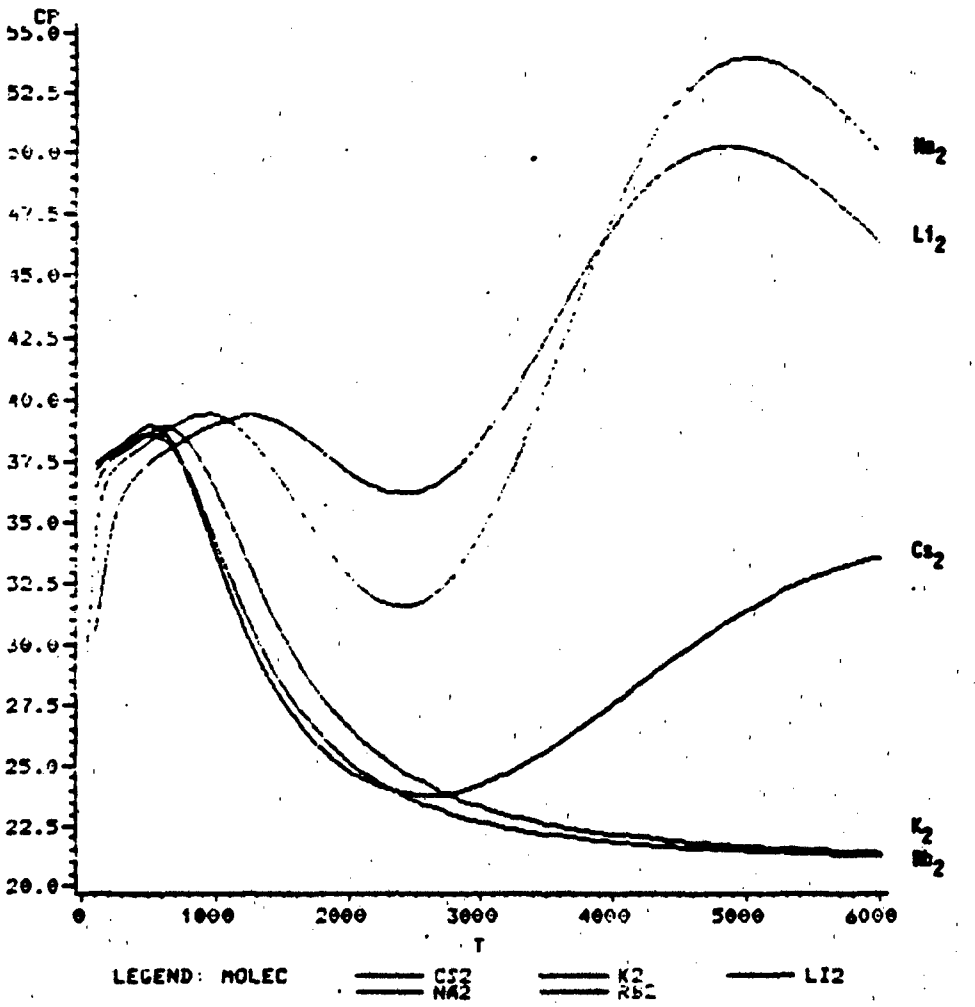

Figure 1

DEPENDENCE OF HEAT CAPACITY ON MODE OF CALCULATION

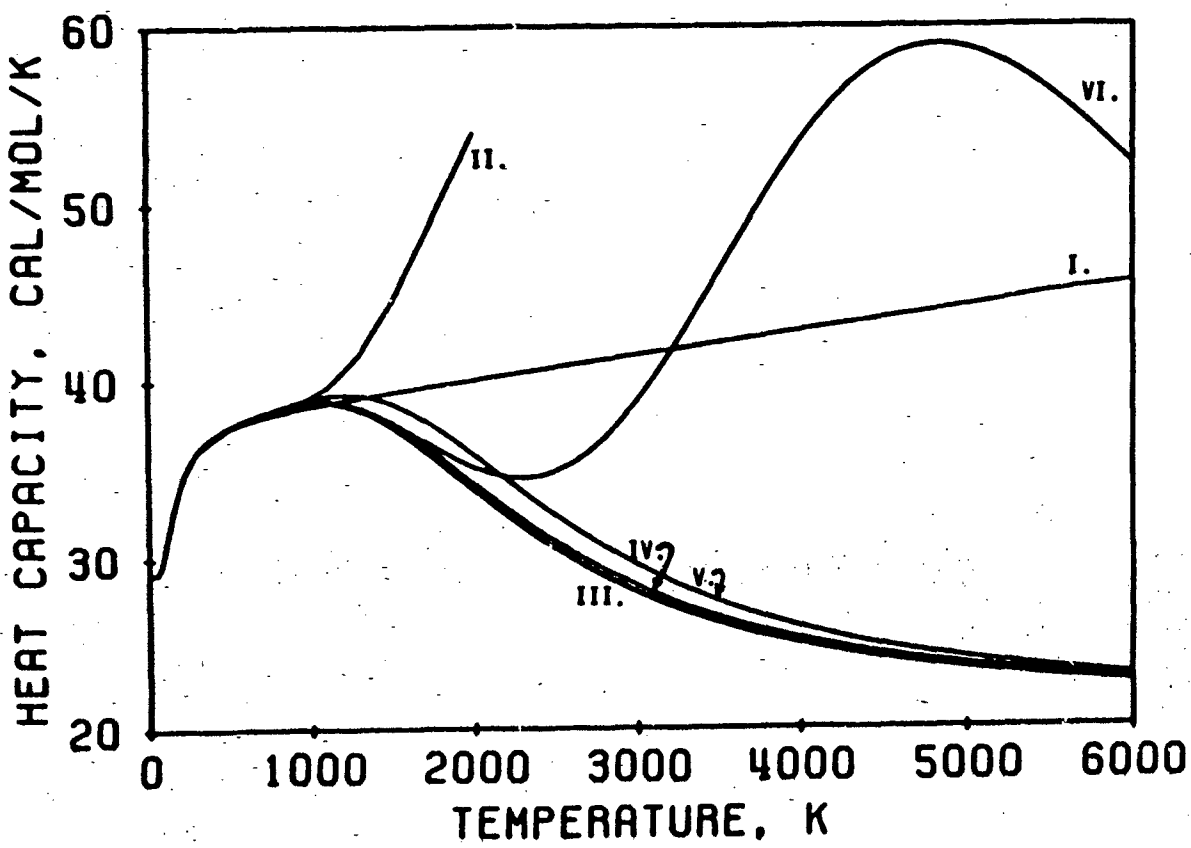

ELECTRONIC GROUND STATE ONLY

I. INTEGRAL (vibration and rotation)
II. DIRECT SUM (vibration) and INTEGRAL (rotation)
III. DIRECT SUM (vibration and rotation)
IV. DIRECT SUM and QUASI-BOUND LEVELS

GROUND STATE AND EXCITED STATES

V. DIRECT SUM - includes shallow excited state
VI. DIRECT SUM - includes four lowest excited states

Figure 2

CRITICAL EVALUATION OF HIGH TEMPERATURE CHEMICAL KINETIC DATA

Norman Cohen and Karl Westberg
Aerospace Corporation
P. O. Box 92957
Los Angeles, CA. 90009

The rapid growth in chemical kinetic data and in the number of nonspecialist users of such data in DOD-related work has created a need for a reliable, easy-to-use compilation of evaluated rate data and recommended rate coefficients. To answer this need, a program for the evaluation of kinetic data and preparation of consistently formatted data sheets patterned after JANAF Thermochemical Tables was undertaken with the joint support of the Air Force Office of Scientific Research and the National Bureau of Standards.

High-temperature data are of special interest to the Air Force, and this was the first data-evaluation program to extrapolate routinely rate coefficients for bimolecular reactions to higher temperatures using methods more sophisticated than the familiar Arrhenius expression. Theory is also used to predict rate coefficients for important reactions for which there are no experimental data. Because the most rigorous current versions of transition state theory are difficult and costly to apply to all but the simplest reactions, a major part of this year's efforts has been devoted to examining the justification of using a simpler, more approximate version as an extrapolative tool and to determining its limits of reliability. A recent technical report does this for the family of reactions of O atoms with alkanes; the report has been accepted for publication. An important result of that study is a series of simple expressions for estimating the value of the room temperature rate coefficient for the reaction of O atoms with any alkane, and then for extrapolating that rate coefficient to temperatures up to 3000 K. The results of this work were used to aid in the preparation of a new series of data sheets for 15 reactions of O atoms with various alkanes, one of which is shown in Figs. 1 and 2.

As a related effort to the aforementioned work, the experimental data for the reactions of O atoms with methane, ethane, and neopentane at temperatures below ca. 600 K were reexamined. In the case of methane and ethane, a set of elementary reactions was assembled that describes the complex chemistry occurring in the original studies. With the aid of previously written computer codes, the original data were reanalyzed. It was found in both cases that the measurements were especially sensitive to errors caused by secondary reactions not taken into account originally and to impurities in the reagent alkane. It appears, qualitatively, that the values for the $O + CH_4$ and $O + C_2H_6$ rate coefficients were overestimated by approximately factors of 2 to 3 in the 250 to 600 K temperature range. This work has also been written up in a technical report and submitted for publication.

During the remainder of the fiscal year, we plan to prepare data sheets for reactions of O and OH with NH_3 and N_2H_4, and for reactions of OH with a series of haloalkanes. Previous work on $H + F_2$ and $F + H_2$ will be updated and prepared for publication. Methods for treating unimolecular reactions will also be examined.

$$CH_3 + OH \underset{-1}{\overset{1}{\rightleftharpoons}} O + CH_4$$

ΔH°_{298} = -11.7 ± 2 kJ mol^{-1} (-2.8 kcal mol^{-1}) ΔS°_{298} = 30.4 ± 1.2 J mol^{-1}K^{-1} (7.3 cal mol^{-1}K^{-1}

$K(T) = 0.14\ T^{-0.3} \exp(1400/T)$

The uncertainty in log K is ±0.2 at 298 K, decreasing to ±0.1 at 2000 K.

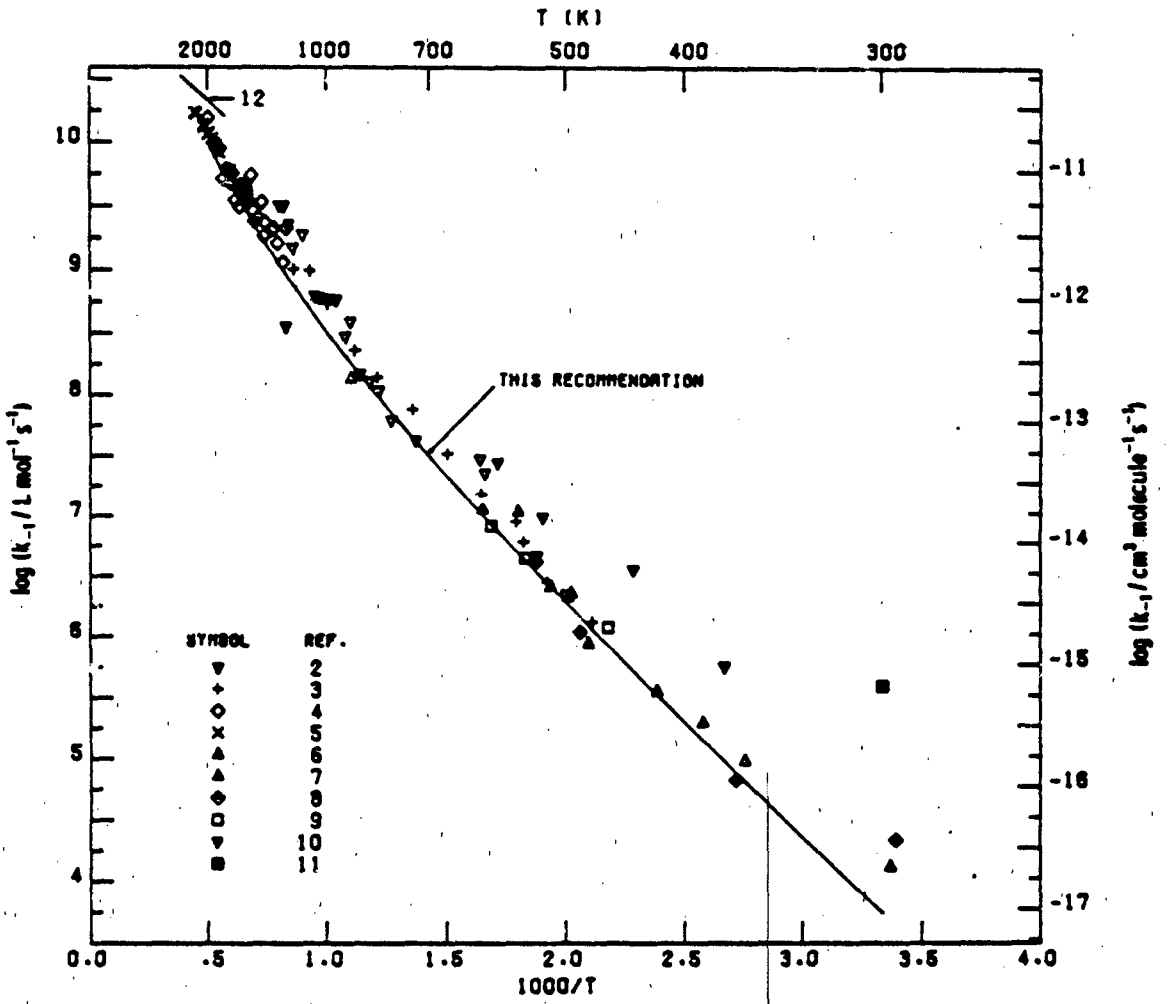

RECOMMENDED RATE COEFFICIENTS

	k(T)	Range	k(298)	Units
k_1	$94\ T^{2.1} \exp(-2070/T)$	298 - 2000 K	1.5×10^{4}	L mol^{-1}s^{-1}
	$1.6 \times 10^{-19}\ T^{2.1} \exp(-2070/T)$		2.6×10^{-17}	cm^3 molecule^{-1}s^{-1}
k_{-1}	$6.7 \times 10^{2}\ T^{2.4} \exp(-3670/T)$	298 - 2000 K	5.6×10^{3}	L mol^{-1}s^{-1}
	$1.1 \times 10^{-18}\ T^{2.4} \exp(-3670/T)$		9.3×10^{-18}	cm^3 molecule^{-1}s^{-1}

Uncertainty in log k_1: ±0.3 near 300 K, decreasing to ±0.4 at 2000 K. Uncertainty in log k_{-1}: ±0.3 throughout the range of 298 - 2000 K. The uncertainty in log k_1 reflects uncertainties in both log k_{-1} and log K(T).

Fig. 1

$OH + CH_3 \xrightarrow[k_{-1}]{k_1} O + CH_4$

THERMOCHEMICAL DATA

Thermochemical data for CH_4 and CH_3 were taken from JANAF Thermochemical Tables (1971), except that the enthalpy of formation of CH_3 at 298 K is taken to be 146.9 ± 0.7 kJ/mol, in accordance with recent measurements[1]. Data for O and OH were taken from unpublished supplements to these tables dated March 1977 and June 1977, respectively. The analytical expression chosen for K(T) matches equilibrium constants calculated from the above data to within 10% between 298 and 2000 K.

MEASUREMENTS

The reaction has been studied only in the reverse direction. The products of the reaction of O with CH_4 both react much more rapidly with O than CH_4 does; in addition, OH reacts with CH_4 faster than O does. Consequently reaction (1) is almost always followed by nonnegligible secondary processes. Two approaches to measuring k_{-1} have been tried: (a) $[O]_o \approx [CH_4]_o$; (b) $[O]_o \ll [CH_4]_o$. If method (a) is used, the stoichiometry must be accurately measured for each set of experimental conditions, since it is a function of $[CH_4]:[O]$, extent of reaction, and temperature. With method (b) the reaction will be pseudo-first order if $[O]_o$ is small enough and $[CH_4]/[O]$ exceeds $\sim 10^5$ at 400-500 K. If O atoms are in excess, the constraints are considerably less stringent, but the reaction has not been studied by this method.

Impurities must be carefully evaluated, especially at low temperatures. For example, at 300 K, 0.1% C_2H_2 (or 0.03% C_2H_6 or 2 ppm C_2H_4) in the CH_4 will contribute 10% to the rate of O consumption if $[CH_4]_o \gg [O]_o$. C.P. grade CH_4 from Matheson typically contains 0.03% C_2H_6. No published studies below 450 K provide enough information to ensure the reader that questions of stoichiometry and purity have been adequately dealt with; however, the unpublished extension of work by Volder and Pentijn[2] may qualify. Consequently, there is no reliable measurement of k_{-1} at 300 K. Between 300 K and 1200 K the best results are those of Volder and Pentijn, obtained by pulsed photolysis in slowly flowing mixtures; and of Klemm et al.,[3] using discharge-flow resonance fluorescence, but the latter require some corrections for secondary reactions, particularly at the lower end of the temperature range.

At higher temperatures, the results of Stubbe and Bruhn[4] are preferred, though they were obtained by elaborate numerical modeling in a complex chemical system. The shock tube results of Roth and Just[5] are consistent with them, but insufficient data are given for proper evaluation. Earlier work[6-12] was reviewed by Warnatz and Hein[13].

CALCULATIONS

A transition-state-theory calculation was carried out assuming log $k_{-1}(300) = 3.75$ and using the structure of the activated complex reported by Walsh and Benning.[14] However, their high values for the C-H-O degenerate bending frequencies (approx. 720 and 630 cm^{-1})[15] gave poor agreement with experimental data, regardless what value of k(300) was assumed. Better agreement was obtained with a much lower bending frequency of 240 cm^{-1}, as calculated by a 4-atom INDO program. Tunneling was quantitatively accounted for assuming an unsymmetrical Eckart barrier (barrier heights of 38.9 and 40.7 kJ/mol) and a transmission (see Ref. 16 for further details.) The calculated values of $k_{-1}(T)$ were well-fitted by the expression $k_{-1}(T) = 670\ T^{2.4} \exp(-3670/T)$ L $mol^{-1}s^{-1}$. This agrees with the best experimental data within a factor of approximately 2 between 300 and 2000 K. Another TST calculation has been described by Michael et al.[17]

DISCUSSION

The usefulness of the TST calculation is impaired by the lack of a reliable experimental value of $k_{-1}(300)$. Although experimental values of log $k_{-1}(300)$ of 4.1 and 4.3 have been reported, it is likely that the true value is lower — probably between 3.3 and 3.8. We recommend the expression derived from the TST calculation described above, which gives good agreement with experiments: $k_{-1}(T) = 670\ T^{2.4} \exp(-3670/T)$, with an uncertainty of a factor of 2 throughout the temperature range of 300-2000 K.

References

1. S. P. Sharpless, P. A. Knost, and S. W. Benson, Int. J. Chem. Kinet. 13, 677, (1981).
2. W. Volder and A. Pentijn, Chem. Phys. Lett. 67, 33 (1979); A. Pentijn, 18th Symp. (Int.) Combust. 797 (1981); W. Volder and A. Pentijn, Tech. Mtg. Eastern Sect. Comb. Inst., Oct 1980.
3. R. R. Klemm, T. Tanzawa, F. G. Sholeth, and J. V. Michael, 18th Symp. (Int.) Combust., 785 (1981).
4. T. A. Stubbe and R. S. Bruhn, 15th Symp. (Int.) Combust., 893 (1975).
5. P. Roth and Th. Just, Ber. Bunsenges. Phys. Chem. 81, 572 (1977).
6. A. A. Westenberg and N. DeHaas, J. Chem. Phys. 46, 490 (1967); ibid., J. Chem. Phys. 50, 2512 (1969).
7. E. L. Wong and A. E. Potter, Jr., Combst. J. Chem. 45, 367 (1967).
8. R. R. Cadle and E. R. Allen, J. Phys. Chem. 66, 1611 (1965).
9. J. M. Brown and B. A. Thrush, Trans. Faraday Soc. 63, 630 (1967).
10. L. L. Avramenko, E. V. Kolesnikova, and G. L. Savlenova, Izvest. Akad. Nauk SSSR, Otdel. Khim. Nauk 630 (1963), as reported in Ref. 13(b).
11. F. M. Preston, Ber. Bunsenges. Phys. Chem. 72, 906 (1968).
12. A. M. Dean and G. B. Kistiakowsky, J. Chem. Phys. 54, 1718 (1971).
13. (a) J. T. Herron, Int. J. Chem. Kinet. 1, 527 (1969); (b) J. T. Herron and R. E. Huie, J. Phys. Chem. Ref. Data, 2, 467 (1973); (c) R. E. Huie and J. T. Herron, Prog. Reaction Kinet. 8, 3 (1975).
14. R. P. Walsh and T. H. Benning, Jr., J. Chem. Phys. 73, 3221 (1980).
15. R. P. Walsh, private communication, 13 Jan. 1983.
16. H. Cohen, to be published.
17. J. V. Michael, D. G. Keil, and R. B. Klemm, Int. J. Chem. Kinet. 15, 709 (1983).

Fig. 2

FUNDAMENTAL STUDIES OF AZIDE DECOMPOSITION AND COMBUSTION

Joseph E. Flanagan, Dean O. Woolery, Wallace W. Thompson
Rocketdyne Division
ROCKWELL INTERNATIONAL
Canoga Park, CA 91304

The utilization of azide ($-N_3$) ingredients is rapidly increasing in a wide spectrum of Air Force applications. Azide materials are primarily characterized by their high positive heats of formation in addition to unique combustion features such as inherent high-burning rates and self-extinguishment at pressures above ambient.

This study will elucidate the decomposition and combustion characteristics of various azide ingredients via high temperature, high heating rate pyrolysis-gas chromatography-mass spectrometry.

The approach will be threefold:

1. Definition of azide decomposition chemistry with structure.
2. Effect of azide decomposition chemistry upon selected propellant ingredients.
3. Correlation of decomposition phenomena with propellant burn rates.

The effort during the first year has resulted in a determination of azide decomposition chemistry via high pressure (30-500 PSIG), high heating rate pyrolysis of various azide ingredients consisting of: (1) Aliphatic azides; (2) Azidonitramines; (3) Azidoalcohols; (4) Multi-substituted azides; (5) Cyclic azide monomers; (6) Azide polymers - a) GAP; b) AZOX; c) AMMO; d) BAMO; (7) GAP gumstocks.

The effect of pressure upon the pyrolysis of liquid GAP polymers of 600, 2000, 2500, and 3800 molecular weight at 30, 100, 250 and 500 PSIG was determined. Increase in CO and decreases in H_2O yields were found with increasing pressure for all polymers. N_2 and other product yields remained essentially constant with pressure increase. These results indicate more efficient carbon oxidation with pressure increase.

The effect of pressure upon the pyrolysis of the respective GAP polymer gumstocks cured with HMDI was determined. These propellants self-extinguished up to 50 PSIG. Gas product distributions from pyrolysis were determined at 100, 250, and 500 PSIG. These product distributions were influenced by HMDI concentration dictated by GAP hydroxyl equivalent weight. In all cases, CO yield increased with increasing pressure indicating more efficient carbon oxidation.

Burn rate studies have demonstrated three pressure dependent azide polymer deflagration phenomena consisting of very rapid combustion, self-extinguishment, and smooth regression over the pressure region of 0 to 3000 PSIG.

Preliminary data shows good correlation between weight percent GAP, flame temperature, and burning rate for cured gumstocks of various GAP samples.

SCIENTIFIC APPROACH

- FIRST TIME EVER ELUCIDATION OF AZIDE DECOMPOSITION CHEMISTRY VIA

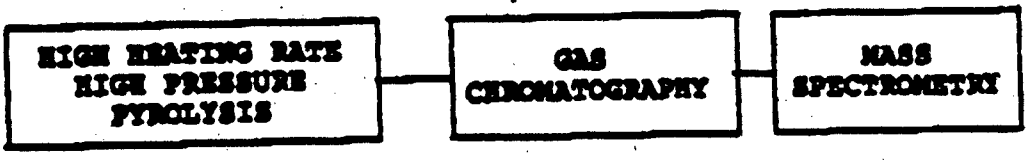

  - ALIPHATIC AZIDES, AZIDONITRAMINES, AZIDOALCOHOLS, CYLIC AZIDE MONOMERS, AZIDE POLYMERS

- CORRELATION OF PYROLYSIS DECOMPOSITION CHEMISTRY WITH BURN RATE
  - GAP POLYMERS 600, 2000, 2500, 3000 MOLECULAR WEIGHT
  - GAP - HMDI GUMSTOCKS

CO AND H_2O YIELD FROM NEAT GAP (370-1940 EW) PYROLYSIS

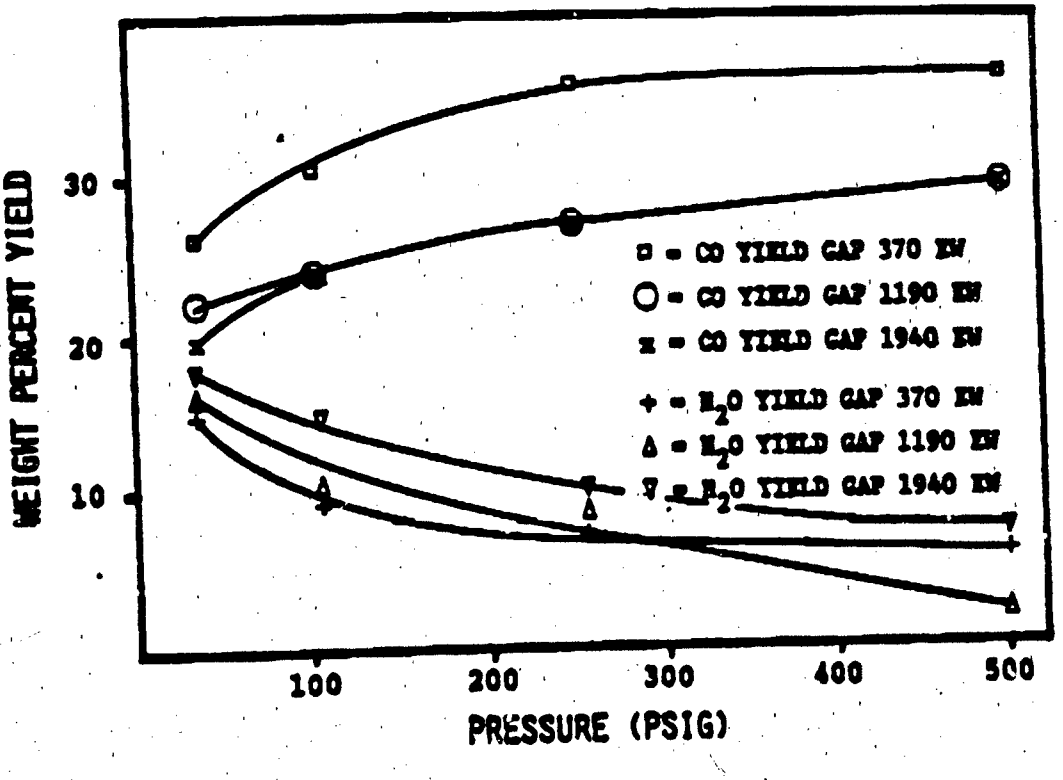

PRIMARY ACCOMPLISHMENTS

- ELUCIDATION AND IDENTIFICATION OF AZIDE DECOMPOSITION CHEMISTRY
  - INFLUENCE OF OTHER FUNCTIONAL GROUPS
  - INFLUENCE OF POLYMERIZATION
- CORRELATION OF INCREASED CARBON OXIDATION FROM PYROLYSIS WITH PRESSURE INCREASE AND BURN RATE
- FIRST TIME DEMONSTRATION OF THREE PRESSURE DEPENDENT AZIDE POLYMER BURNING PHENOMENA CONSISTING OF
  - VERY RAPID COMBUSTION
  - SELF-EXTINGUISHMENT
  - SMOOTH REGRESSION

GAP (370-1940 EW) HMDI GUMSTOCK BURN RATES

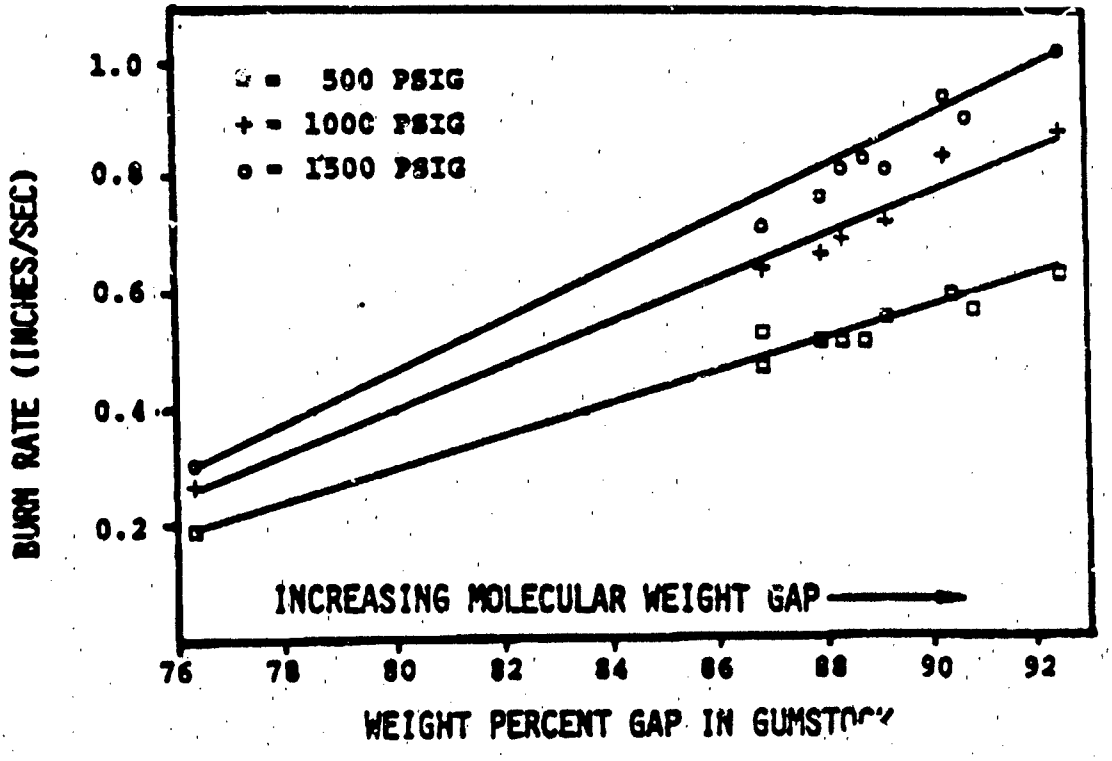

STABILITY OF RDX, AP, AND BTTN NEAR ROOM TEMPERATURE

Douglas B. Olson and Robert J. Gill

AeroChem Research Laboratories, Inc.
P.O. Box 12, Princeton, NJ 08542

The overall objective of this work is to gain a more fundamental understanding of the chemical reaction mechanism and kinetics responsible for aging of solid rocket propellants at near ambient temperature. The chemical aging process is envisioned to result from the slow decomposition of some ingredients producing highly reactive species which then chemically attack other ingredients, especially the polymer binders. The present studies include the decomposition kinetics of selected pure ingredients as well as the degradation reactions of two binders. Mechanisms will be postulated, using the measured kinetic parameters, and the predictions of this chemical aging "model" will be compared with available data. A noteworthy aspect of this program is the use of highly specific and ultrasensitive analytical probes which allow studies to be performed at realistic storage temperatures, over short time spans, and with little degradation, compared to the more usual accelerated testing at high temperatures, which then requires extrapolation of rate coefficients over many decades.

Progress to date has included measurements of the low temperature decomposition rate coefficients of RDX, AP, and BTTN using gas evolution analysis, as schematically illustrated in Fig. 1. A carrier gas is passed over small samples of the ingredient under test in heated isothermal cells ($T \approx 20$–$100°C$). A highly sensitive NO/O_3 chemiluminescence analyzer is used to measure the real-time NO_x concentration (or NH_3 concentration from AP) evolved from the samples to compute a decomposition rate coefficient. This is performed at several temperatures to establish the Arrhenius parameters of the process. The technique is capable of measuring rate coefficients as small as about 10^{-12} s^{-1} (half-lives greater than 10^4 years). Using the same apparatus, the reactivity of decomposition products, such as NO_2, with individual ingredients and mixtures is also being measured over short, 1–100 hour, storage times.

Figure 2 shows low temperature kinetic data measured in this program on RDX, AP, and BTTN as well as some earlier AeroChem data on other materials. The activation energy for RDX decomposition is a surprisingly low 25 ± 1 kcal mol^{-1}, although when the rate expression is extrapolated to 450 K reasonable agreement is obtained with previous estimates. The rate coefficients shown for two perchlorates, AP and CP, illustrate their high stability. The AP data are in good agreement with some of the previous high temperature measurements.

Results are also shown for three nitrate esters, NC, PETN, and BTTN. Because of some experimental difficulties and a large disagreement between these data and an earlier Hercules/Allegany Ballistic Labs. study, we report this BTTN rate coefficient as a preliminary value. Note that the measured activation energy for BTTN (E_a=41 kcal mol^{-1}) is similar to that of the other two nitrate esters, although the previously reported BTTN value (E_a=26 kcal mol^{-1}) is much smaller.

This work is continuing and will concentrate on the reactions of decomposition products with propellant ingredients and the aging mechanism of HTPB-containing propellants.

PROPELLANT AGING RESEARCH

Approach

* *NO_x OFFGAS ANALYSIS*

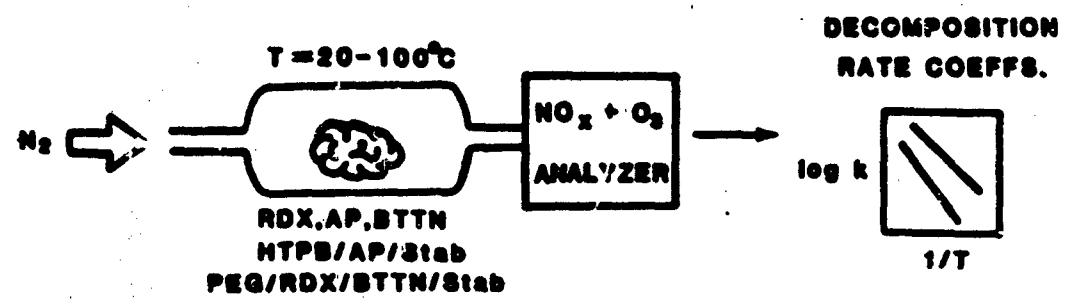

* *BINDER REACTIVITY*

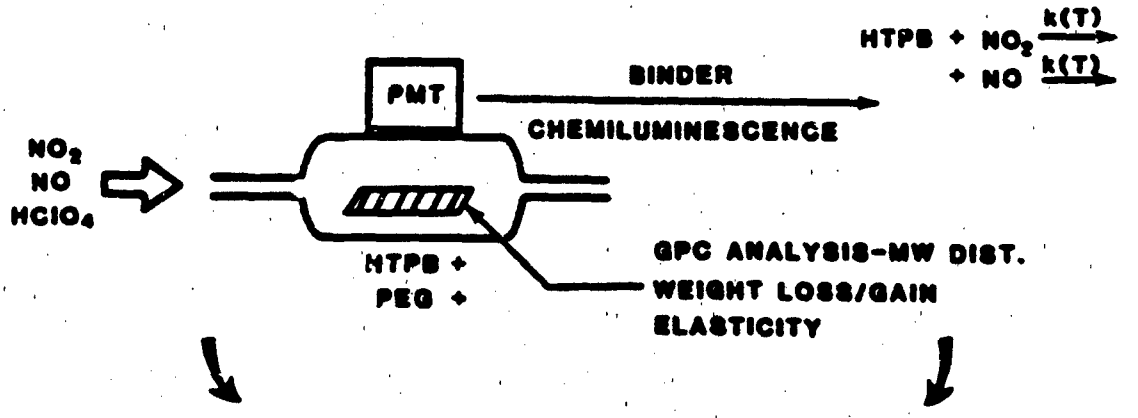

* *POLYMER OXIDATION/PROPELLANT AGING MECHANISM*

INITIATOR (NO_2?) → R·

R· + O_2 → RO_2

RO_2 + RH → RO_2H + R·

etc.

NITRATE ESTER → NO_2

NO_2 + Stab → UNREACTIVE PROD.

NO_2 + BINDER → DEGRADED BINDER

FIGURE 1

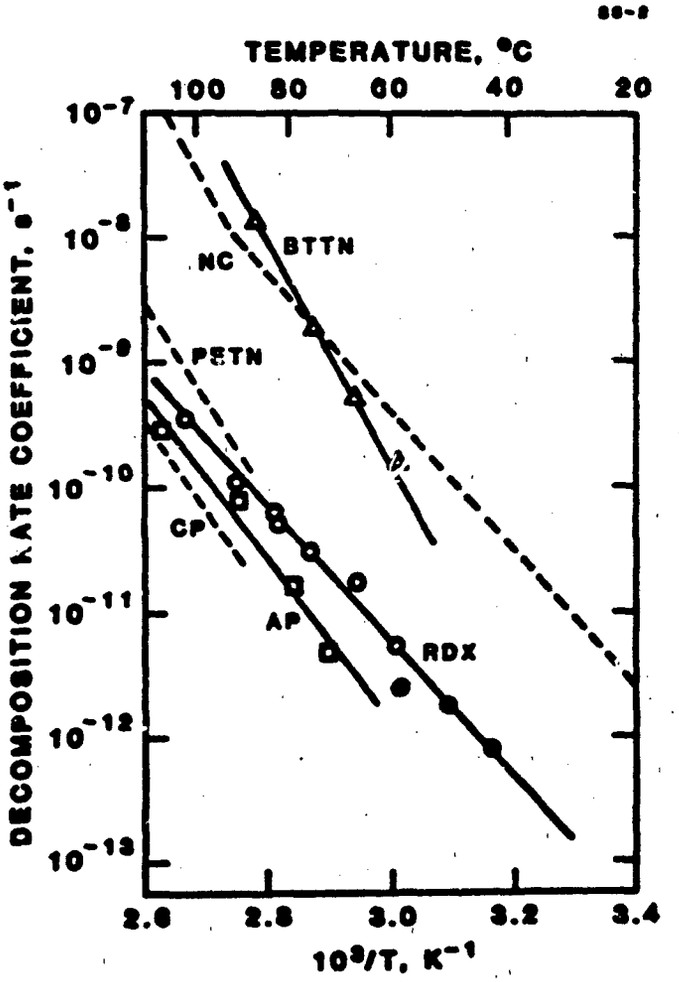

FIGURE 2 DECOMPOSITION RATE COEFFICIENTS OF PROPELLANT INGREDIENTS

Activation energies in kcal mol^{-1} for: nitrate esters - NC (E_a(T < 90°C) = 25, E_a (T > 90°C) = 43), PETN (E_a = 40), and BTTN (E_a = 41); the nitramine RDX (E_a = 25; and perchlorates AP (E_a = 30) and CP (E_a = 32).

FUEL-RICH SOLID PROPELLANT BORON COMBUSTION

Merrill K. King and James J. Komar
Atlantic Research Corporation
Alexandria, Virginia

Boron particle combustion is retarded by initial presence of an oxide coating. In current boron ignition models, oxygen is assumed to dissolve in the oxide and diffuse to the B/B_2O_3 interface for reaction. Measurements of exotherms for oxide-coated particles in hot O_2/N_2 mixtures have quantified oxidation rates, but have not unequivocally established whether oxygen or boron (suggested by theoretical solubility considerations) moves across the oxide. Possible non-equilibrium condensation of boron oxide/hydroxide products during rapid cooling (e.g., nozzle expansion) is also important - significant performance is lost without such condensation. Past condensation studies have been conducted under unrealistic conditions or involved limited diagnostics, inadequate for mechanism definition.

Regarding the first problem, a unique experiment (Figure 1A) utilizing two sealed vessels (one containing argon, the other an argon/oxygen mixture) separated by a controlled thickness/temperature liquid B_2O_3 film on a porous platinum disk, will be performmed. Oxygen permeability will be determined by monitoring O_2 concentration rise in the argon vessel with a mass spectrometer or NDUV detector. Oxide film temperature will be controlled by resistance or inductive heating and measured by two-color pyrometry and/or thermocouples, while thickness will be established by oxide volume and disk area. Equal pressures will be maintained in the vessels by bellows sections or use of a manometer connected across chambers with controlled bleeds as needed. Several temperature, oxide thickness, and oxygen level combinations will be studied. Results will be compared with calculations from previously referenced oxide-coated boron particle exotherms (Figure 2A).

In Task 2, a unique combination of laser diagnostics and a 2-D windowed expansion section (with pressure taps) attached to a gaseous combustor will be used to quantify boron oxide/hydroxide condensation processes at realistic conditions. (Figure 1B). Wet and dry, unseeded (homogeneous) and seeded (heterogeneous) systems will be studied. A long-residence-time combustor using oxygen, CO or propane, nitrogen, and B_2O_3 or triethylborane will produce well defined (composition, temperature) products. Various throat sizes and nozzle contours provide various controlled temperature-pressure-time profiles. Optical ports permit use of laser-based diagnostics for measurement of flow velocity, composition, temperature, particulate concentration, and condensate sizes versus distance (time). From analysis of changing gas composition and particle quantity and size along the nozzle (for various initial conditions and expansion rates) condensation mechanisms will be defined.

1A. APPARATUS FOR DETERMINATION OF SOLUTION/TRANSPORT (PERMEABILITY) RATE OF OXYGEN ACROSS A BORIC OXIDE FILM

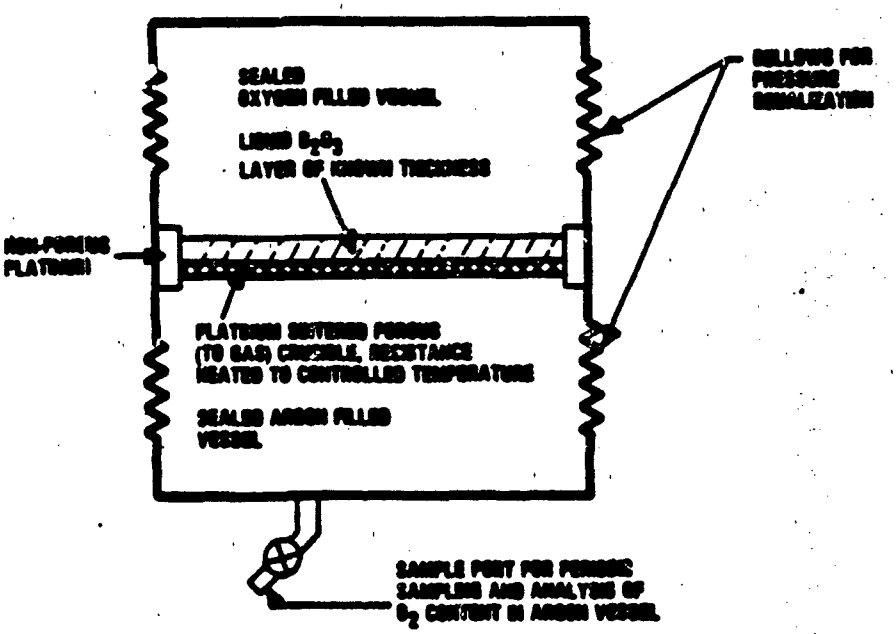

1B. STUDY OF CONDENSATION PROCESSES OF BORON OXIDES AND HBO_2

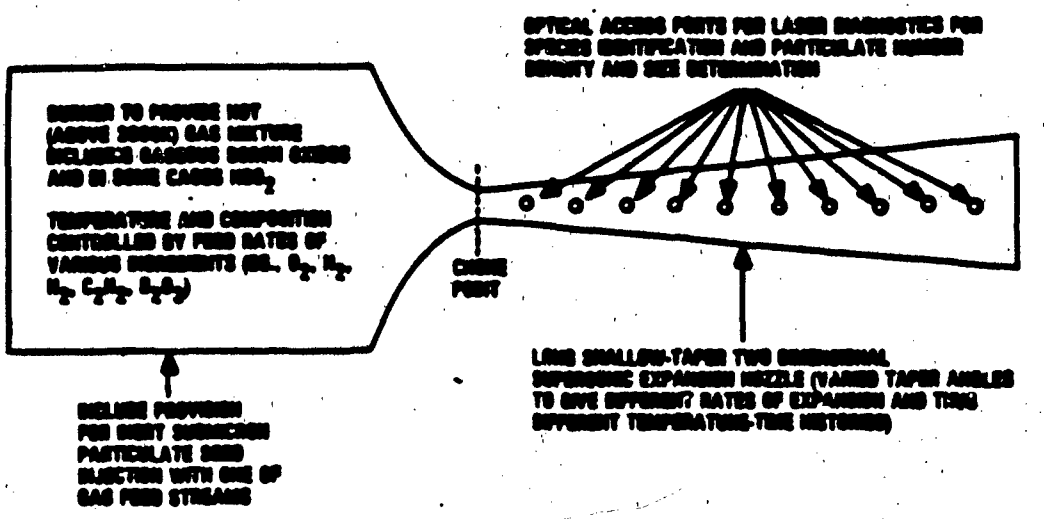

2A. PERMEABILITY EXPERIMENT——ANTICIPATED RESULTS

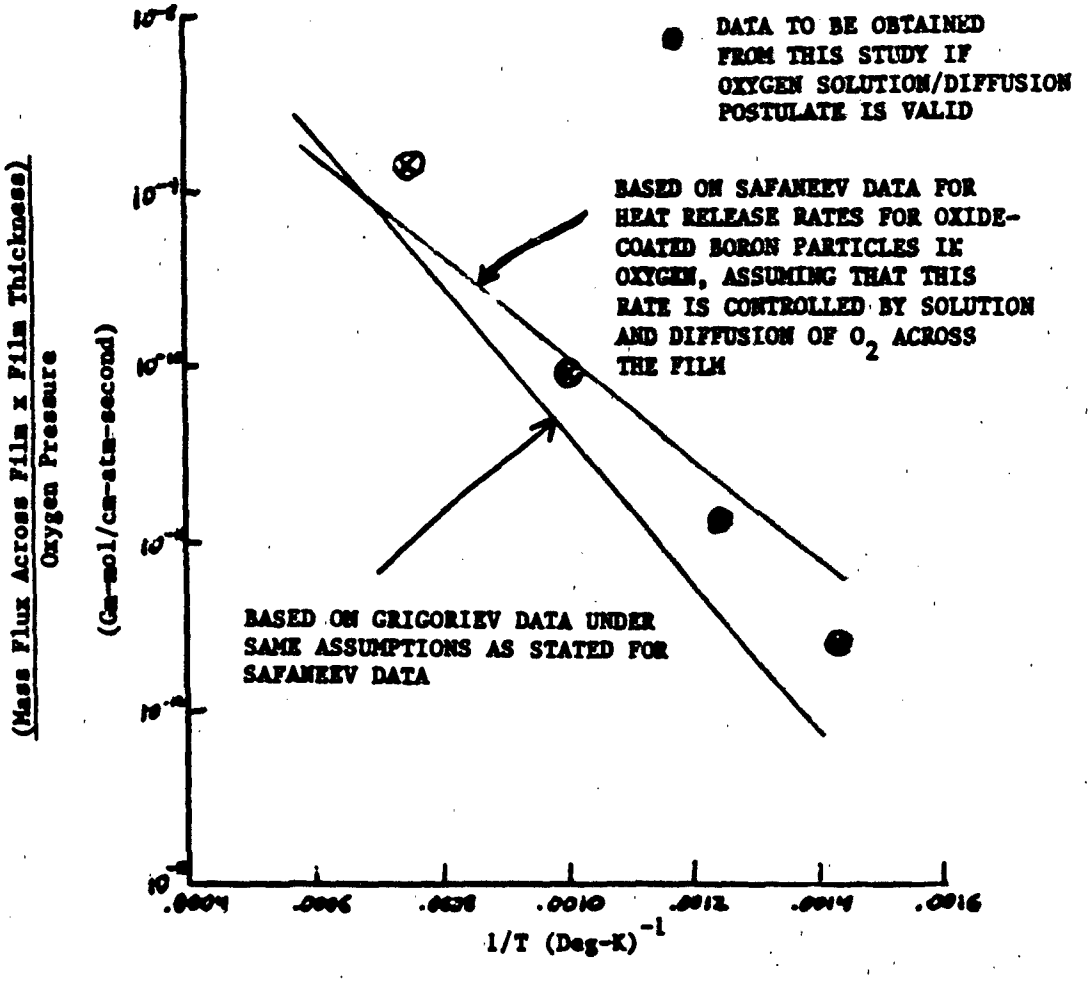

2B. CONDENSATION EXPERIMENT OUTPUT

For Various Chamber Gas Temperatures, Pressure, and Composition, and Various Rates of Change Of Temperature (Controlled By Nozzle Contour),

Obtain
- Temperature
- Major Species Concentration
- Pressure
- Amount of Condensed Oxide
- Minor Species Identification

} vs Distance (Time)

Leading to Model of Nucleation/Condensation Processes Capable of Being used to Predict Degrees of Supercooling in Various Situations

CRACK GROWTH BEHAVIOR IN A COMPOSITE PROPELLANT WITH STRAIN GRADIENTS

C. T. LIU
Air Force Rocket Propulsion Laboratory
Edwards AFB CA 93523-5000 (805) 277-5502

The main objective of the Structural Mechanics Research Program is to advance the current understanding of the crack growth behavior in solid propellants. The specific objective of this present research program is to investigate the crack growth behavior in solid propellant in the presence of nonuniform, gross applied strain fields.

In this study, the crack growth behavior in a highly filled composite propellant with strain gradients was studied through the use of precracked biaxial specimens. Two different shapes of biaxial specimens were considered; namely, the rectangular shape and the wedge shape. Through cracks with different crack lengths and eccentricities, with respect to the vertical centerline of the specimen, were cut along the horizontal centerline of the specimen. Crack propagation tests were conducted under a constant strain rate condition at room temperature. The measured crack length, load, and time served as input to a computer program that calculated the crack growth rate and the stress intensity factor, and then determined the functional relationship between these two parameters.

In analyzing the data, time was selected as the independent variable, whereas crack length and load were selected as the dependent variables. With this selection of independent and dependent variables, the crack length and the load were measured every three seconds (i.e., $\Delta t = 3$ seconds), which was selected just for convenience. Based on the measured a versus t data, the crack growth rate, $\frac{da}{dt}$, was calculated by four different methods for five different time intervals, $\Delta t = 3$, 6, 9, 12, and 15 seconds.

At the time of this writing, progress has been made toward developing a crack growth model to predict the crack growth behavior in solid propellants, and the data analysis had been completed. Based on the results of the data analysis for the condition considered in this study, the following conclusions are drawn:

1. The spline fitting method introduces the least error into the crack growth rate.

2. There is an optimum Δt measurement increment that will minimize the error in crack growth rate calculation.

3. The time range of the crack growth transition zone is insensitive to the change of the initial crack length and the nonuniform gross strain field.

4. The crack growth resistance curve is insensitive to the initial crack length.

5. In the stable crack growth stage, the effect of the initial crack length and the nonuniform gross strain field on the crack growth behavior is negligibly small.

6. A power law relationship exists between the crack growth rate $\frac{da}{dt}$ and the stress intensity factor K_I.

7. The eccentricity of the crack has no significant effect on the crack growth behavior.

8. When the crack grows into a lower nonuniform, gross strain field, the crack growth behavior shows a pronounced cyclic fluctuation.

Crack Growth Behavior in the Presence of Strain Gradients....

OBJECTIVE: Investigate Effect of Gross Strain Gradients on Crack Growth Behavior in Solid Propellant.

APPROACH:

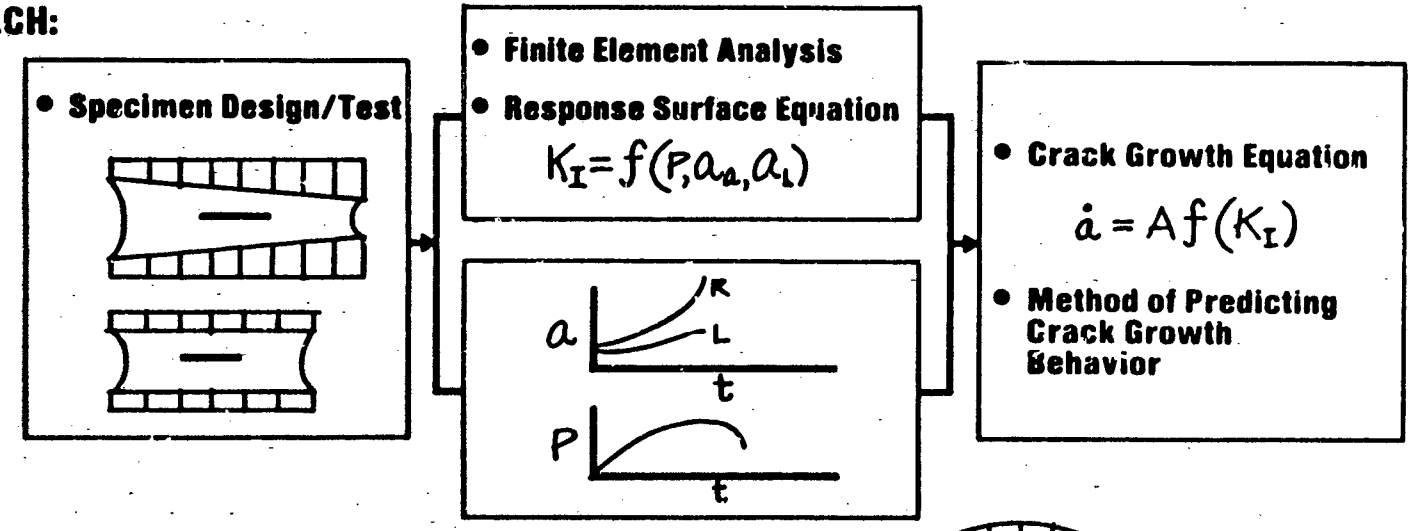

ISSUES:

- How does Nonuniform Gross Strain Affect Crack Initiation and Propagation?
- Is Instantaneous Crack Growth Behavior Controlled by Instantaneous Stress State Near Crack Tip?

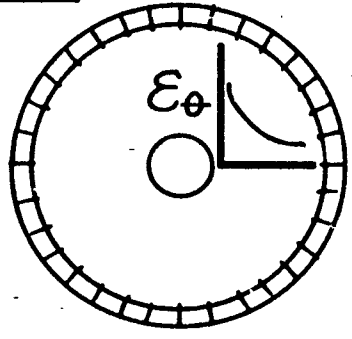

Figure 1 Schematic Representation of Basic Approach

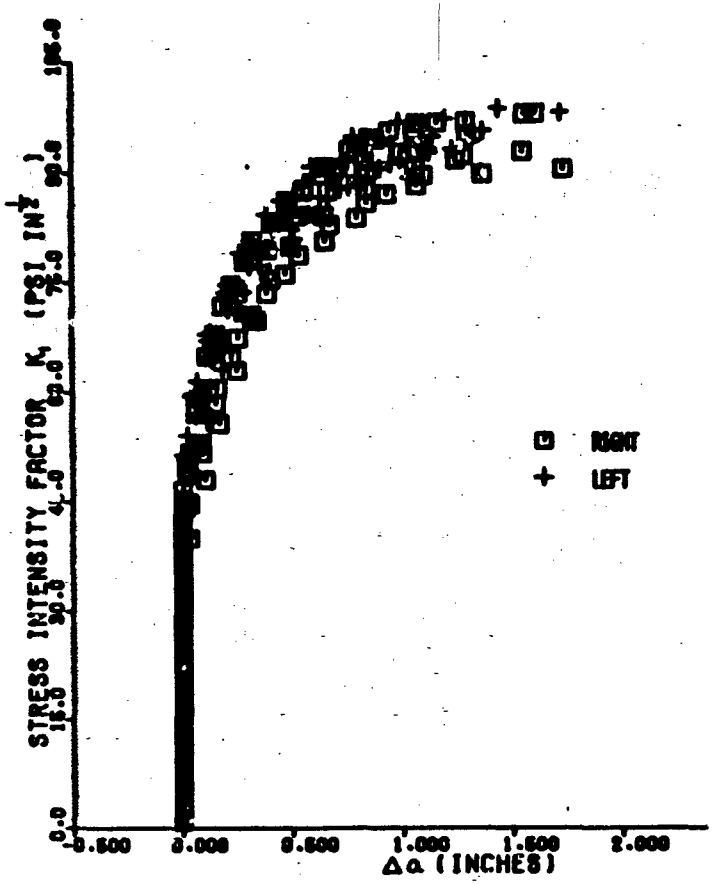

(a) Stress Intensity Factor K_I VS Crack Increment Δa

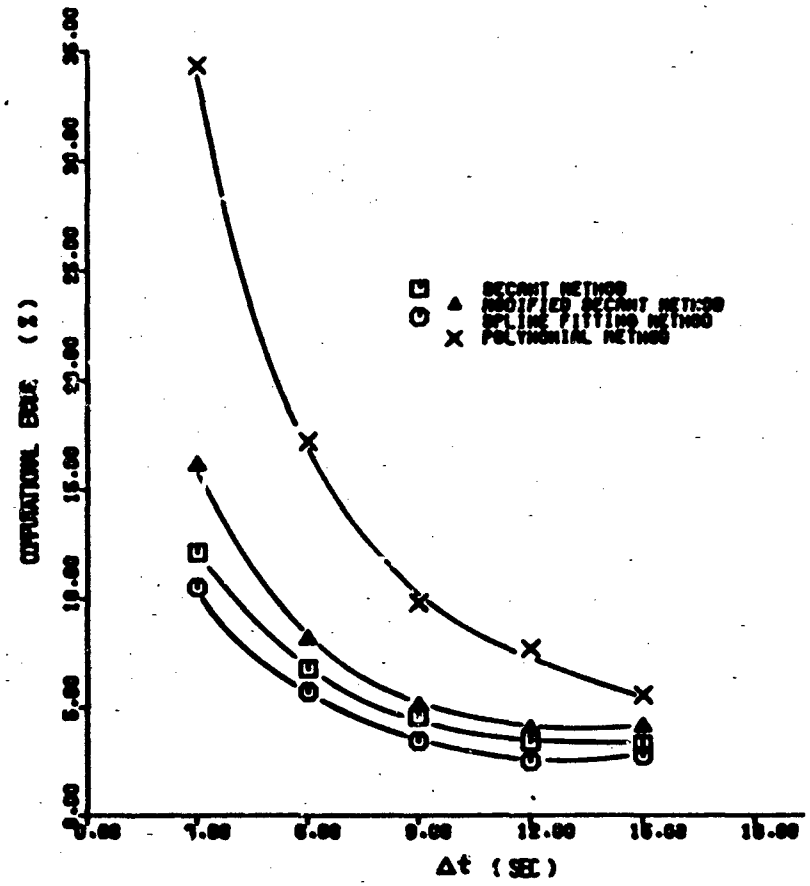

(b) Computational Error VS Time Increment Δt

Figure 2 Experimental Results

NONLINEAR MODELING AND METHOD OF PREDICTING CRACK GROWTH

C. T. LIU
Air Force Rocket Propulsion Laboratory
Edwards AFB CA 93523-5000 (805) 277-5502

In the past decade, many experimental studies were directed primarily toward the characterization of fracture behavior in solid propellants under various loading conditions. The experimental results revealed that despite the nonlinear nature of these types of materials, linear viscoelastic fracture mechanics theory or slightly modified nonlinear versions had been successfully used in characterizing the crack growth behavior in some propellants. However, it should be pointed out that the verifications were limited to rather ideal stress states and simple loading conditions. Therefore, in order to characterize the fracture behavior in solid propellant, under realistic and general loading conditions, the effect of material nonlinearity on the crack initiation and the subsequent crack growth is required.

The objective of this study is to develop a nonlinear crack growth model which can be used to characterize crack growth under large deformation conditions and to determine the range of applicability of the linear theory in predicting crack growth.

The approach will involve a combination of analytical and experimental studies. Experiments (destructive and nondestructive) will be conducted to determine the failure process, the damage zone, the failure property, and the strain field ahead of the crack tip. This information will be used to determine the damage parameters associated with the nonlinear viscoelastic constitutive equation and to determine, together with the criteria developed from the theoretical analysis, the failure process zone. The material response near the crack tip will be modeled by the 2-D nonlinear viscoelastic constitutive equation. This crack tip model and the generalized path-independent J-integral, developed by Schapery, will be incorporated into a computer code to calculate the value of the J-integral. This information will be used to predict crack initiation and propagation in solid propellants under various loading conditions.

The preliminary damage zone study was conducted by using the acoustic imaging technique. A typical result is shown in Figure 2. The contours shown in Figure 2 are the acoustic fringes of a strained propellant which indicate the intensity of the damage developed in the material. It can be seen that, near the crack tip region, the shape of the contours or the damage zones are commensurate with the stress fields developed in the material and they resemble the plastic zones near the crack tip in ductile metals. This preliminary study suggests that the acoustic imaging technique can be a promising technique to determine the damage zone size in solid propellants.

Nonlinear Modelling and Method of Predicting Crack Growth....

OBJECTIVE: Investigate Crack Tip Damage and Develop Crack Tip Model for Predicting Crack Tip Growth

APPROACH:

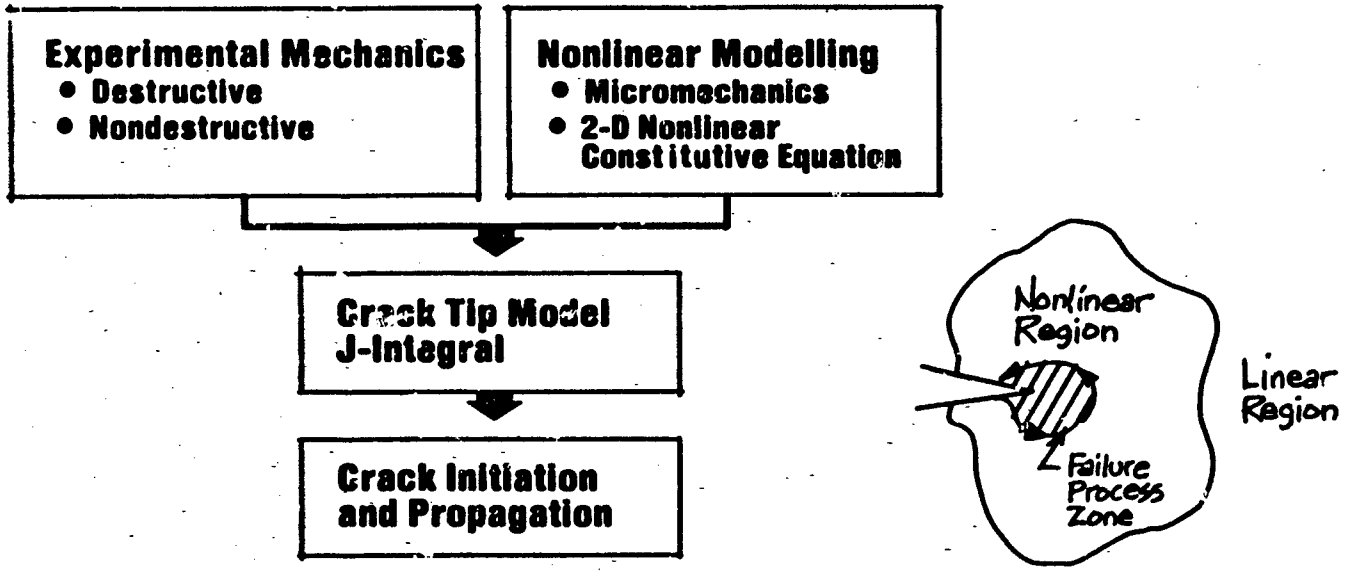

ISSUES:
- What is Definition of Faiure Process Zone?
- How does Nonlinear Behavior Near Crack Tip Affect Crack Growth?
- Is Schapery's J-Internal Theory for Predicting Crack Growth Behavior Valid?

Figure 1 Schematic Represcntation of Basic Approach

Figure 2 Acoustic Fringe Pattern of Strained Propellant Specimen

HIGH-RESOLUTION MOVIES OF PROPELLANT DEFLAGRATION

Roger J. Becker, Paul F. Luehrmann, and Janet L. Laird
University of Dayton Research Institute
Dayton, Ohio 45469

This program has been designed to enhance our understanding of the behavior of the particles at the surface of a grain during deflagration. A special emphasis has been placed on qualitative knowledge of particles and agglomerates ranging in size from 20 to 70 μm. Cooperative behavior and the nature of the immediate particle environment are of particular concern. The ultimate goal of this initiative is experiments correlating particle behaviour with external parameters, such as the flow field and pressure oscillations.

Our approach has been to exploit the unique capability of the newly developed copper-vapor laser as a light source for front-lit cinephotography. The 30 ns pulse width, 1.2 mJ pulse energy, and 5 kHz repetition rate of this laser are ideal for front-lit cinephotography. The short pulse width freezes the motion, the high-energy, monochromatic pulse penetrates the flame, and the 5 kHz repetition rate captures dynamic phenomena. We have also developed a diode-array detector for our servo positioner, due to severe depth-of-field restrictions.

We have succeeded in making movies during pressured burns on wide-distribution propellants. Our diode-array detector has worked well and our movies are immune to flame brightness, show no motion blur, and have enabled us to photograph the intermediate sized (20 μm) particles and their agglomerates. In all movies using different formulations, the intermediate sized particles are seen to undergo rapid and large amplitude oscillations, as if tethered to the surface by fine fibers.

We are developing an improved inhibitor for strand burns that gives no smoke, causes little flaking, and is relatively successful in preserving the strand profile. We have also built and tested an optical correlator for quantitative analysis of our films. An optical approach allows for parallel data processing, and is therefore both fast and economical. Preparations for stereo movies are in progress.

APPROACH

- IN-SITU, HIGH-RESOLUTION CINEMATOGRAPHY

TIMING SEQUENCE

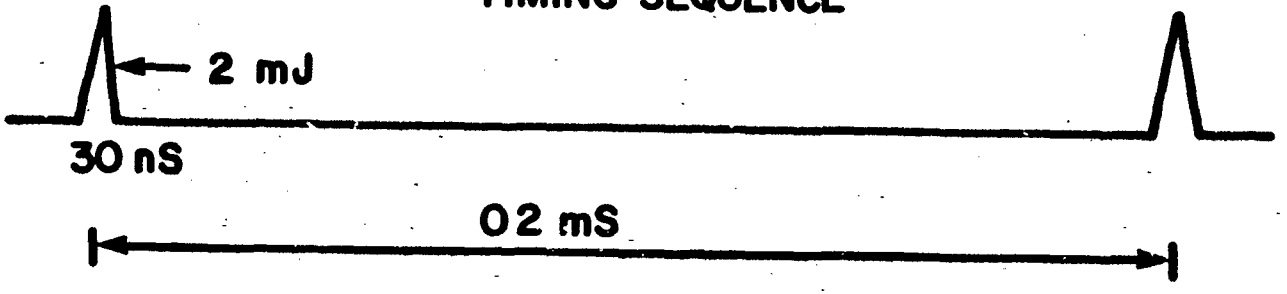

- ELIMINATES MOTION BLUR
- PIERCES FLAME INCANDESCENCE
- AMPLE LIGHT FOR FINE-GRAINED FILM

RESULTS

- NO MOTION BLUR
- PUNCHES THROUGH FLAME
- RESOLVES INTERMEDIATE SIZED PARTICLES
- INTERMEDIATE PARTICLES DANCE ON SURFACE AT UP TO 200 PSI

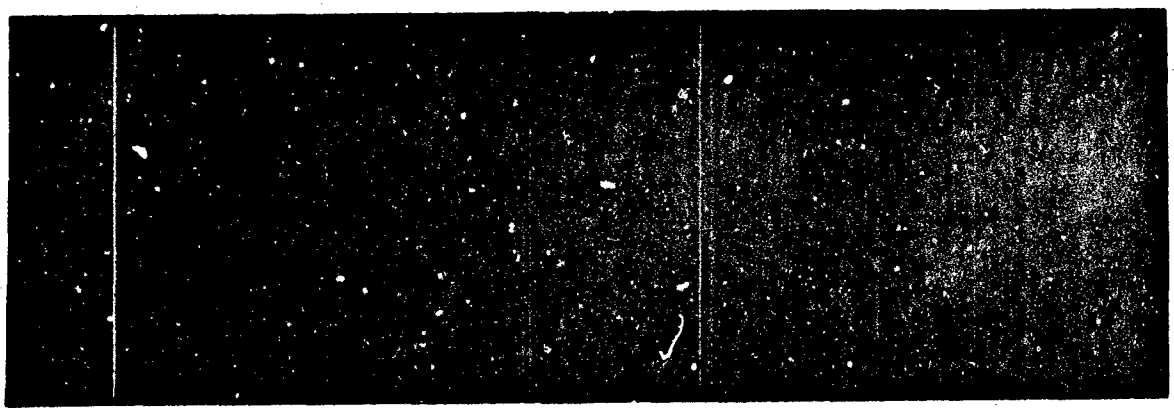

- DEVELOPING IMPROVED INHIBITOR
- DEVELOPING OPTICAL CORRELATOR

WIDE DISTRIBUTION PROPELLANTS

Robert A. Frederick, Jr. and John R. Osborn
School of Aeronautics and Astronautics
Purdue University
West Lafayette, Indiana 47907

Composite propellants containing a wide AP particle size distribution have exhibited unpredictable ballistic properties. Highly loaded propellants of this type do not burn continuously but show local stepwise burning patterns at the propellant surface. The propellant burns quickly for a short period of time, then "rests" for a short period of time. The increments of burning occur over distances comparable to the diameter of the coarse AP, while the rest period has been linked to the energetic properties of the binder for IPDI and DDI formulations.

These observations challenge previous conclusions that propellant burning rate is controlled largely by the deflagration of individual oxidizer crystals and their surrounding binder. Scenarios which describe propellant combustion as strictly a time average or area average process are inadequate to describe this local intermittent combustion. It now appears possible that AP particle ignition and binder pyrolysis are controlling combustion mechanisms, at least for wide distribution formulations.

The goal of this research program is to identify conditions which produce local stepwise burning of solid propellants and to identify the physical processes that control the duration of the burn periods and "rest" periods. Perfecting a technique to continuously measure the local burning rate is a major task in achieving this goal. Measurements will first be completed using high-speed photography as a preliminary screening tool. The desired technique, however, is a direct measurement using a laser position detector (LPD). This LPD is being designed and developed to continuously record spatially local (40 micron diameter circle), high resolution (20 micron) distance measurements. With an adequate technique perfected, systematic composition variations will be examined to determine the role of AP ignition and combustion properties, and the energetic nature of the binder on the local and average burning rate. Specifically, the binder curative, oxidizer modal size ratio, and pressure will be investigated as independent variables.

The significant achievement to date has been the continuous measurement of average burning rate of solid propellant burning at atmospheric pressure by sensing the position of a modulated laser beam reflected from the propellant surface. The instrument tested compensated for the variable optical properties of the propellant surface and the combustion gases.

FEATURES OF APPROACH

- o HETEROGENEOUS SURFACE CHEMISTRY
  - LARGE SIZE DIFFERENCE BETWEEN COARSE AND FINE AP
- o FIRST DIRECT MEASUREMENTS
  - MEASUREMENT OF LOCAL MICROSCOPIC NON-STEADY BURNING
- o SYSTEMATIC VARIATIONS
  - AP DECOMPOSITION CHARACTERISTICS
  - BINDER ENERGETICS

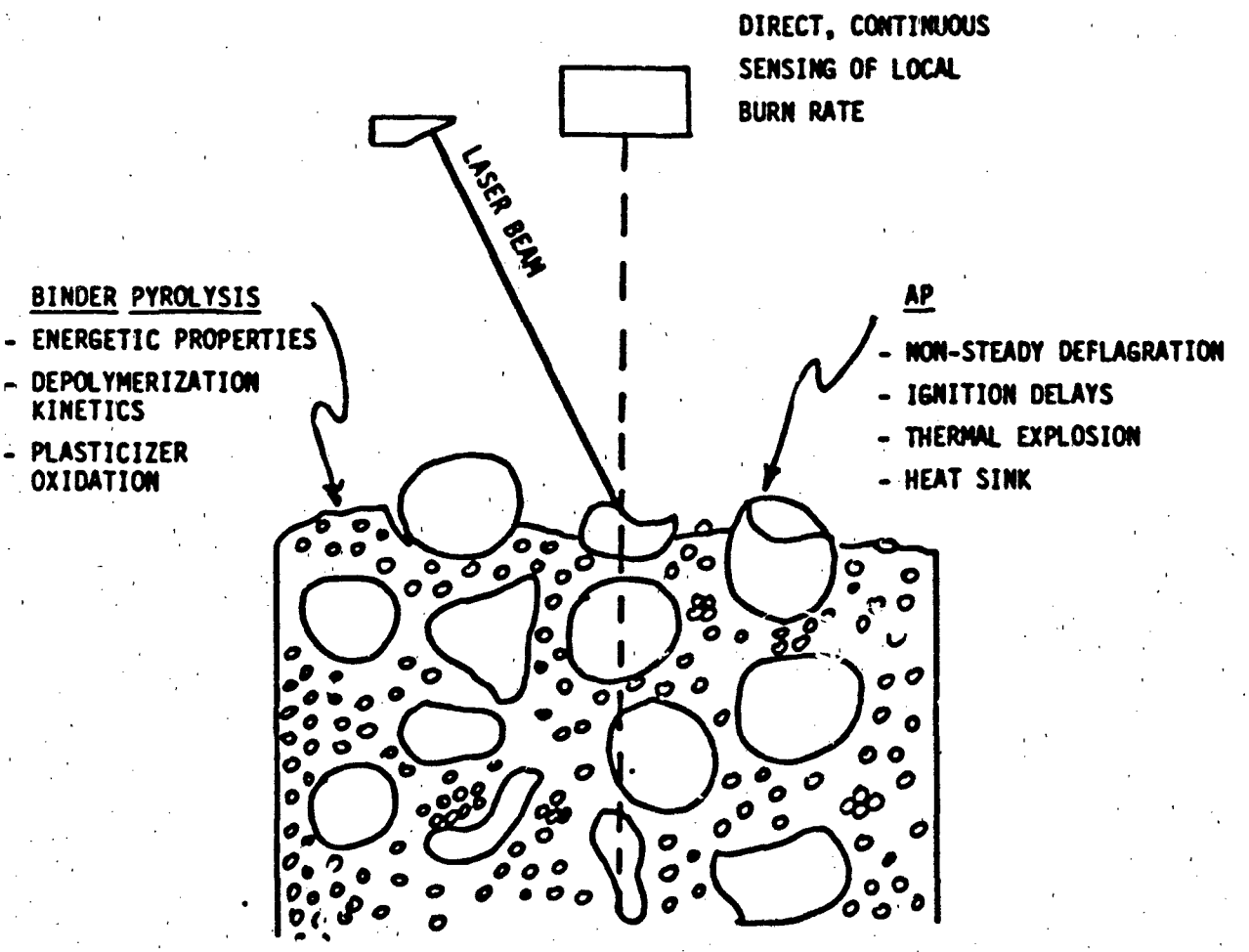

PRIMARY SCIENTIFIC ACCOMPLISHMENTS...

o ACHIEVED

- CONTINUOUS MEASUREMENT OF SURFACE HEIGHT AT ATMOSPHERIC PRESSURE

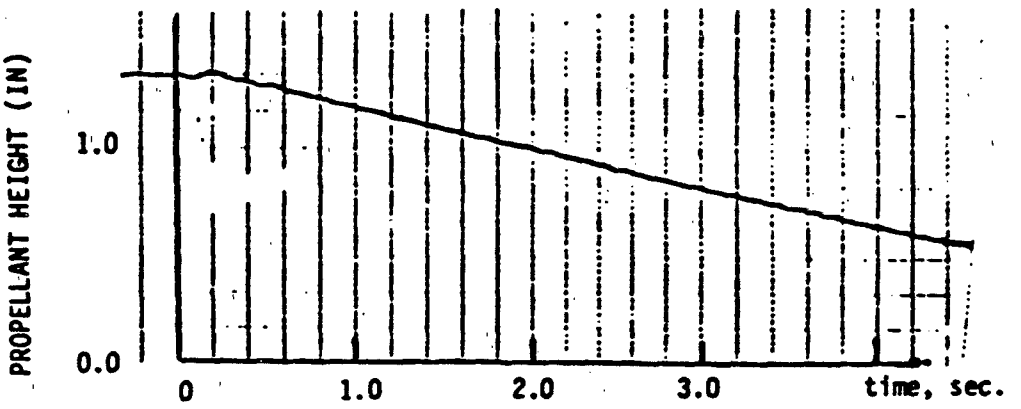

o ANTICIPATED

- EFFECT OF BINDER ENERGETICS ON MICROSCOPIC NON-STEADY COMBUSTION
- EFFECT OF SURFACE HETEROGENEITY ON AP IGNITION DELAYS

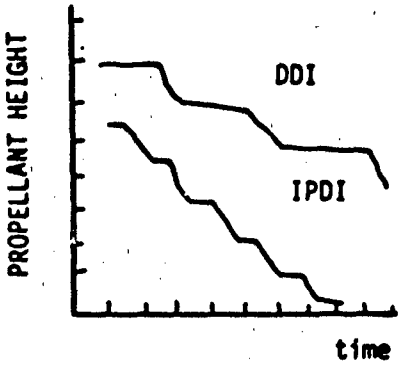

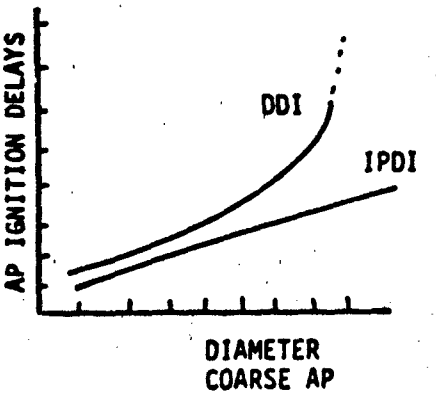

Coupling Between Velocity Oscillations and Solid Propellant Combustion

R. S. Brown, A. M. Blackner, P. G. Willoughby, and R. Dunlap

United Technologies/Chemical Systems Division
San Jose, CA 95150-0015

Cold-flow studies are being conducted to define and characterize the basic flowfield and heat transfer mechanisms controlling the coupling between the acoustic velocity and the solid propellant combustion zone. This coupling produces a substantial effect on the overall stability of the combustion pressure, yet substantial deficiencies exist in the current basic knowledge.

Previously reported measurements of the oscillatory heat transfer demonstrate that this coupling is extremely nonlinear at relatively low acoustic pressures (< 0.4%). The data also show that the current heuristic model for velocity coupling (which is incorporated into the Standard Stability Prediction Program) is largely wrong; the differences in the head-end and aft-end coupling are reversed from those predicted by the conceptual model.

Radial profiles of the acoustic velocity have been measured at several axial stations for two surface Mach numbers, frequencies, and acoustic pressure levels. The data, when normalized to the head-end acoustic pressure, show that at low acoustic pressures (i.e., 0.05%), the acoustic waves extend across the entire cross-section in the region upstream of the transition in the mean velocity profile, with nonplanar and nonlinear behavior observed in the near surface regions. Downstream of the velocity transition, the acoustic waves do not penetrate through the near wall turbulence. At higher acoustic pressures (i.e., 0.4%) the upstream nonlinearities increase in magnitude and extend across the entire port. Downstream of the velocity transition the core nonlinearities decay while the linear component penetrates through the turbulence to the wall. These results are completely consistent with the oscillatory heat transfer measurements. They further substantiate the large error in the conceptual model of the fluid mechanics used to predict velocity coupling effects in motor stability predictions.

Based on these results, some important characteristics of an improved velocity coupling model for linear stability predictions can now be formulated. There is a threshold position along the propellant grain upstream of which the propellant surface responds to the acoustic velocity. Downstream of this position, the propellant does not respond to the acoustic velocity. The threshold position appears to be defined by the growth of turbulence in the flow near the propellant surface. Wall blowing/acoustic interactions produce surface heat transfer oscillations which are not "in phase" with the centerline acoustic velocity. This proves that the combustion response based on driving by the centerline velocity must quantitatively account for both propellant and flowfield effects.

Figure 1. Velocity Coupling with Propellant Combustion

- Goal
  - Characterize Interactions of Acoustics Turbulence and Heat Transfer to Blowing Surface
- Experiment
  - Cold Flow Simulation
- New Observations
  - Velocity Coupling Models Wrong
  - Acoustic Waves Very Nonplanar Large Radial Amp./Phase Shifts
  - Strong Turbulence/Acoustic Interaction - Coherence Shifts
- Future
  - Is Coherence Decay Turbulence Damping or Refraction?
  - Has Significant Effect on Turbulent Acoustic Interaction

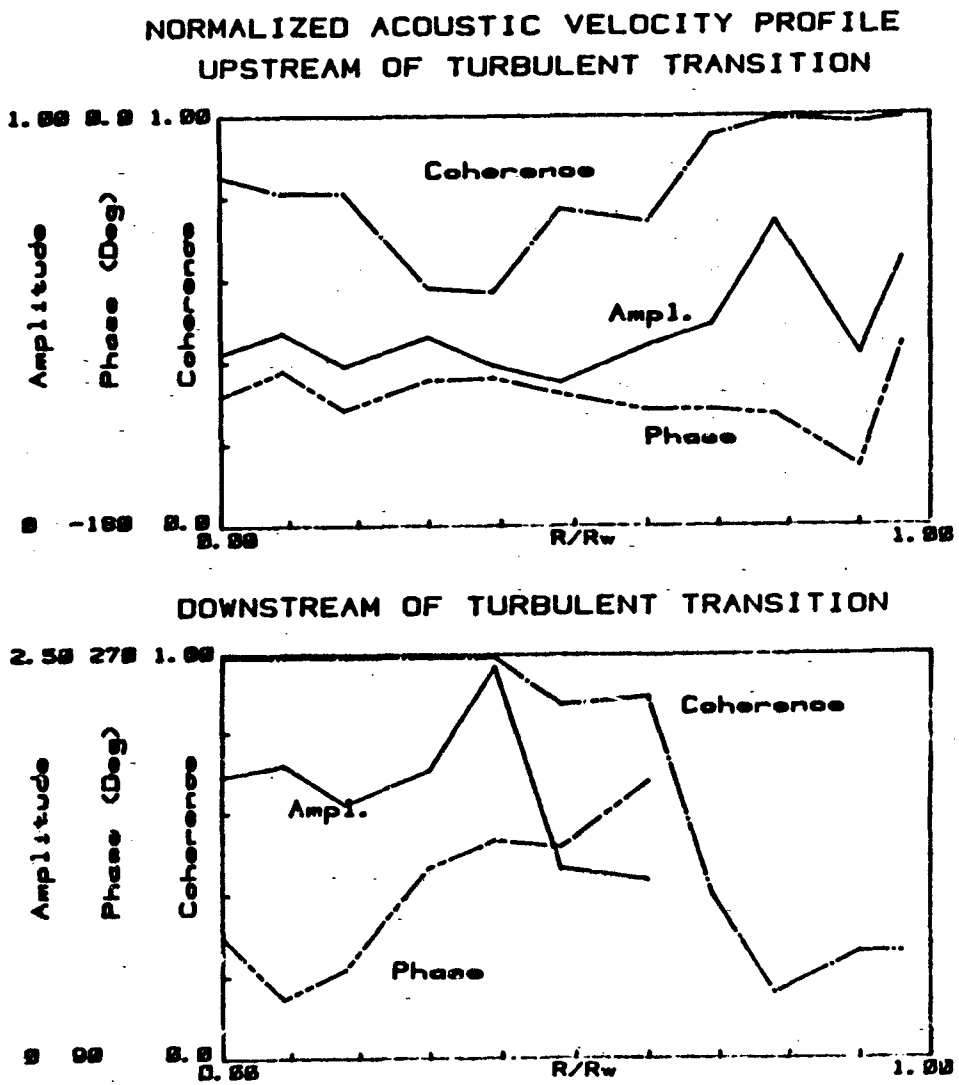

FIGURE 2. CURRENT QUALITATIVE FLOWFIELD MODEL

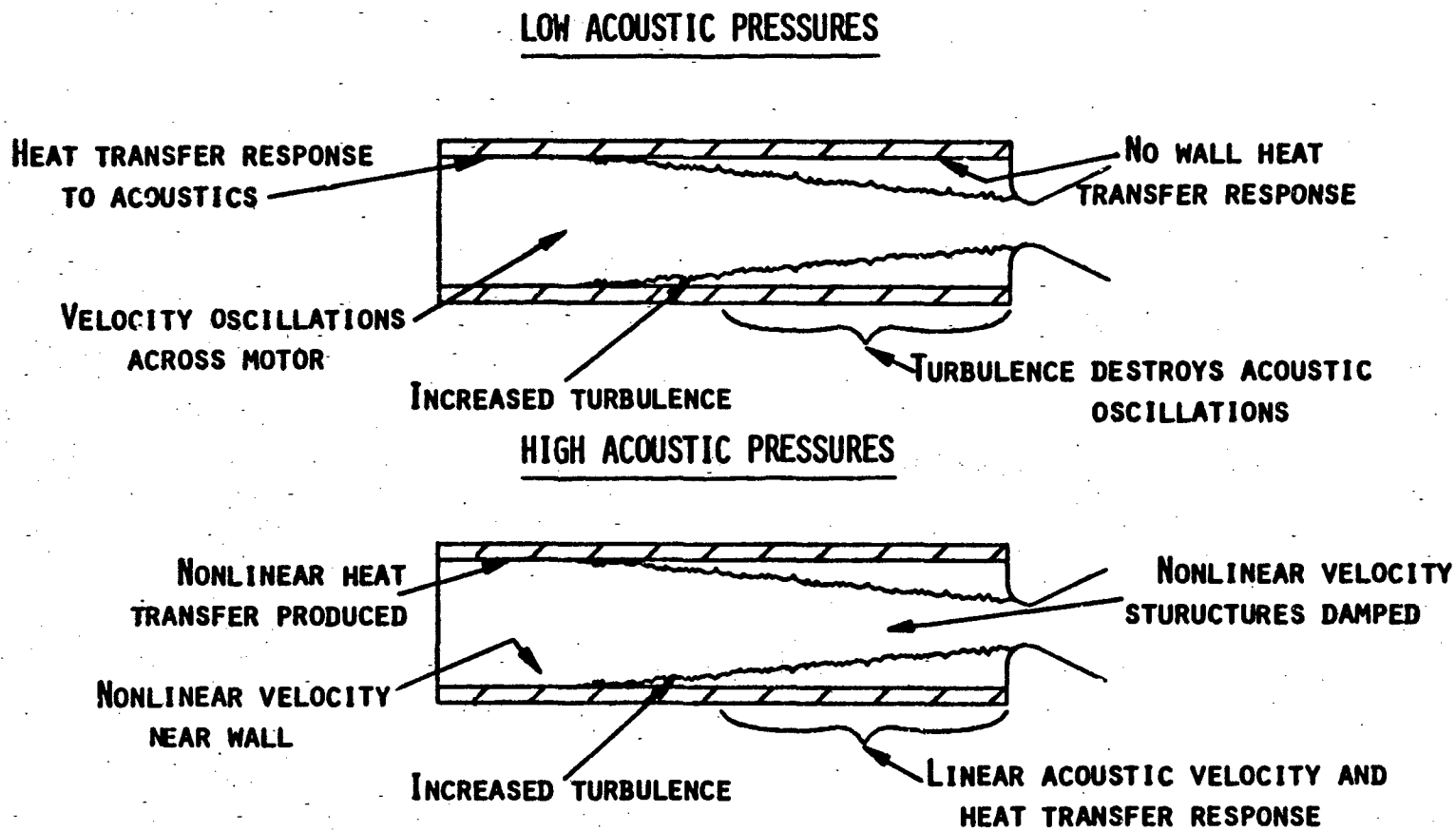

FLAME-ACOUSTIC WAVE INTERACTION DURING AXIAL SOLID ROCKET INSTABILITIES

Ben T. Zinn, Brady R. Daniel, Jechiel J. Jagoda, Uday Hegde and Subra V. Sankar

Aerospace Engineering,
Georgia Institute of Tecnhlogy
Atlanta, Georgia, 30332

This theoretical and experimental research program is concerned with the determination of (1) the processes which control the driving of axial instabilities by solid propellant flames and (2) whether existing models can indeed determine the interactions between solid propellant flames and oscillatory flow fields. Since experimental investigation of actual solid propellant flames is currently not possible because of the extremely small dimensions of their combustion zones, the present study investigates the characteristics of a premixed, flat flame stabilized within an acoustic boundary layer next to a porous side wall in a specially developed experimental setup, see Fig. 1. In this setup, a combustible mixture enters the duct through the porous side wall and it burns in a flat flame stabilized at some distance downstreem of the wall which permits performing the indicated diagnostics. Simultaneously, the response of this flame to acoustic excitation is modeled using an approach similar to those utilized to model the responses of solid propellant flames. This model requires the steady temperature distribution within the flame $\bar{T}(y)$, the wall admittance Y_w, the acoustic pressure p'_e and the steady wall velocity $\bar{v}(y=0)$ as inputs and it predicts the normal acoustic velocity at the boundary layer edge v'_e which determines the local flame driving. To check the validity of the developed model, both the required input data and the predicted quantity (i.e., v'_e) will be measured and v'_e will be compared with the model predictions. In addition, the experimental efforts will investigate the possible presence of unusual features such as vortex sheets, distortions and turbulence within the flame. These studies will be conducted for combustible mixtures having different compositions, for different wave amplitudes and frequencies and for flames located on different portions of the standing acoustic wave structure.

Todate, the development of the theoretical model has been completed and typical predictions of the distributions of the acoustic solutions in the flame are shown in Fig. 2. Interestingly, these solutions show that driving occurs(i.e., v'_e increases) in the region of the flame heat release. In addition, this model shows that (1) contrary to earlier analyses, the steady shear $\partial\bar{u}/\partial y$ cannot be neglected in the vicinity of acoustic pressure nodes, (2) periodic vortices are present within the flame and (3) the flame driving depends upon the steady velocity at the wall, the wall response and the steady state flame characteristics. Finally, computations were performed to determine the ranges of frequencies and steady velocities at the wall for which the model is valid.

RESEARCH OBJECTIVES (1) Determine the gas phase processes which contribute to flame driving during combustion instabilities.

(2) Determine whether state of the art models can describe the driving provided by oscillatory gaseous flames.

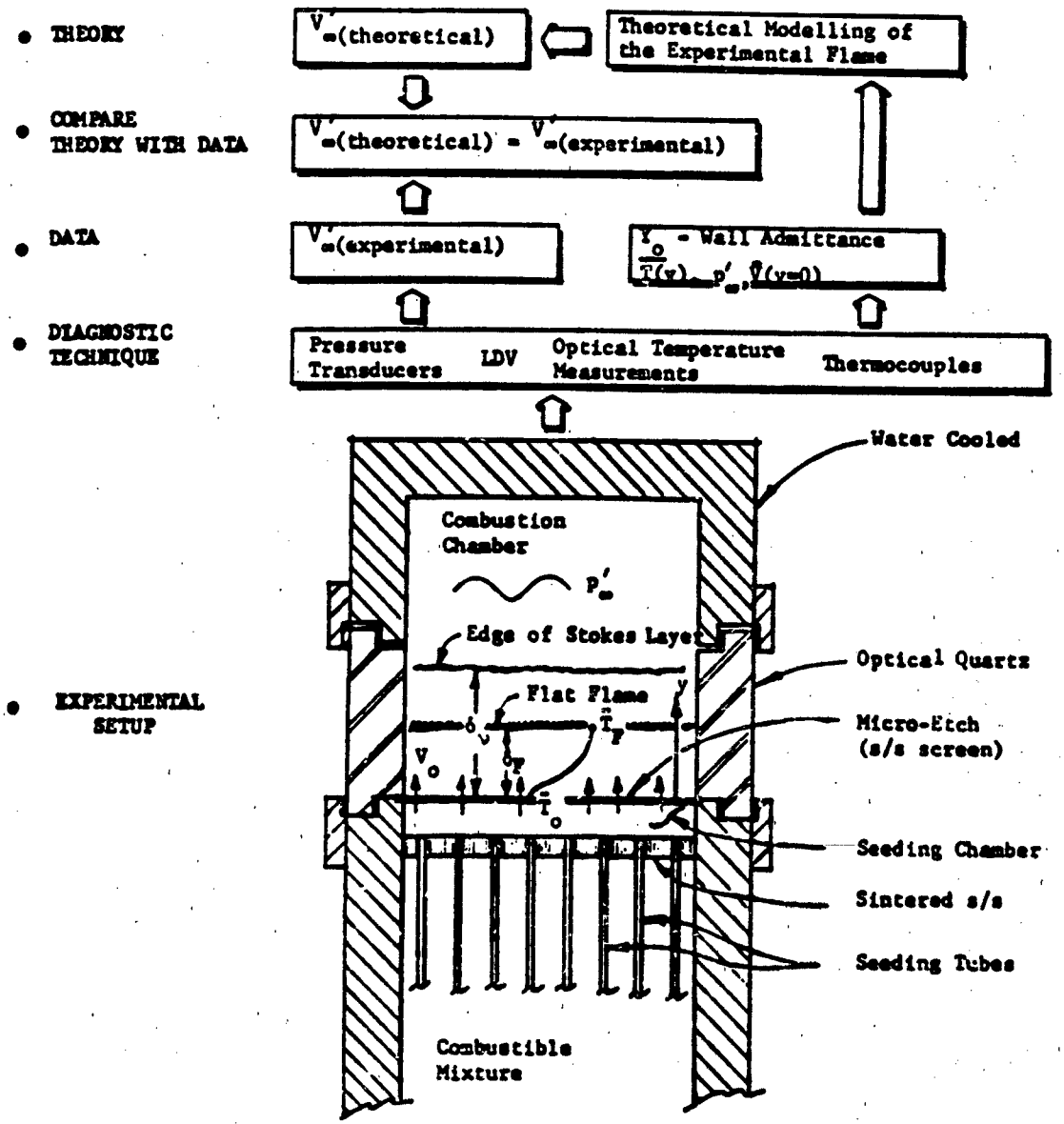

Figure 1. An Outline of the Proposed Research Approach (top) and a Schematic of a Cross Sectional View of the Developed Experimental Setup and Flat Flame

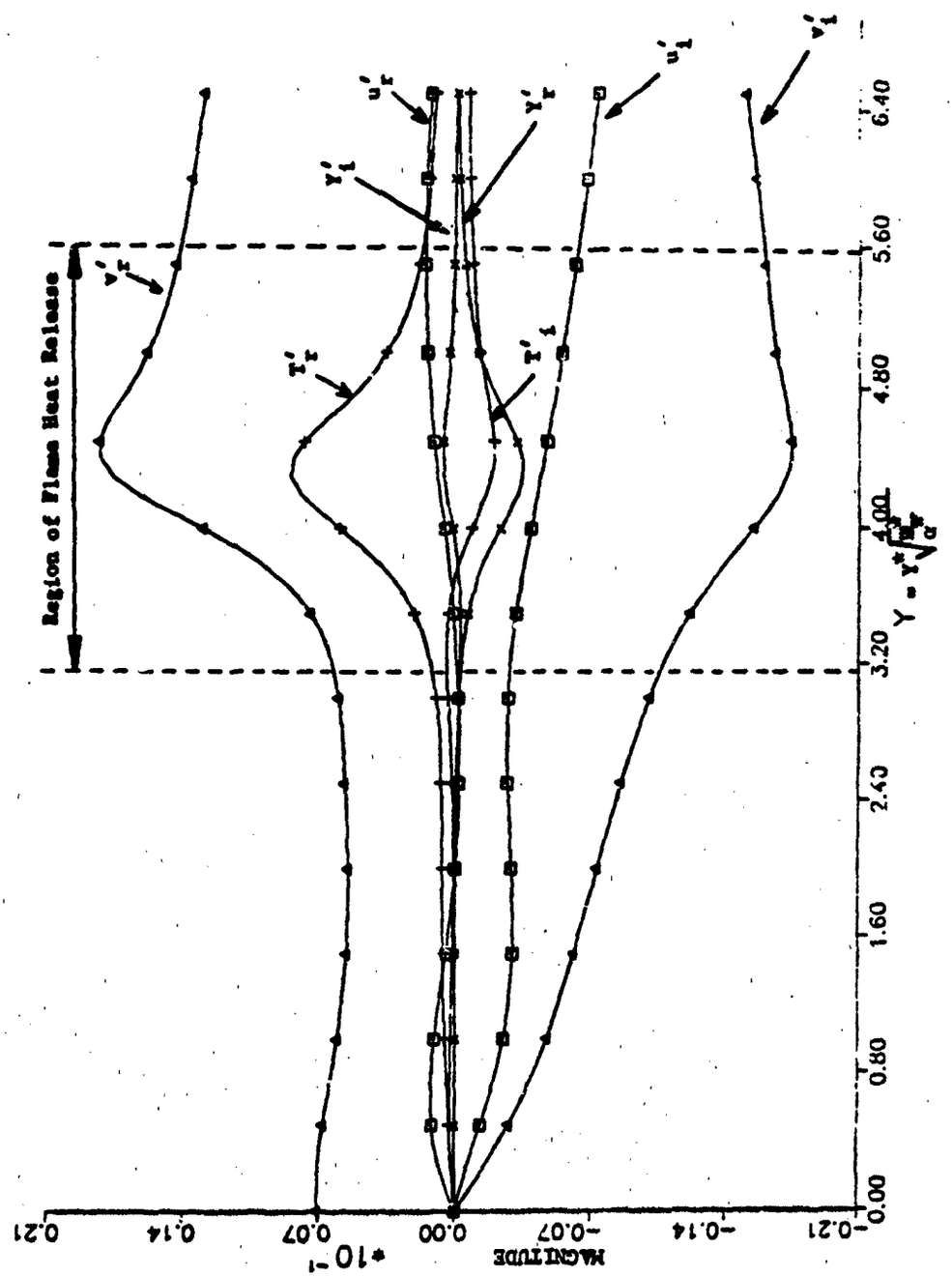

Figure 2. Predicted distributions of the real and imaginary parts of the normal v′ and axial u′ velocity components, the fuel mass fraction Y and the temperature T′ within the acoustic boundary layer. V′ describes the driving provided by the flame region. Note that the driving increases in the region where energy is released by the flame.

MECHANISMS FOR ACOUSTIC SUPPRESSION

Principal Investigator: Merrill W. Beckstead
Coinvestigator: R.L. Raun
Brigham Young University, Provo, Utah 86402

Acoustic suppressants are commonly added to low smoke and smokeless propellants to avoid the problem of combustion instability. Suppressants apparently work by one or more of three mechanisms: (1) energy loss due to viscous dissipation due to drag forces, (2) modification of the propellant combustion response function, or (3) energy interchange due to distributed combustion.

Viscous dissipation of acoustic energy by drag forces on a suspended particle is the most commonly recognized mechanism, being a direct analogy to suspended moisture in a fog. A second mechanism can occur with solid additives within the propellant that has a catalytic influence on the combustion response. The third mechanism considered is due to the effect of a particle burning as it traverses a relatively large portion of the system. As it does so, the interchange of energy between the burning particle and the acoustic environment can result in either a driving or damping contribution to the acoustics of the system. This third mechanism is the primary area of study of the current contract.

The principle objective of this work is to identify and develop an understanding of the mechanisms whereby acoustic suppressants modify an acoustic wave. Figure 1 is a graphic illustration of the approach, some of the technical advantages, the data to be collected and the data analysis to be performed. In the past, T-burners have usually been used to make measurements to study additives. The experimental basis for the technical approach of this study is the Rijke burner. The Rijke burner is a gas burner with a paddle to control (stop and start) combustion oscillations, over frequencies ranging from 500 to 1500 Hz. The unique advantage of this approach (i.e. using the gas fired Rijke burner), allows separation of the three mechanisms mentioned above by testing an additive independent of the propellant burning surface. Other advantages include avoiding use of solid propellants, and allowing for independent control of frequency, O/F ratio, temperature and particle addition.

Figure 2 summarizes the most significant data obtained during the past year. Al and ZrC are commonly added to solid propellants and exhibit significantly different combustion characteristics, Al being very reactive and ZrC slightly reactive. The experimental results obtained using Al and ZrC in the Rijke burner (Figure 2) indicate that both additives do cause a increase in the acoustic growth rate when compared to growth rates obtained without any particles in the system. The increase caused by Al is greater than that caused by ZrC. Because the reaction of Al releases more than twice the energy ZrC does, it would be expected to have a greater influence on the system than ZrC. The increase in the acoustic growth rate is apparently the result of energy being added to the system by the distributed combustion of the particles.

MECHANISMS FOR ACOUSTIC SUPPRESSION

How Do Suppressants Work in Solid Propellant Rocket Motors?

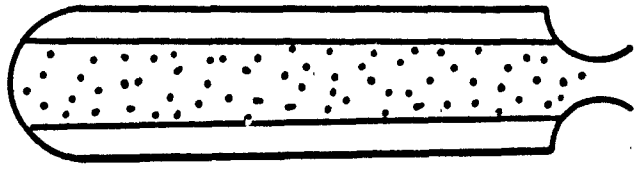

Mechanisms of Acoustic Suppressants:

Viscous dissipation due to drag forces
Modification of propellant response function
Effect of distributed combustion

CURRENT PROGRAM:

- Separate Effects of Different Mechanisms Using
- Unique Experiments

- The Modified Rijke burner

  - Use gas (eliminates solid propellant)
  - Evaluate acoustics w/o particles
  - Can feed particles independently
  - Vary particle type, size and concentration
  - Evaluate reactive or inert particles
  - Use paddle to control acoustic growth

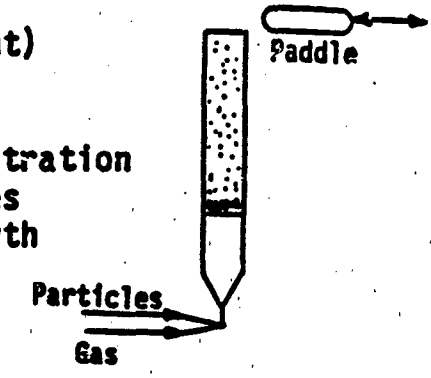

- Results

  - Monitor particle combustion with high speed movies
  - Evaluate acoustic growth rates with and without particles
  - Evaluate mechanisms of reactive versus inert particles
  - Measure effect of pertinent parameter

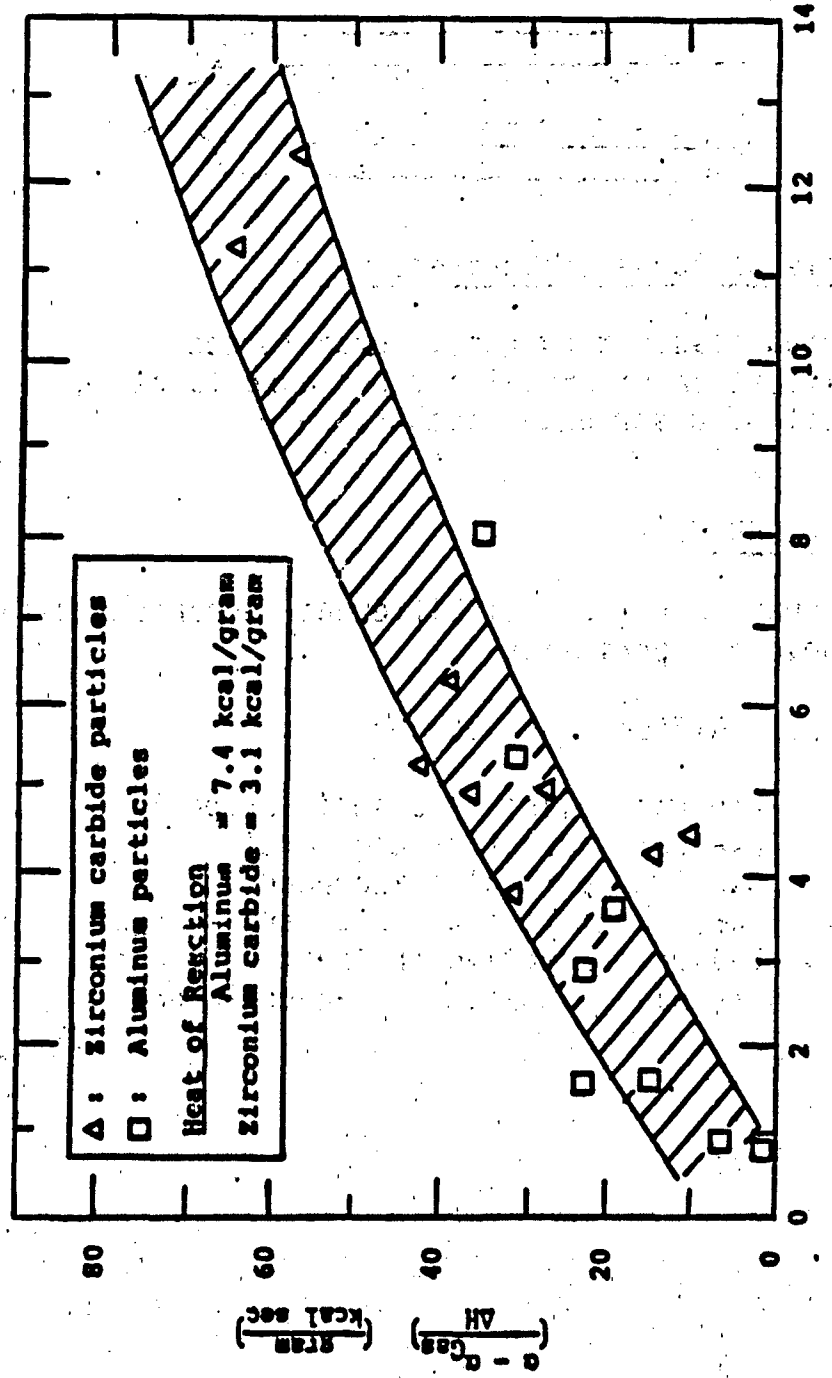

Figure 2. "Pseudo" acoustic growth rate vs. mass fraction of 13 micron aluminum and 7 micron zirconium carbide (mass mean diameter)

FLOW FIELD EFFECTS ON COMBUSTION INSTABILITY

T.J. Chung

Department of Mechanical Engineering
The University of Alabama in Huntsville

The main topic of research during the past two years has been the theoretical and numerical studies of the coupling mechanism of acoustic and hydrodynamic wave oscillations and its effects on combustion instability. The so-called "hydrodynamic stability boundary" concept is well known, as illustrated in Fig. 1a. A question arises: What happens if acoustic oscillations are coupled with the hydrodynamically oscillating system?

To see this phenomenon, consider the rocket motor simulator in Fig. 1b. We derive, by means of Green's function integrals, an expression for the growth constant in the form, $\alpha=\alpha_A + \alpha_H$, where α_A and α_H refer to the growth constants corresponding to acoustic and hydrodynamic oscillations, respectively. α_A is a function of the mean flow velocity, acoustic pressure and frequencies, whereas α_H is a function of additional variables such as the vortical component of velocity and hydrodynamic (vortical) frequencies as well as those for α_A. Finite elements are utilized for calculations of mean flow fields, eigenvalue analyses, and the evaluation of the growth constant integrals. For a given excited acoustic frequency and Reynolds number, we plot the α_H versus hydrodynamic frequencies, as shown in Fig. 2a (solid lines). This information leads to acoustic-coupled hydrodynamic stability boundaries (see Fig. 2b). Similar graphs can be constructed for other combinations of excited acoustic frequencies to identify the most critical cases.

Based on this research, we conclude that an acoustic coupling with hydrodynamic oscillations causes the hydrodynamic stability boundaries to expand into higher as well as lower frequency regions. Furthermore, there are some regions of damping (stable) due to acoustic coupling otherwise unstable. This phenomenon divides the single hydrodynamic stability boundary region into several (typically three) regions. It suggests that there are certain combinations of acoustic and hydrodynamic frequencies at which stable and unstable situations arise, and the method of analysis described herein provides such predictions. Can this be substantiated by laboratory measurements? This subject is considered as a challenging future laboratory experimental task.

Other research activities during this period include particle damping based on multi-dimensional flow field analysis and two-dimensional response function calculations as listed below.

Chung, T.J. and Sohn, J.L., "Interactions of Unsteady Acoustic and Vortical Oscillations in Axisymmetric Cylindrical Cavity", AIAA Paper No. 84-1635, 1984.

Chung, T.J. and Chan, S.K., "Particle Damping Effects on Combustion Instability", AIAA Paper No. 84-0373, 1984.

Chung, T.J. and Kim, P.K., "A Finite Element Approach to Response Function Calculations for Solid Propellant Rocket Motors", AIAA Paper No. 84-1433, 1984.

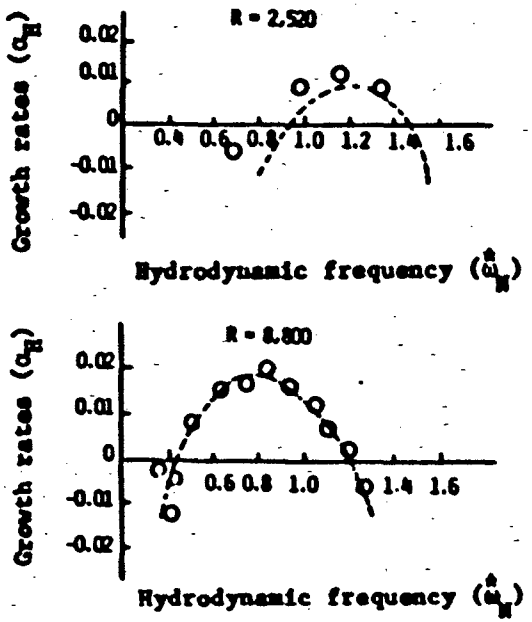

Fig. 1a Measurements of growth rates vs hydrodynamic frequency for various Reynolds numbers by Schubaur and Skramstad [1947] using hot wire anemometers on a flat plate and calculations by Kaplan [1964] for hydrodynamic instability

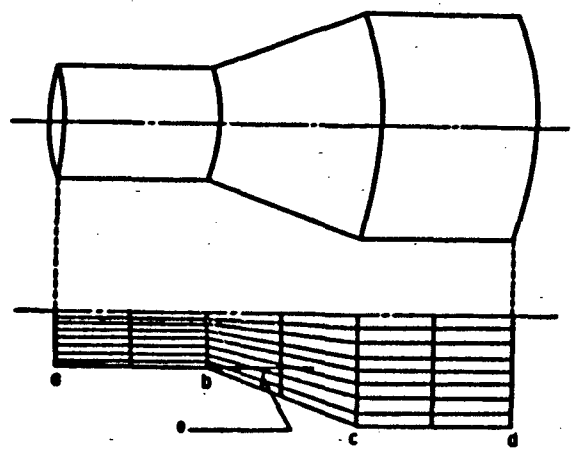

Fig. 1b Axisymmetric cylindrical geometry of a solid propellant rocket motor simulator and finite element modeling for calculations of coupled acoustic-hydrodynamic growth constants (α_A, α_H) for combined hydrodynamic-acoustic stability boundaries

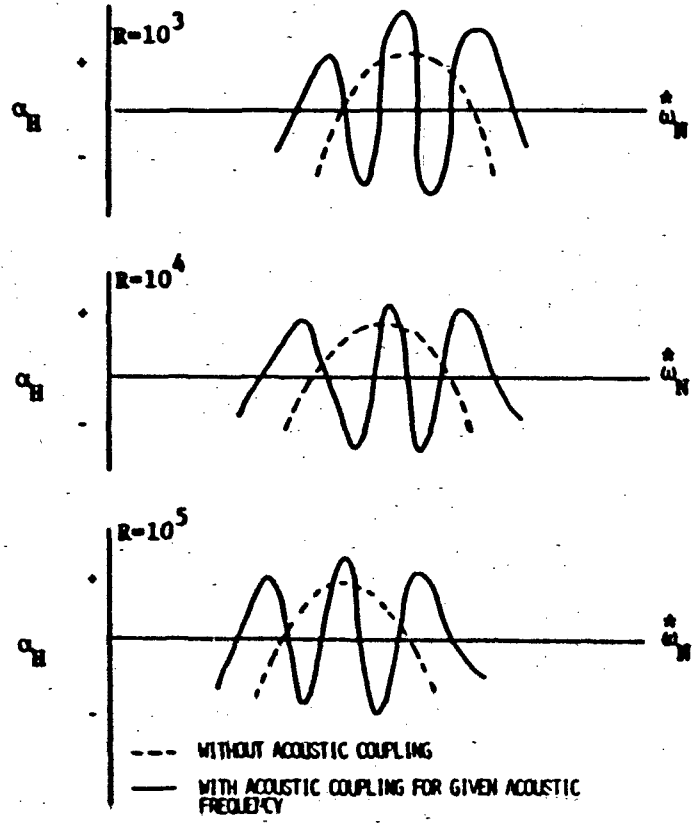

Fig. 2a Hydrodynamic growth constants (α_H) vs hydrodynamic (vortical) frequency ($\hat{\omega}_H$), α_H=0 indicating the stability boundaries

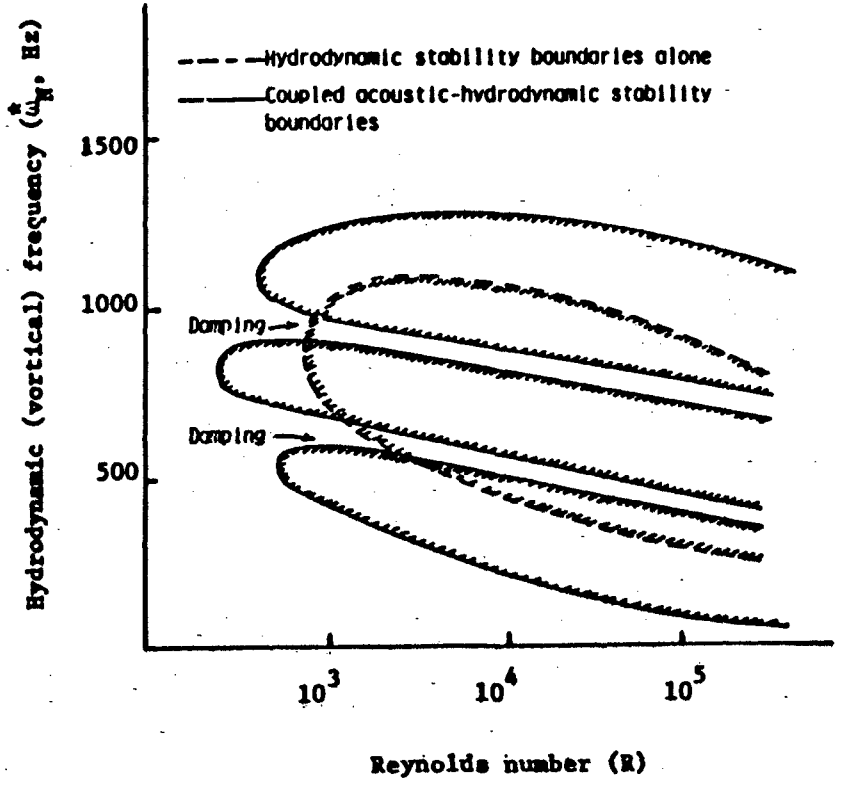

Fig. 2b Coupled acoustic-hydrodynamic stability boundaries

ROCKET MOTOR FLOW-TURNING LOSSES

Alan S. Hersh
Hersh Acoustical Engineering, Inc.
Chatsworth, CA 91311

"Flow-turning" losses represent one of the least understood mechanisms in the acoustic gain and loss estimates used in rocket motor stability calculations. According to theoretical models proposed by Culick, acoustic energy is absorbed during the energy exchange process governing the interaction between mean flow and longitudinal waves within the interior of rocket motors. To validate his model, Culick undertook a series of tests which proved inconclusive because of experimental difficulties. A series of experimental investigations were undertaken to provide fundamental understanding of the "flow-turning" acoustic loss mechanisms. The experimental investigation was unique in four important ways. First, meaningful test data was collected using injection volume flow rates on the order of 100 times the values used in Culick's tests. Second, detailed two-dimensional surveys of the mean and acoustic profiles across the injection test section were conducted. Third, the effects of mean flow turbulence were removed by signal processing. And fourth, acoustic energy flux losses across the injection test section were directly measured. The accuracy of the acoustic energy flux measurements will be improved this year by conducting hot-wire measurements of the acoustic particle velocity across the injection test section.

Figure 1 is a schematic of the experimental facility. Sound was introduced at one end of the faciltiy. Uniform transverse flow was injected into the test section through individual air plena. This was necessary to compare the test results to theoretical models which assume uniform transverse injection rates. The amplitude and phase of the sound pressure within the test section was measured using the probe tube arrangement shown. The measurement program consisted of measuring the sound pressure within the test section as a function of lateral injection flow rate. The idea here is that if "flow-turning" losses indeed absorb sound, then the sound pressure amplitude should decrease with increasing injection flow.

Figure 2 summarizes the current findings of the study. The symbols represent the measured acoustic energy flux losses across the injection test section as a function of injection flow rate. The solid line represents an one-dimensional estimate of the acoustic losses while the dashed line represents a refraction corrected one-dimensional estimate.

It is clear that the "flow-turning" process absorbs sound. The measurements show that most, if not all, of the energy absorption takes place at the finite admittance side wall panels. A reasonably accurate one-dimensional model of the sound energy absorption was derived providing the efficiency of the sidewall panel absorption was increased due to injected mean flow gradients/refraction amplification of the local sound pressure at the sidewalls. The refraction effects are clearly two-dimensional and were incorporated in an ad-hoc manner into the one-dimensional model. The identification of the redistribution of the sound pressure is new, at least in rocket motor stablility calculations, and many have important applications to other rocket motor stability mechanisms.

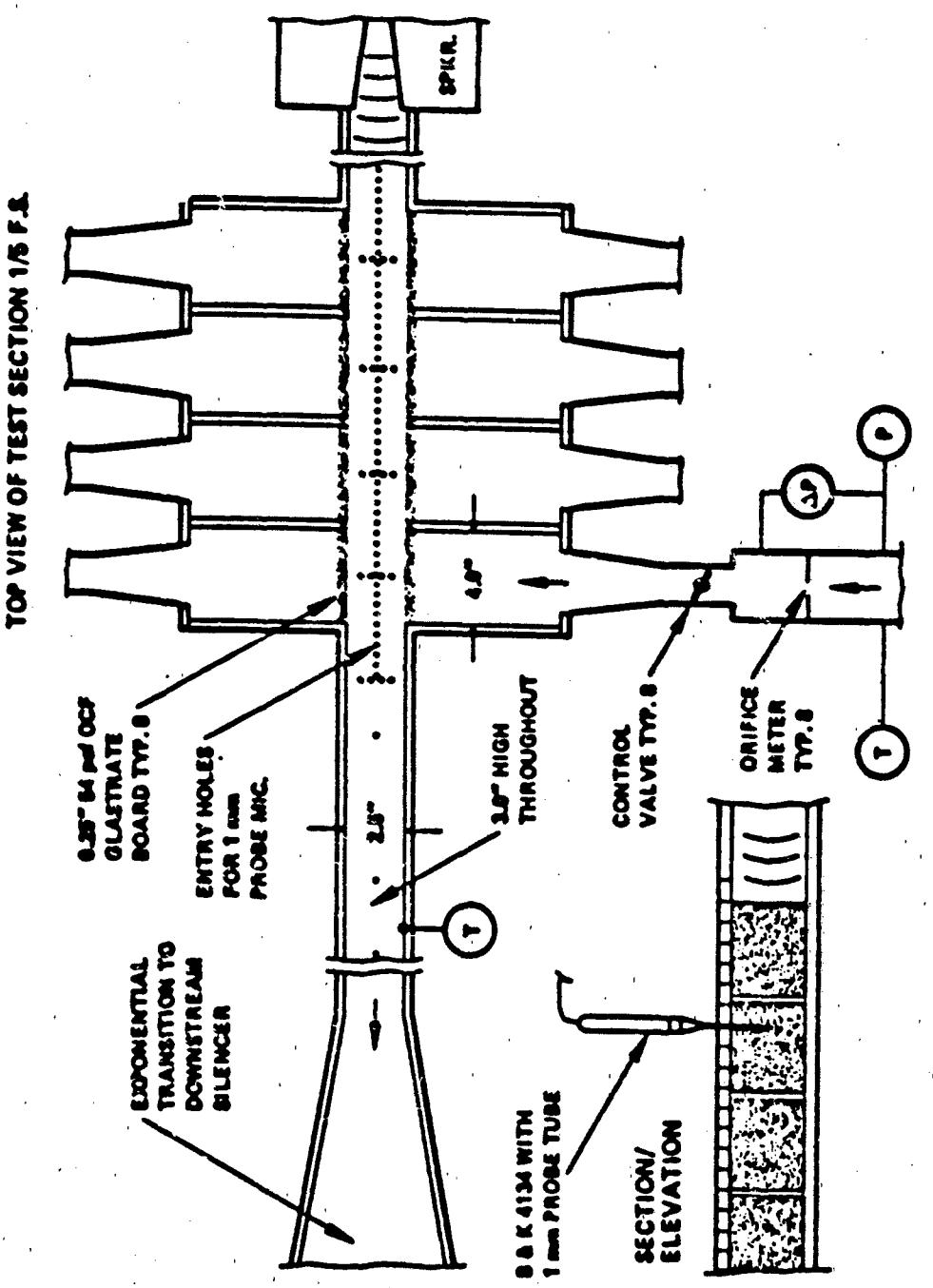

Figure 1. Schematic of the Flow-Turning Test Facility

Notes:
1. Data corrected for grazing flow past probe tube
2. Sound Frequency = 100 5 Hz
3. ⊙ Two-dimensional area-averaged data

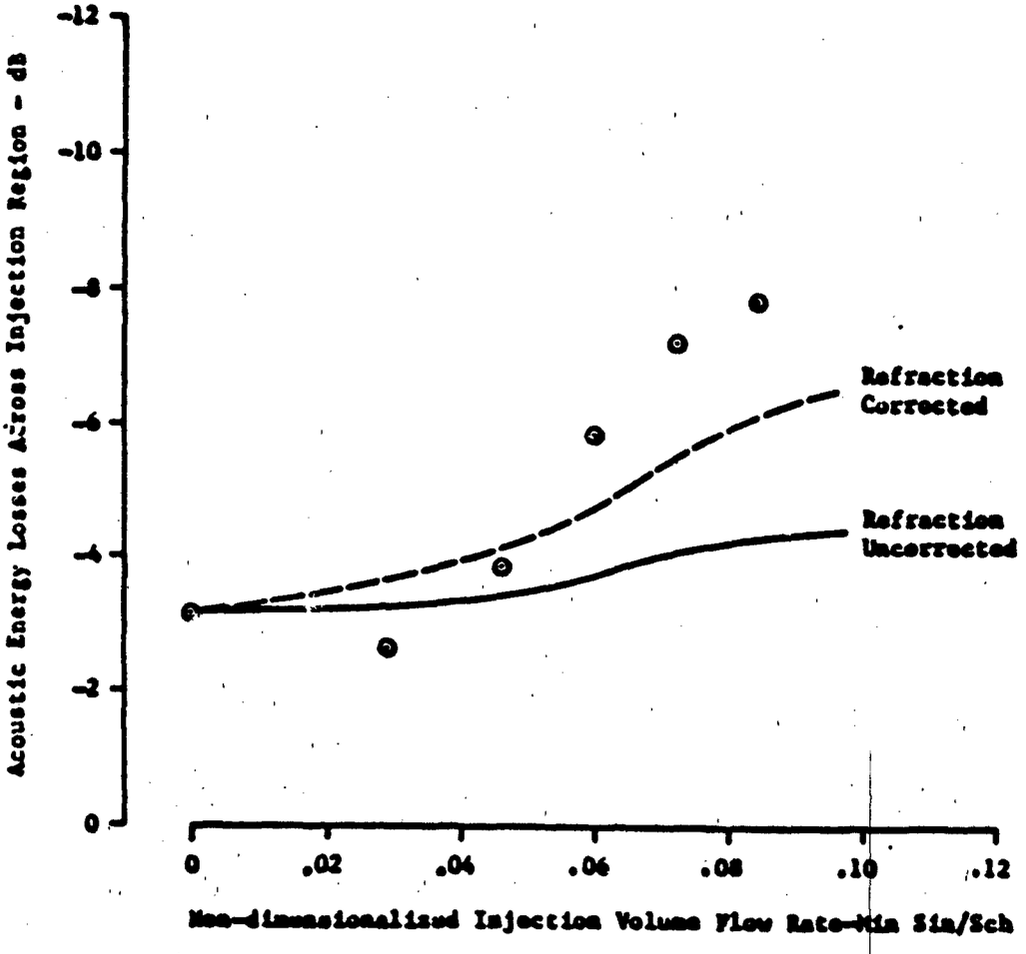

Figure 2 .Comparison Between Measured and Predicted Acoustic Energy Losses Across Injection Section

OVERVIEW: AFOSR INTERESTS IN ROCKET PROPULSION

Leonard H. Caveny
Air Force Office of Scientific Research
Bolling AFB
Washington, DC 20332-6448

Rocket propulsion requirements, both present and planned, present important challenges that are not addressed adequately by present technologies. Future propulsion systems must be improved to assure that the winning edge is maintained. As the conventional propulsion technology matures, the need persists to attain yet another round of performance gains. Thus, the technology challenges become even greater since the obvious advancements are being implemented. Also, broad classes of problems (e.g., costs, hazards, combustion instability, service life, signature, low-temperature structural integrity, light weight thermal protection) are never solved entirely and recur often as important considerations (and compromises) prior to propulsion system qualification.

Powerful motivations continue for basic research on topics such as reacting flows, energetic materials, stability, refractory materials, and propulsive processes. Many phenomena, not explained adequately, are accommodated by specific designs. Periodically, this lack of understanding is the precursor to major setbacks. Clearly, rocket motor processes present scientific challenges suggesting that properly conceived research will continue to provide the foundation for higher performance, reduced risk, lower development costs, longer service life, etc.

This meeting is the first review following the increased emphasis in advanced energetic materials. Accordingly some introductory comments will be provided by several of the investigators to help put portions of this research into perspective.

The recent emphasis on space and the reusable launch vehicle capability to low Earth orbit present new considerations for advanced propulsion for orbit transfer. Transferring the projected large payloads using conventional propulsion imposes severe limitations on the missions. For example, 70% of the mass delivered to low Earth orbit may be the chemical propulsion system required to raise the other 30% (i.e. the active payload) to geosynchronous Earth orbit; nonconventional propulsion offers the promise of reversing this ratio of propulsion and payload masses. The technology issues are necessarily complex; controversial approaches are to be expected. Much of the research is coupled to optimistic projections for technological advances by the 1995 to 2000 time period.

The Wednesday afternoon session treats fundamental processes related to beamed energy and solar propulsion, i.e., radiation transmission and absorption in flowing media, plasma initiation, and chamber configurations. The immediate advantage of beamed and solar energy is high specific impulses obtained by using low molecular weight working fluids heated by external power sources to temperatures greatly above combustion gas temperatures. The premise of the beamed energy approach is that suitable megawatt laser sources will be available and justified for applications other than propulsion. Recent studies support the thesis that ground based free-electron lasers operating at suitable short wave lengths will enable attractive transmission efficiencies and compact collection optics.

The Thursday morning session on electric propulsion emphasizes concepts which lend themselves to sustained operation at megawatt power levels. This represents a major departure from millinewton thrust, pulse-mode electric propulsion considered for station keeping or planetary probes, e.g., millisecond pulses driven by a capacitor bank charged by a dedicated kilowatt power source. Present mission analyses are exploring the dual mode premise of the megawatt nuclear power supply onboard for the main mission being available for propulsion power. Thus, propulsion does not take all the weight penalty for the power source. When large total impulses are required, thruster mass is small compared to the fuel mass; thus, a premium is placed on increasing fuel efficiencies and the low thrust densities of the thrusters become less important. Electrode and insulator lifetimes have been identified as primary barriers to sustained, high power density operation of magnetoplasmadynamic thrusters. Accordingly a major portion of the research is directed at mass loss mechanisms and conditions leading to abusive environments and inefficient operation.

Ample opportunity exists for new approaches. During the last year, several investigations into the synthesis of energetic ingredients were initiated; complementary research is needed to improve the characterization techniques for these higher energy (and more temperamental) ingredients and propellants. Good progress is being made on understanding the origins of combustion instability; more attention must be given to the mechanisms of deliberate suppression. The advent of quantitative flow visualization for turbulent reacting flows has not been accompanied by corresponding theoretical treatments to fully exploit array data, capable of revealing rapid evolution of flow structure and flame fronts. The remarkable advances in optical diagnostic techniques present new approaches to investigate plasma flows which must be understood and controlled under magnetoplasmadynamic and beamed energy thruster conditions. The research on life limiting processes which occur at the surfaces of electrodes, electrical insulators, and refractories will benefit from advances in remote sensing of surface temperatures, composition, and structure. Space missions will present entirely new autonomous operation challenges; a theoretical basis must be established to anticipate and guide the advances in sensors, adaptive control, thruster configuration options, etc. Sustained megawatt operation of space thrusters will be limited by the inability to reject heat; research is needed to enable advances in light weight radiators and thermal management systems. We will welcome discussion on these and other topics pertinent to the Air Force basic research program on energy conversion.

INTERACTION OF MULTI-DIMENSIONAL MEAN AND ACOUSTIC FIELDS IN SOLID ROCKET COMBUSTION CHAMBERS

Joesph D. Baum and Jay N. Levine
Air Force Rocket Propulsion Laboratory/DYCR
Edwards AFB, CA 93523-5000

The objective of the present research project is to seek an understanding of the physical mechanisms by which energy is exchanged between the mean and acoustic flow fields in resonance combustion chambers (in particular, solid rocket motors). These processes which have the potential of contributing significantly to the growth or decay of pressure oscillations in solid rocket chambers, have been the subject of much speculation in the past, but have never been thoroughly investigated. Specifically, the phenomena to be investigated are the interaction between the acoustic field in a chamber and a free shear layer (i.e., vortex shedding) and the so called "flow turning effect" (i.e. energy transfer between the acoustic field in the combustor and the mean flow of combustion products entering the chamber parallel to its axis). The presentation this year will detail efforts, to date, to develop the computational capability to properly address such problems via a solution of the compressible, turbulent, time dependent Navier-Stokes equations, and will report progress made toward the understanding of flow turning and acoustic refraction (which results from the interaction between sound waves and a coexisting mean sheared flow, as shown in Figs 1a and 1b for downstream and upstream wave propagation, respectively).

Acoustic refraction effects had to be investigated since they result in redistribution of acoustic pressure and velocity (and thus acoustic energy) in the radial direction. When sound waves travel with the sheared mean flow in a combustion chamber, acoustic refraction results in increase of acoustic pressure and velocity near the burning propellant surface thereby enhancing the propellant burning rate (due to the coupling between the pressure and velocity fields and the burning rate of the propellant). This results in further enhancement of acoustic energy production, in contrast with the coexisting phenomenon of acoustic energy dissipation that results from acoustic energy absorption by the incoming flow of combustion products.

A computer program was developed to solve the time dependent, turbulent, compressible Navier-Stokes equations that describe the flow in a combustion chamber and a hard wall tube (utilized to study the phenomenon of sound wave propagation in a coexisting sheared mean flow). Studies were conducted to evaluate explicit versus implicit codes (implicit was chosen as more computationally efficient) and proper definition of the boundary conditions. The results obtained in the acoustic refraction study demonstrate significant distortion of the initially plane waveform as the wave traverses the tube length, as shown in Figs 2a and 2b for the pressure and axial acoustic velocity, respectively. After 600 time steps, when the solution is terminated, the amplitude of the acoustic pressure at the wall is 39.5% larger than at centerline, while the amplitude of axial velocity oscillations near the wall is 31% larger than at centerline. The results for downstream propagation demonstrate significant increase of acoustic pressure and velocity near the wall with respect to the corresponding values at the centerline. For upstream propagation the reverse phenomena occurs. Additional results demonstrate that acoustic refraction effects: a) increase with frequency; b) increase with Mach number; c) are higher for upstream wave propagation; d) are significantly lower than predicted by classical acoustic theory; and e) acoustic refraction effects which have not been previously considerd in motor stability analysis, should be included in the models. To the best of our knowledge, these are the first solutions demonstrating acoustic refraction effects that are obtained through solution of the complete Navier-Stokes equations.

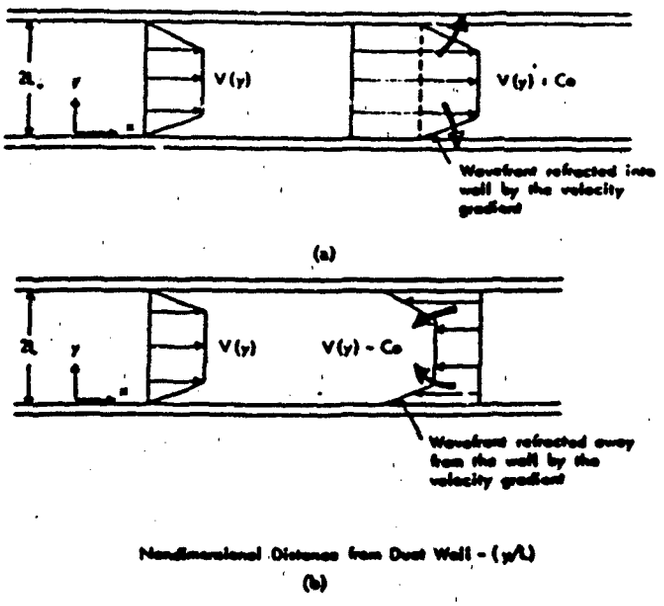

Fig. 1. (a) Schematic of Downstream Sound Propagation; (b) Schematic of Upstream Sound Propagation.

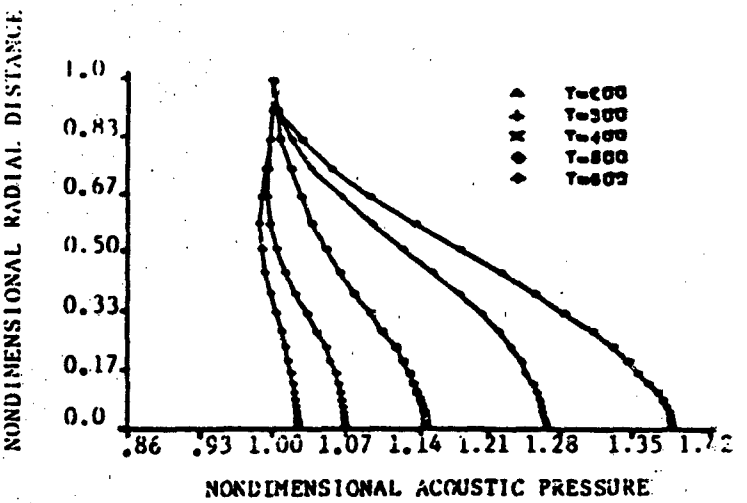

Fig. 2a Time Evolution of the Radial Distribution of Acoustic Pressure, f=6000 Hz, $M_{c.l.}$ = 0.1, Downstream Propagation.

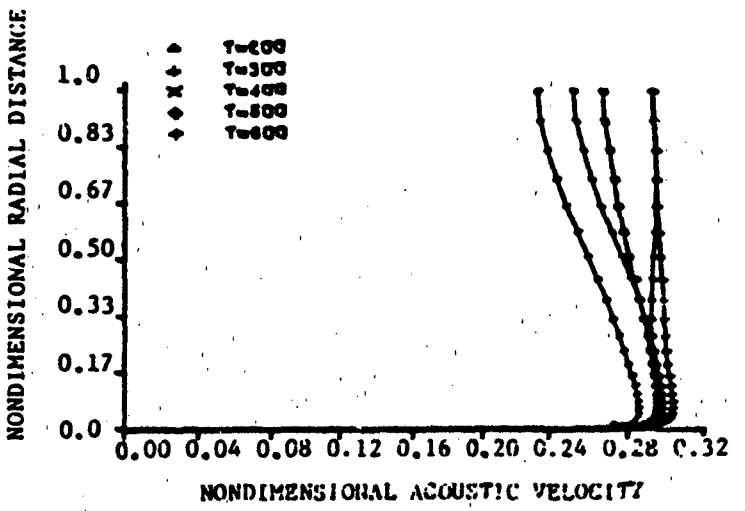

Fig. 2bTime Evolution of the Radial Distribution of Acoustic Axial Velocity, f=6000 Hz, $M_{c.l.}$ = 0.1, Downstream Propagation.

LASER THERMAL PROPULSION

Dennis Keefer, Carroll Peters,
Herbert Crowder and Richard Welle
Center for Laser Applications
University of Tennessee Space Institute
Tullahoma, Tennessee 37388

Laser sustained plasmas (LSP) have been proposed as a means of converting beamed energy from a remotely located laser to provide efficient propulsion for orbital transfer. Successful implementation of this concept requires that the detailed energy conversion processes that control plasma stability and fractional energy absorption within the LSP be thoroughly understood. An experimental study of these mechanisms is being conducted using argon plasmas sustained by a continuous wave carbon dioxide laser in a controlled, forced convection flow. Detailed measurements of the plasma temperature field are obtained using digital images of the plasma continuum radiation within a narrow spectral wavelength band. Using the measured temperature field, the interaction among the absorbed laser power, thermal conduction, and thermal radiative transfer can be calculated at each point within the plasma.

Experiments have now been performed, using both 8-inch and 12-inch focal length lenses at incident power levels to 1 kW, pressures from 1 to 3 atm. and flow velocities to 21.4 cm/s. The data has been reduced to provide the measured temperature fields for most of these experiments, but the calculation of absorbed laser power was delayed by the need to perform real-ray analyses of the focusing optics to account for spherical aberrations. One of the most important questions concerning LSP behavior was the effect of forced convective flow, since no previously reported experiments were performed under these conditions. It was found from our experiments that, at a given condition of pressure, incident power and focusing geometry, the LSP is relatively insensitive to the incident flow velocity. This can be seen from Figure 1 where images of the plasma have been computer enhanced to show the isoradiance contours. The plasma shape and volume remain nearly constant, and the principal effect of increased velocity is to move the plasma closer to the focal plane. No instability of the LSP has been observed as a result of forced convective flow.

For the range of parameters which we have studied to date, the LSP was found to be most sensitive to pressure and to the focal length of the lens. These effects can be seen in Figure 2. These data were acquired at a constant volume flowrate of 3.2 standard liters/min using the 8-inch focal length lens, and shows that the plasma radiance increases with pressure, reaching a maximum at about 2 atm. The sequence of images in Figure 2b was obtained at the same conditions except that the 12-inch focal length lens was used. In this sequence, the maximum radiance is smaller, and occurs for a pressure of 1.7 atm. As the pressure is increased, the plasma moves closer to the lens and decreases in length until it becomes unstable and extinguishes. This result is somewhat surprising since, as a result of reduced spherical aberrations, the peak intensity of the laser beam is greater for the 12-inch lens. Further explanation of this effect must await the detailed analysis of the laser beam absorption within the LSP.

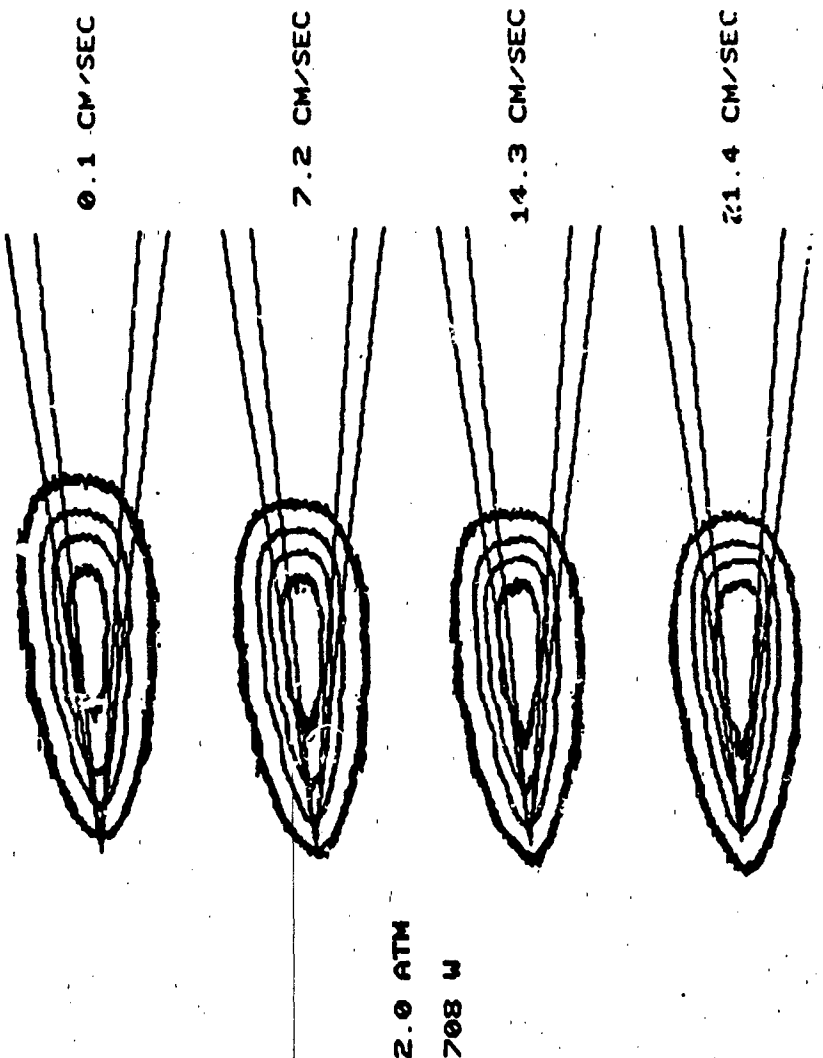

Figure 1. Spectral images of the LSP computer processed to indicate isoradiance contours. Indicated flow velocities are the average upstream values based on volumetric flow measurements.

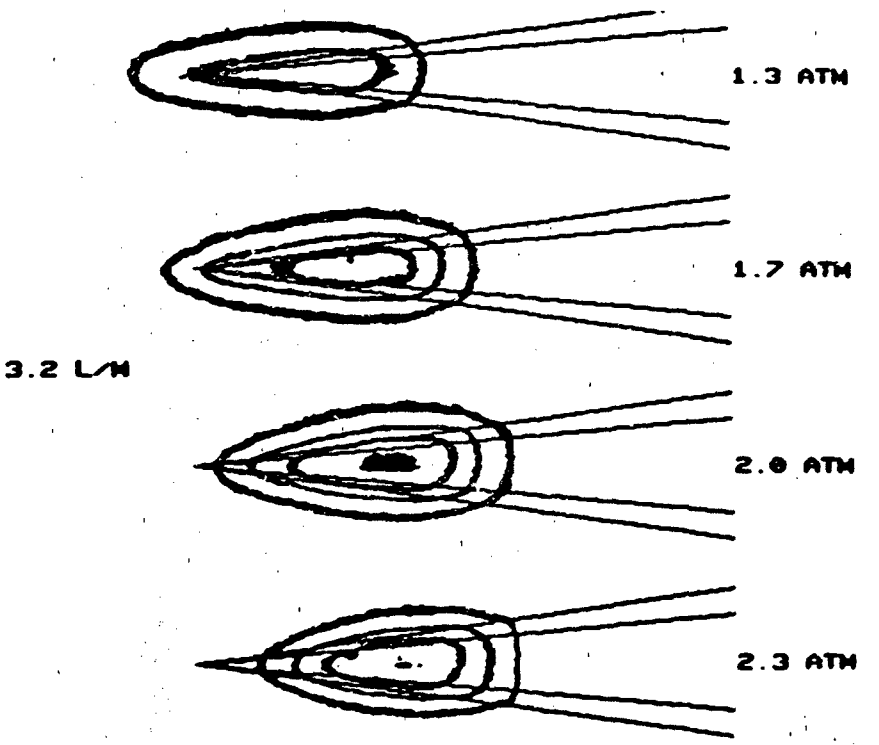

a. The sequence was obtained using the 8-inch focal length lens.

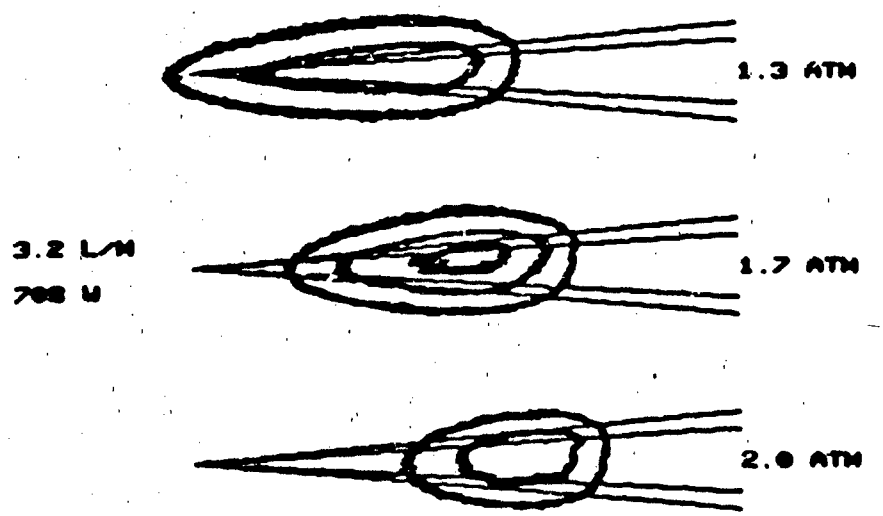

b. The sequence was obtained using the 12-inch focal length lens.

Figure 2. The effect of pressure for two different focusing lenses.

ANALYTICAL MODELING OF STRONG RADIATION GAS-DYNAMIC INTERACTION

Charles L. Merkle
The Pennsylvania State University
University Park, PA 16802

The principal objective of this research program is to determine the dominant characteristics of the interaction between a high power laser beam and a flowing gas. The method of investigation is by numerical analysis with primary emphasis on the steady two-dimensional problem. The one-dimensional problem and the stability characteristics of the interaction are also being considered. The geometry of interest is the convergent portion of a converging-diverging nozzle. This geometry, along with the major physical phenomena included in the analysis, is shown in Fig. 1. In particular, the analysis includes the effects of a converging laser beam with an arbitrary intensity profile. (Present calculations are using a Gaussian beam.) The mass flow through the nozzle is fixed by the back pressure when the nozzle is unchoked, and by the choking condition when the nozzle is operated supercritically. Real gas properties, including viscosity and thermal conductivity, corresponding to those of equilibrium hydrogen are used for all thermodynamic variables. Gas absorptivities corresponding to hydrogen-seedant mixtures have been chosen for the calculations to date. The location of the heat absorption zone and the fraction of power absorbed are found by satisfying the complete conservation laws.

The numerical procedure is a linearized, block implicit time-dependent scheme. To ensure accurate mass and energy balances, both the fluid equations and the radiation equation are expressed in fully conservative form. Boundary conditions are expressed in proper characteristics form, and all calculations are done in a body-fitted coordinate system.

Some representative results of a parametric study currently in progress are shown on Fig. 2. These calculations represent the first ever two-dimensional analysis of the laser absorption problem. The left side of Fig. 2 shows temperature contours for three different laser powers. Note that the heating zone exhibits steeper gradients in the radial than in the axial direction. For the conditions computed, much of the absorption is accomplished in the diverging part of the beam, but the resulting interaction remains stable. The fraction of laser power absorbed in these cases ranges from 50 to 70%. The fractional power absorbed can be increased and the heat addition zone can be moved forward by raising the stagnation pressure or the back pressure or by further increases in the laser power.

The variation in the cross-beam intensity is shown on the right side of Fig. 2. At and near the nozzle inlet (x=0 and 0.5) it remains Gaussian, but preferential absorption by the hotter gases on the axis destroys the Gaussian shape toward the end of the nozzle. At the exit, almost the entire amount of energy on the centerline has been absorbed, but substantial power remains in the outer portions as seen by the x=1.5 curve.

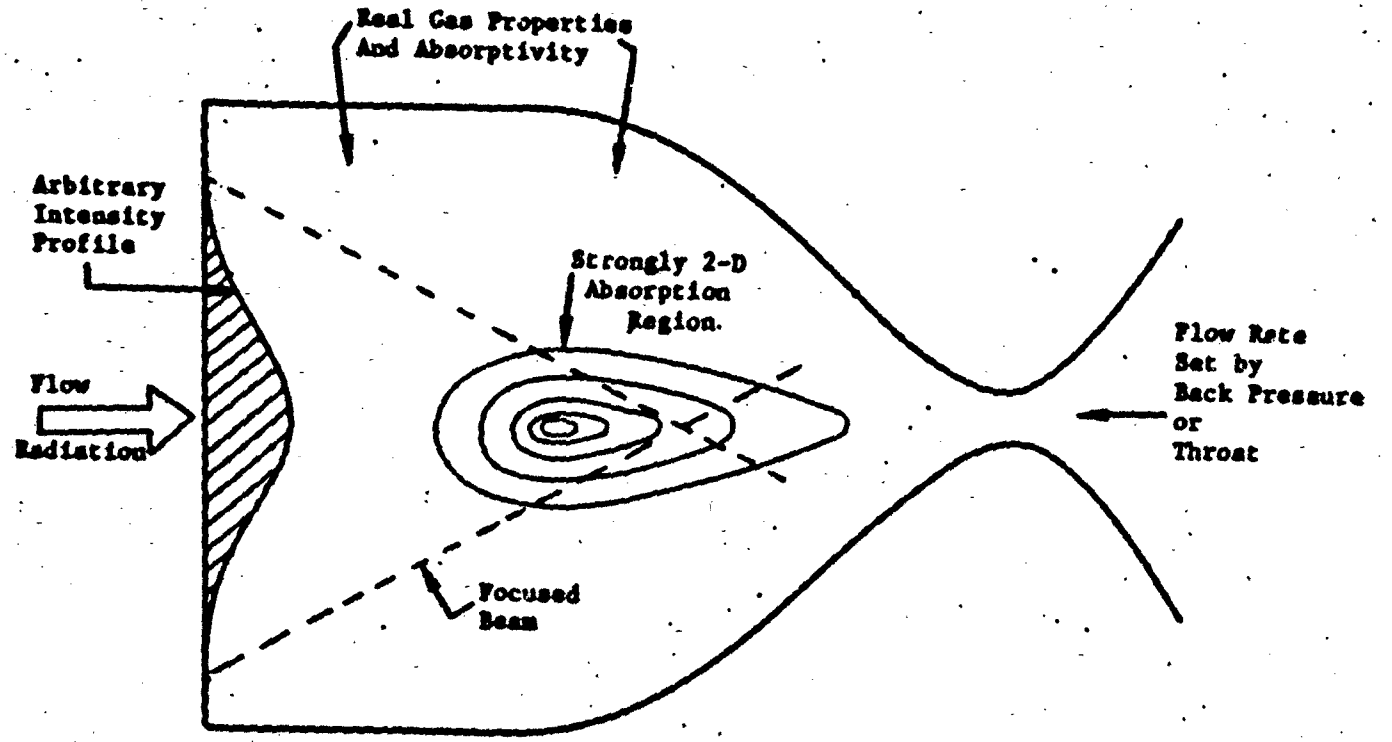

Fig. 1. Physical Phenomena Included in Model of Laser-Gasdynamic Interaction

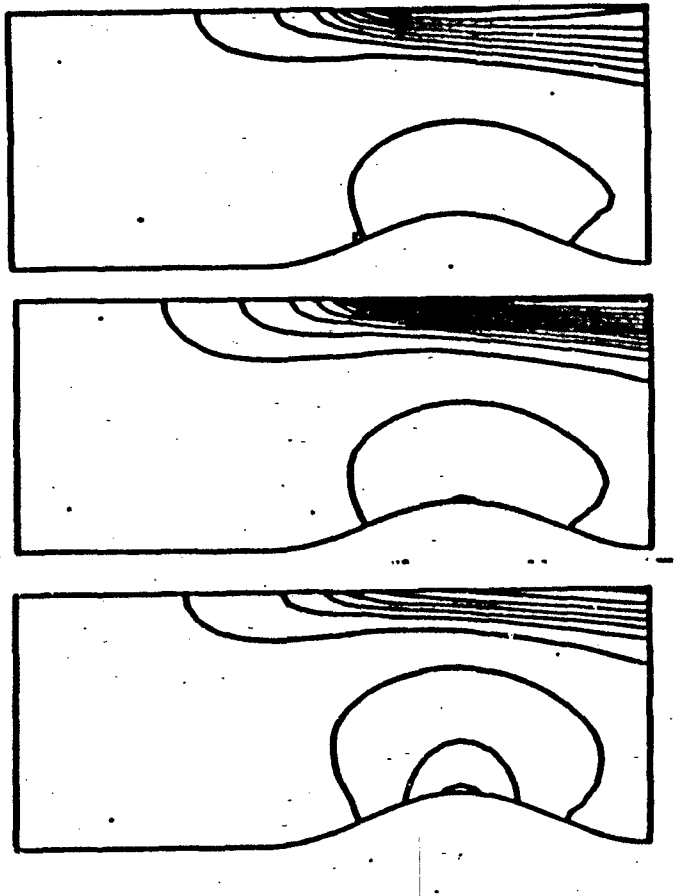

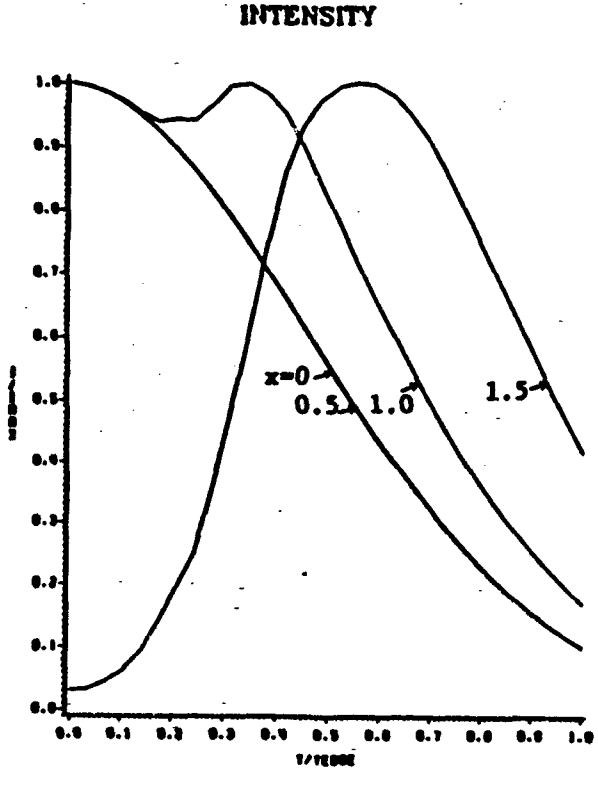

Fig. 2. Effect of Laser Power on Location and Shape of Temperature Contours and Nonuniform Absorption of Radiation in Representative Laser Propulsion Configuration

Experimental Studies of Laser-Sustained Argon Plasmas For CW Laser Propulsion Applications

Herman Krier and Jyoti Mazumder
University of Illinois at Urbana-Champaign

Experimental studies of laser-sustained plasmas in pressurized flowing argon are now underway. Figure 1 presents preliminary global absorption data, as measured calorimetrically, over a range of laser power for air and argon at 1.1 atm. Such absorption data for flowing argon at these power levels has not been presented before.

The data shows strong laser energy absorption by argon, approaching 80% at higher powers. The argon absorption is considerably stronger than that of air, due mainly to its higher absorption coefficient. The absorption coefficient of air is degraded by the presence of extraneous species with larger electron collisional cross sections. These tend to deexcite free electrons and lower electron temperature, reducing inverse Brehmsstrahlung absorption, the dominant absorption mechanism.

The data also indicates a tendency for global absorption to rise with laser power. This is most likely a geometric effect. Total absorption depends both on absorption coefficient and on plasma size. Plasma size is an eigenvalue solution of the steady state energy balance equations (see Fig. 2), producing a finite plasma size for a given laser power and flow conditions. As laser power increases, the plasma size and therefore the absorption length grow, causing a net increase in global absorption.

The data also suggests asymptotic behavior at high power (see Fig. 2b). As laser power increases, the plasma grows until it reaches a point where radiative losses from the enlarged surface area offsets the increase in power, preventing further growth in absorption length. Thus there is probably an upper limit to absorption percentage, depending largely on beam geometry and radiative behavior.

Minimum maintenance powers are also indicated. One reason for the difference is again the lower absorption coefficient of air (see Fig. 2c). Near plasma extinguishment, the plasma is held near the focal volume, where absorptive area and length are comparable for the two gases. Since the absorption coefficient of argon is higher, it can be maintained at the focus at lower power levels. Minimum powers will be lower once our optics are optimized, and when higher gas pressures are used.

The dashed line above the argon data represents an analytic correction for the heated gas that becomes trapped in our calorimeter; it is based on thermocouple readings taken inside the calorimeter. Actual measurements of the correction factor are now being made using calorimeter windows.

In addition to these absorption studies, we are currently: 1) examining plasma initiation using targets and aerosols, 2) producing detailed temperature and number density measurements in the plasma core using spectroscopic relative-line-intensity and line-broadening techniques, 3) extending the temperature data downstream using infrared thermography and thermocouple grids, and 4) developing an LIF diagnostic system for studying convective mixing behavior.

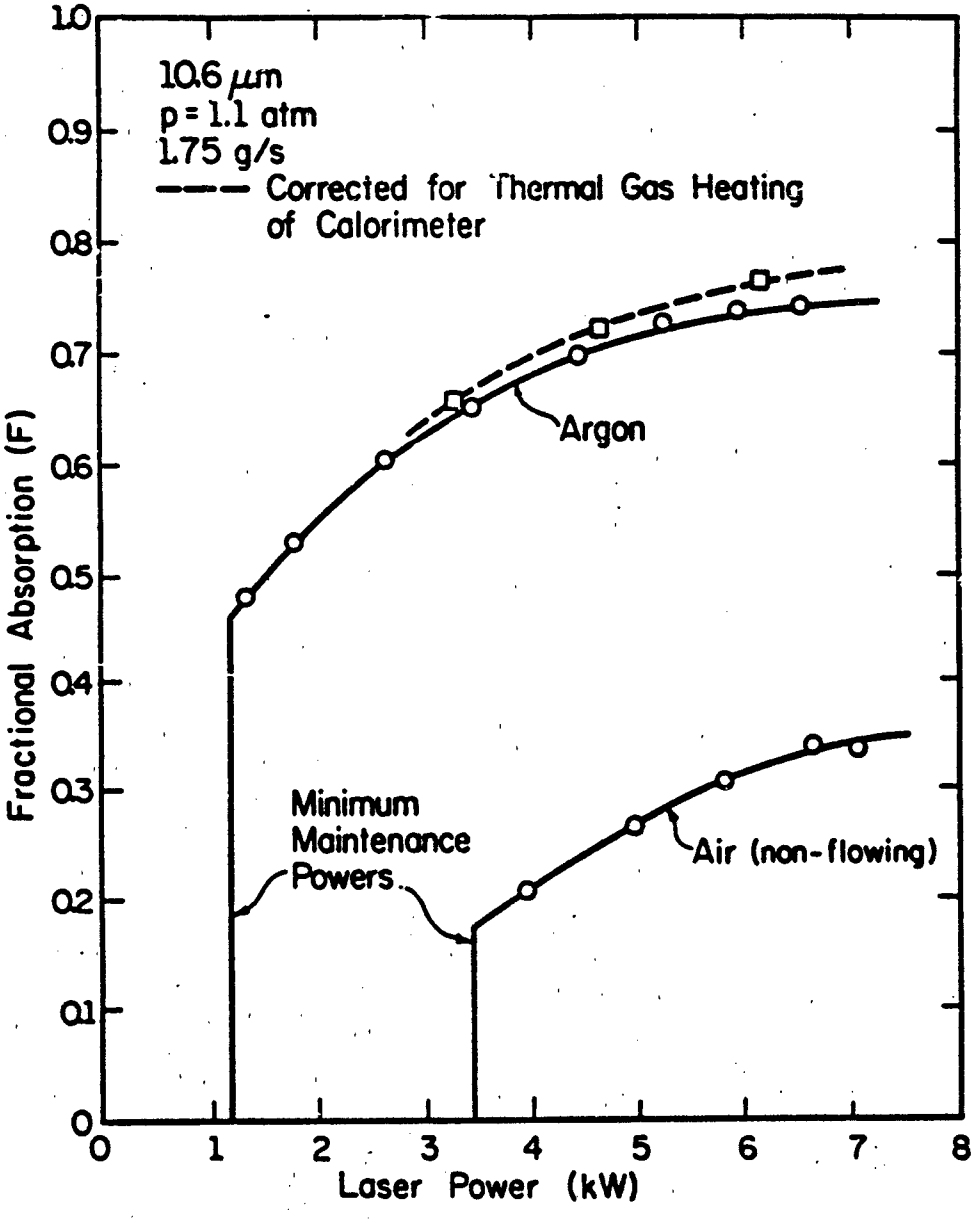

Figure 1 Measurements of fractional energy absorption versus power for plasmas in argon and air. The dashed line is an analytical correction for hot gas that builds up inside the calorimeter.

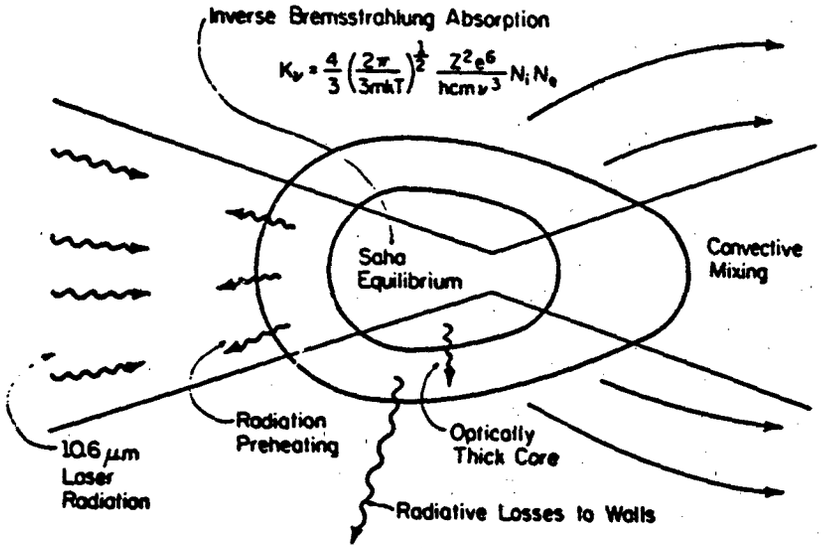

Fig. 2a Physical mechanisms affecting the energy balance of the LSP. The plasma stabilizes at a point in the focused beam where the absorbed power equals all loss mechanisms.

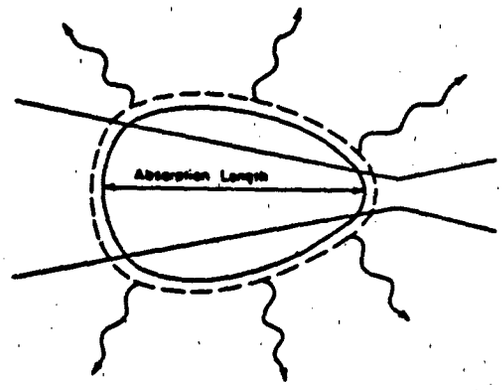

Fig 2b Increased radiative losses due to larger surface area offset increases in laser power and fix an upper limit to plasma size and global absorption fraction.

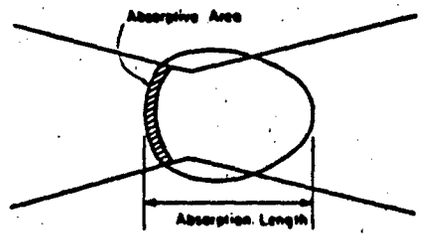

Fig 2c Near plasma extinguishment, absorption area and length are fixed by the focal volume. Thus, minimum maintenance power is a function of absorption coefficient only.

LINEAR AND SATURATED ABSORPTION OF LASER RADIATION IN HEATED GASES

Robert H. Krech, Lawren M. Cowles,
George E. Caledonia and David I. Rosen
Physical Sciences Inc.
Dascomb Research Park, P.O. Box 3100
Andover, MA 10810

The physical processes involved in heating the working fluid of a rocket engine with a high power CW laser beam can be simply described. The gas is injected into the stagnation/absorption zone at a temperature most probably determined by regenerative cooling requirements. As the gas flows toward the throat it is heated by absorption of laser radiation. With hydrogen as the primary propellant constituent, the equivalent of nine 10.6 μm photons per molecule must be absorbed to reach a stagnation condition that yields a specific impulse of ~1000 s.

The absorption scheme originally considered required the laser-induced breakdown of the H_2 "fuel" followed by the formation of a stable laser-supported combustion (LSC) wave. The principle absorption mechanism in this case is inverse electron bremsstrahlung which requires significant ionization levels in the gas. For pure H_2, ionization becomes significant at ~10,000 K with the development of a stable LSC wave requiring temperatures of ~20,000 K. It has been suggested that the introduction of alkali seeds, which will begin to thermally ionize at temperatures of ~3000-3500 K, would allow operation at temperatures of <10,000 K, thus providing a less severe thermal environment for thruster design.

Although the use of alkali seeds appears promising, an LSC wave mechanism is required to heat the gas to T ~3000-3500 K to initiate alkali ionization. Alternatively, other "seed" molecules can absorb the laser radiation via vibration-rotation band transitions. Such absorbing molecules can provide for gas heating to temperatures of ~3000-3500 K, so that heating from the initially "cold" gas to stagnation conditions can be continuous rather than through laser-induced breakdown. Furthermore if such species can absorb to T ≈4500-5000 K, then specific impulses of 1000-2000 s can be achieved without the need for ionization (and thus alkali seeds).

The present program has been directed towards studying the absorption properties of potential "high temperature" molecular absorbers over the temperature range of 1000-3500 K and at CO_2 (~10.6 μm) and DF (3.8 μm) laser wavelengths. These measurements have been performed behind incident and reflected shockwaves. Species studied to date include H_2O, CO_2, NH_3, SF_6 and NF_3. Small signal (linear) absorption coefficients have been measured for these species (including effects due to dissociation fragments). These measurements have been performed under pressure and temperature conditions, and within non-equilibrium chemical kinetic regimes, appropriate to the propulsion application. In addition observations of saturation phenomena in the intensity range of 10^3-10^6 W/cm^2 have been performed at CO_2 laser wavelengths for the species CO_2 and NH_3.

A brief overview of the technical issues involved and research approach used to address these issues is provided in Figure 1. Figure 2 provides a summary of our small signal absorption observations for the CO_2 P(20) transition.

INFRARED LASER ENERGY ABSORPTION BY SEED MOLECULES
IN WORKING FLUID OF CW THRUSTERS

- **ISSUES**
  - Overlap of Laser Transitions with Resonant V-R Transitions in Molecules
  - Contributions of 'Hot Band' Transitions at Elevated Temperatures
  - Possible Saturation or Bleaching Effects at High Irradiance (10^3 ÷ 10^6 W/cm^2)
  - Stability of Absorbing Species at High Temperatures (T > 3500 K);
    ⇒ Detailed Dissociation Kinetics May be Important
- **APPROACH**
  - Review and Screen Potential Candidates for Absorption of CO_2 (~10 μm) and DF (~4 μm) Laser Radiation
  - Assess High Temperature Absorption Behavior Through Laser Absorption Measurements in Shock-heated Mixtures of Interest
  - Assess Absorption "Saturation" Behavior at High Flux (10^3 -10^6 W/cm^2) Using Laboratory Scale Pulsed Probe Lasers
  - Utilize Experimental Results to Develop Absorption Algorithms

Figure 1. Scientific Approach to Research on Molecular Absorption Scheme for CW Laser-Heated Thruster.

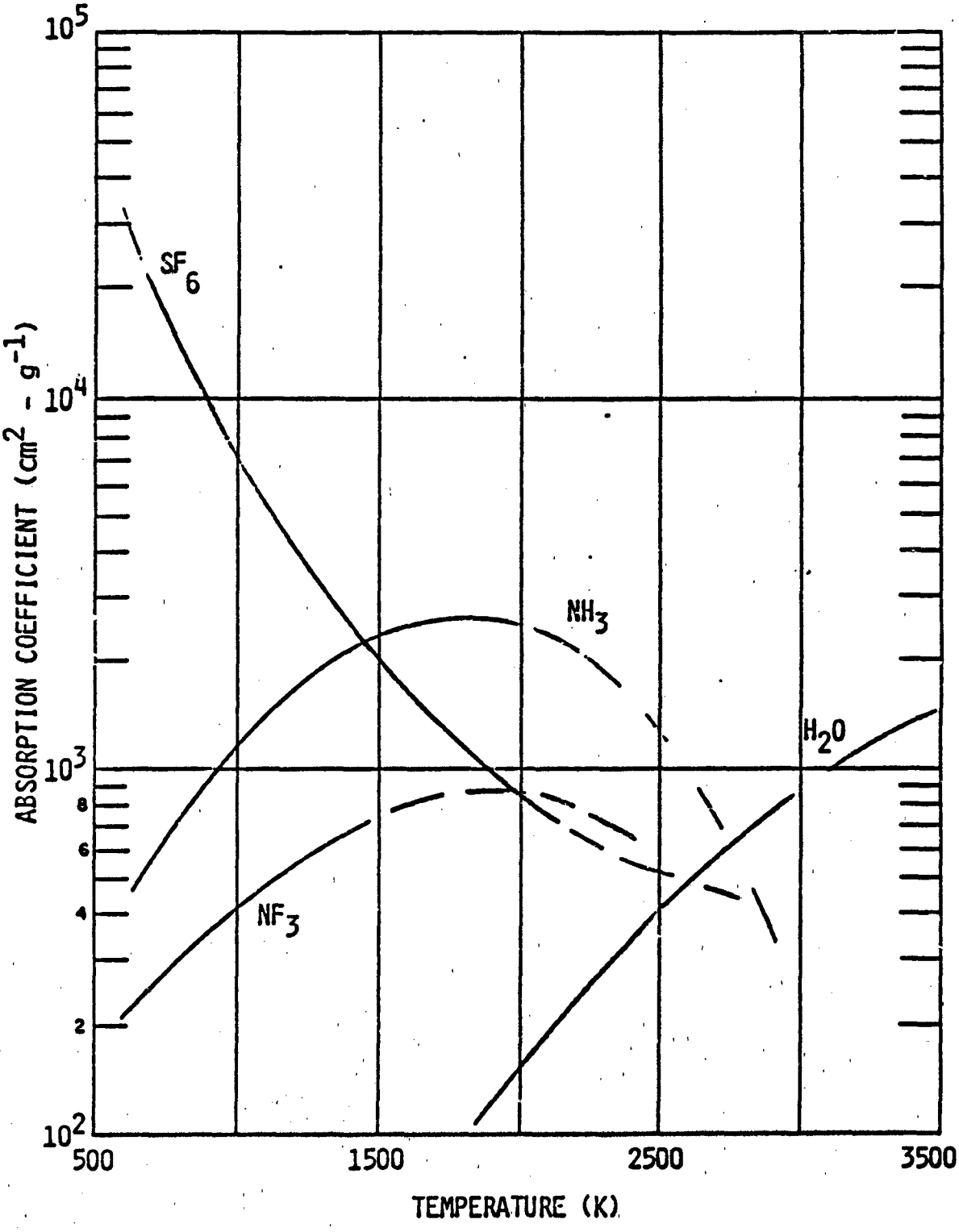

Figure 2. Measured High Pressure Absorption Coefficients for the CO_2 P(20) Transition.

ENERGY DEPOSITION OF PULSED ONE MICRON LASER RADIATION IN H_2 AND AR

David I. Rosen and Nelson H. Kemp

Physical Sciences Inc.
Dascomb Research Park
P.O. Box 3100
Andover, MA 01810

In RP (repetitively-pulsed) laser propulsion the propellant energy is supplied by the absorption of short, repetitive laser pulses beamed to the thruster from a remote laser power station. In the RP thruster concept shown in Figure 1 parabolic nozzle walls focus the incoming beam to yield propellant breakdown at the focal point of this parabola. Depicted schematically in Figures 1a to 1d are the four principal stages in the operation of the pulsed laser-heated thruster: (1) ignition/breakdown, (2) post-breakdown plasma absorption and growth under the influence of the laser radiation field, (3) blast wave propagation into the surrounding gas, and (4) late-time expansion and cooling of the laser-heated gas.

In a previous study at PSI experimental and theoretical investigations of laser-induced gas breakdown at short laser wavelengths (< 1 μm) were carried out for a variety of propellant gas candidates. The results of those studies have helped to establish the threshold irradiances required to initiate an optically absorbing plasma and the scaling of those irradiances with gas density, pulse duration, and concentration of low ionization potential additives. With the ignition/breakdown criteria thus established, the next step was to evaluate the subsequent laser energy deposition that occurs in the post-breakdown plasma.

In the present study, we have performed experiments to investigate the degree of laser optical absorption and the resulting plasma-dynamics which occurs when high energy pulses of 1.05 μm laser radiation are focussed into various gases at focal intensities above the breakdown threshold (10^{10}-10^{13} W/cm^2).

The amount of laser energy absorbed into the gas was inferred from a combination of experimental measurements and computer modeling calculations. In the experiments, the laser beam attenuation was found by optical transmission measurements, and the shock wave trajectory was measured from time-resolved interferometric measurements. A computer model of quasi-one dimensional flow was adapted to calculate spherical expansion of a heated gas sphere, including thermochemical equilibrium. The measured shock trajectories were compared with the calculated ones to infer the energy absorbed by the gas from the laser. Details of the work will be discussed in the talk to be presented.

A summary of the results based on our preliminary analysis can be found in Figure 2 for hydrogen and argon. The results indicate that, under appropriately chosen conditions, conversion efficiencies of pulsed laser energy to blast wave energy can be achieved that approach 100%. The data analysis also reveals, however, that a proper treatment of 'real gas' effects, i.e., energy partitioning into internal degrees of freedom of the gas, is essential to any modeling analysis.

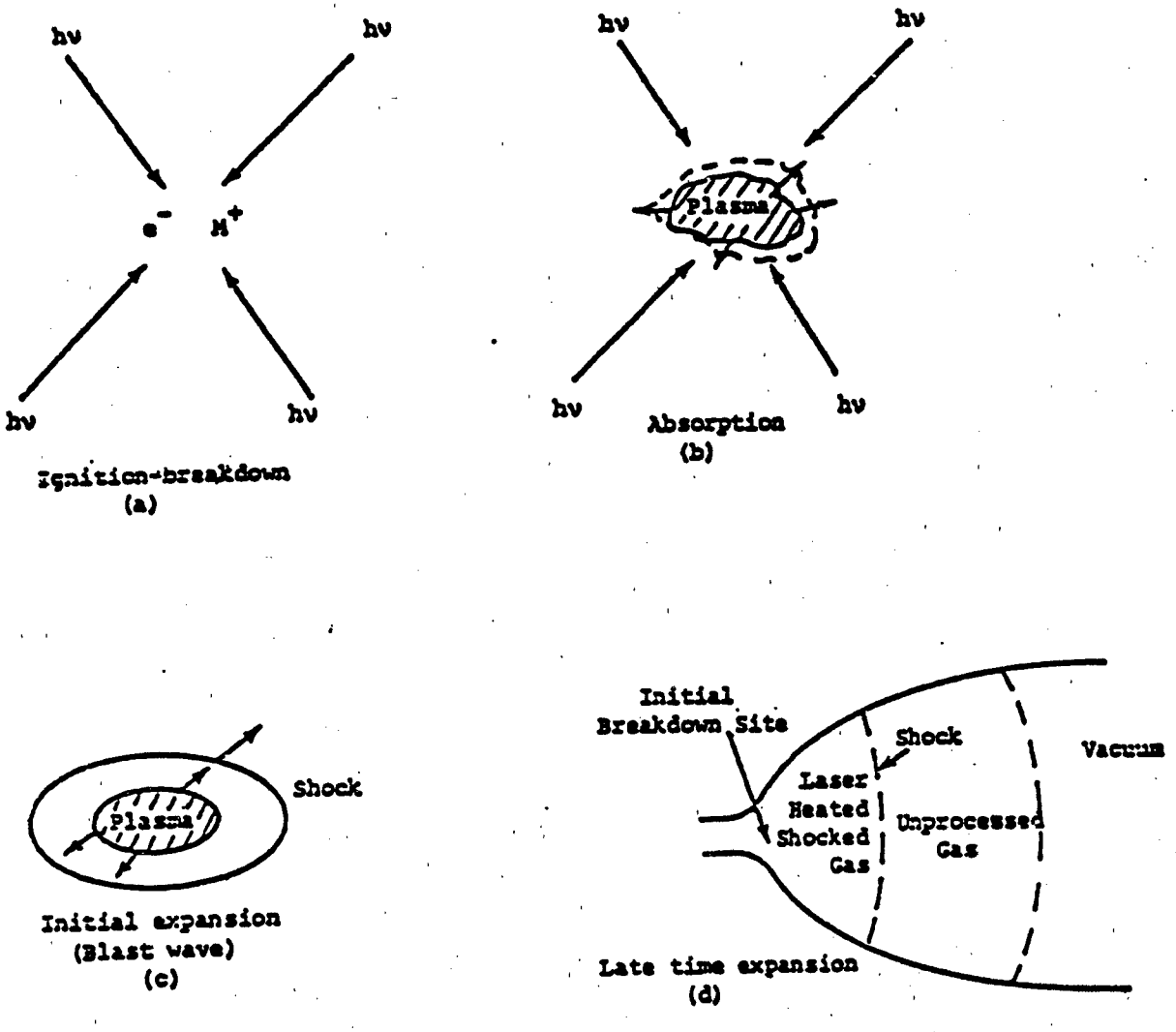

Figure 1. Different stages in pulsed laser thruster. (Sequence a-d is repeated after initial gas has expanded out of nozzle and fresh gas enters.)

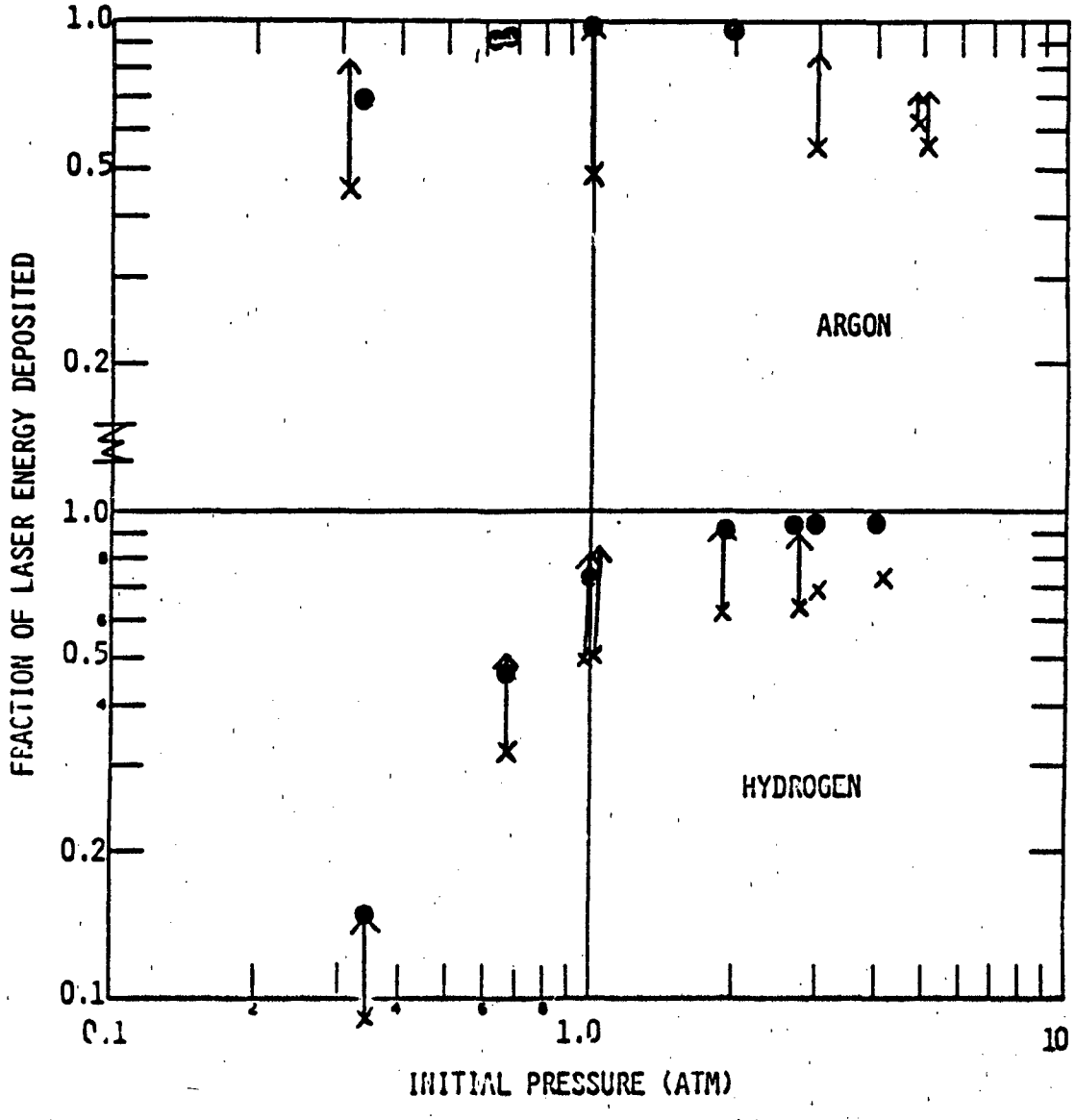

Figure 2. Results of Laser Energy Deposition Measurements in Argon and Hydrogen. ● - from optical transmission measurements, x - from "blast wave:" analysis without real gas effects, and † - from "blast wave" analysis including real gas effects.

ADVANCED ENERGY CONVERSION CONCEPT FOR MICROWAVE BEAMED-ENERGY PROPULSION

Professor Leik N. Myrabo
Department of Mechanical Engineering,
Aeronautical Engineering & Mechanics
Rensselaer Polytechnic Institute
Troy, New York 12180

The principal objective of this study is to perform basic research investigations on an innovative electrostatic force generation principle. Basically, microwave energy is beamed directly to remote RF linear accelerators (LINAC) enclosed by a specially-shaped envelope/body within a planetary atmosphere. A number of low current (1A peak, 100 mA average) 5 MeV LINACs eject free-electron charge to a distance of 5 to 10 m from the body, thereby establishing a "charge cloud" and resultant high electric field between the cloud and body. In less than a microsecond, these free electrons attach to previously neutral oxygen and water molecules (forming negative ions), and drag the largely neutral air-mass "cloud" back to the body which is now positively charged. Force generation is postulated to occur on a millisecond time scale, and may be limited to some extent by ion-slip processes. As shown in Figure 1, repetitively-pulsed operation (e.g., 1000 Hz) of the LINACs could give rise to quasi-steady electrostatic forces, which accelerate the air-mass working fluid within a stream tube of a given capture area — as established by the radius of the E-beam at the point of maximum range from the accelerator.

The research program proposes to examine the physics of global body electrostatic charging and artificial atmospheric charging, formulate a model for electrostatic force generation and finally, conduct an analysis of the cloud/ body interaction physics. Figure 2 graphically presents the results of a "first-order" calculation of anticipated surface-field thrust, free charge, and stored energy.

a) Charge emitted near body surface:

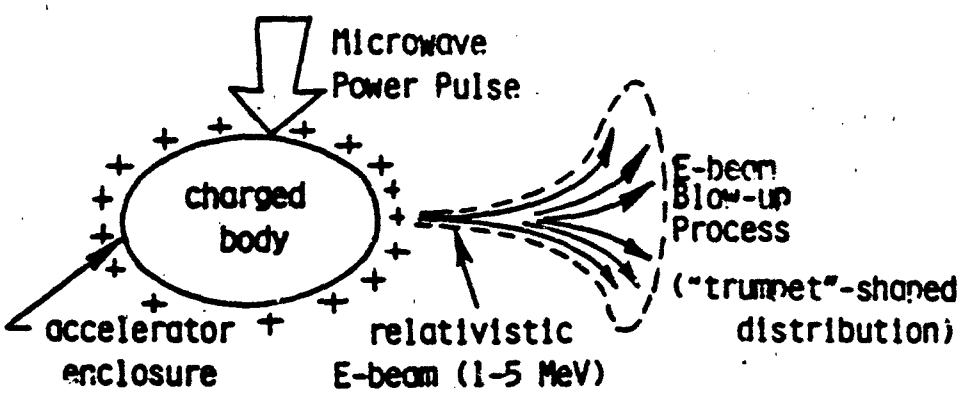

b) Creation of surface field:

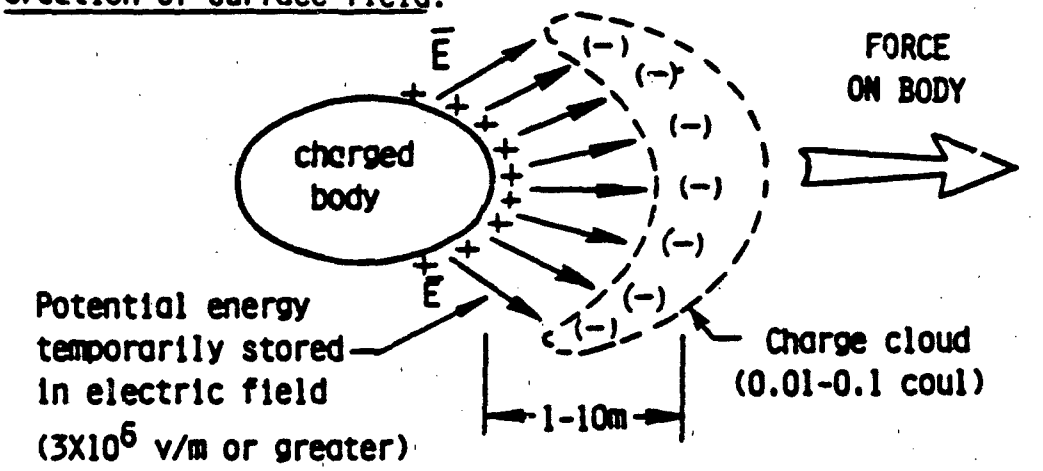

c) Acceleration of "Charge Cloud" Reaction Mass:

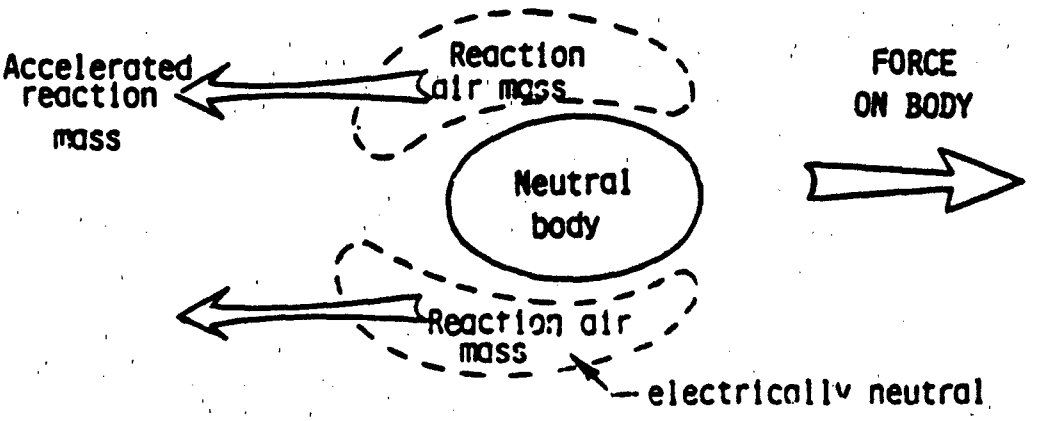

Figure 1 "Surface Field" Electrostatic Force Model

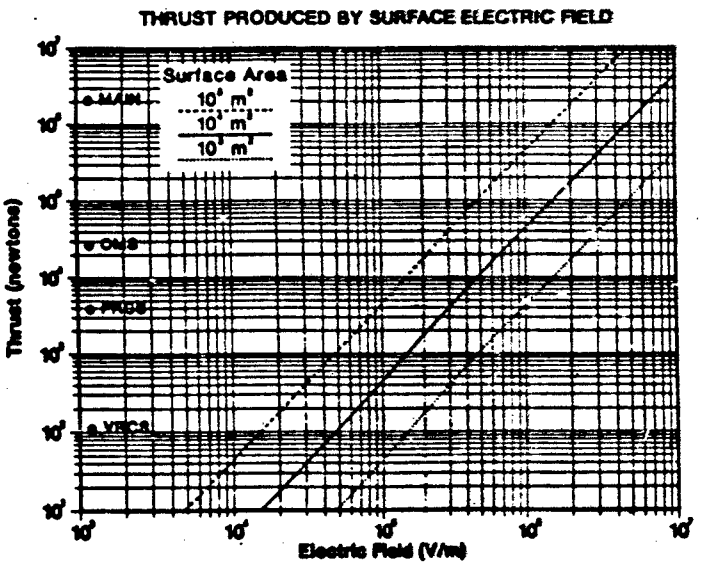

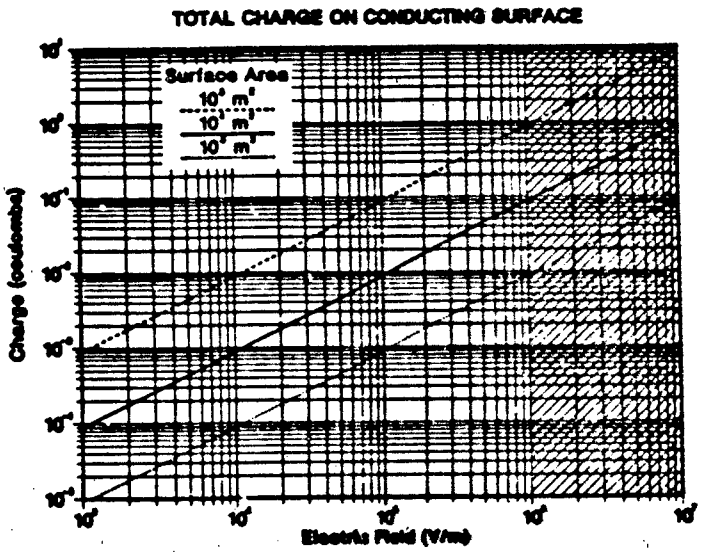

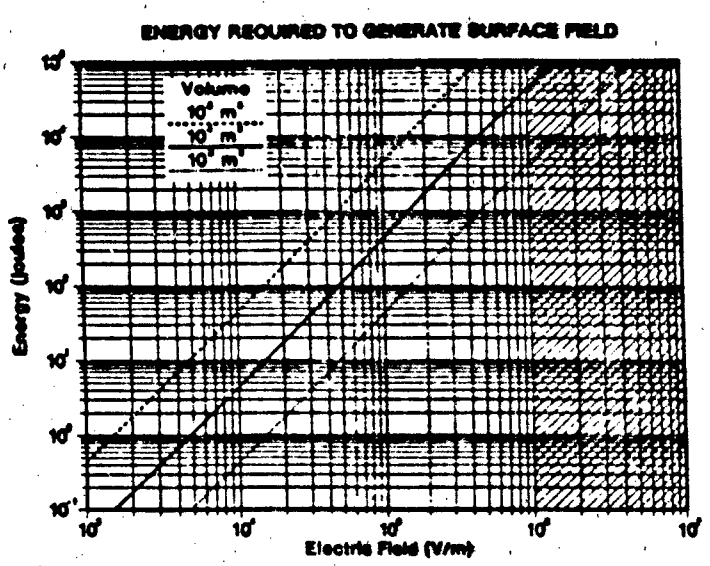

Figure 2 "First Order" Calculation of Electrostatic Surface-Field Thrust.

Basic Processes of Plasma Propulsion

Herbert O. Schrade
Institut für Raumfahrtantriebe der Universität Stuttgart

The goal of this program is to get a better understanding of a) the acceleration mechanisms and b) the electrode effects in self magnetic pulsed and continuous MPD-arc thrusters. In order to assess the applicability of these thrusters as space propulsion systems such an investigation is mandatory. Moreover, since similar problem areas can be found in many other low to medium pressure arc devices, the results of this study should be also of interest for electrically induced gasdynamic lasers, MPD-power generators and power switching devices.

a) the magnetic thrust of a MPD-arc propulsion device increases with the square of current. Unfortunately by increasing the current above a critical value, one observes strong voltage fluctuations and simultaneously a detrimental increase of electrode and insulator erosion. This fact, which has been found in all steady and quasi steady self field thrusters severely limits their performance. So far besides the two known explanations of this "onset phenomenon",- the first of which is an anode sheat failure due to plasma starvation caused by a radial magnetic pressure increase (Hügel) and the second which is an excessive back EMF (Lawless and Sabramanian)- another explanation could be put foreward which also accounts for the electrode and insulator erosion. This new explanation is based on a plasma instability, which leads to a deviation off the axisymmetrical current distribution and hence to a current concentration on the anode surface (see Fig. 1a). The derived onset conditions for this instability phenomenon agree quite well with those found in experiments. However in order to relate this onset conditions to the overall quantities of any thruster type like mass flow rate and total current,one has to know the average current contour and flow lines within the thruster. Therefore a simplified rotationally symmetric, twodimensional numerical methode to calculate the flow pressure and current density field for different thruster geometries has been set up and will be successively improoved. The current contour and constant pressure lines of such a numerical calculation for the Stuttgart MPD-Thruster assuring isothermal conditions for the electrons and an isotropic behavior of the heavy particles are shown in Fig. 1b.

b) In order to gain a better understanding of the cathode phenomenon and in order minimize the erosion rate in MPD-arcs an experiment has been initiated in addition to the theoretical work. The experimental set up is schematically shown in Fig. 2 and is placed in a vacuum test vessel which allow pressure variations between 10^{-3} and 10^{4} Pa for different gases. The cathode sample which can have different shapes (cylinder, flatt plate, etc) is mounted between two rods. The arc discharge is struck between the cathode sample and an anode of variable length. The electrode system is energized by a pulse forming network of electrolytic capacitors delivering a rectangular current pulse lasting about 2 ns with currents which can be varied between several hundred amperes up to 10 kA. By means of an auxiliary electric current through the cathode sample the cathode can be preheated and/or a transverse magnetic field of different strength can be applied. By means of this test apparatus the cathode attachment behavior, the mass loss, erosion rate and surface damage for different cathode materials under various aperating conditions will be determined and investigated.

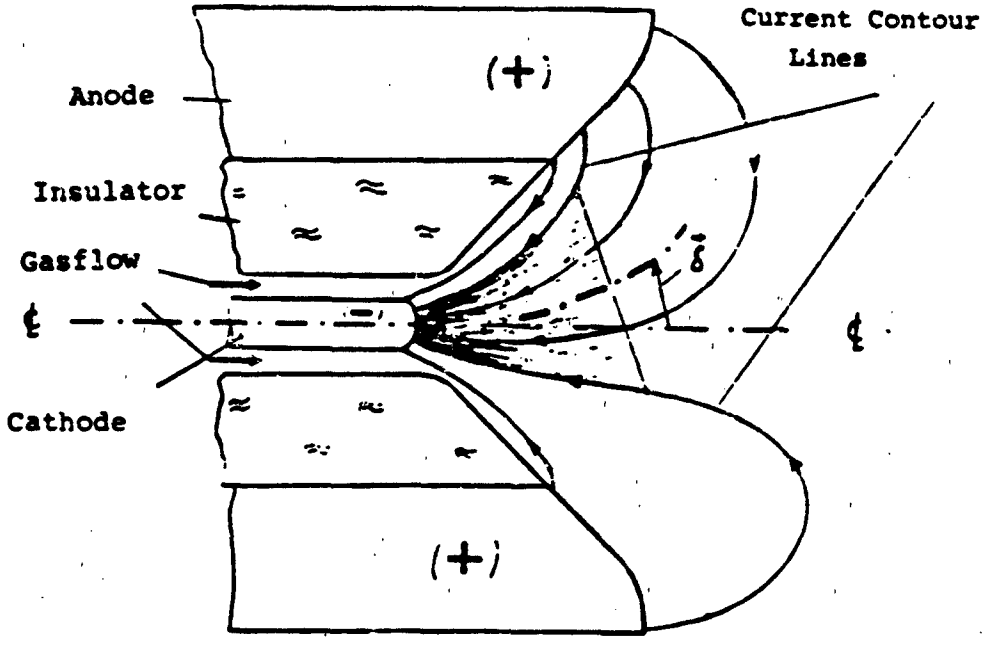

Fig 1a: MPD-Arc with Disturbed Current Contour Lines

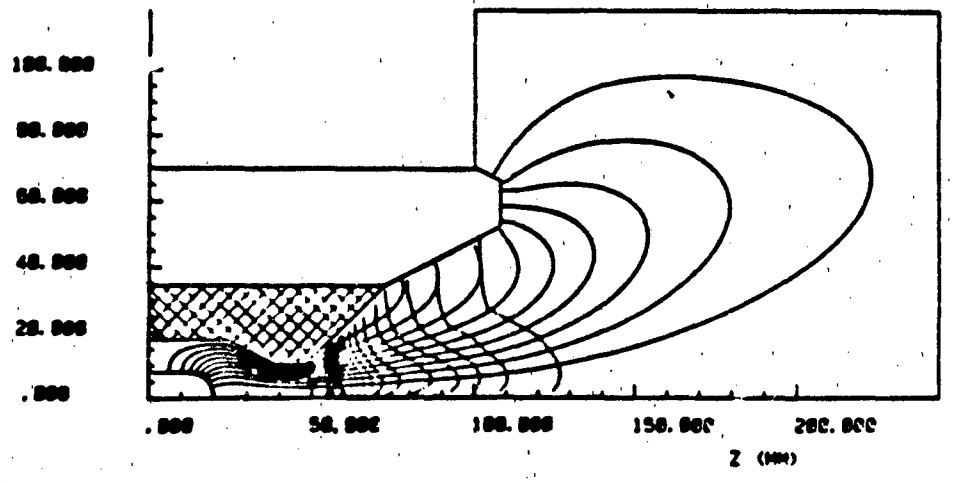

Fig 1b: Calculated Current Density and Constant Pressure Lines within the Stuttgart MPD-Thruster

ELECTRODE TEST CONFIGURATION

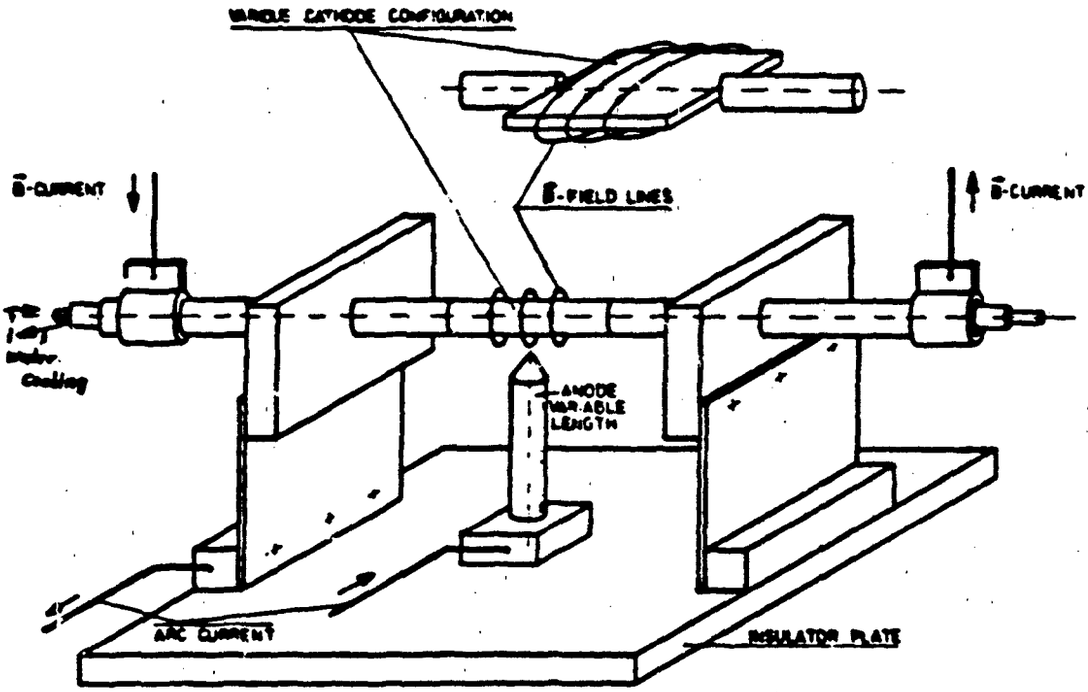

Tasks:

- Determine the mass loss and the erosionrate by weighing the cathode sample before and after a series of discharge pulses
- Investigation of arc traces (craters) on the cathode surface by means of optical and scanning electron microscopy
- Observe by means of high speed cameras the arc attachment motion

Fig. 2: Cathode Experiment: Scheme of Electrode Test Configuration; proposed Tasks.

PERFORMANCE-LIMITING FACTORS IN MPD THRUSTERS

By Manuel Martinez-Sanchez, Daniel Heimerdinger, Mark Chanty and David Melanson
M.I.T., Dept. of Aeronautics and Astronautics
Cambridge, Massachusetts 02139

Continuing our research effort into the physics and design of MPD thrusters, we are this year addressing three primary questions: (a)Based on a simplified model of the plasma physics (but still retaining the Hall effect), how should an MPD channel be lofted to insure a smooth current distribution? (b)Developing a numerical simulation code for off-design or off-shape channels. (c)Development of experimental tests and diagnostics to verify the above. This approach differs from the more traditional route , in which the channel shape is arrived at in a purely empirical manner, and also from earlier plasma flow analyses, where the crucial role of the Hall parameter (particularly for onset) was not accounted for. We are also hoping to bring to bear advanced diagnostic techniques (fiber optics, fine spectral measurements and active laser probing).

During the past few months we have formulated the governing dynamic equations for a fully ionized plasma with tensor conductivity in terms of axial distance and stream function, using boundary layer approximations for a slender geometry. The distribution of total pressure (ordinary plus magnetic) along the channel is prescribed, which nearly prescribes the current density, and the axial and transverse profiles of the remaining quantities are then computed, among them the cross-sectional area. Insight is derived from the existence of a simple analogy to gas-dynamic nozzle flow when the magnetic Reynolds number is high; thus, choking at the throat occurs at the magneto-acoustic velocity, and Prandtl-Meyer expansion fans, whose fanning constant-density lines are also the current lines of the commonly observed anode-exit arc, are seen as a natural effect at the channel end. Finite magnetic Reynolds number effects modify these results. The theory also yields a simple design showing no axial current, and hence no side force tending to produce onset phenomena, but this requires an axial field, hence segmentation. Even in designs with no axial field (monolythic electrodes), the possibility of reducing the inlet and outlet current concentations is likely to lead to a delay in the onset of instability. We hope to use our computer code based on the above theory to design a longer life, higher onset channel.

In parallel with this, several other activities are being pursued. They include a full 2-D, time-varying numerical simulation of plasma flow for a prescribed geometry, which is undergoing tests, and preparation for experimental testing of a channel designed according to our theoretical work. These tests will be in cooperation with RDA, Washington office.

ISSUES:

HOW TO DESIGN MPD THRUSTERS WITH MINIMAL CURRENT CONCENTRATIONS AND DELAYED ONSET PHENOMENA

APPROACH:

A) INVERSE (DESIGN) CALCULATION OF AREA DISTRIBUTION
B) DIRECT NUMERICAL MODELING (GIVEN SHAPE)
C) EXPERIMENTAL VERIFICATION

A) DESIGN

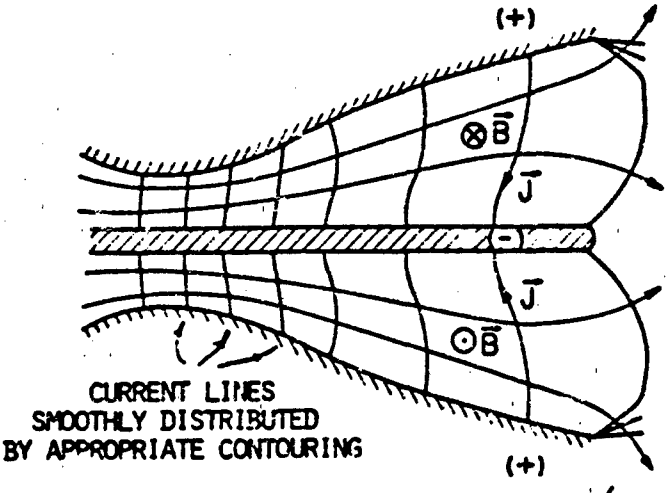

B) ANALYSIS

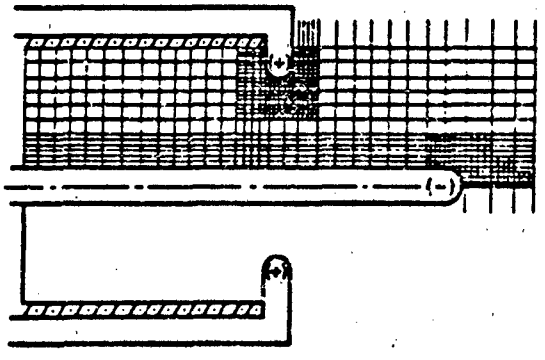

REFINED GRID USED
IN CRITICAL AREAS

TIME MARCHING, AXISYMMETRIC FINITE
DIFFERENCE MODEL

NEW RESULTS AND WORK IN PROGRESS

A) HAVE FORMULATED ANALOGY OF HIGH INTERACTION MPD TO ORDINARY GASDYNAMICS

B) HAVE FOUND LIMITING CONFIGURATION WITH NO AXIAL CURRENT - REQUIRES CONTOURING AND SEGMENTATION OF ELECTRODES

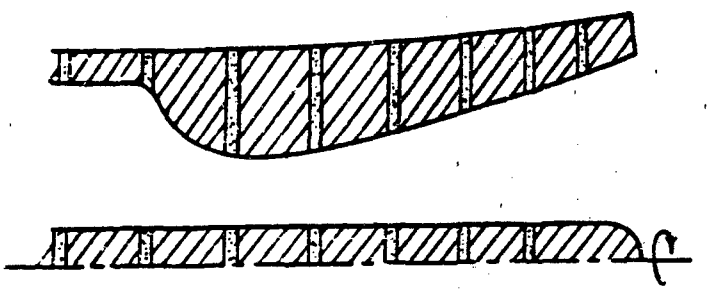

C) HAVE DEVELOPED DESIGN CODE FOR NON-SEGMENTED, CONTOURED CHANNELS WITH SMOOTH CURRENT DISTRIBUTION

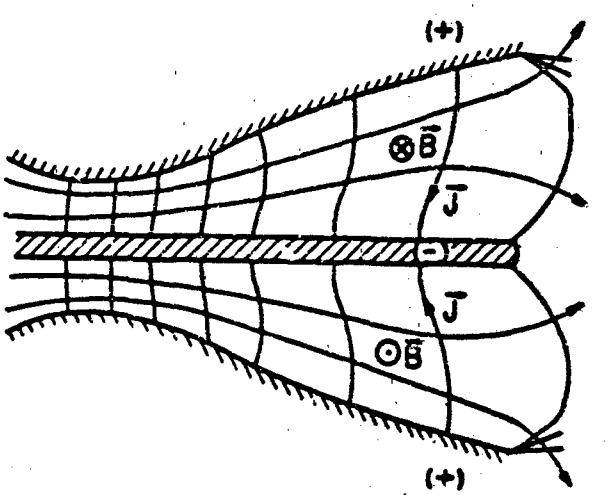

D) ARE PLANNING PULSED TEST OF CONCEPTS, USING FLOW DIAGNOSTICS TO VERIFY ANALYSIS. ALSO TWO-DIMENSIONAL CODE DEVELOPED.

EROSION AND ONSET MECHANISMS IN MAGNETOPLASMADYNAMIC THRUSTERS

John L. Lawless
Carnegie-Mellon University
Pittsburgh, Pennsylvania 15213

Although erosion is a major concern in MPD thruster design, very little is presently known about it. To minimize erosion, it is desirable to operate in the diffuse as opposed to spot mode of current conduction. The goal of this work is (1) to determine the limits of diffuse mode operation and (2) to quantify its erosion rates. Since, at present, there are no theories to answer either question, this work is unique. Also, it is hoped to clarify the relationship between erosion and the experimental phenomenon of 'onset.'

Erosion is believed to be due to evaporation and sputtering. Evaporation is a serious concern with tungsten electrodes if the surface temperature reaches 3000K, as it might in steady-state operation. The surface temperature is determined by a heat transfer problem involving the plasma, the sheath structure, and the electrode cooling mechanisms. The importance of sputtering is determined by the rate with which energetic ions strike electrode or insulator surfaces. A major unknown here is how such high energy ions are created. One hypothesis, due to Kuriki and Onishi, is that they are created in a high voltage region of the anode sheath. Another possibility is that they are created by thermal means within the plasma, possibly in the relatively hot boundary layer. The above considerations are illustrated in figure 1. The importance of sputtering may be strongly affected by the density of second ions. The importance of second ions is currently being studied.

To quantify erosion, knowledge of plasma temperature and compositional profiles is needed. To this end, a flow model is being studied. This model includes the effects of pressure gradients, magnetic forces, ohmic heating, and convection in a quasi-one-dimensional approximation similar to that of King et. al.(1981). The effects of ionization on the otherwise ideal gas flow have been studied. The results show that ionization greatly affects the choking condition and hence the electrical characteristics of the thruster. This is illustrated in figure 2.

The primary scientific accomplishment to date has been the prediction of a new onset mechanism. This mechanism predicts that the back emf rises rapidly enough to limit the current to some critical value. This mechanism is distinct from the anode sheath failure mechanism analyzed by Baksht et. al.(1974) among others. It should be possible for experiments to distinguish between these two mechanisms. The Baksht mechanism would be observed as a rapid increase in the voltage drop of the anode sheath near the exit as onset is approached. The proposed new mechanism would be observed as a rapid drop in current density in the middle of the thruster. The preliminary evidence exists to support the existence of both mechanisms but is inconclusive about which occurs first under different flow conditions. Current work shows how these onset limitations are altered by the presence of ionization.

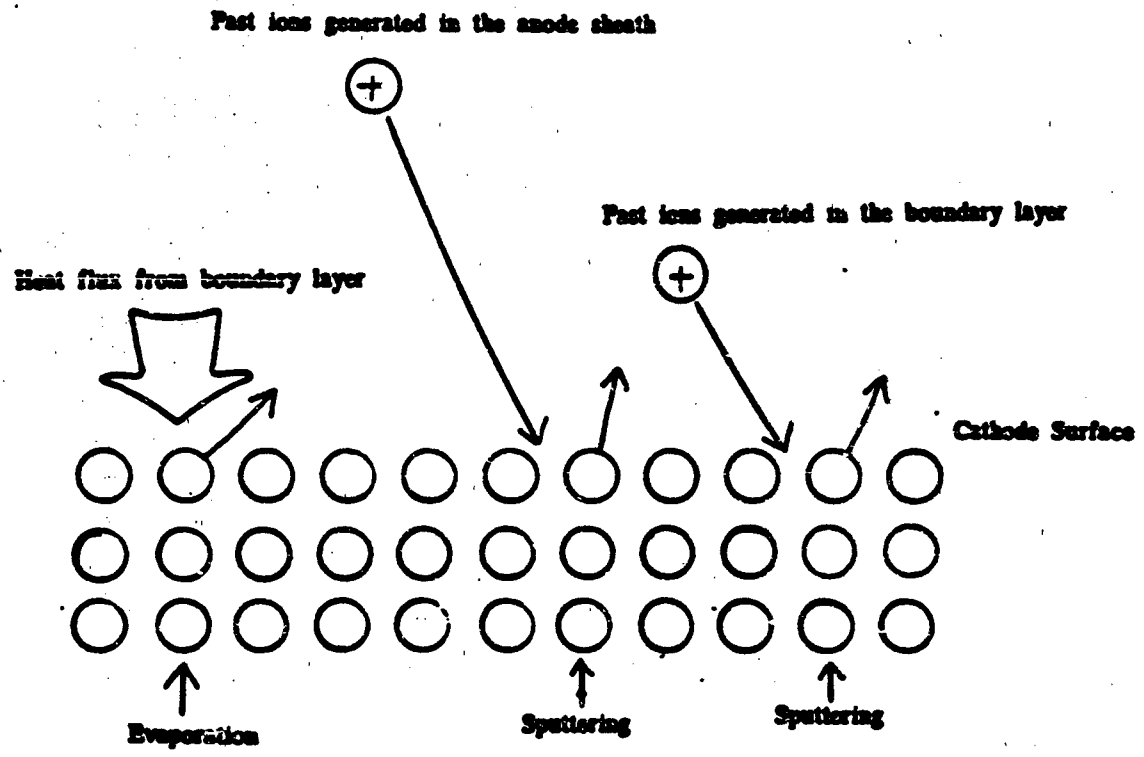

FIGURE 1: Some erosion mechanisms for an MPD thruster cathode are shown.

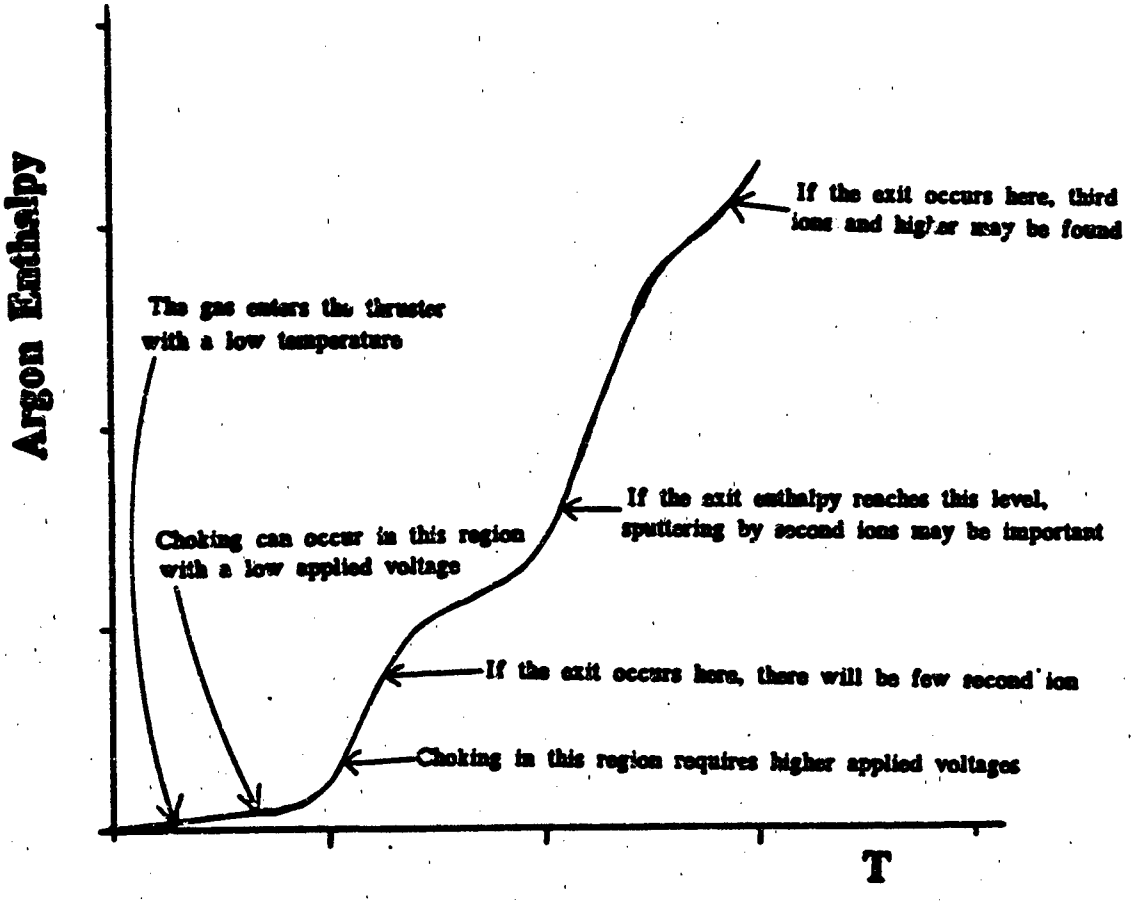

FIGURE 1: A plot of enthalpy versus temperature for argon is shown. The sharply rising portions indicate a new ionization stage.

MAGNETOPLASMADYNAMIC THRUSTER EROSION RESEARCH

David Q. King
Jet Propulsion Laboratory
California Institute of Technology
Pasadena, California 91109

Magnetoplasmadynamic thruster (MPDT) lifetime at sustained multi-megawatt power levels is unknown but will be governed by plasma erosion of thruster surfaces. Before the thruster can be developed for an orbital propulsion application the physics of the erosion mechanisms must be studied. The research proposed herein addresses the following key questions that must be resolved in order to understand erosion:

1) What are the erosion mechanisms on the anode, cathode, and insulator and what are the quantitative rates for each?

2) What governs the cathode heat balance at high current density (>200A/cm^2) and megawatt power levels.

3) What governs the anode heat balance.

4) How does the cathode work function change with time, and what effect does this have on erosion.

The approach is unique in that it aims at developing an understanding of the erosion of the electrode and insulator surfaces by conducting experiments on a steady-state, scaled-down MPD device, and by analysis of key processes. Figure 1 shows the cathode and cathode sheath region and identifies two types of emission processes, one of which is destructive the other non-destructive.

The primary accomplishment this year is to have shown, by steady-state tests and analysis that the cathode operates in a diffuse, thermionic mode which can be considered non-destructive in some cases. Figure 2 shows thoriated tungsten cathode tip temperatures measured by an optical pyrometer that are commensurate with high current density, field-enhanced thermionic emission.

Analysis of the data provides a further insight by exposing two key processes in the cathode heat balance. Here, a large flux of low energy ions bombard and heat the cathode as they are drawn into and accelerated by the cathode sheath. Each thermionic electron emitted from the cathode removes the work function in energy thereby providing a cooling effect that increases with current density. The bottom of Figure 2 shows that at lower current densities, ion bombardment dominates the heat balance and can cause temperatures high enough to evaporate cathode material quickly. The bottom curve, at a lower plasma density ($5\times10^{20}/m^3$) incurs reduced ion bombardment and indicates reduced temperatures commensurate with experiment. The temperature at various plasma densities are driven to a common point at extremely high current densities by the effect of electron cooling.

The design of multi-megawatt MPD engines is advanced by the realization that high current densities demanded by size and efficiency constrains are in fact necessary to keep the cathode cool enough, by electron emission, to prevent severe temperatures and evaporation.

FIGURE 1 - TECHNICAL APPROACH

APPROACH: OPERATE SCALED-DOWN ELECTRODE MODEL TO DETERMINE CONDITIONS CAUSING MICRO-SPOT-MODE OR DIFFUSE MODE CURRENT EMISSION, AND CATHODE TEMPERATURE

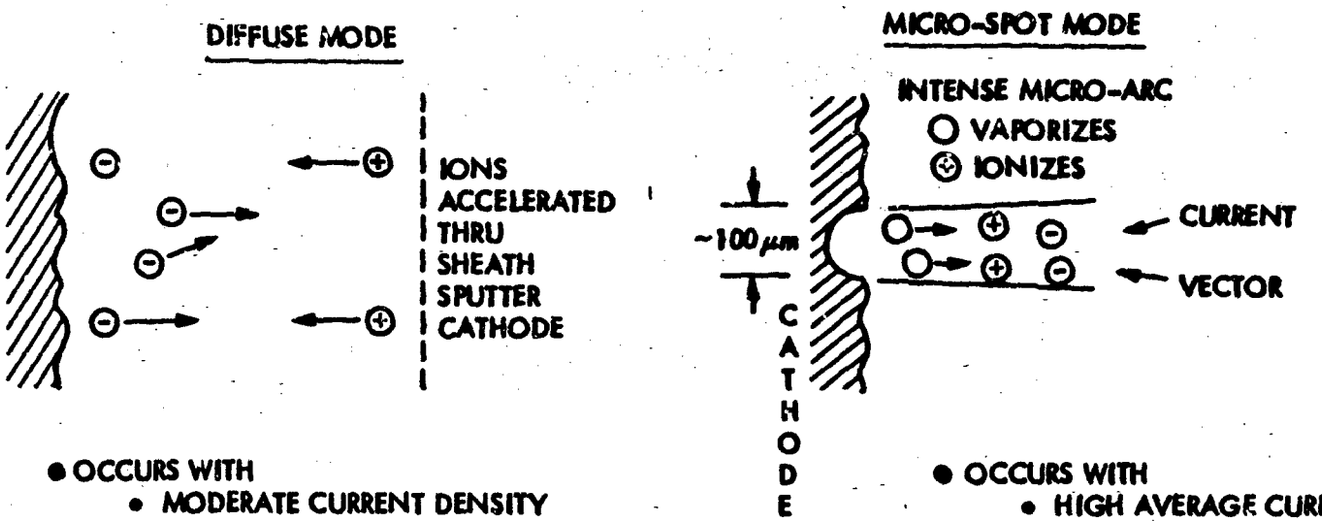

- OCCURS WITH
  - MODERATE CURRENT DENSITY
  - HOT CATHODES
  - LOW WORK FUNCTION CATHODES
- LOW EROSION RATE (10^{-3} - 10 Å/SEC)
  - SPUTTERING
  - EVAPORATION

- OCCURS WITH
  - HIGH AVERAGE CURRENT DENSITY
  - LOW PLASMA DENSITY AND PRESSURE
  - COLD CATHODES
- HIGH EROSION (10^{3} Å/SEC)

MODE DEPENDS UPON AVERAGE CURRENT DENSITY, PLASMA DENSITY, CATHODE TEMPERATURE, AND FIELD ENHANCED WORK FUNCTION, NONE OF WHICH HAVE BEEN QUANTIFIED.

FIGURE 2 — MPD THRUSTER EROSION RESEARCH — RESULTS

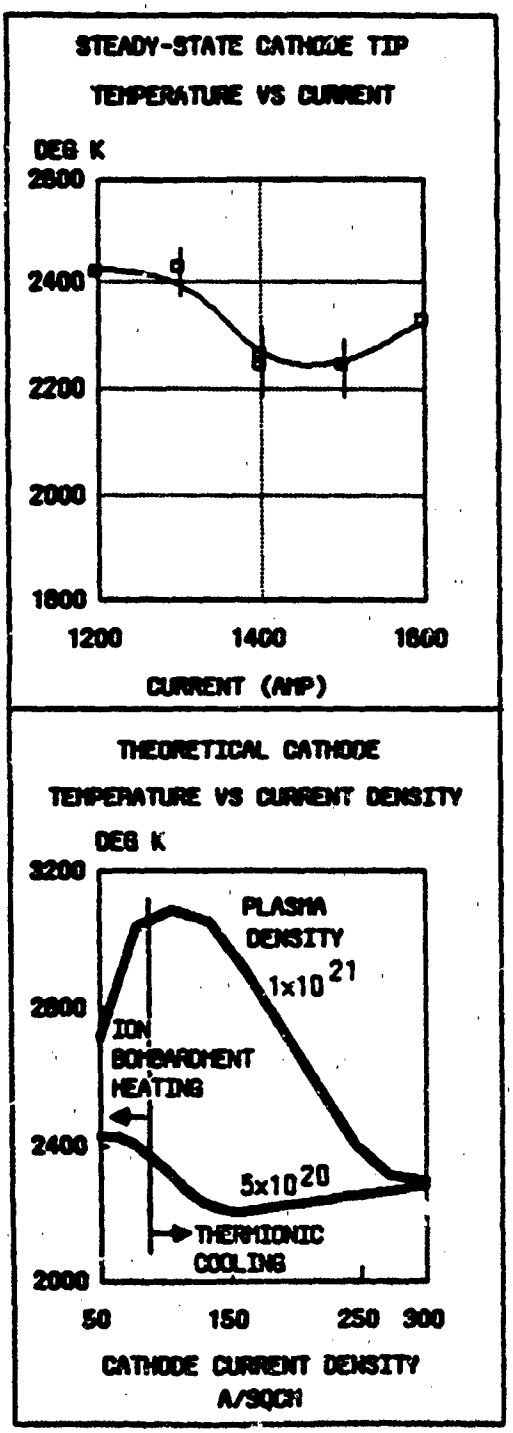

- SUBSCALE STEADY-STATE, RADIATION COOLED MPD DEVICE OPERATIONAL
- PROVIDES ESSENTIAL DATA FOR COMPARISON WITH THEORY
- OPERATES OVER A WIDE RANGE OF CURRENTS AND MASS FLOWS YEILDING ORDERS OF MAGNITUED VARIATIONS IN PLASMA PROPERTIES

- **PRIMARY RESULT:** THE MPD CATHODE OPERATES IN A DIFFUSE, THERMIONIC EMISSION MODE

- ANALYSIS CONCURS WITH EXPERIMENT THAT CATHODE OPERATES IN A THERMIONIC EMISSION MODE
- ANALYSIS SHOWS HEAT BALANCE IS STRONGLY COUPLED TO PLASMA SHEATH AND THERMIONIC EMISSION ABOVE ~40 A/SQCM
- HEAT BALANCE MAY BE DOMINATED BY:
  1) ION BOMBARDMENT-HEATING POTENTIALLY CAUSING TEMPERATURES HIGH ENOUGH TO RAPIDLY EVAPORATE THE CATHODE
  2) THERMIONIC ELECTRON EMISSION-COOLING PROVIDING TEMPERATURES "SAFE" FROM EVAPORATION

COMPLETELY MAGNETICALLY CONTAINED ELECTROTHERMAL THRUSTER

George R. Seikel
SeiTec, Inc.
P.O. Box 81264
Cleveland, OH 44181

Results of previous major MPD arc thruster experiments with applied magnetic fields are summarized in Ref. 1. The highest measured performances were: 1) a thrust efficiency of 37% at 2200s specific impulse with a xenon propellant thruster operating at a power of 0.48kW, and 2) a thrust efficiency of 34% at 2500s specific impulse with an argon propellant thruster with a 1T superconducting magnet at a power of 25kW.

Results for both this 25kW thruster and a MW quasi-steady thruster also demonstrated that efficiency significantly increases with the applied magnetic field strength up to the experimental limits, 1 and 2T respectively. At these field strengths the cyclotron radius of the propellant ions becomes smaller than the anode diameter, and heating, containment, and acceleration of the plasma ions can be directly accomplished by the applied radial electric field and expanding axial magnetic "nozzle" field.

These prior experiments all had inefficiencies, operating limits, and life limits associated with their physical upstream thruster backplates. One such problem is illustrated in Fig. 1.

Fig. 1 shows a 0.5kW thruster which was life-tested for 1332 hours. Also shown are cross-sectional sketches of the upstream boron nitride insulator after 735 and 1332 hours of operation. This wear was life limiting and reflected a large inefficiency. Efficiency was improved over 10 points, to the previously cited 37%, by modifications providing a stronger upstream magnetic mirror field. However, this higher efficiency thruster was limited in power level by heating of the backplate. As it became heated to a dull red, the efficiency decreased.

Backplate problems have also limited higher power MPD thrusters which to date have all used coaxial cathodes and anodes. In the only life test of a radiation cooled 25kW thruster, testing had to be terminated at 553 hours because of rapid erosion of the thrusters boron nitride insulator.

The subsequent, previously mentioned, superconducting magnet thruster used a hollow cathode to better control current attachment; however, for stable operation it required all the propellant to be introduced into the cathode which penalizes performance. A downstream cathode could eliminate this problem but will not eliminate backplate heating and erosion problems.

The present research is developing conceptual designs of a novel thruster concept which avoids backplate inefficiencies, operating limits, and life limits. This concept, Fig. 2, provides for complete upstream magnetic containment of the plasma. The magnetic field is designed to insure both stable plasma containment in the upstream "U" and efficient expansion in the downstream magnetic nozzles. Two designs are being defined. The first for quasi-steady (1ms) MW operation with 1T fields. The second for steady-state radiation cooled operation at a few kW with 0.03T fields. Both will have the same size and geometry, but will have different thickness coil turns and number of turns (to limit voltage). The plasma containment tube will be the anode and a single downstream cathode will be used. Anticipated performance improvements over that of prior thrusters will also be estimated.

1 Seikel et all, P. in Astro. and Aero., Vol. 89, 1984, L.H. Caveny editor, pp. 260-302.

0.5kW MPD THRUSTER LIFE-TESTED FOR 1332 HOURS

REF.: NASA TN D-7616, 1974

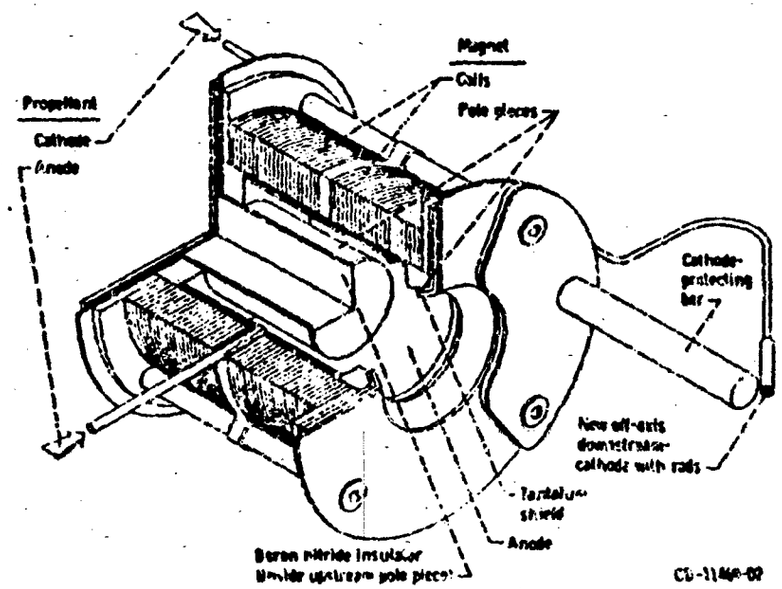

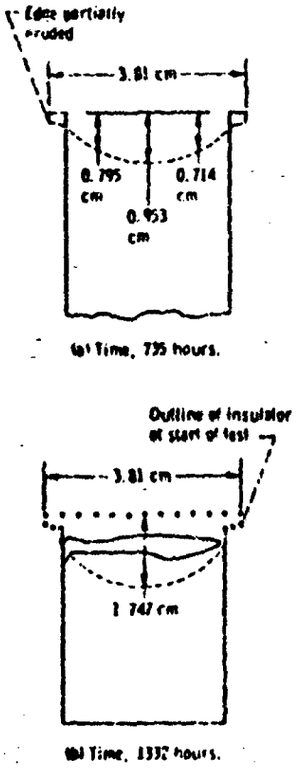

BORON NITRIDE INSULATOR

MAGNETICALLY CONTAINED ELECTROTHERMAL THRUSTER

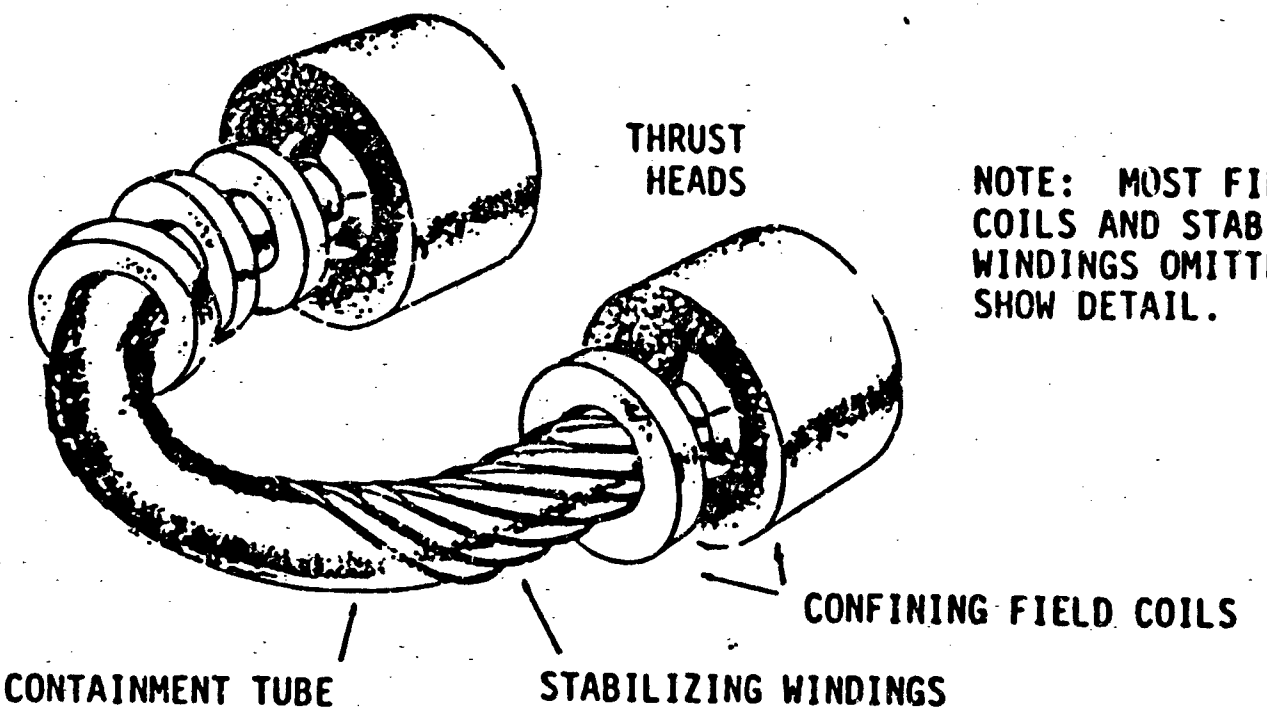

NOTE: MOST FIELD COILS AND STABILIZING WINDINGS OMITTED TO SHOW DETAIL.

Figure 2

PLASMA-GAS INTERACTION STUDIES IN A HYBRID PLUME PLASMA ROCKET

F. R. Chang,† W. A. Krueger, T. F. Yang, J. L. Fisher††

Plasma Fusion Center
Massachusetts Institute of Technology
Cambridge, MA 02139

A hybrid plume is here defined as one where the fluid properties exhibit a drastic variation from one region to another. The concept[1] has a potential application in magnetic divertors for energy recovery and impurity control in fusion reactors, as well as in rocket propulsion using high temperature plasmas. In a hybrid plume plasma rocket, for example, the temperature at the core of the exhaust is extremely high; whereas, near the edge, the temperature is quite low. Furthermore, the variation in temperature from the plume centerline to the outside can be many orders of magnitude. While the exhaust fluid at the center is a fully ionized plasma (at .5 to 1 keV), it actually becomes a neutral gas at the edges (at .1 to .3 eV). The net result is a plume, cool at the edges, thereby relaxing the heating constraints on the nozzle material, but hot at the center, thus preserving and even enhancing the allowable power density and specific impulse of the device.

In principle, such a hybrid configuration could be achieved by surrounding the hot plasma flowing out of one of the end cells of a tanden mirror[2] with a coaxial flow of high speed gas (Fig. 1). The gas would be injected through a hypersonic annular nozzle immediately downstream of the mirror end cell. The hypersonic gas would have the dual purpose of: (1) effectively insulating the nozzle walls from the the hot plasma, and (2) increasing the available mass flow rate and hence the overall thrust of the system.

The physics of high temperature hydrogenic plasma, interacting with hypersonic gas jets are not well understood. Analytical and numerical modeling of these interactions requires the simultaneous, self-consistent solution of particle, momentum and energy transport equations for each particle species. Moreover, the solution approach must have sufficient spatial granularity to resolve small regions of the flow pattern.

The present research covers the area of plasma/gas interaction and describes the basic mechanisms for energy and particle transport. The solution approach assumes cylindrical geometry and includes a multiplicity of atomic reactions, as well as the presence of a strong magnetic field. The principal reactions are electron and ion impact ionization, as well as charge exchange between hot ions and cold neutrals. Radial particle and energy transport is mainly by diffusion. Accordingly, the present description includes a modified Bohm diffusion model for plasma in the core of the plume, and classical neutral particle diffusion in the cooler regions of the flow. Neutrals are allowed to "free stream" in the low density regions, where the collision mean-free-path becomes comparable, or even larger than the characteristic dimensions of the system.

---

†Astronaut Office of the NASA Johnson Space Center, Houston, TX
††Southwest Research Institute, San Antonio, TX

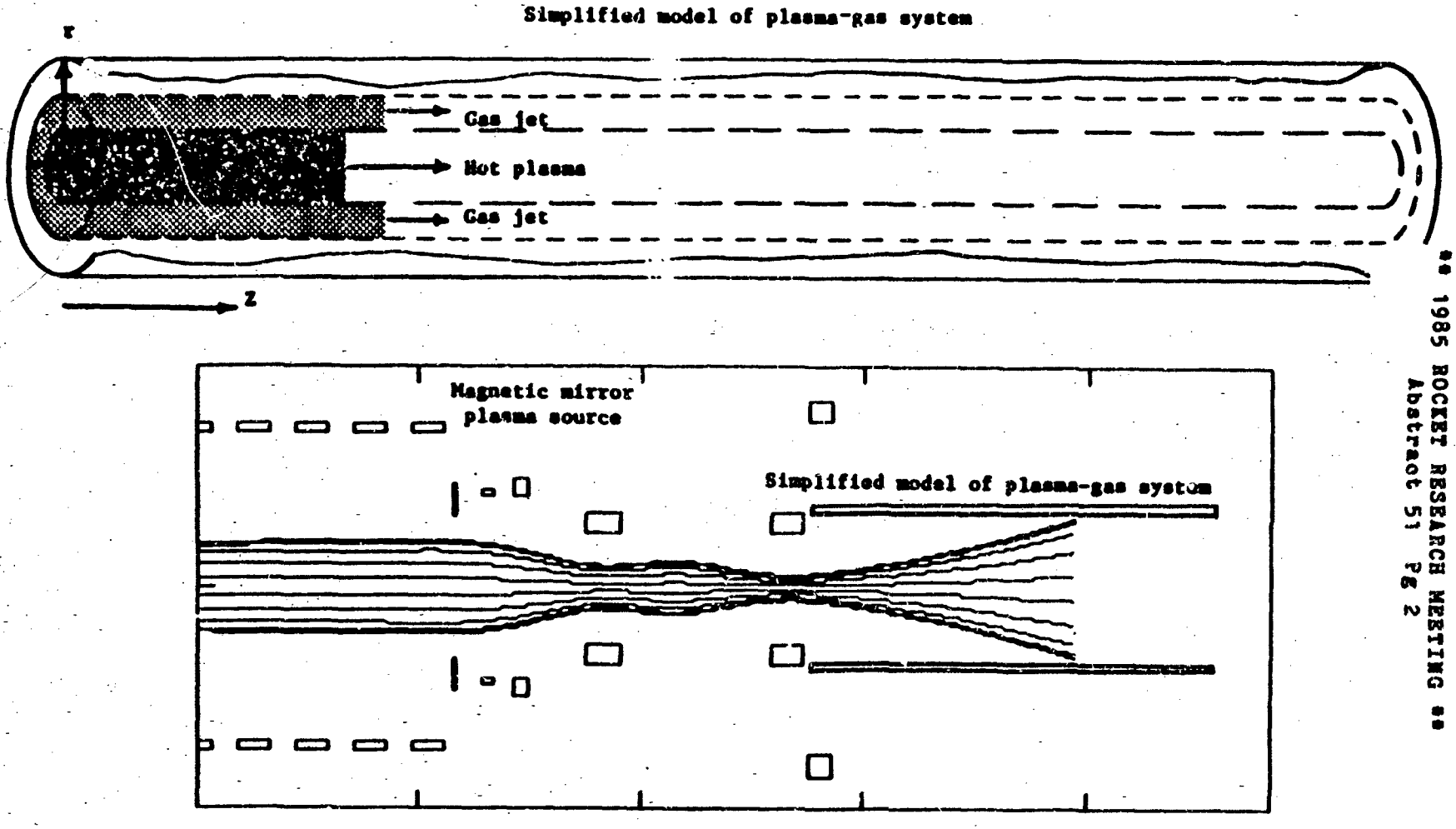

Figure 1: Model of plasma-gas system; the figure at the top shows the simplified cylindrical model for numerical simulation; the figure at the bottom shows the plasma source into the cylindrical duct from the designed mirror device.

A TANDEM MIRROR PLASMA SOURCE FOR HYBRID PLUME PLASMA STUDIES

T. F. Yang, F. R. Chang,†, R. H. Miller,
K. W. Wenzel, W. A. Krueger

Plasma Fusion Center
Massachusetts Institute of Technology
Cambridge, MA 02139

This paper describes a tandem mirror device to be considered as a hot plasma source for the hybrid plume rocket concept discussed in Ref. 1. The hot plasma from this device is injected into an exhaust duct, which will interact with an annular hypersonic layer of neutral gas. Such a device can be used to study the dynamics of the hybrid plume, and to experimentally verify the numerical predictions obtained with computer codes. The basic system design is also geared towards low weight and compactness, as well as high power density (i.e., several kW/cm^2) at the exhaust. This feature is aimed towards the feasibility of "space testing".

The basic structure of such a device consists of four major subsystems: (1) an electric power supply; (2) a low temperature, high density plasma gun, such as a stream gun, an MPD source or gas cell; (3) a power booster in the form of a tandem mirror machine; and (4) an exhaust nozzle arrangement. The configuration of the tandem mirror section is shown in Fig. 1.

A tandem mirror machine appears attractive for this particular application. These devices[2-4] can produce the necessary plasma conditions with minimal further technological development. In present day tandem mirrors, the plasma density varies from 10^{11} to 10^{13}cm^{-3} and the confinement time varies from hundreds of microseconds to tens of milliseconds. The power output ranges from a few kW to 100 kW. Advancement in both understanding of physics and technology to bring such a device to a high power level can be expected.

Presently these machines are large and heavy because they aim to achieve a high confinement time and the temperatures of 5 to 10 keV required for a fusion reactor. However, relaxing the confinement and temperature requirements translates directly to lower magnetic fields. For example, the maximum field required for a fusion reactor is usually about 15 T. In comparison, the maximum field needed for this application is 0.5 T, or 30 times smaller.

Another important consideration in an experimental arrangement of this nature is the basic method for plasma heating. In the present configuration, the tandem mirror section behaves as a power booster. The mechanism selected for energy coupling to the flowing plasma is ion cyclotron resonance heating, or more simply stated, microwave injection at the ion cyclotron frequency. This is a proven method for heating ions in fusion grade plasmas. The ions in the system absorb approximately 53% of the power, while the electrons receive 3%. This is a desirable result since energy transfer from the ions to the neutrals is more efficient than from the electrons to the neutrals. Efficiencies of 30% to 50% have been obtained.[7]

---

†Astronaut Office of the NASA Johnson Space Center, Houston, TX

Another aspect under investigation is the overall stability of the plasma column. In general, the plasma in linear devices such as this one is rich in wave phenomena, and simple magnetic mirrors exhibit "bad curvature" (i.e., the field lines bulge away from the axis of symmetry). The plasma in these configurations tends to be MHD unstable. Stability, however, can be readily attained in the tandem mirror geometry by the influence of the end cells. The outermost cell at each end of the mirror is appropriately designated as an "anchor". Notwithstanding these arguments, the MHD stability of these devices must be evaluated on an individual basis, particularly in relation to the axial asymmetry in this particular application (i.e., a source at one end and an exhaust at the other).

A generic device for this experimental application has been investigated in light of the above requirements and considerations. Preliminary results on its mode of operation, critical machine parameters, overall size, plasma stability, as well as an evaluation of the microwave heating requirements will be presented.

ACKNOWLEDGMENT

This work was supported, in part, by the Office of Scientific Research, US Air Force.

REFERENCES

1. F. R. Chang, W. A. Krueger, T. F. Yang and J. L. Fisher, "Plasma-Gas Interaction Studies in a Hybrid Plume Plasma" to be presented at this meeting.
2. N. Hershkowitz, R. A. Bruen et al., Proc. IAEA on Plasma Phys. and Cont. Nucl. Fus. Res. 1982, 1, 553, Vienna (1983).
3. W. C. Turner et al., "Recent Experimental Progress in the TMX-U Thermal Barrier Tandem Mirror Experiment", LLNL Report UCRL-90879, preprint, (1984).
4. M. E. Mauel, D. K. Smith, R. S. Post, J. Irby, et al., APS Bulletin 29, No. 8, paper 4S3 (1984).
5. W. A. Krueger, F. R. Chang, J. L. Fisher, T. F. Yang, Bull. Am. Phys. Soc., 28, No. 8, paper 1U4 (1983).
6. W. A. Krueger, F. R. Chang, T. F. Yang, internal reports to be published and paper to be presented at the same meeting.
7. S. N. Golovato, D. Brouchous, J. R. Ferron, Bull. Am. Phys. Soc. 29, No. 8, paper 9S3 (1984).

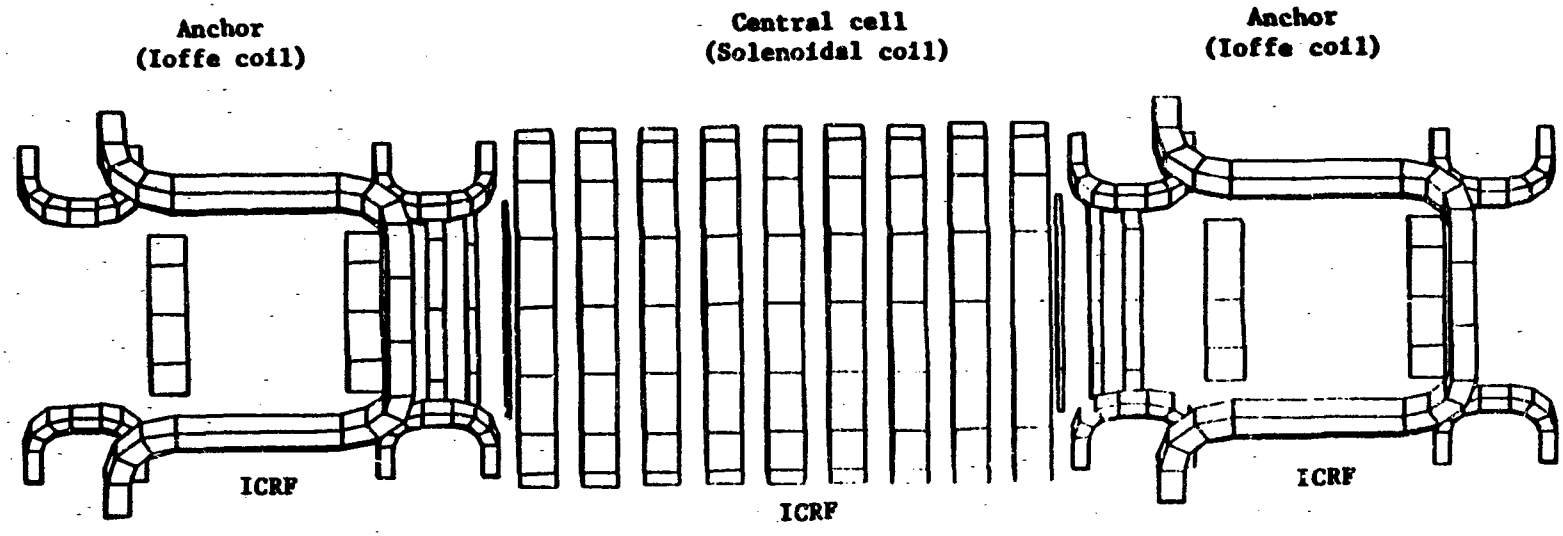

Figure 1: Position relationship between field intensity and mirror device.

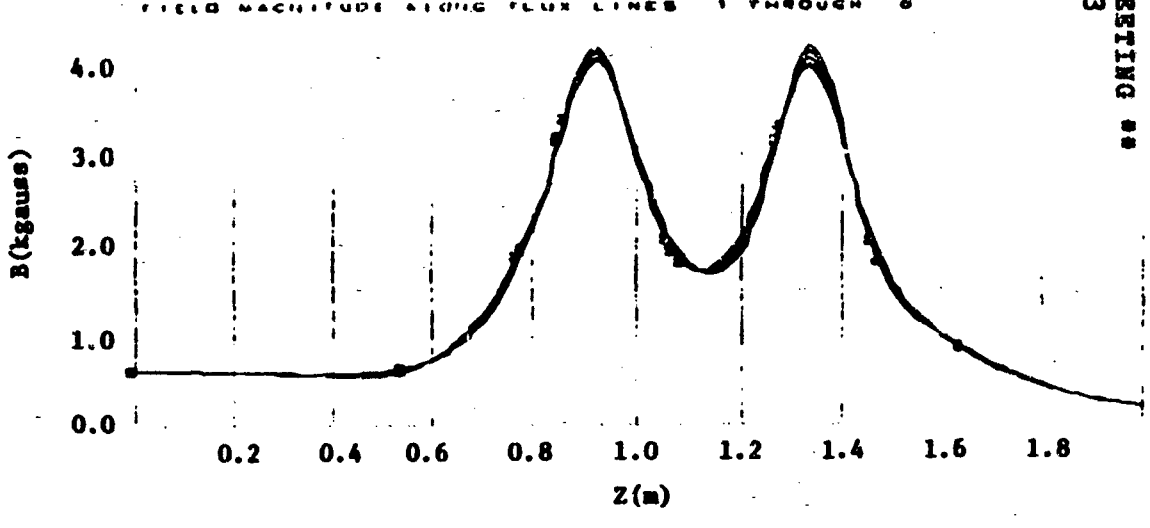

COUPLING BETWEEN GAS DYNAMICS AND MICROWAVE ENERGY ABSORPTION

Michael M. Micci
The Pennsylvania State University
University Park, PA 16802

Microwave energy can be absorbed by a gas in one of several modes in order to heat the gas to a high temperature. Because the region of energy deposition can be located away from any material walls, a higher temperature can be obtained than in devices which utilize wall heating. Allowing the high temperature gas to expand through a nozzle converts the internal thermal energy to directed kinetic energy to produce thrust. Hydrogen is the gas of choice for this application since its low molecular weight gives the highest exhaust velocity for a given chamber temperature. There is an understanding of the process of microwave energy addition to a high pressure gas for some of the available absorption modes but no unified comparison of all the modes in terms of absorption efficiency, maximum temperature, etc. Also there is little knowledge of the coupling of the absorbed energy to the gas dynamics required to obtain propulsive thrust. The proposed research will be the first experimental effort to examine and compare free floating filamentary and toroidal microwave absorbing plasmas and planar propagating plasmas in hydrogen gas as well as the first examination of the coupling of the energy absorption to the gas dynamics in order to convert internal thermal energy of the gas to directed kinetic energy by means of a nozzle expansion. Figure 1 illustrates the three absorption modes to be examined along with the three modes of heat transfer which may couple the absorption region with the interior gas dynamics.

This program will consist of analytical modeling of the microwave absorption regions both with and without gas flows and experimental measurement of key physical parameters such as gas temperature and heat fluxes. Heat losses from the absorption region and the amount of cooling gas required and its effects on final exhaust velocity and efficiency will be examined. Questions to be resolved include the relative roles of conduction, convection and radiation in transferring the absorbed microwave power to thrust power, the stability of such flows and the mixing processes of cold gas with the microwave sustained plasma. Figure 2 illustrates the anticipated scientific accomplishment of this program. The research will provide insight to the entire field of high temperature gas flows driven by radiation absorption.

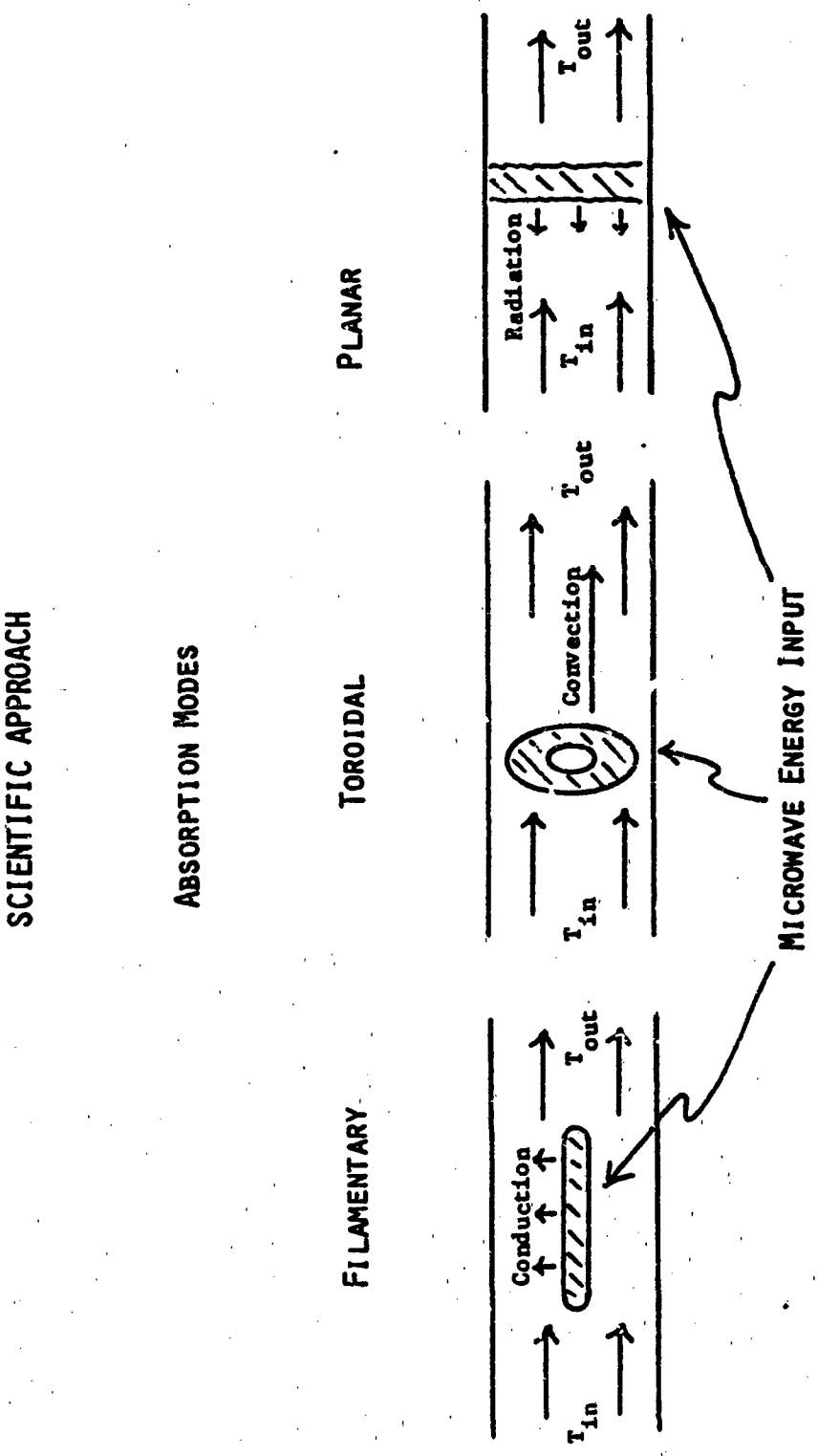
SCIENTIFIC APPROACH
ABSORPTION MODES
FILAMENTARY
TOROIDAL
PLANAR
Conduction
Convection
Radiation
T_{in}
T_{out}
MICROWAVE ENERGY INPUT

FIGURE 1

EXPECTED SCIENTIFIC ACCOMPLISHMENT

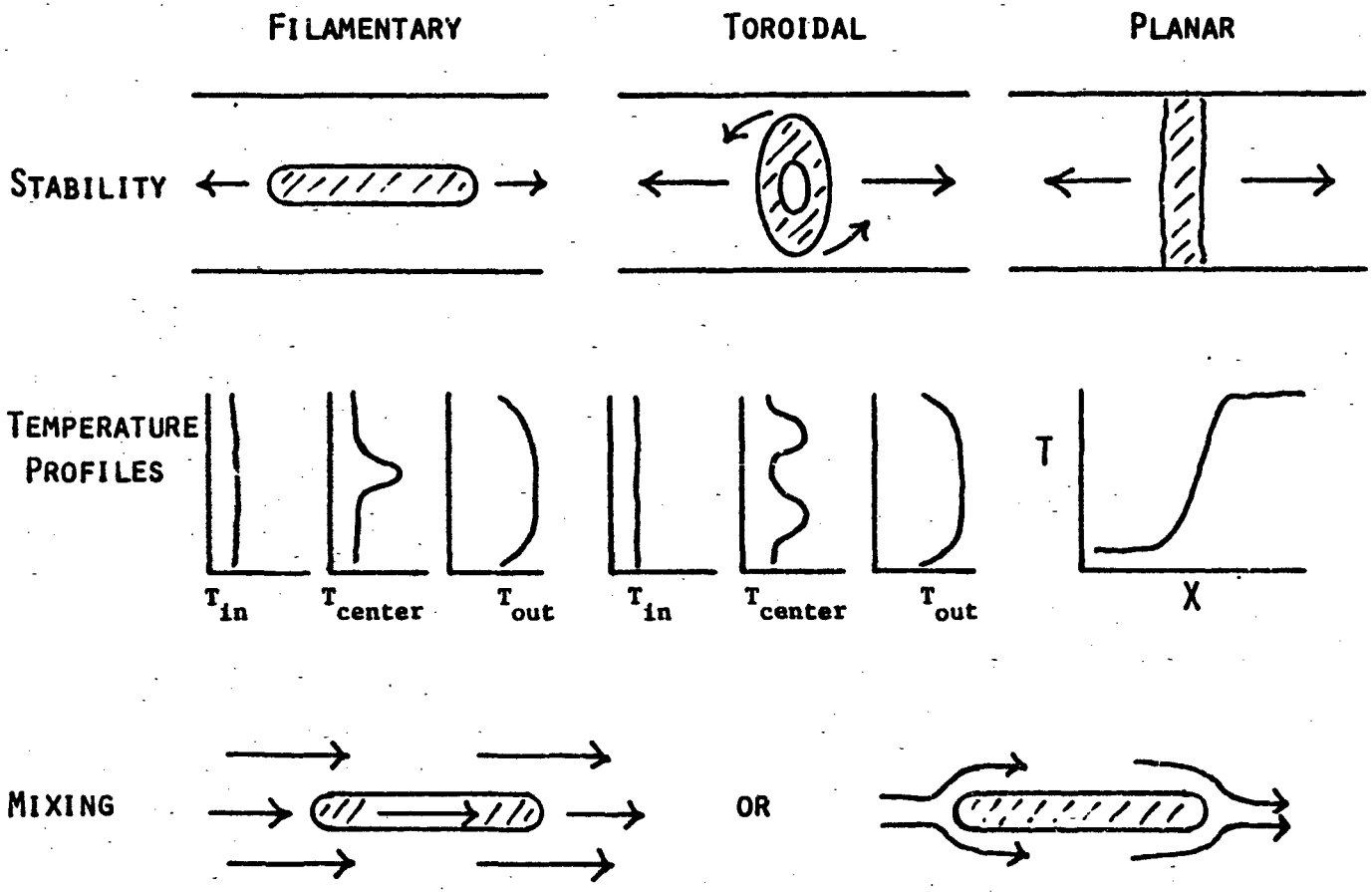

FIGURE 2

PULSED INDUCTIVE ENERGY TRANSFER

Peter P. Mongeau and Douglas P. Hart

Electromagnetic Launch Research, Inc.
625 Putnam Avenue
Cambridge, MA 02139

Advances in electrical propulsion have inspired a variety of approaches for orbit raising propulsion. One such technique, the metallic induction reaction engine, uses a solid metallic reaction mass rather then a gas or plasma to achieve a high thrust density and efficiency. The reaction mass is inductively accelerated by a magnetic pulse coil, thereby eliminating the problems of erosion and wear.

During the past two years, Electromagnetic Launch Research, Inc. has been investigating the pulsed inductive acceleration process. It is the goal of this research to establish the basic energy transfer mechanisms and the performance limitations of this device.

Experimental and numerical simulations of the pulsed inductive acceleration process indicates that the performance of the metallic induction reaction engine is more dependent on the density of the reaction mass material then it is on the conductivity of the material (Figure 1). Furthur analysis performed numerically indicates the existence of a back EMF saturation effect which can inhibit energy transfer to the pulsed inductive system. This saturation effect can be greatly reduced by using a compound pulse coil rather then a face coil to accelerate the reaction mass.

The high initial conductivity of metals such as aluminum, sodium, and lithium greatly reduce the energy transfer losses normally associated with inductive plasma excitation. Also, because these low density metals are accelerated in a solid form, a high degree of mass utilization is achieved. Ohmic heating during acceleration can melt and even vaporize these metals and in the process decrease the reaction materials conductivity. However, it is assumed that if sufficient voltage is induced by the pulse coil, the metal will ionize and continue to conduct electricity well past its vaporization point.

A compound pulse coil and an experimental aparatus has been constructed to observe and analyze the effects of back EMF and reaction mass ionization (Figure 2).

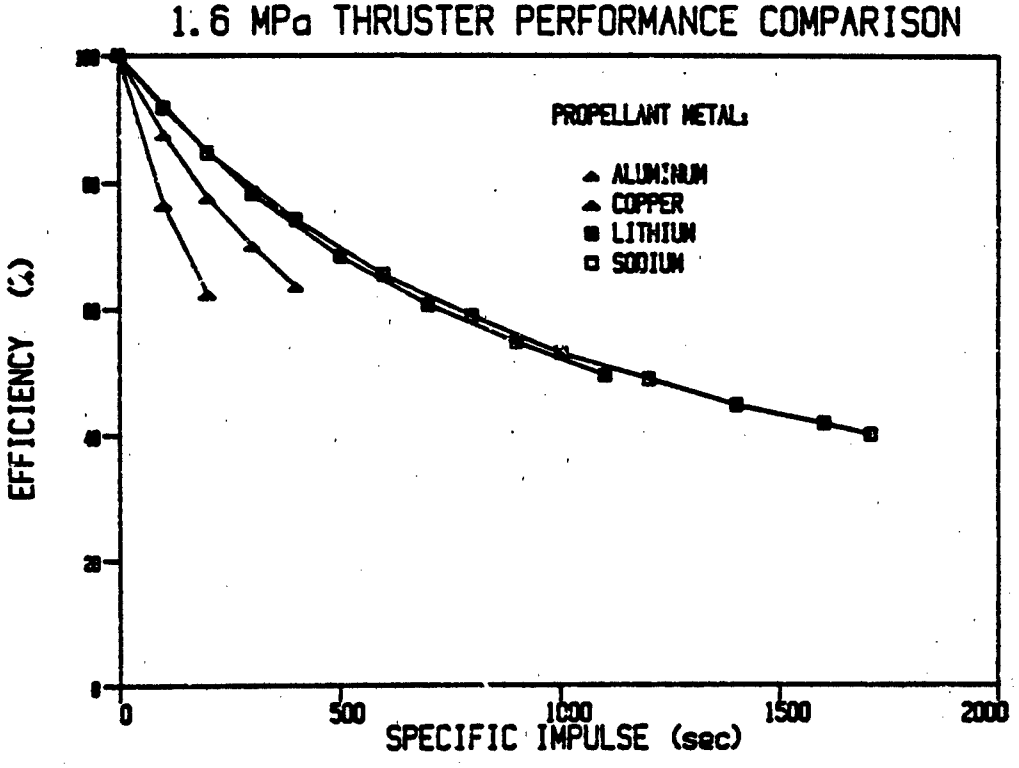

Figure 1: Reaction Mass Comparison

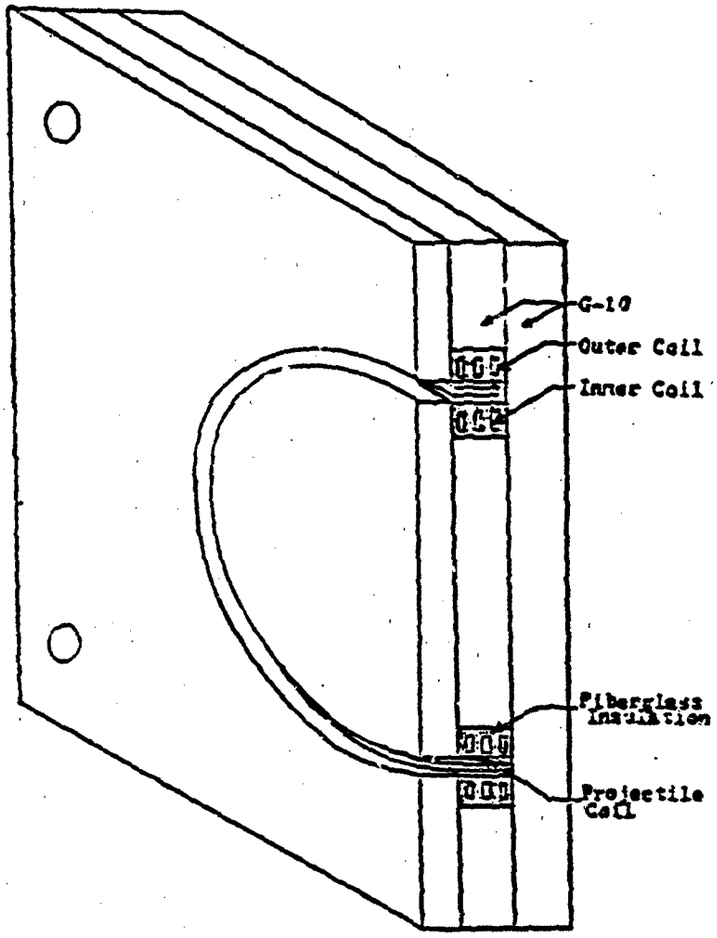

Figure 2(a): Experimental Compound Coil

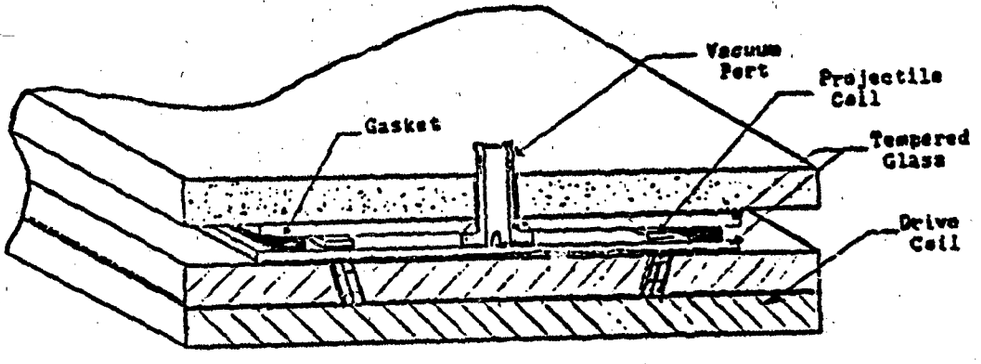

Figure 2(b): Ionization Aparatus

LASER DIAGNOSTICS FOR ELECTRIC FIELD MEASUREMENTS

Roger J. Becker, Blair A. Barbour, Alan T. Buswell

The objective of this program is to develop accurate means of measuring the electric field strength in transient plasmas with good spatial resolution. This requires a nonintrusive (optical) measurement that will provide reliable data in a conducting medium.

Our approach is to use selection rule breakdown in a laser scattering measurement. The selection rule breakdown is very sensitive to external perturbations such as electric fields. Its application to electric field measurements is, to our knowledge, totally unique. Two scattering spectroscopies will be explored. One of these, Rayleigh Depolarization Scattering (RDS), is directed at gas atoms and ions and highly symmetric molecules. The second method will use CARS to measure selection rule breakdown in Raman scattering, and will be applied to a wide class of molecules. This program is scheduled for completion by October 1, 1987.

Initial measurements are being made using RDS and a (cw) argon-ion laser on gases. These measurements will be followed by experiments in partially ionized gases. The cw measurements will then be supplanted by pulsed measurements using a copper-vapor laser. The experiments are being augmented by calculations of the electric-field induced depolarization.

The second half of the program will focus on the setup and testing of the Raman selection rule technique using CARS. This will require the construction of a dye laser for use with a copper-vapor laser. All measurements will be made in DC electric fields. A synchronization circuit will be built for the pulsed measurements.

SCIENTIFIC APPROACH

LASER LIGHT SCATTERING

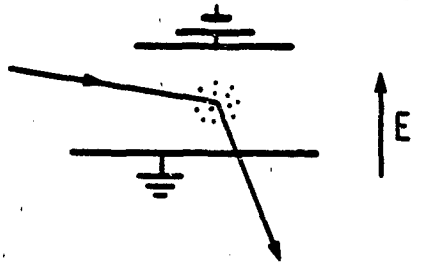

GOOD SPATIAL RESOLUTION
STRONG SIGNAL STRENGTH

SELECTION RULE BREAKDOWN

a		
	a	
		a
	↓	
a		c
	a	c
c	c	b

DISTORTION OF RAMAN AND RALEIGH SCATTERING TENSOR BY E FIELD

ANTICIPATED RESULTS

- DEMONSTRATION OF PHYSICAL EFFECT
- DEMONSTRATION OF TEMPORAL AND SPATIAL RESOLUTION CAPABILITY
- ESTIMATION OF RANGE OF APPLICABILITY
- DETERMINATION OF LIMITING FACTORS
- CALCULATION AND MEASUREMENT OF TENSOR COEFFICIENTS
- PUBLICATION IN REFEREED JOURNALS

OPTICAL TECHNIQUE TO MEASURE ELECTRODE EROSION

James D. Trolinger and David F. Schaack
Spectron Development Laboratories, Inc.
Costa Mesa, California 92626

The failure mechanism in a number of extremely important components and systems is electrical erosion, for example, in electrical propulsion systems or other components exposed to plasmas and arcs. Lifetime improvement and testing of such systems is extremely important and is difficult because erosion is sometimes extremely slow, requiring thousands of test hours. The present research will determine the ability and provide the required technology for highly sensitive optical methods to serve as a diagnostic for miniscule amounts of surface erosion.

Such methods, while relatively straight forward when applied to optically smooth surfaces or to surfaces which the microscope structure remains unchanged, become much more difficult for an eroding surface undergoing changes in microscopic surface structure.

A major question to be addressed concerns the effect of such a surface on optical properties which are relevant to the measurement of erosion. Perhaps, the most important of these is the change in the coherent speckle which will occur as the surface structure changes.

Three candidate optical methods will be analyzed for erosion measurement. They are (1) holographic interferometry, (2) diffuse point interferometry, and (3) an astigmatic ranging probe. All three methods possess the potential for measuring during lifetime testing of electrical systems with resolutions of one micrometer or better. Each method would be considered applicable to the high resolution contouring of a surface which changed profile without the associated change in microscopic surface features anticipated with electrically eroding surfaces. When surface changes are monitored with classical interferometry the change is manifested in a measureable shift in the phase of an optical wavefront. The surface microstructure adds a random phase term to the wavefront undergoing measurement. This term could be easily subtracted from the measurement unless it is changing. When it changes with time the change must be accounted for by either measuring it or averaging it out. The measurement of this change may not only allow the use of interferometry but may also provide itself an extremely sensitive measurement of erosion.

The most favored candidate will be assembled on a research breadboard experiment in which an electrically eroding surface simulating a useful application will be monitored. The technique will be further expanded and refined laying the groundwork for production of a diagnostic instrument which can ultimately be applied in a lifetime testing facility.

INSTRUMENTS FOR SURFACE EROSION MONITORING

- DIFFUSE POINT INTERFEROMETER

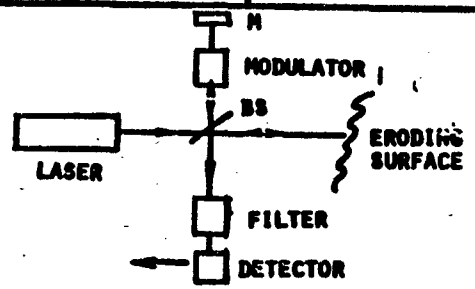

- HOLOGRAPHIC INTERFEROMETER

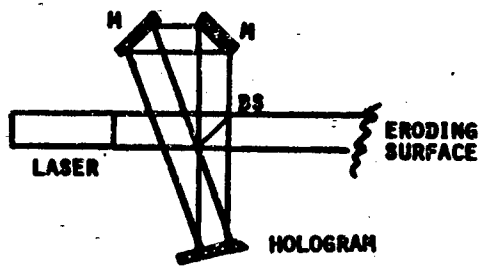

- ASTIGMATIC RANGING PROBE

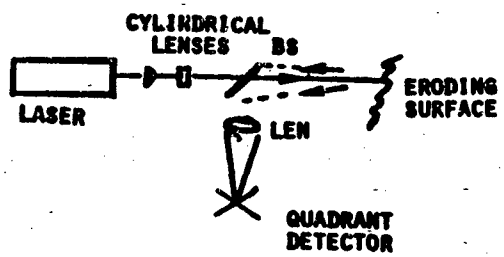

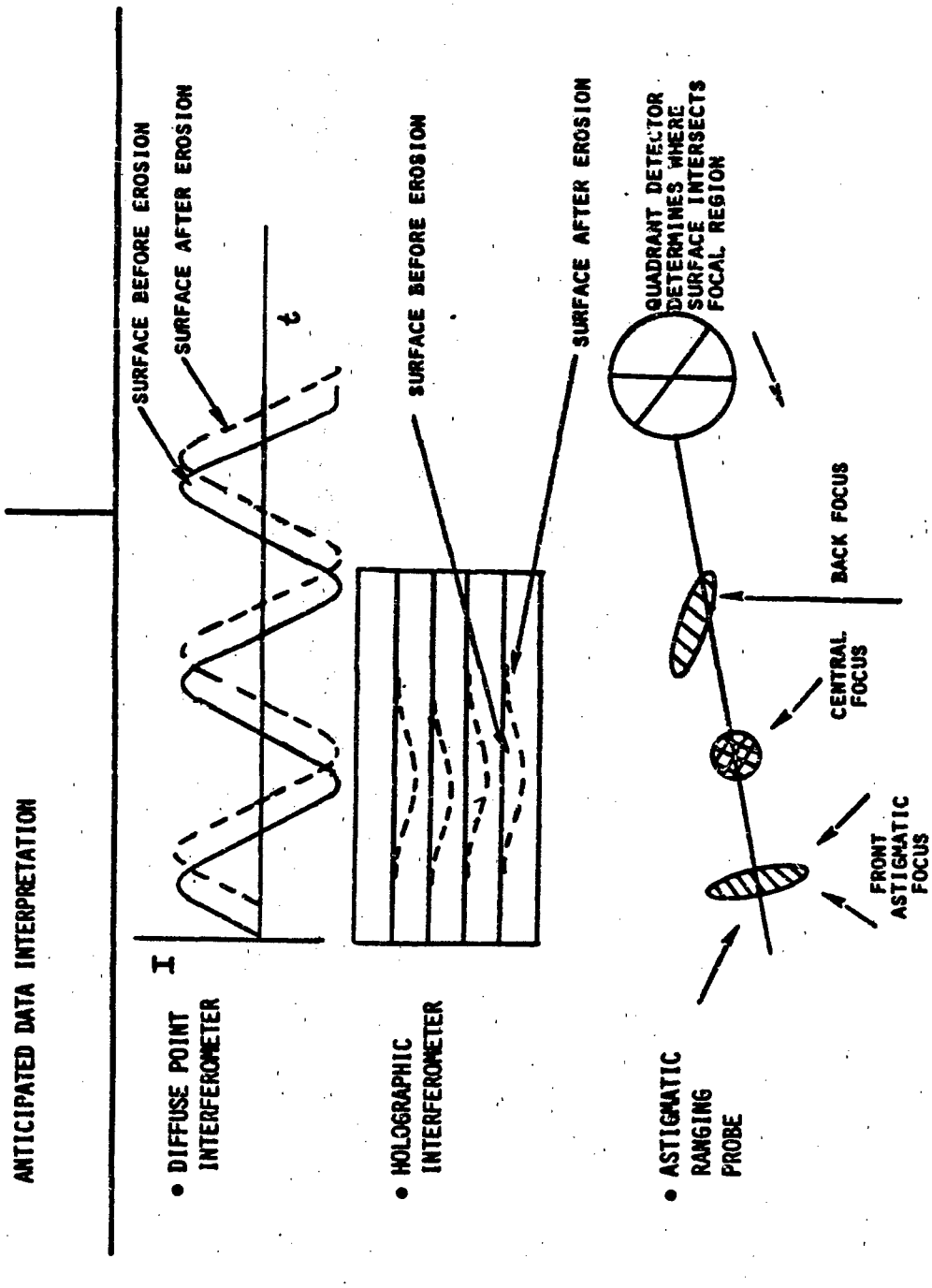
ANTICIPATED DATA INTERPRETATION
• DIFFUSE POINT INTERFEROMETER
I
SURFACE BEFORE EROSION
SURFACE AFTER EROSION
t
• HOLOGRAPHIC INTERFEROMETER
SURFACE BEFORE EROSION
SURFACE AFTER EROSION
• ASTIGMATIC RANGING PROBE
QUADRANT DETECTOR DETERMINES WHERE SURFACE INTERSECTS FOCAL REGION
BACK FOCUS
CENTRAL FOCUS
FRONT ASTIGMATIC FOCUS

VARIABLE FIELD EFFECTS FOR THE ROTATING FLUIDIZED BED REACTOR

Owen C. Jones
Rensselaer Polytechnic Institute
Troy, New York 12180-3590

The rotating fluidized bed nuclear reactor is a concept which has the potential for very large power densities, one to two orders larger than those currently available, very large turn-down ratios, and, for propulsive purposes, very high specific impulses of ~ 25-50% higher than those associated with chemical rockets. The scientific questions which must be addressed to determine the technical feasibility of this concept include material studies of nuclear fuels and thermal-hydraulic studies of the behavior of rotating fluidized beds of various shapes and under centrifugal g-fields up to several thousand g's. The latter questions are the subject of this research program.

The approach used in this research includes a combination of analytical and experimental methods. The first year of the program was devoted, by mutual agreement, to questions of a scoping nature. Specific results of this scoping effort included: 1) An evaluation of fluid-bed expansion and development of new predictive techniques; 2) evaluation of the quasi-1-dimensional coupled thermo-nuclear stability of reactor operation; 3) examination of the hydrodynamic stability of fluidized beds, development of some initial predictive methods, and initiation of a simple experiment to evaluate the results; 4) evaluation of the potentially concept-killing problems associated with thermal stress in the blind end plate of the reactor.

Figure 1 shows the fluid bed geometry of concern indicating the question of bed expansion. Bed bubbling instability would result in pockets of gas forming and percolating through the expanded bed. Figure 2 indicates the results of our modelling applied to fluid bed slugging instability in pipes. Similar modelling applied to bubbling instability appears reasonable, but cannot be tested due to a total lack of data, hence our initiation of experiments in this area. These simple experiments directed to bubbling instabilities are unique in that all important variables will be determined and a broad range of fluid-solid combinations will be studied in one configuration. Even exact combination of controlling parameters had not heretofore been identified.

Our analysis related to coupled thermo-neutronic stability has determined the effects of zone lumping and, more recently, been directed to the 2-D effects of neutron leakage out the exhaust path. Conservation analysis of the two-phase gas-solid fluidized bed behavior shows that in the averaging processes used to obtain the field equations there are many terms which cannot be evaluated using current knowledge. These averaging processes are similar to those which yield the beta factors in simple pipe flow or lead to the usual turbulent shear stress quantities in the estimation of turbulent flows. In addition, closure of the two-phase flow problem requires knowledge of the interactions at phase interfaces, behavior of assemblages of particles near solid boundaries, and other interaction effects which can only be crudely approximated using simple single-particle relationships. Therefore, progress can only be achieved through the study of these very basic questions in the long term and, in the short term, treating the problem as if these covariance and interaction effects either do not exist or can be approximately formulated in parametric forms which seem to make sense. This is the direction in which our future analysis will be directed.

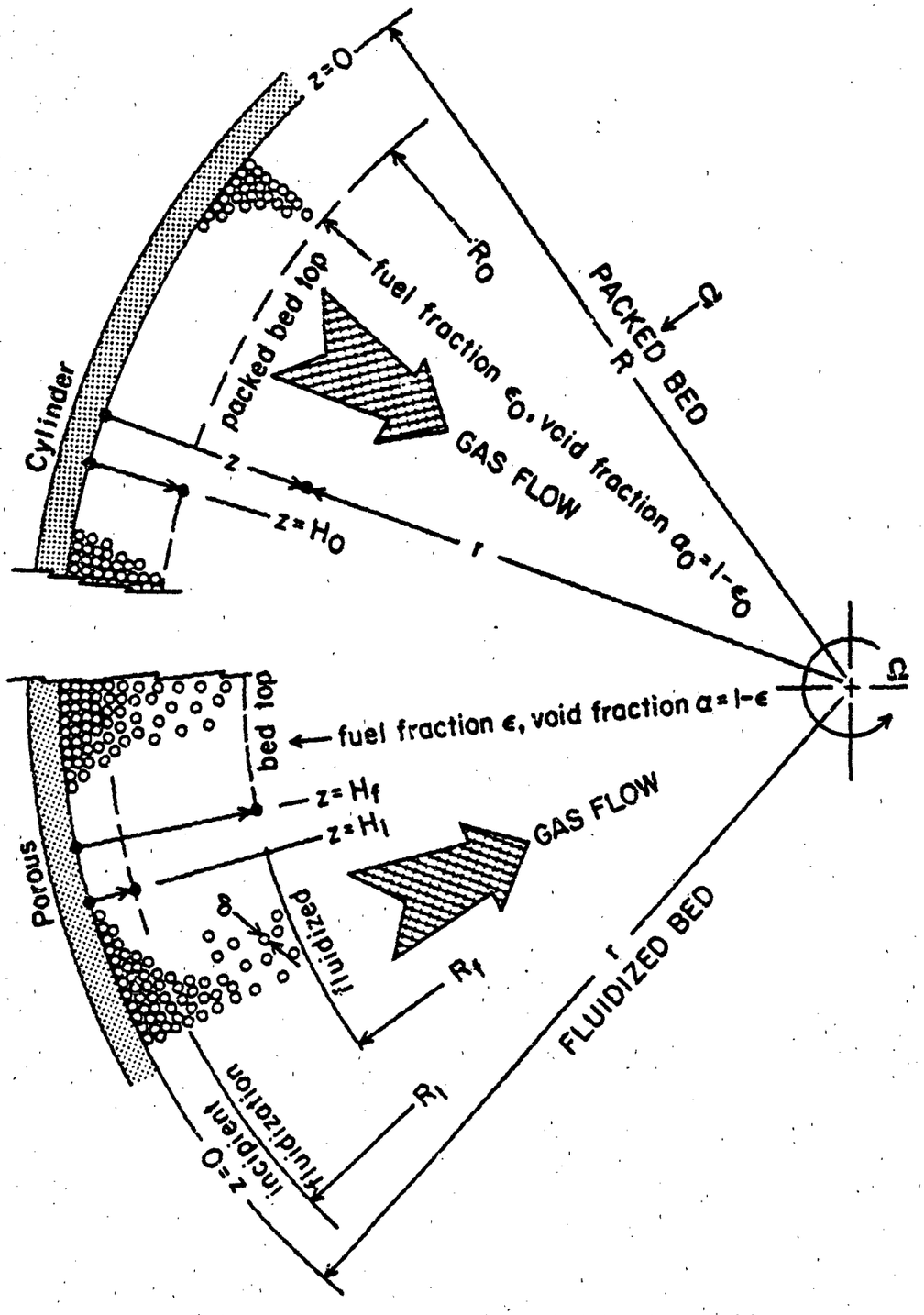

Figure 1. Schematic of geometry of consideration for the fluidized bed reactor research showing both bed expansion and bubbling instabilities.

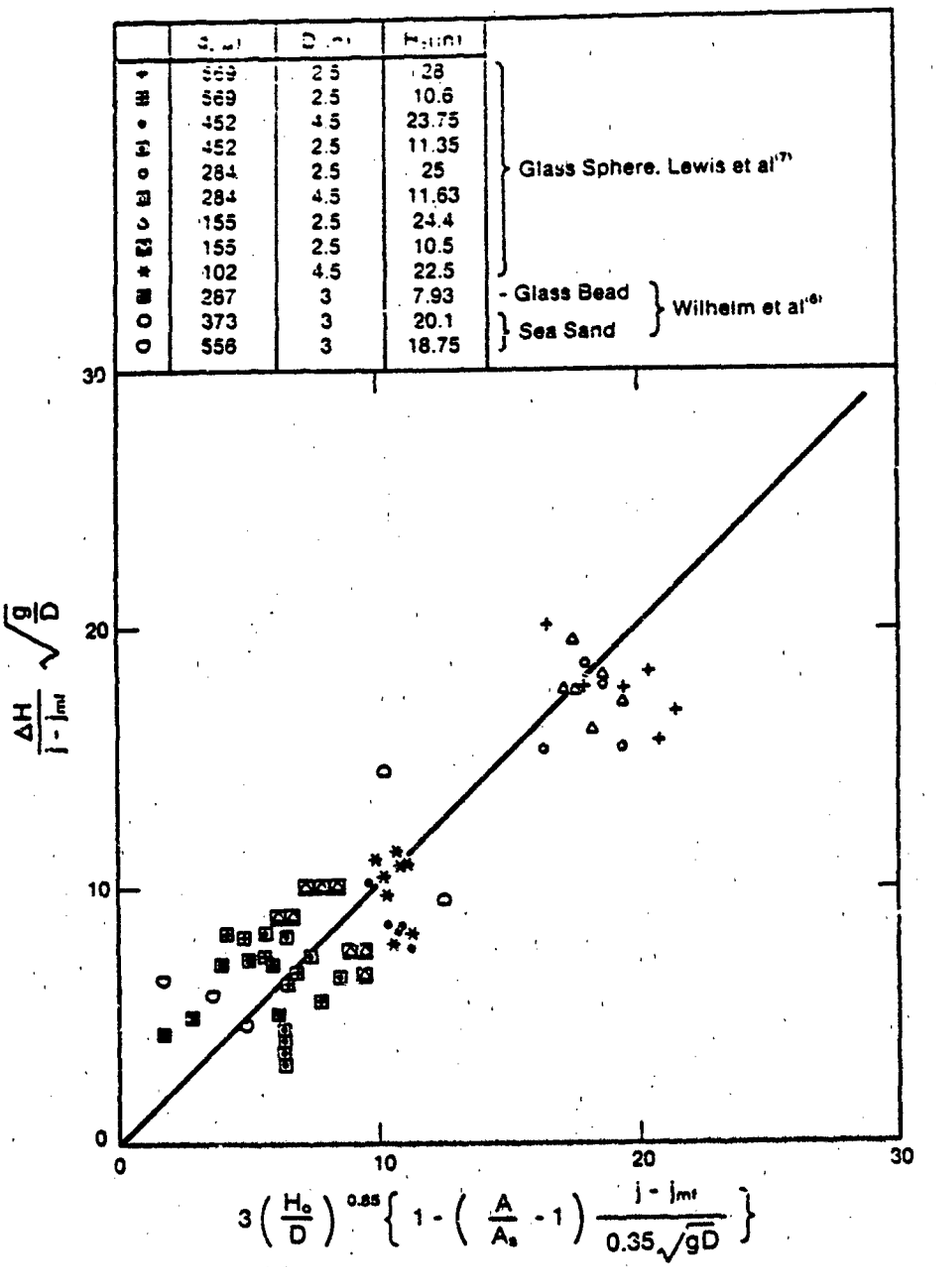

Figure 2. Comparison of prediction of slugging instability data with the model developed in the program.

EFFECT OF INTERFACIAL PHENOMENA ON CONTACT LINE HEAT TRANSFER

Peter C. Wayner, Jr.
Department of Chemical Engineering and Environmental Engineering
Rensselaer Polytechnic Institute
Troy, NY 12180

Very little is known concerning the stability and heat transfer characteristics of the contact line region of an evaporating thin liquid film. Our objectives are to measure and model the processes of heat, mass and momentum transfer in the film thickness region $\delta < 10^{-5}$ m. Our experimental work is unique in the use of a miniaturized heat transfer cell on the stage of a microscope equipped with a scanning microphotometer. Our theoretical work is unique in the combined use of the interfacial concepts of disjoining pressure, spreading pressure, fluid microstructure and surface tension to analyze the transport processes and to develop a macroscopic suction potential model for the integral heat sink.

Figure 1 illustrates the unique use of a scanning microphotometer to determine the steady state evaporating liquid film profile as a function of the integral heat transfer rate. The thickness profile is needed to calculate fluid flow and heat transfer in thin liquid films.[1] The figure also illustrates the use of small temperature sensors to measure the surface temperature profile which is needed to calculate the heat transfer rate for comparison with the fluid flow rate based on the thickness profile. We note that the exact location of the temperature sensors in the evaporating film can be determined during evaporation. By varying the concentration of the liquid charge we can determine the effect of concentration by analyzing the measured changes in the thickness and temperature gradients with concentration and heat flow rate.[2] The use of a new circular cell design eliminates edge effects. These measurements along with the concepts of disjoining pressure, surface tension, surface pressure, and fluid microstructure will be used to develop an integral heat transfer suction potential model.

Figure 2 illustrates the new small circular heat transfer cell which we designed and built during the first six months of the contract. We note that since the cell is passive in that the interfacially induced flow rates are controlled by the heat input, the selection of the liquid composition and cell dimensions are critical. It is currently being tested for its' response to the following variables: the volume of liquid charge, the external heat input, the bulk liquid composition, and the external heat sink. Our initial tests indicate that the cell design dimensions are approximately correct in that the internal flow fields are desirable. We are still in the process of developing small temperature sensors.

1. R. Cook, C.Y. Tung, and P.C. Wayner, Jr., "Use of Scanning Microphotometer to Determine the Evaporative Heat Transfer Characteristics of the Contact Line Region", A.S.M.E. Journal of Heat Transfer, 103, 325-330 (1981).

2. C.Y. Tung and P.C. Wayner, Jr., "Effect of Surface Shear on Fluid Flow in an Evaporating Meniscus of a Mixture of Alkanes", Proceedings of the 5th International Heat Pipe Conference, Tsukuba, Japan, May 14-17, 1984, Part I, 201-207.

INTERFACIAL HEAT TRANSFER CONTACT LINE REGION

GOAL

UNDERSTANDING OF TRANSPORT MECHANISMS IN EVAPORATING THIN LIQUID FILM (THICKNESS $< 10^{-6}$ m)

GENERAL PRINCIPLE

HEAT, MASS, AND MOMENTUM TRANSFER ARE CONTROLLED BY INTERFACIAL PHENOMENA RESPONDING TO GRADIENTS IN THE THICKNESS, TEMPERATURE AND CONCENTRATION

TECHNIQUES

1. MEASURE LIQUID THICKNESS PROFILE, $\delta(r)$, AS A FUNCTION OF BULK CONCENTRATION AND EVAPORATION RATE IN NEW CIRCULAR MINIATURIZED HEAT TRANSFER CELL USING SCANNING MICROPHOTOMETER.

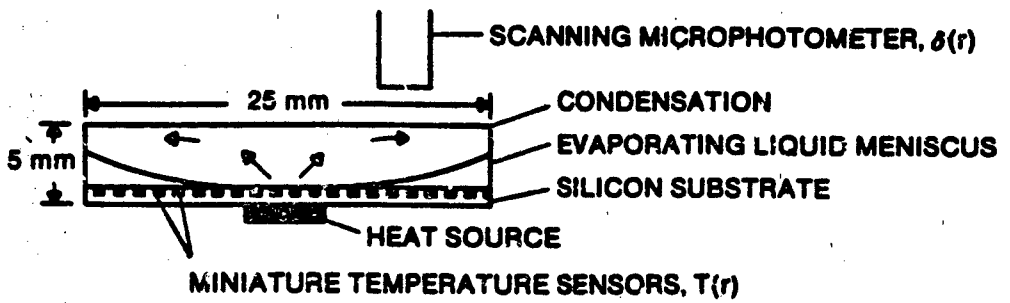

2. MEASURE SUBSTRATE TEMPERATURE PROFILE, T(r), USING SMALL TEMPERATURE SENSORS.

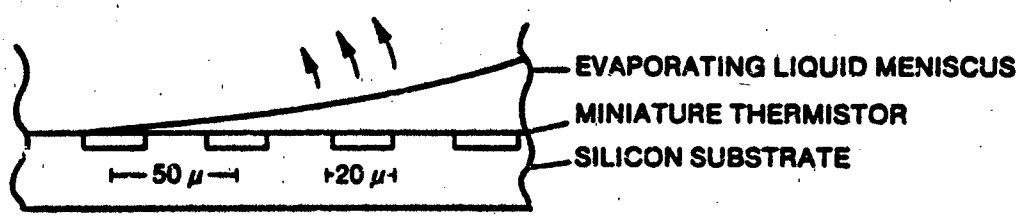

3. COMBINE THE FOLLOWING CONCEPTS INTO HEAT TRANSFER SUCTION POTENTIAL MODEL: DISJOINING PRESSURE, FLUID MICROSTRUCTURE, SURFACE TENSION, APPARENT CONTACT ANGLE, $\delta(r)$, T(r).

ACCOMPLISHMENTS

1. A SMALL CIRCULAR HEAT TRANSFER CELL WAS DESIGNED AND BUILT

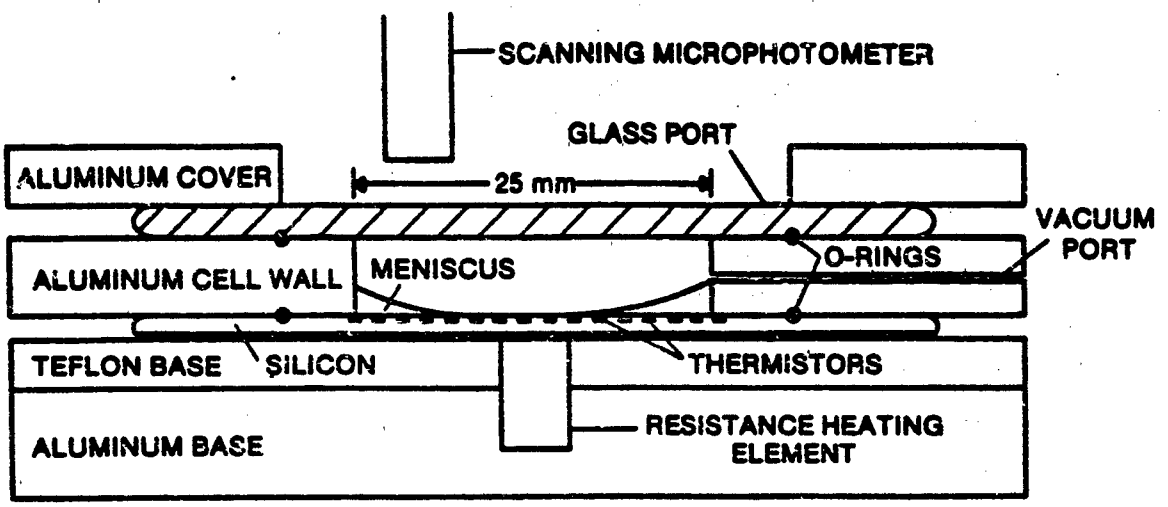

2. CELL DESIGN IS BEING TESTED FOR RESPONSE TO:
   a. VOLUME OF LIQUID CHARGE
   b. EXTERNAL HEAT INPUT
   c. LIQUID COMPOSITION
   d. EXTERNAL HEAT SINK

3. SMALL TEMPERATURE SENSORS ARE UNDER DEVELOPMENT

UNIFIED STUDY OF PLASMA-SURFACE INTERACTIONS FOR SPACE POWER AND PROPULSION

Peter J. Turchi, John F. Davis III,
Joseph Norwood, Jr., Craig N. Boyer

R & D Associates, Washington Research Laboratory
301A S West Street, Alexandria, VA 22314

The efficiency and lifetime of high specific power/high specific impulse space power and propulsion devices often depend on particle and energy transport at electrodes and insulators in low temperature (0.5-5 eV) plasma flows. In the present study, actual measurements of particle and field distributions near solid surfaces in controlled plasma flows are performed and used to develop models for particle and energy transport. A unique advantage in such model development is our ability to vary flow conditions, surface orientation, and material properties (plasma and solid) and to compare data within a unified experimental framework, thereby allowing complicated interactions to be delineated.

The basic arrangement is depicted in Figure 1, indicating a quasi-steady MPD arcjet that provides plasma flow over a surface sample. The orientation of the sample to the flow, placement in different regimes of density and velocity, and choice of electromagnetic boundary conditions can all be adjusted while maintaining diagnostic access. The magnified insert suggests one of the many possible interactions near the surface, specifically, transport of neutral surface atoms into the local plasma a distance scaled by the mean-free path for electron-atom ionization λ^I_{eA}, followed by Coulomb collisions, with mean free path λ^D_{ii}, that prevent the surface particle from returning to the local surface (if $\lambda^D_{ii} << \lambda^I_{Es} << \lambda^D_{Ai,A}$ the mean free path for atomic momentum-transfer collisions). Measurements of particle densities, temperatures, flow conditions, and electric sheaths, combined with variation of atomic properties can be used to assess the actual ordering of mean free paths and establish proper modeling.

A quasi-steady MPD arcjet plasma source has been designed, built and installed in the existing 6 m long x 0.6 m diam vacuum facility. The arcjet is powered by a rectangular current pulse ($\leq$20 kA, 160 μsec). Figure 2 shows a time-integrated photo of the overall arcjet flow onto a sample. An RDA-built microchannel plate camera system is used with a 1.5 m spectrograph to obtain time-, space-, and spectrally-resolved photos. For example, with the slit normal to the surface, measurement of the Stark-broadened H_β-linewidth provides the electron density ($n_e \approx 2\text{-}5 \times 10^{15}$ cm^{-3}) near a polyethylene sample stagnating an argon plasma flow ($u \approx$ 17 km/s) at selected times during flow operation.

RDA WASHINGTON RESEARCH LABORATORY

PLASMA-SURFACE INTERACTION STUDY

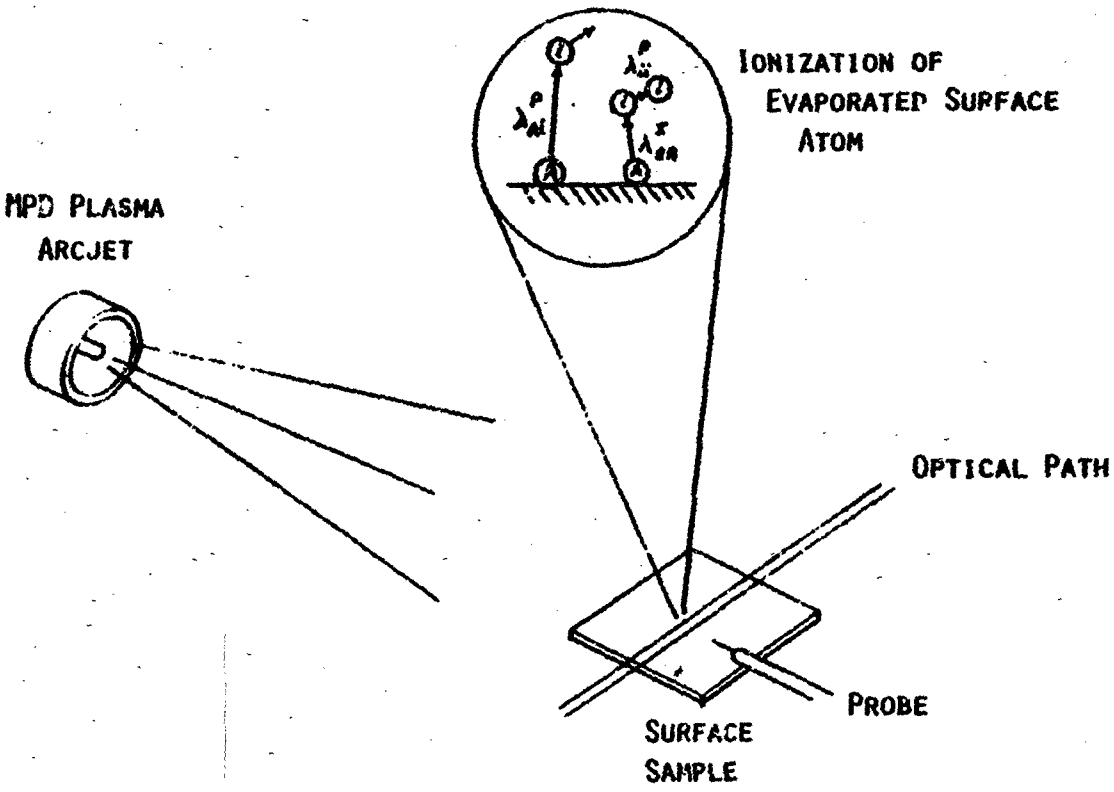

FIGURE 1

RDA WASHINGTON RESEARCH LABORATORY

PLASMA/SURFACE INTERACTION STUDY

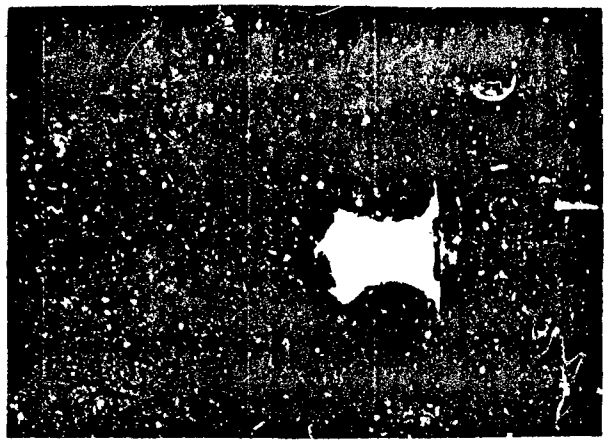

TIME-INTEGRATED

LINE SPECTRA

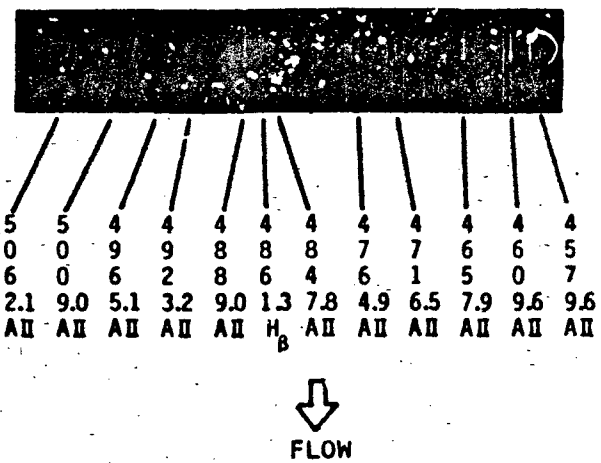

TIME RESOLVED H_β

DELAY TIME (μs)

FIGURE 2

** 1985 ROCKET RESEARCH MEETING **
Abstract 59 PR 3

CLOSE-SPACE, HIGH TEMPERATURE KNUDSEN FLOW

JOHN B. McVEY

RASOR ASSOCIATES, INC.
253 Humboldt Ct.
Sunnyvale, CA 94089

The objective of this research is to investigate the discharge processes and performance characteristics of thermionic energy conversion systems operating in the collisionless (Knudsen) mode. The specific processes under study are shown in Fig. 1. The interelectrode space charge can be reduced by close interelectrode spacings ("vacuum" mode), contact ionization of cesium at the emitter surface (unignited mode), or introduction of ions produced in an externally generated arc. Soviet results suggest that structured emitters can increase the current and power densities in the unignited mode by a factor of four. Our experimental approach has been to use small diode structures called SAVTECs, with spacing set by thermal expansion, to measure converter performance at interelectrode spacings below 20 μm. Measurements have covered both the "vacuum" and unignited regimes. Two variable-spacing planar converters containing mixed cesium and barium vapor are planned in order to verify and investigate the structured emitter effect. Theoretical studies and computer models of the collisionless thermionic converter and its interaction with an external arc supplement the experimental work. A two-dimensional analysis of the particle kinetics associated with structured emitter is planned.

During the first year of the program, experimental results were obtained from a close-spaced diode (d = 6.5 μm) at emitter temperatures up to 1250 K. The performance characteristics agreed well with vacuum diode theory. In the second year a diode with 18-20 μm spacing has been tested. Maximum output power as measured at the electrical leads is shown in Fig. 2 as a function of emitter temperature. Up to about 1580 K, the data are well characterized by vacuum diode theory. Above that temperature the data follow the higher performance predicted by unignited mode theory. A beneficial effect was produced by the presence of oxygen in the system, which increases the adsorption of cesium on the emitter surface and lowers the cesium pressure necessary to achieve a low emitter work function.

The rest of the program will concentrate on the structured emitter effect. This is more applicable to the high-power regime than SAVTEC, which was proposed for low-power systems. Analysis has ruled out associative ionization as an important mechanism in such converters; we will therefore, concentrate on understanding the particle kinetics. Two converters are planned, one with a structured and one with a smooth emitter in order to make a comparative study of performance. The second converter is being substituted for a planned experiment on breakdown effects between SAVTEC diodes. This is consistent with the shift in emphasis in the national program to high-power systems.

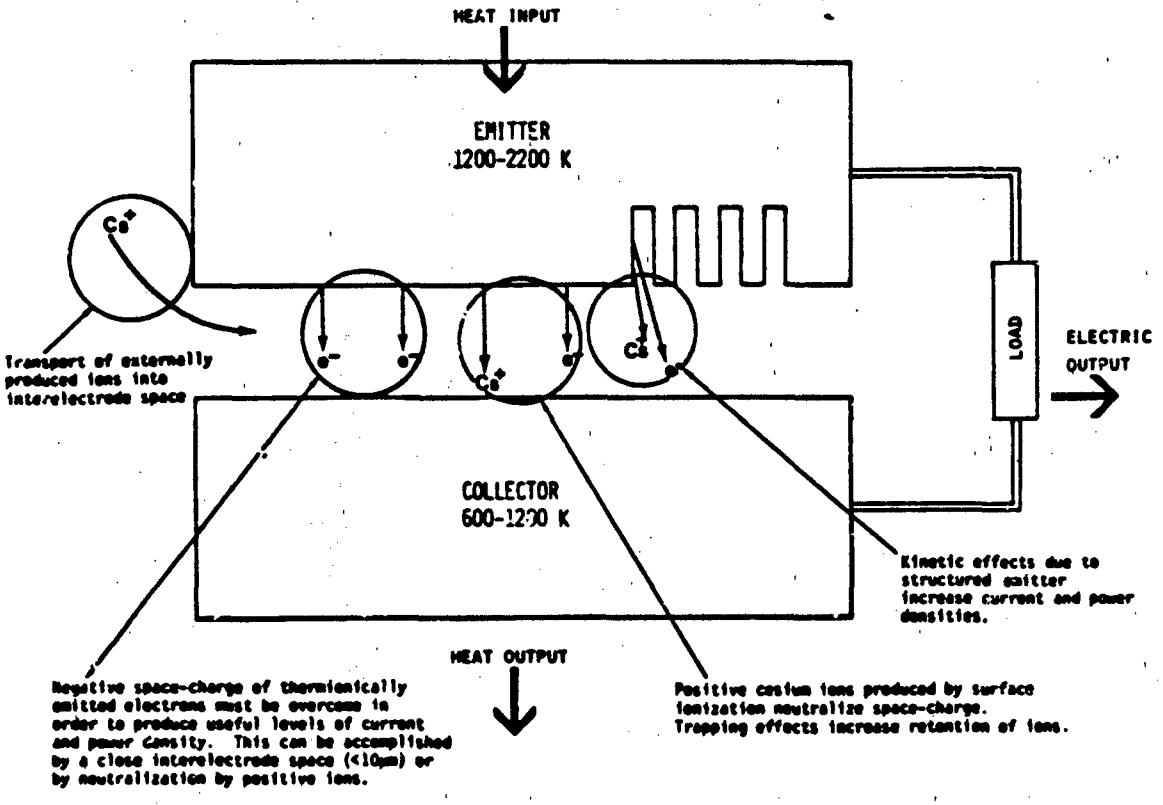

Fig. 1 Discharge Mechanisms in a Knudsen-Mode Thermionic Energy Converter

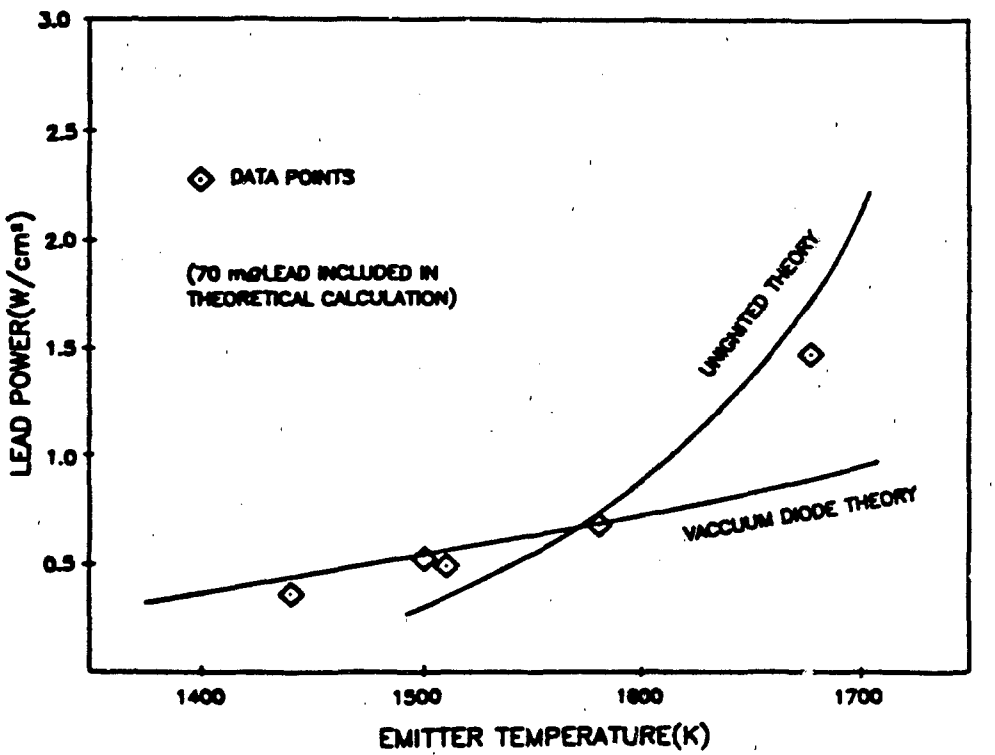

Fig. 2 Measured Maximum Output Power from a SAVTEC Diode

TWO-PHOTON DETECTION TECHNIQUES FOR ATOMIC FLUORINE

William K. Bischel
SRI International
Chemical Physics Laboratory
Menlo Park, CA 94025

The remote detection of atomic fluorine is an extremely difficult problem that needs to be solved for a variety of applications. The fact that all optically allowed single photon transitions to excited states occur at wavelengths below 100 nm greatly hampers efforts to develop optical detection techniques. Consequently, there are currently no laser based detection techniques for F atoms that combine high sensitivity with a point detection capability.

We address this problem by examining two-photon excitation processes in fluorine. Unfortunately, there is very little data concerning the spectroscopy and kinetics of the two-photon accessible electronic states. Data concerning two-photon excitation cross sections, radiative lifetimes and quenching rate, and photoionization cross sections for these electronic states are crucial to the development of a viable detection technique based on two-photon excitation. We have therefore started a research program to obtain data on the spectroscopy and kinetics of the odd parity electronic states of atomic fluorine while demonstrating two different types of detection techniques.

The electronic states of primary interest here are shown in Figure 1. The two states that will be the focus of the experiments are the $^2P_{1/2}$ state at 404 cm^{-1} and the $^2D_{5/2}$ state at 117,624 cm^{-1}, both of which have two-photon allowed transitions from the ground state. Two different types of experiments will be utilized to detect and study the properities of these excited states. The experiment conducted during the first year of the project will be the Raman excitation of the $^2P_{1/2}$ state as illustrated in Figure 1. The apparatus for this experiment is illustrated in Figure 2. This experiment will use two visible lasers: a pulsed dye laser laser and a CW krypton ion laser with the frequency difference between the two lasers equal to 404 cm^{-1}. The Raman gain induced on the CW laser by the pulsed laser will be recorded as a function of frequency. From this data we will determine the spectroscopy of the fine structure Raman transitions, the Raman gain cross section, and the collisional Raman linewidth. This data is critical for the determination of the sensitivity of this detection technique.

The second experiment is the direct two-photon excitation of the $^2D_{5/2}$ state. As shown in Figure 1, fluorescence emission at 775 nm will form the observed signal. This experiment requires laser radiation at 170 nm. Hence an important part of this experiment is the generation of the vuv radiation at the required intensity. Different generation techniques will be studied during the first year of the project.

We anticipate that the results of both experiments will be two fold: (1) new remote detection techniques for atomic fluorine will be demonstrated and, (2) a wealth of new data concerning its excited states will be generated.

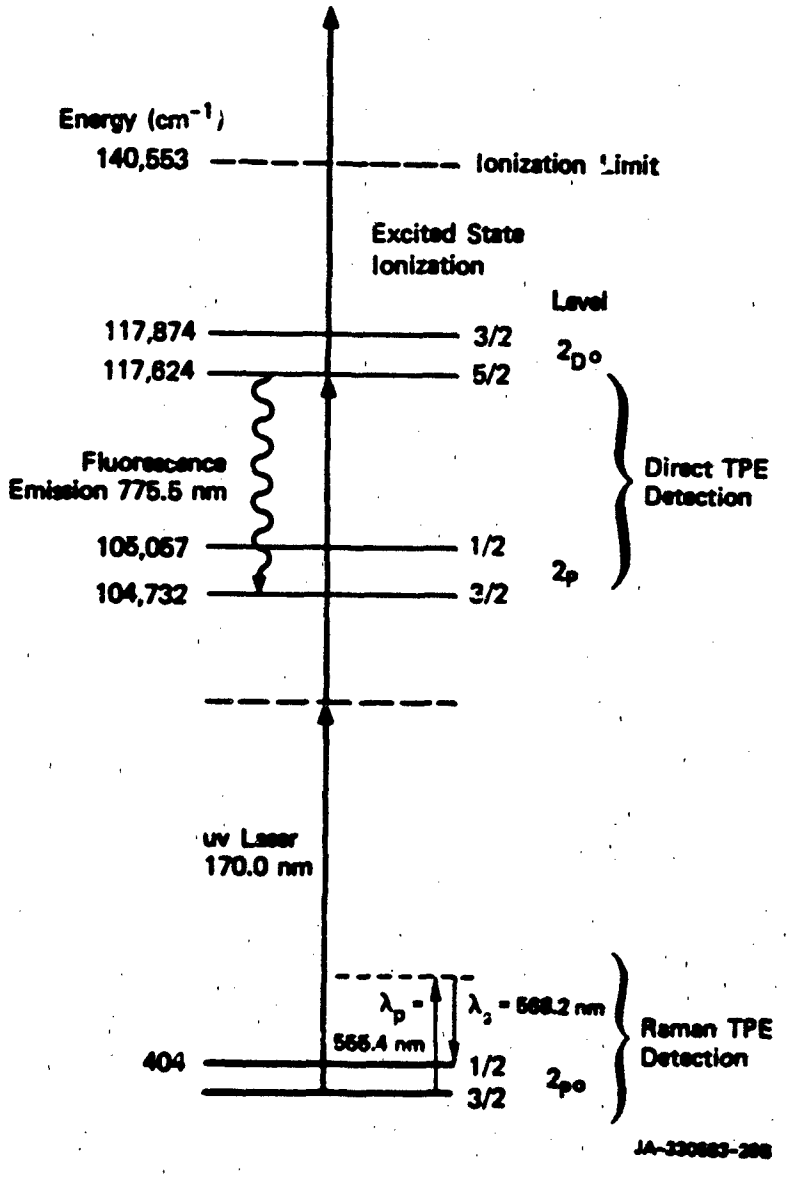

FIGURE 1 FLUORINE EXCITED STATES RELEVANT TO THE TWO-PHOTON DETECTION TECHNIQUE

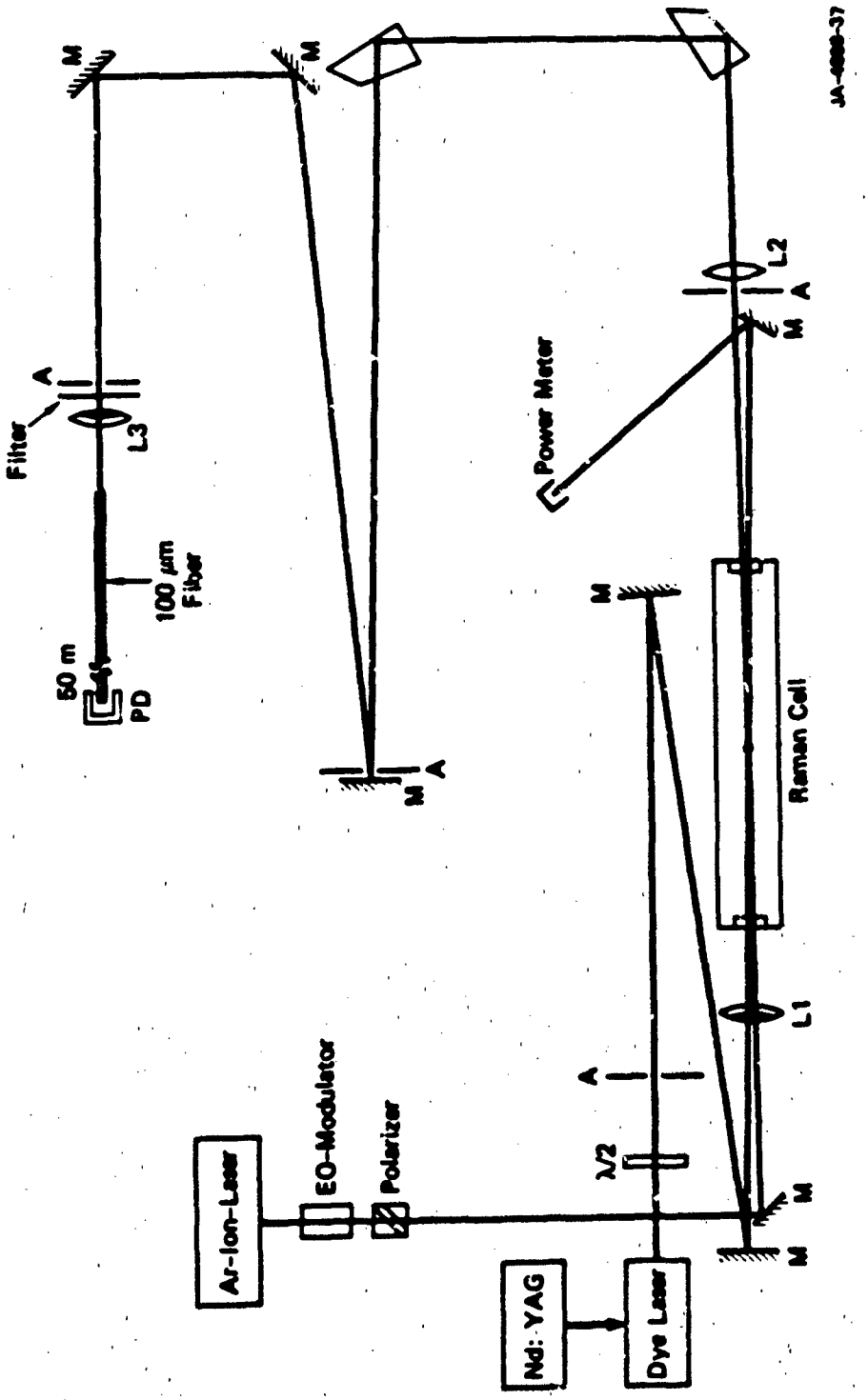

FIGURE 2 EXPERIMENTAL SETUP FOR THE DETECTION OF ATOMIC FLUORINE USING QUASI-CW STIMULATED RAMAN GAIN SPECTROSCOPY

The F atoms will be generated using a microwave discharge (not shown).
(L1 – 40 cm f.1. achromatic lens; L2 – f.1 lens, L3 – 7 cm f.1. achromatic lens, A – variable apertures, M – dielectric mirrors, λ/2 – half-wave plate, PD – photodiode)

COHERENT OPTICAL TRANSIENT SPECTROSCOPY IN FLAMES

John W. Daily

Department of Mechanical Engineering
University of California
Berkeley, Ca 94720

Coherent optical transient spectroscopy is a technique in which the transient response of a group of molecules to laser excitation is observed. The uniqueness of the method lies in the fact that when transient experiments are conducted on a time scale short compared to collisional relaxation times, coherent phenomena occur which enable one to directly observe the rates of a variety of collisional processes. Furthermore, the coherent pheenomena can be quite strong, resulting in large signals and thus high data rates. Processes such as state-to-state energy transfer, optical dephasing and velocity redistribution can be studied.

An example experiment is shown in Figure 1. An actively stabilized CW dye laser is used as a source. By passing the beam through a traveling wave modulator to which a high voltage pulse has been applied, the frequency may be shifted up to 15 GHz within 150 psec for periods of several nanoseconds. Thus, one may shift into or out of resonance with an absorption line of interest and observe the transient behavior that results. The type of transient we will be observing is Free Induction Decay in which the laser beam is suddenly shifted out of resonance with an absorption line and the transient absorption signal observed. The decay rate of the transient signal is the collisional dephasing rate for that transition. Also illustrated in Figure 1 are several other types of excitation, the transient they produce and the quantities one can obtain.

We have been focusing on studying CH in our low pressure flame facility. A complete layout of our equipment in two configurations, one for COTS and another for making high resolution absorption measurements, is shown in Figure 2. A risetime curve for the traveling wave modulator is shown demonstrating a less than 200 psec electrical rise time. Emission profiles through the flame are also shown as are Boltzmann plots showing that the excited CH is fairly well equilibrated. Also shown is a high resolution laser induced fluorescence line profile and an example of the resolution obtained in the absorption configuration. Coupled with a thorough study of CH in our flame by emission and high resolution flurescence and absorption spectroscopy, the COTES measurments will provide information essential for making accurate fluorescence and coherent Raman measurements in practical combustion devices.

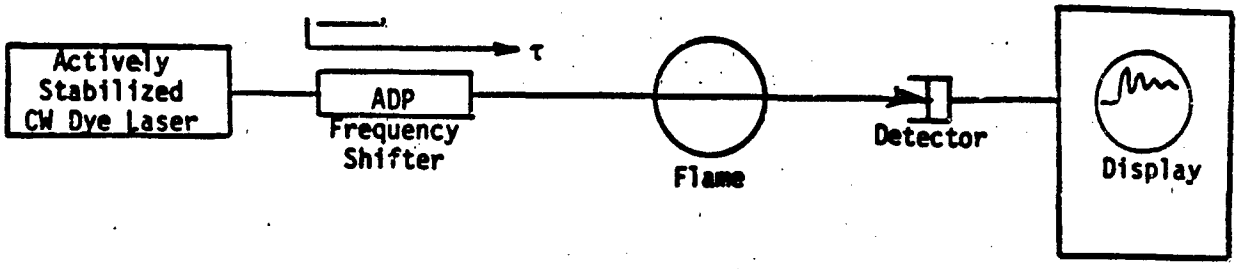

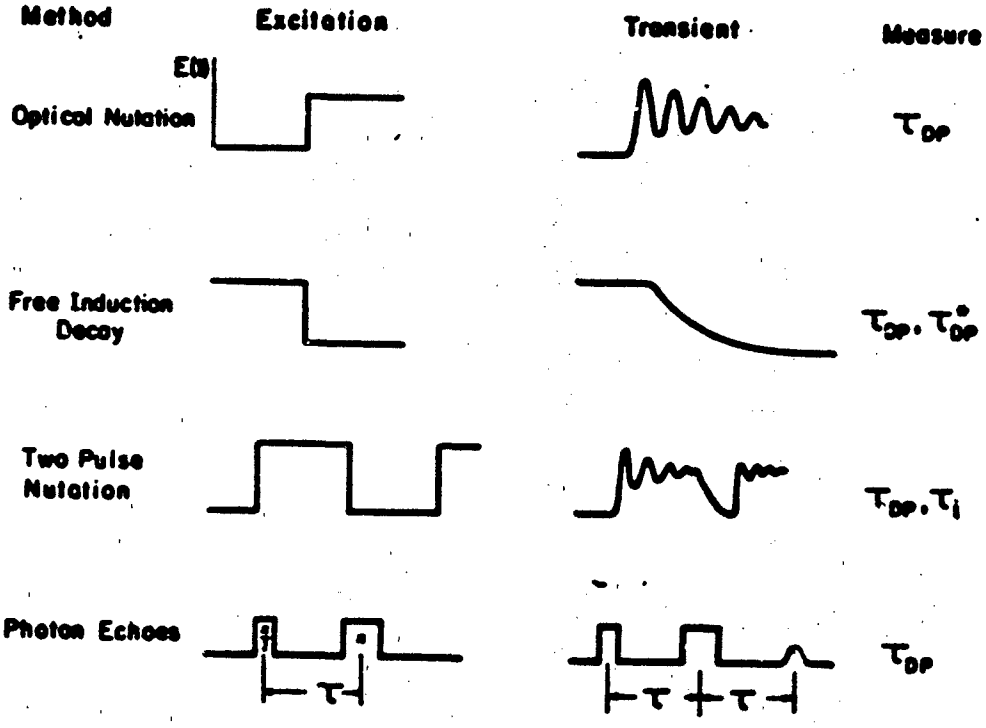

Measure	Learn	Why Important
τ_{DP} Optical Dephasing	Line Widths	Interpret Raman Spectra
τ^*_{DP} Doppler Dephasing	Velocity Redistribution Rates	Leads to Transport Properties
τ_1 State Decay Rates	State to State Energy Transfer Rates	Interpret Fluorescence Signals
	Chemical Relaxation Rates	State to State Chemistry

Figure 1

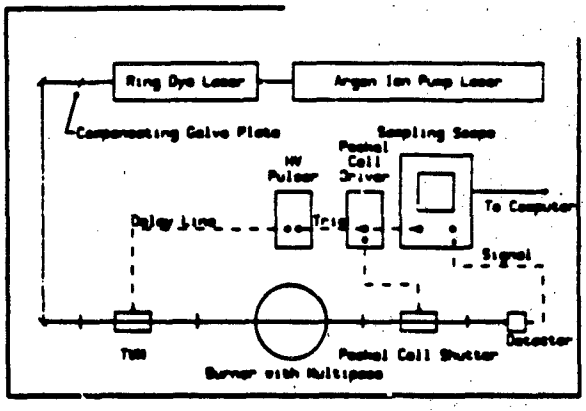

COTES System Apparatus

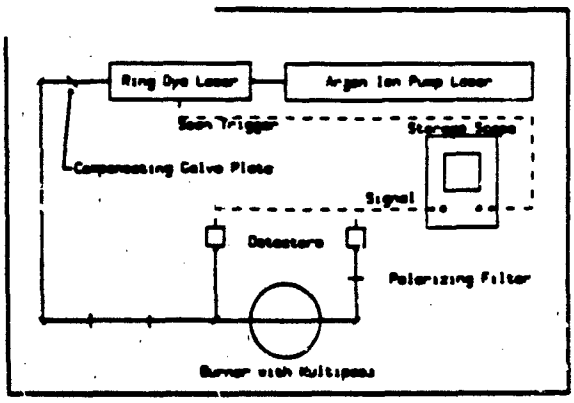

Absorption System Apparatus

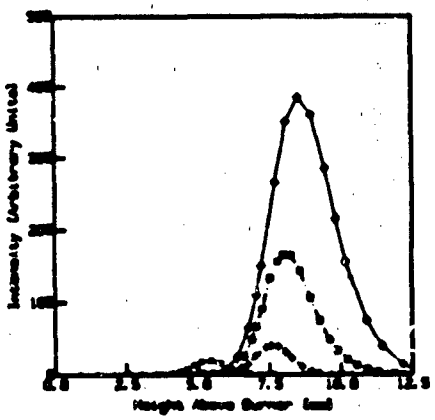

Emission Intensity vs. Height

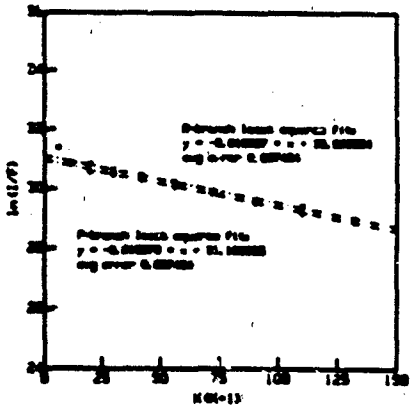

OH emission of P and R branches plotted as ln(I/P) vs. K(K+1)

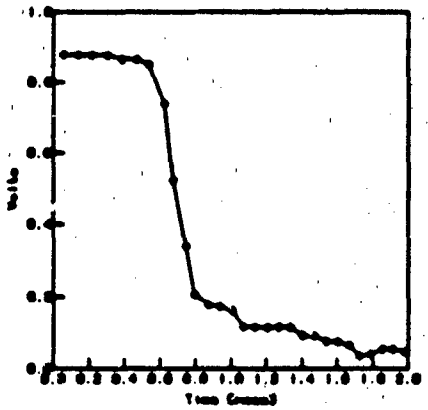

Reaction of Voltage Pulse to TDM

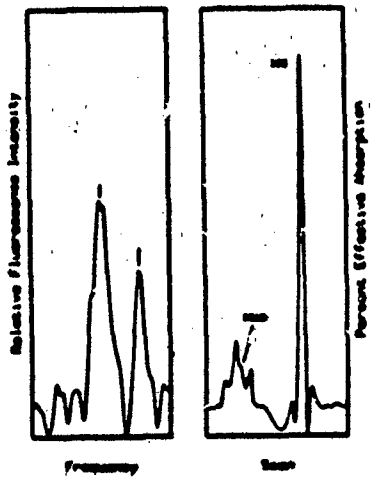

Figure 2

Development of Velocity Measurement Technique by Pulsed Laser Doppler Anemometry

Department of Chemical Engineering and
Fuel Technology, The University of Sheffield,
Sheffield, England

B.C.R. Ewan and J. Swithenbank

The objective of the present study is to extend the conventional point measuring ability of laser Doppler anemometry to a line measurement. Such a facility will be an important advance and of particular use in transient flow situations such as periodic combustion systems or small rocket firings, where it is impractical to traverse the field of interest in the time available.

Two immediate requirements follow from this modification. The first is that of monitoring several points along the line measuring volume simultaneously, leading to a multi-channel data collection and analysis system. The second stems from the diminished beam intensity in the measuring volume due to its extension and the need to restore scattered light intensity by increasing laser power or scattering particle diameters. The present approach aims at investigating these requirements by two parallel lines of study.

The first aims at developing the optics and signal processing necessary to produce and analyse the Doppler signals. This is being done using a CW argon ion laser operating in a conventional laser Doppler configuration, with the exception of the output lens , which is cylindrical and produces a line intersection within the measurement field. Scattered light from this line is imaged on to an array of detector elements, which for the argon laser, consists of five single core fibre optic heads. Each of these leads to a separate photomultiplier tube producing five parallel output channels.

Two hardware options are being pursued to analyse these channels.

The first is to use a multi-channel disc or tape recorder to store the individual Doppler bursts for subsequent analysis, channel by channel. The interfacing and software to analyse these functions already exists.

At the same time a five channel real time processor is being built, the output from which can easily be monitored with a micro-computer. Due to the higher frequency handling ability of such a processor, compared with the 2 MHz available with magnetic tape, this is a preferred solution, since with an increase in frequency, measuring volume width can be reduced leading to better signal to noise ratios. Figure 1 shows a schematic of the present system.

Progress with the argon ion system to date consists of the completion of the optical arrangement in conjunction with an air jet and suitable particle seeding, capable of producing sonic jets. An indication that good data can be obtained from the extended line volume is shown in Figure 2, which shows an expanded image of the line intersection and also a typical Doppler burst, both in its raw and filtered state.

The second parallel element of the study aims at overcoming the low light level in the measuring volume using the high powers available with pulsed lasers. In this way it is also intended to switch from PM tubes to solid state detection. For this purpose, a five element photodiode array of the correct bandwidth is being fabricated and this will fill the place of the present fibre optics when the pulsed laser study begins. An important part of this development involves the suitable shaping of the pulsed ruby output pulse in order to match this to the particle transit times. Present pulse widths without Q switching are around 5 μsec whereas transit times of around 10 μsec can be expected. The possibilities being investigated centre around the suitable choice of laser cavity gain and ultimately by applying negative feedback to the gain to extend the pulse.

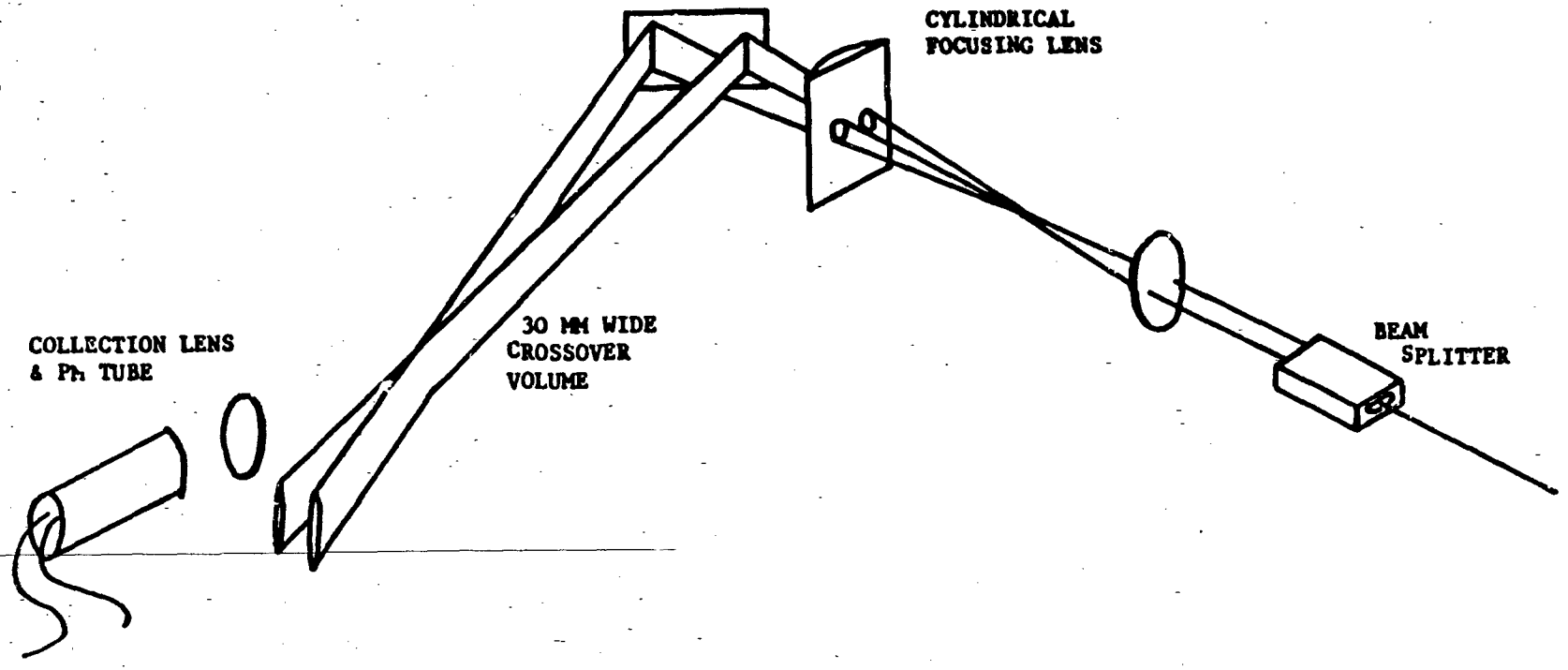

FIGURE 1 Schematic of present laser Doppler anemometry arrangement being developed for pulsed laser measurements showing extended line cross over probe volume.

Enlarged view of extended line fringe volume. This is 30 mm long in present system.

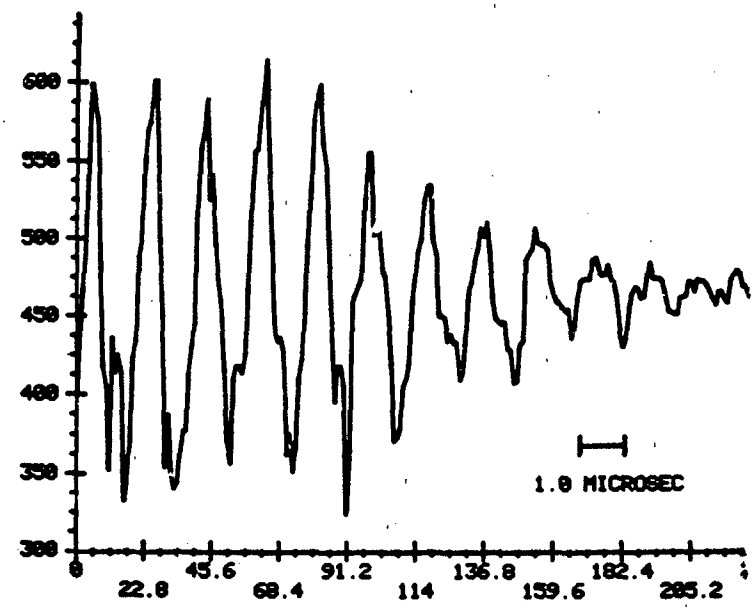

Example of raw Doppler burst from line intersection measuring volume.

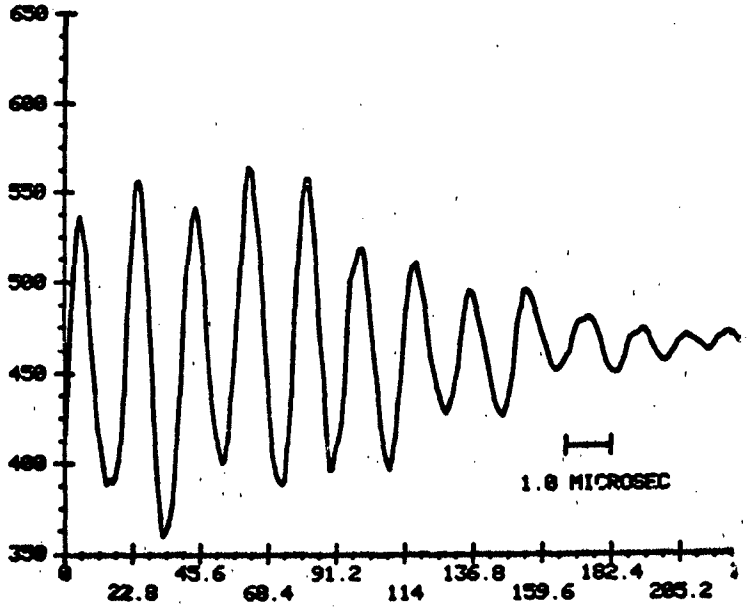

Doppler burst which results when above signal is low pass filtered.

FIGURE 2

QUANTITATIVE FLOW VISUALIZATION

Ronald K. Hanson

Mechanical Engineering Department
Stanford University
Stanford, California 94305

The utility of flow visualization in fluid mechanics is well established. Until recently, however, most visualization techniques have been qualitative and based on line-of-sight approaches poorly suited for flows with three-dimensional characteristics and varying composition. With the development of laser-based light scattering techniques, it has become possible to obtain temporally resolved, quantitative records of flow properties throughout a plane (and ultimately throughout a volume) using sheet illumination and techniques such as Raman, fluorescence and Mie scattering. The aim of the Stanford program has been to establish methods for visualizing a range of flowfield parameters including temperature, velocity, species concentrations, pressure, and, in the case of two-phase flows, droplet or particle distributions. Ideally these techniques should be applicable to nonreacting and reacting flows, including plasmas. Most of our work has utilized planar laser-induced fluorescence (PLIF), except for particle visualization which uses planar Mie scattering (PMS).

The approach and some representative results for temperature and velocity are shown in the following figures. Figure 1 provides an overview of the fluorescence-based temperature sensing strategy, and Figure 2 presents representative results for instantaneous temperature contours in a vertical plane in a rod-stabilized, premixed CH_4-air flame. Figure 3 is a schematic diagram of the two-frequency strategy for monitoring velocity, also based on fluorescence, and Figure 4 provides sample results for the axial velocity component in a subsonic, room temperature nitrogen roundjet. For both temperature and velocity visualization, the recording camera has been an intensified Reticon array (100 x 100) interfaced with a DEC 11/23 laboratory microcomputer for experiment control, data processing and display. For temperature measurements, the light source is a pulsed dye laser system, yielding tunable output near 226 nm, and the absorbing/fluorescing tracer species is nitric oxide. For velocity visualization we employ a tunable cw Ar^+ laser, operating on a single axial mode near 515 nm, and the tracer species is iodine. We should note that the two-frequency velocity scheme also yields a value for the normalized slope of the absorption lineshape function, $(dg/dv)/g$, at each flowfield point. Owing to the sensitivity of this function to pressure, it should therefore be possible to simultaneously infer pressure from the same observations when pressure broadening is significant. Combined pressure and velocity visualization in supersonic flows will be attempted in future work.

2-D TEMPERATURE MEASUREMENT: STRATEGY AND SENSITIVITY

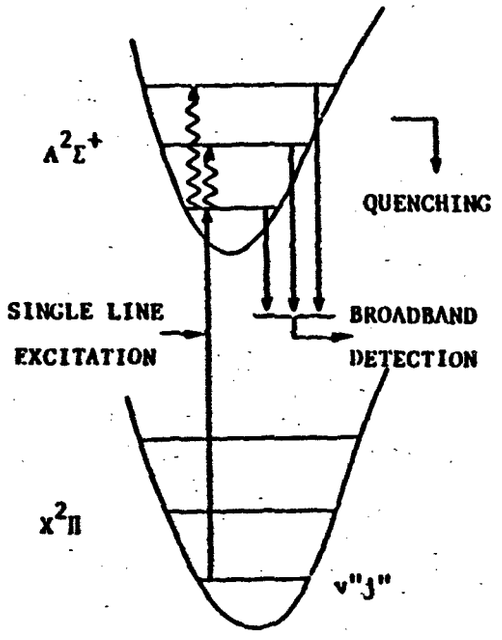

$$\frac{F_{v''J''}}{\sqrt{T}}$$

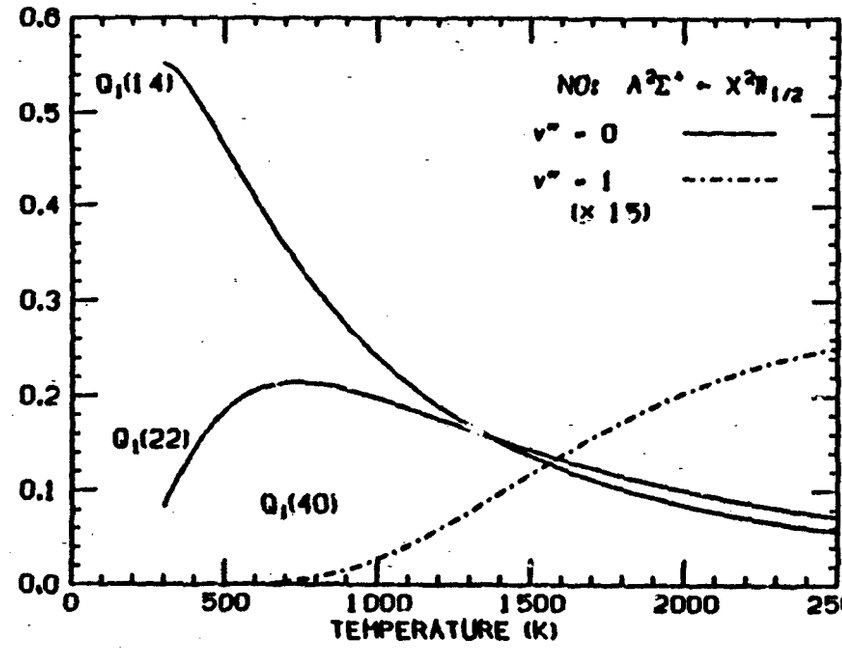

FLUORESCENCE EQUATION → $S \sim N_{NO} \times F_{v''J''} \times \frac{A}{A + Q}$

ASSUMPTIONS → $A \ll Q$, $Q = N \sigma \bar{v}$, $\bar{v} \sim \sqrt{T}$

RESULT → $S \sim [N_{NO}/N] \times [F_{v''J''} / \sqrt{T}]$

Fig. 1 Excitation/detection scheme for temperature visualization and plot of fluorescence signal (S) sensitivity to temperature.

** 1985 ROCKET RESEARCH MEETING **
Abstract 64 Pg 2

2-D TEMPERATURE MEASUREMENT

- LASER INDUCED FLUORESCENCE YIELDS INSTANTANEOUS 2-D TEMPERATURE FIELDS

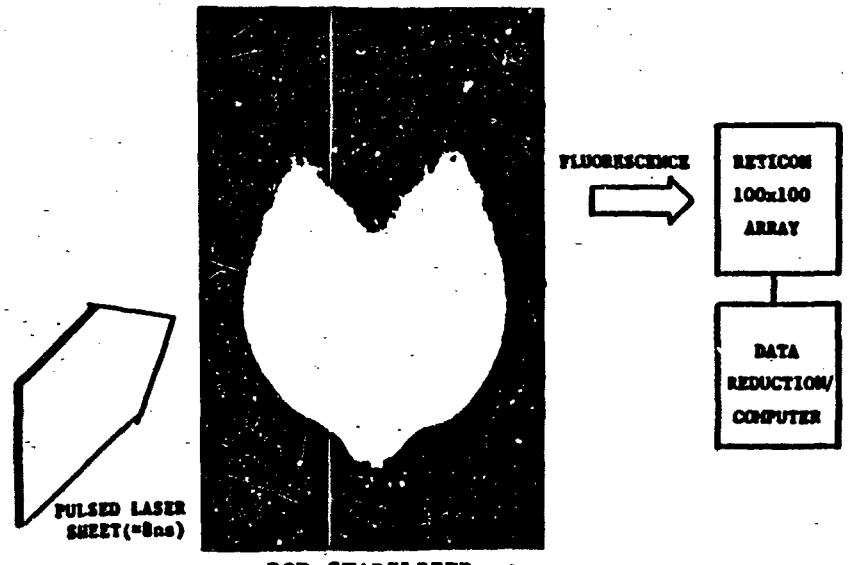

ROD-STABILIZED
CH_4/AIR FLAME

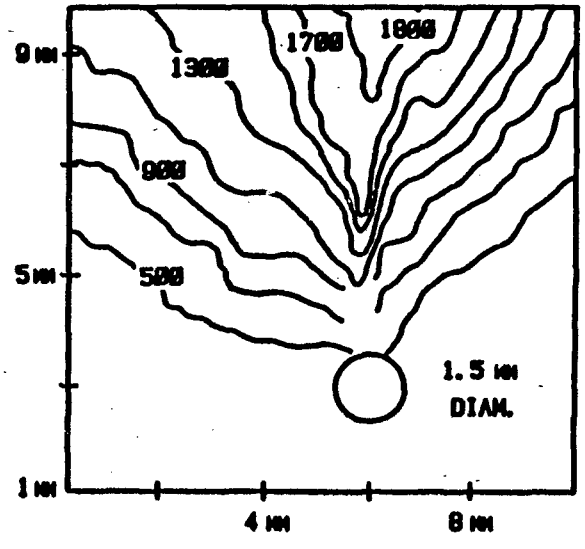

DIGITAL TEMPERATURE CONTOURS
(10mm x 10mm REGION)

- FIRST TECHNIQUE FOR INSTANTANEOUS 2-D TEMPERATURE MEASUREMENTS
- NOVEL SINGLE-WAVELENGTH TECHNIQUE CAN BE SELF-CALIBRATING
- POTENTIAL APPLICATION TO UNSTEADY REACTING AND NONREACTING FLOWS

FIG. 2 APPROACH AND RESULTS FOR TEMPERATURE VISUALIZATION TECHNIQUE

TWO-FREQUENCY STRATEGY FOR VELOCITY VISUALIZATION

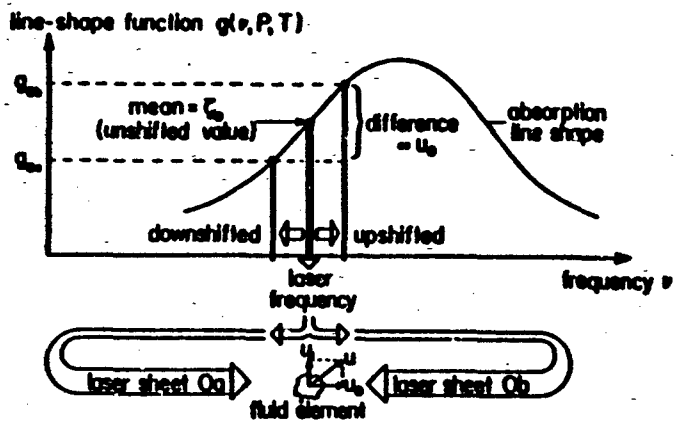

Effect of Doppler-Shift on Absorption Line-Shape Function: Single Frequency

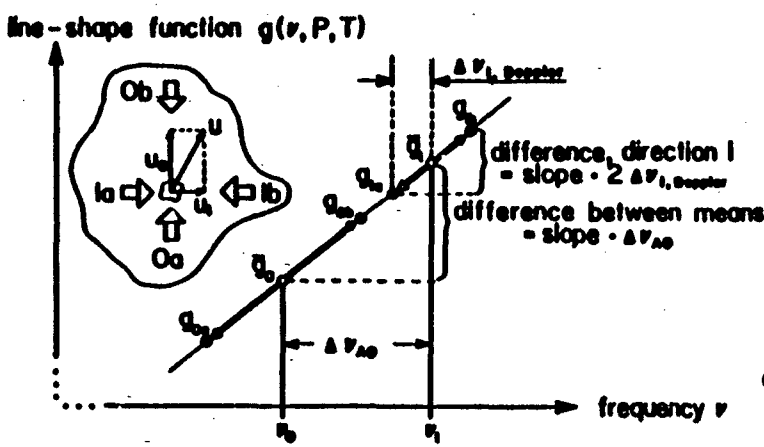

Two Laser Frequencies: Ratio of Differences Provides Self-Calibrated Velocity Measurement

$$u_0 = \frac{c}{\nu} \Delta\nu_{0,Dop} \qquad \Delta\nu_{1,Dop} = \Delta\nu_{A0} \frac{\frac{1}{2}(g_{1b} - g_{1a})}{\bar{g}_1 - \bar{g}_0}$$

FIG. 3 TWO-FREQUENCY STRATEGY FOR VELOCITY VISUALIZATION

1985 ROCKET RESEARCH MEETING
Abstract 64 Pg 4

2-D Velocity Measurement

- SPATIAL VELOCITY DISTRIBUTIONS VISUALIZED WITH LASER-INDUCED FLUORESCENCE

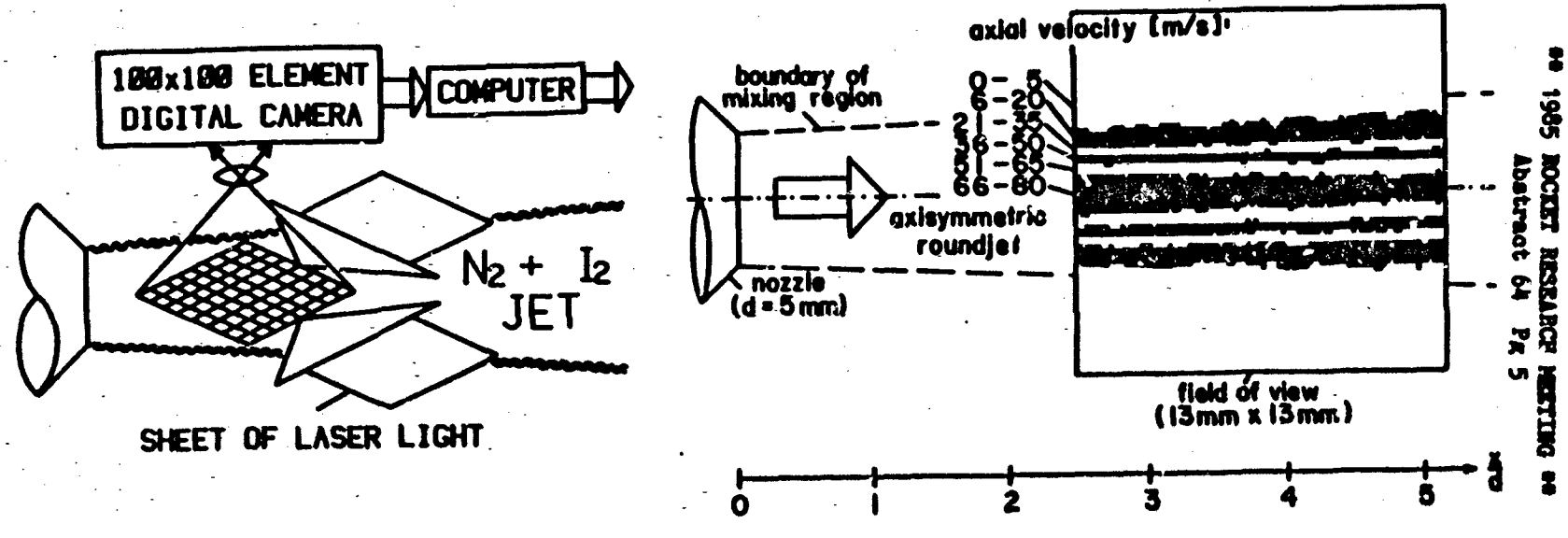

- NOVEL TWO-FREQUENCY TECHNIQUE IS SELF-CALIBRATING
- NO PARTICLE SEEDING REQUIRED
- FAST DATA PROCESSING; PROSPECTIVE TECHNIQUE FOR REAL-TIME MONITOR
- SENSITIVITY DEMONSTRATED TO 5 m/s; ACCURACY IMPROVES WITH INCREASING VELOCITY
- POTENTIAL FOR COMBINED VELOCITY AND PRESSURE MEASUREMENTS

FIG. 4 APPROACH AND RESULTS FOR VELOCITY VISUALIZATION TECHNIQUE

** 1985 ROCKET RESEARCH MEETING **
Abstract 64 Pg 5

OPTICAL PROCESSING AND PHASE CONJUGATION

Lambertus Hesselink
Stanford University
Stanford Cal. 94305-2186

RESEARCH OBJECTIVE The objective of the research program is to investigate innovative new approaches for making quantitative measurements in combusting flows. Techniques under investigation include optical and digital image processing, holography and phase conjugation.

EXPLANATION OF THE APPROACH Two new diagnostic techniques are under investigation. The first technique is a new method for obtaining species concentration in a flame using phase conjugation (DFWM). Two counter propagating laser beams (or sheets) are incident on a flame seeded with sodium, and a third probe beam intersects the other two. The probe and pump beam 1 form a grating in the medium by modulating the index-of-refraction through a nonlinear χ^3 process. The second pump beam is used to read out the hologram in real time and a fourth counter-propagating or phase conjugate probe beam results. The intensity of this beam is directly proportional to the local sodium number density and thus provides a means for measuring species concentration. As an example we have discussed sodium, but reaction species and radicals can be measured in the same fashion as well.

The second technique is a new method for making real-time velocity measurements in a plane using speckle interferometry. A sheet of laser light is used to illuminate a particle laden combusting flow and scattered radiation, called a speckle pattern, is recorded on a high resolution photorefractive crystal. Velocity information can be obtained by superimposing two speckle patterns on the crystal. Upon illumination of the crystal by another laser beam Young's fringes result in the far field diffraction pattern. The fringe spacing and orientation of the fringes are directly related to the velocity vector. It is also possible to record multiple exposures and thus provide a time-sequences of velocity at repetition rates in excess of thousands of frames per second for a total of a few hundred frames. In addition the crystal can be used for optical processing such as determining contour lines of equal velocity.

UNIQUENESS OF THE APPROACH. The new technique of phase conjugation (DFWM) in a flame can be compared with CARS or BOXCARS. DFWM is superior to the alternatives in that the signal strength is substantially higher, which allows for better spatial resolution and S/N for a given amount of laser power. The optical configuration is also very much simpler for DFWM because phase matching is automatically accomplished. In addition, since only light of a single frequency is used no monochromater or other beam separation devices are needed.

The use of a photorefractive recording material for speckle metrology allows real-time measurement of velocity in a plane for the first time. In addition movie data can be obtained at very high rates. Other approaches involving solid state cameras do not have the required resolution for speckle metrology and the conventional technique of using film provides only snap shot velocity information.

RESULTS. The first demonstration of DFWM was achieved in our laboratory a few months ago. The concentration of sodium in a small laboratory flame has been measured using the new DFWM technique; results of this experiment are reported in a publication submitted to Opt. Lett. The technique shows excellent promise as a diagnostic tool for combustion research.

The real-time speckle velocimetry work was started a few months ago, but preliminary results are available. We have demonstrated that indeed photorefractive materials can be used as a recording medium for speckle patterns. A new laboratory facility has been set up, including a small jet facility, optical components and instrumentation for analyzing the fringe patterns. We expect to demonstrate a working system within a few months.

PHASE CONJUGATION

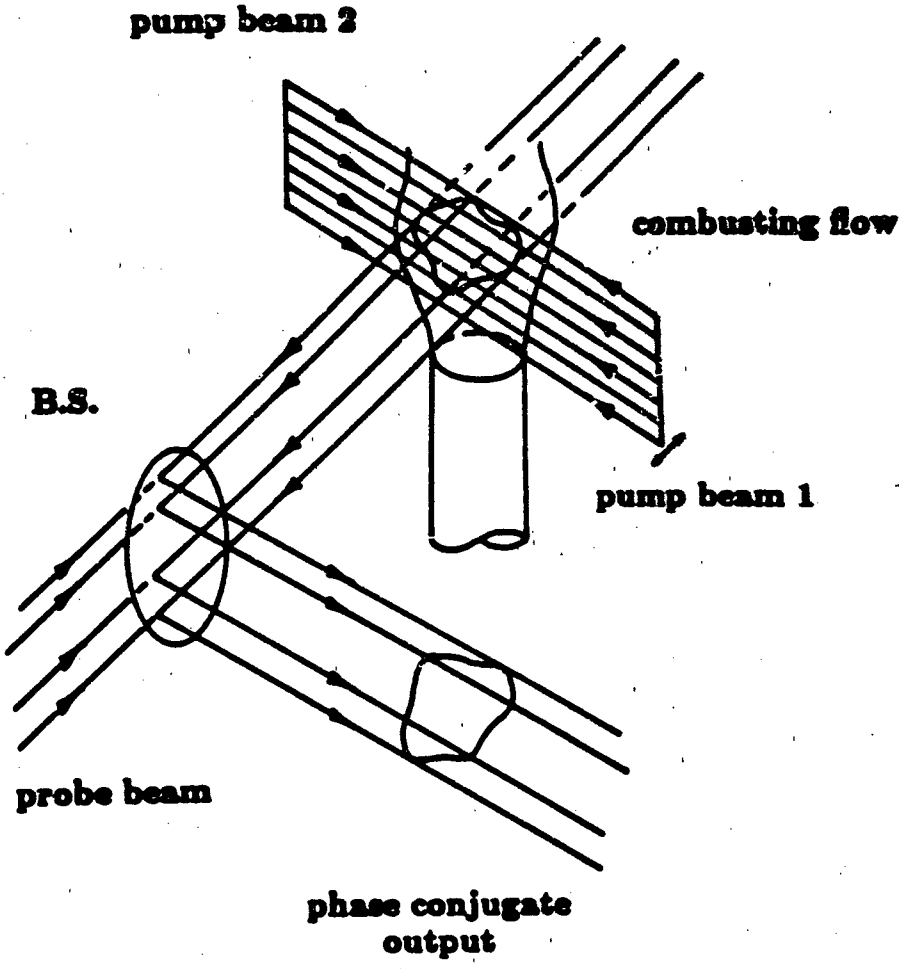

NOVEL ASPECTS

- First demonstration of phase conjugation in a flame.
- Better signal strengths compared with CARS or BOXCARS.
- Excellent spatial resolution.
- Only light of one color required.
- Simple optical set–up.

REAL-TIME SPECKLE VELOCIMETRY

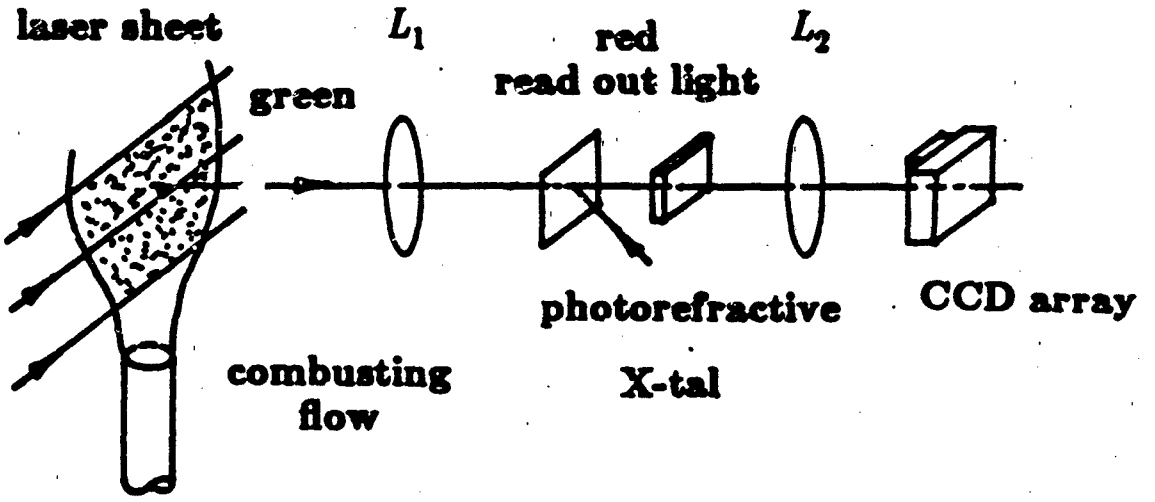

NOVEL ASPECTS

- Real-time velocity measurement in a plane or volume.
- Movie data of velocity can be obtained at very high rates in excess of thousands of frames per second.
- Optical processing can provide, for instance, contour lines of velocity.
- Excellent spatial resolution.

STRATEGY FOR ADVANCED SENSING AND CONTROL OF COMBUSTION

Mark L. Nagurka, Juan I. Ramos and W.A. Sirignano
Department of Mechanical Engineering
Carnegie-Mellon University
Pittsburgh, Pennsylvania 15213

The objective of this research program is to investigate approaches to the sensing and control of combustion processes. In order to achieve this objective a series of control problems are being considered. Each successive problem contains a more detailed model of the combustion process than the previous problem. In the first problem, a model equation describing the temperature distribution through a propagating flame has been studied. The sensing and control problem is formulated such that a suitably defined flame front is driven to or maintained at a desired location. Various definitions for the flame front location have been used to generate control problems for distributed parameter systems (DPS) in a classical format. For example, the flame can be defined as the inflection point of the temperature profile. Using such a definition is possible to state an ordinary differential equation governing the flow velocity and/or mixture ratio. The flow velocity and thermochemical properties of the mixture are collapsed in one parameter V here referred to as velocity. Solution of the partial differential equation governing the temperature distribution together with the ordinary differential equation for V yields the results for the controlled problem. Two sensors at neighboring locations and the temperatures measured by them are employed to determine the velocity V. The gain of the control system is reflected through a characteristic time τ. Figures 1 and 2 present the temperatures measured at the two sensor locations and the controlled parameter V as a function of time. The temperatures and velocity converge to a stable steady solution. For the model problem considered here, an exact analytical solution is known for the steady state and it coincides with our converged result obtained by means of a finite-difference solution of the unsteady problem. (The finite-difference method employed in the calculations shown in Figures 1 and 2 is second-order accurate in both space and time, and is based on a time linearization of the reaction terms.) In this first problem, the location of the sensors was selected a priori and calculations were performed to investigate the effects of the sensor locations, reaction rate, and characteristic time τ on the control problem. In the next class of problems, we will optimize the location of the sensors in order to achieve the research program goals.

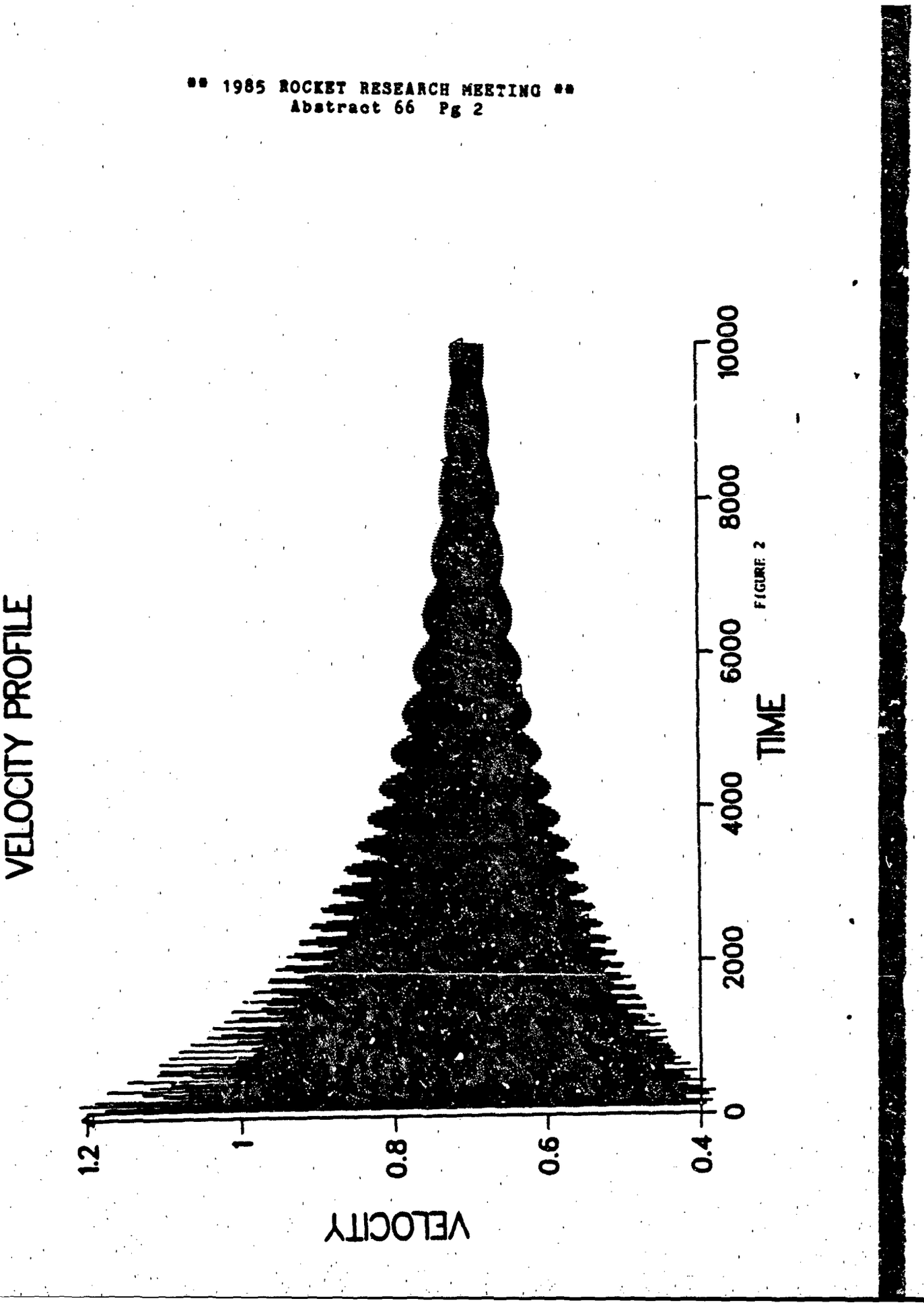
VELOCITY PROFILE
VELOCITY
1.2
1
0.8
0.6
0.4
0
2000
4000
6000
8000
10000
TIME

FIGURE 2

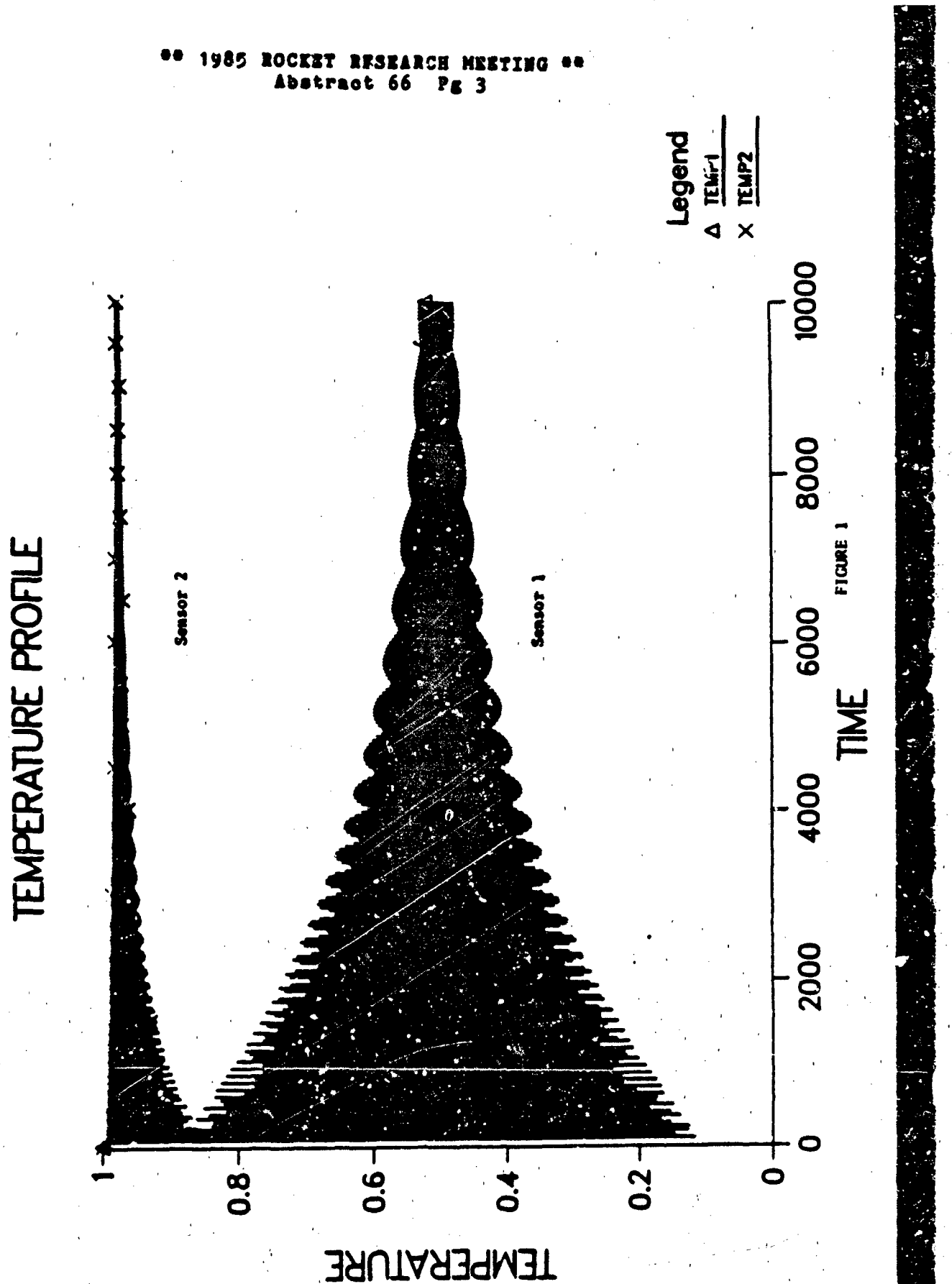
TEMPERATURE PROFILE
Sensor 2
Sensor 1
Legend
Δ TEMP1
× TEMP2
TEMPERATURE
1
0.8
0.6
0.4
0.2
0
0
2000
4000
6000
8000
10000
TIME

FIGURE 1

1-D Laser Doppler instrumentation

Holger T. Sommer
Department of Mechanical Engineering
Carnegie-Mellon University
Pittsburgh, PA 15213

The need for time and space resolved simultaneous velocity information increases with growing sophistication of turbulence models. Theoreticians request initial and boundary conditions for turbulent quantities currently inaccessible to experimental techniques. Laser-Doppler velocimetry has developed to an accepted method for investigating the turbulent flow fields. However the information obtained applying LDV to turbulent flows is restricted to measuring velocity components locally and simultaneously. In addition to velocity data obtained at one point in the flow, turbulence is influenced by the local, instantaneous velocity gradient.

This project focuses on the development of the reliable measurement of instantaneous velocity gradients by obtaining profiles of one component of the velocity vector instantly. The instrument consists of the standard transmitting optics of a LDV-system modified with cylindrical lenses to form laser sheets. The laser sheets cross and form a cylindrical LDV-measurement volume. The fringes of the volume are oriented perpendicular to the velocity component of interest and scattered light from paticles moving through the volume transmits the velocity information to the photo diode array. The signal from the photodiodes is processed in two different ways. The analog LDV-burst is stored on tape. Later on it is digitized and numerically analyzed to obtain the relevant velocity information. The second method of reducing the data involves optical frequency analysis developed earlier with AFOSR support. The laser doppler signal detected by the photodiodes is high-pass filtered and amplified. This signal drives a Bragg-cell which acts as an optical frequency analyzer. The displacement of the first order of deflection of a laser beam passed through the Bragg-cell is proportional to the signal frequency. By feeding the laser doppler bursts observed by different photodiodes to the Bragg-cell, and correlating the frequency proportional displacement of the analyzing laser beam with the location along the LDV-volume, a velocity profile can be obtained. In order to obtain instantaneous velocity profiles, a time window is opened which is sufficiently short to time resolve the turbulence of the flow. The coincidental property of these measurements is of importance to measure turbulent properties like the dissipation rate of turbulence, $\overline{\varepsilon}$.

$$\overline{\varepsilon} = \overline{\left(\frac{\partial v}{\partial x}\right)^2}$$

In which the gradient of the fluctuating velocity dissipates the kinetic energy of turbulence.

Figure 1 shows a schematic of the transmitting and receiving optics of the system developed with AFOSR support. Figure 2 illustrates the diagnostic electronics of the first method to record the data and reduce them to useful information. Figure 3 shows the optical frequency analyzer.

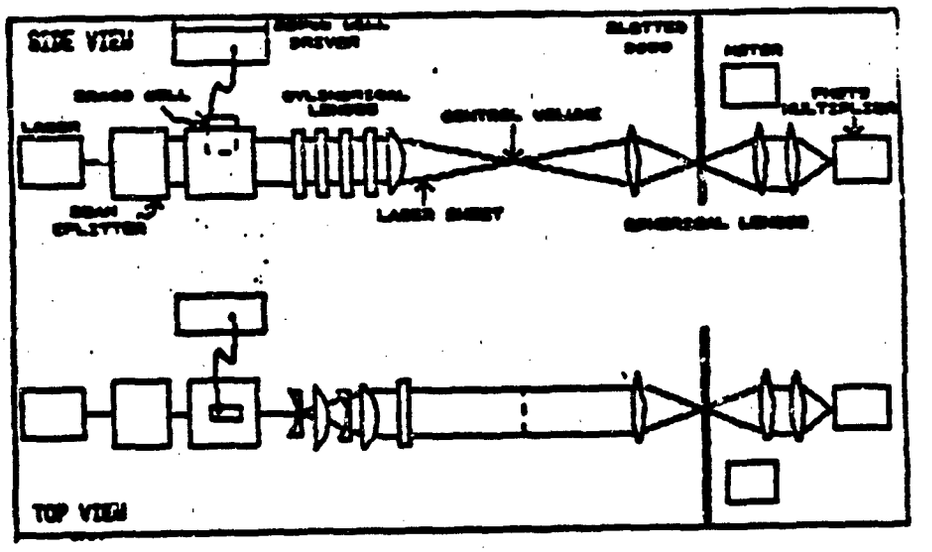

Figure 1 Optics set up to measure instantaneous velocity profiles

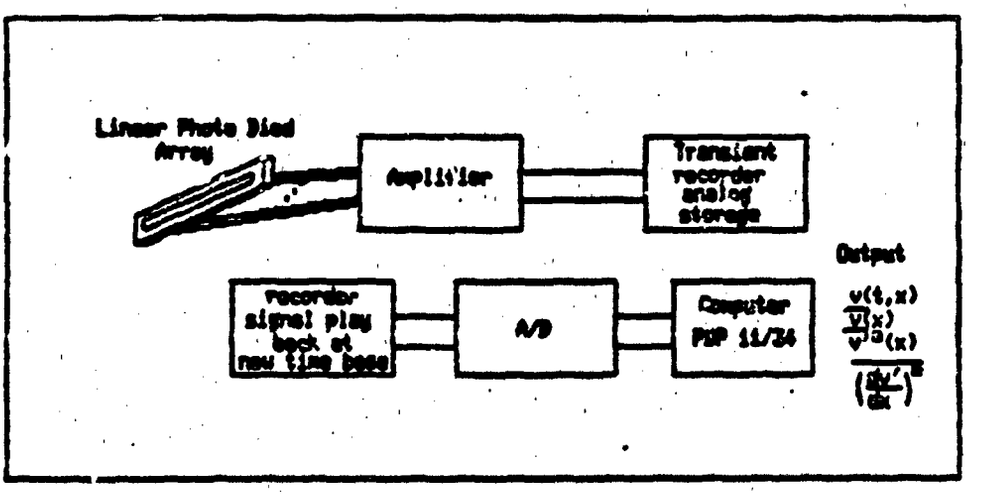

Figure 2 Multi-channel LDV data processing

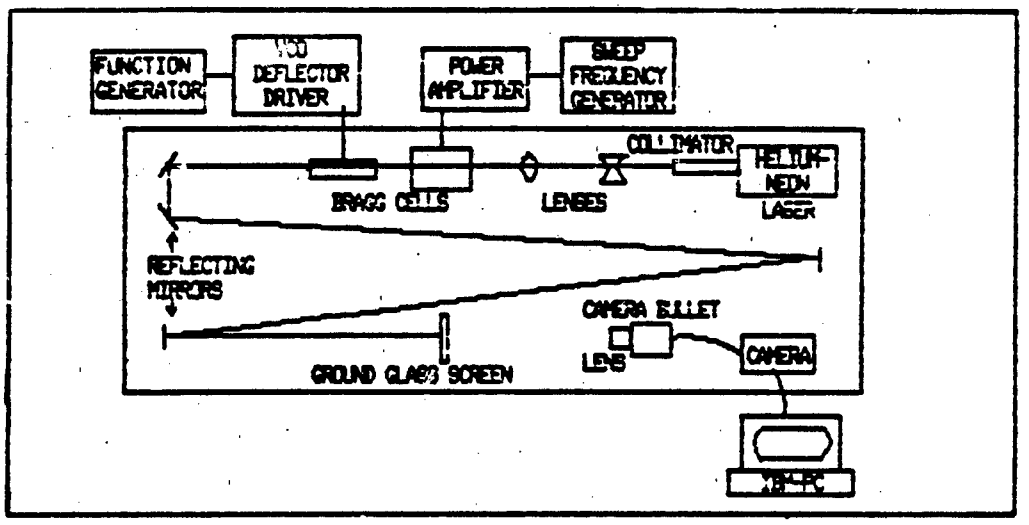

Figure 3 Optical frequency analyzer

RESONANT CARS DETECTION OF OH RADICALS

James F. Verdieck
United Technologies Research Center
East Hartford, CT 06108

Coherent anti-Stokes Raman spectroscopy (CARS) is an important spectroscopic technique which fulfills several requirements for probing hostile combustion environments that are of primary interest to the Air Force. The several advantages and numerous applications of CARS diagnostics have been well-chronicled elsewhere. A limitation of normal CARS is that, at atmospheric pressure, detection requires a species concentration of about 1 percent or greater. The aim of this program has been to extend CARS diagnostics to minority species, in particular radicals, through the technique of resonant CARS. The essentials of resonance CARS are illustrated in Fig. 1. The hydroxy radical was chosen as a candidate molecule because of its seminal importance in both combustion and atmospheric chemistry. The approach taken throughout this program has been to achieve an understanding of the basic physics of electronic resonant CARS in OH, including effects of tuning, laser linewidth dependence, choice of electronic transition, and saturation considerations.

At UTRC the first observation of resonant CARS in OH has been made under several conditions, including several different choices of the electronic resonant frequency. The amplitude and shape of a particular CARS spectrum are very sensitive to the precise tuning to the electronic resonance. The OH resonant CARS spectrum has a much greater amplitude than the adjacent water (conventional) CARS spectrum. In addition to the experiments, the theory of resonant CARS in OH has been treated. Agreement between theory and experiment is generally good, except for the experimental observation of satellite structure about the central line. This observation is shown in Fig. 2, which compares the theoretical spectrum predicted for excitation into Q1(2) of the X to A transition, with the experimental spectrum. The major discrepancy, highlighted by the expanded inset of Fig. 2, is the asymmetrically disposed fine structure about the strong central line. This satellite structure is now the subject of investigation. Several causes have been proposed, among them are: (1) Saturation, which can lead to power-induced extra resonances,whose spacing depends upon the optical power, (2) Rotational redistribution in either the upper or lower states, (3) Overlap of electronic resonance, so that two spectra are superposed. Other future work involves determining the applicability of resonant CARS as a diagnostic technique for OH (and other radicals), against LIF as a standard. Does resonant CARS have an advantage at high pressure? Another problem is to explore whether saturated CARS can be employed for concentration measurement, and, if so, the concentration range of applicability.

RESONANT CARS DETECTION OF OH RADICALS

Scientific Approach

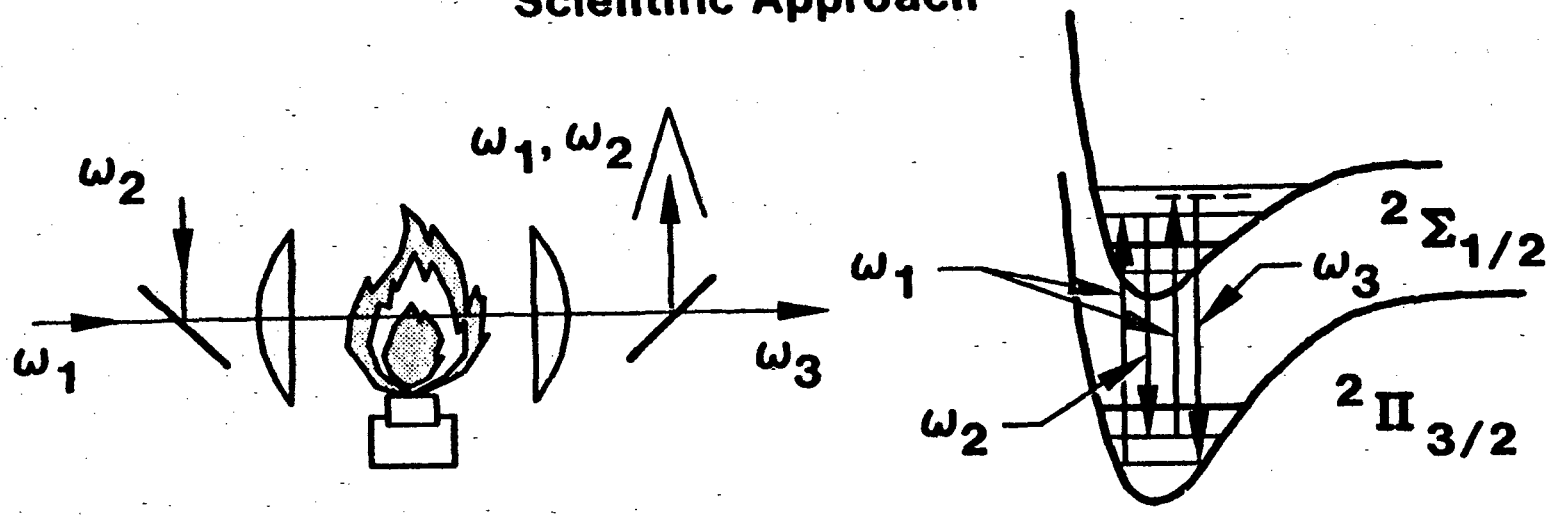

GOALS

- Improve CARS species detectivity via electronic enhancement
- Study the physics of resonant CARS spectroscopy
- Investigate multiple electronic resonances
- Determine the CARS detectivity limit for OH

RESONANT CARS DETECTION OF OH RADICALS

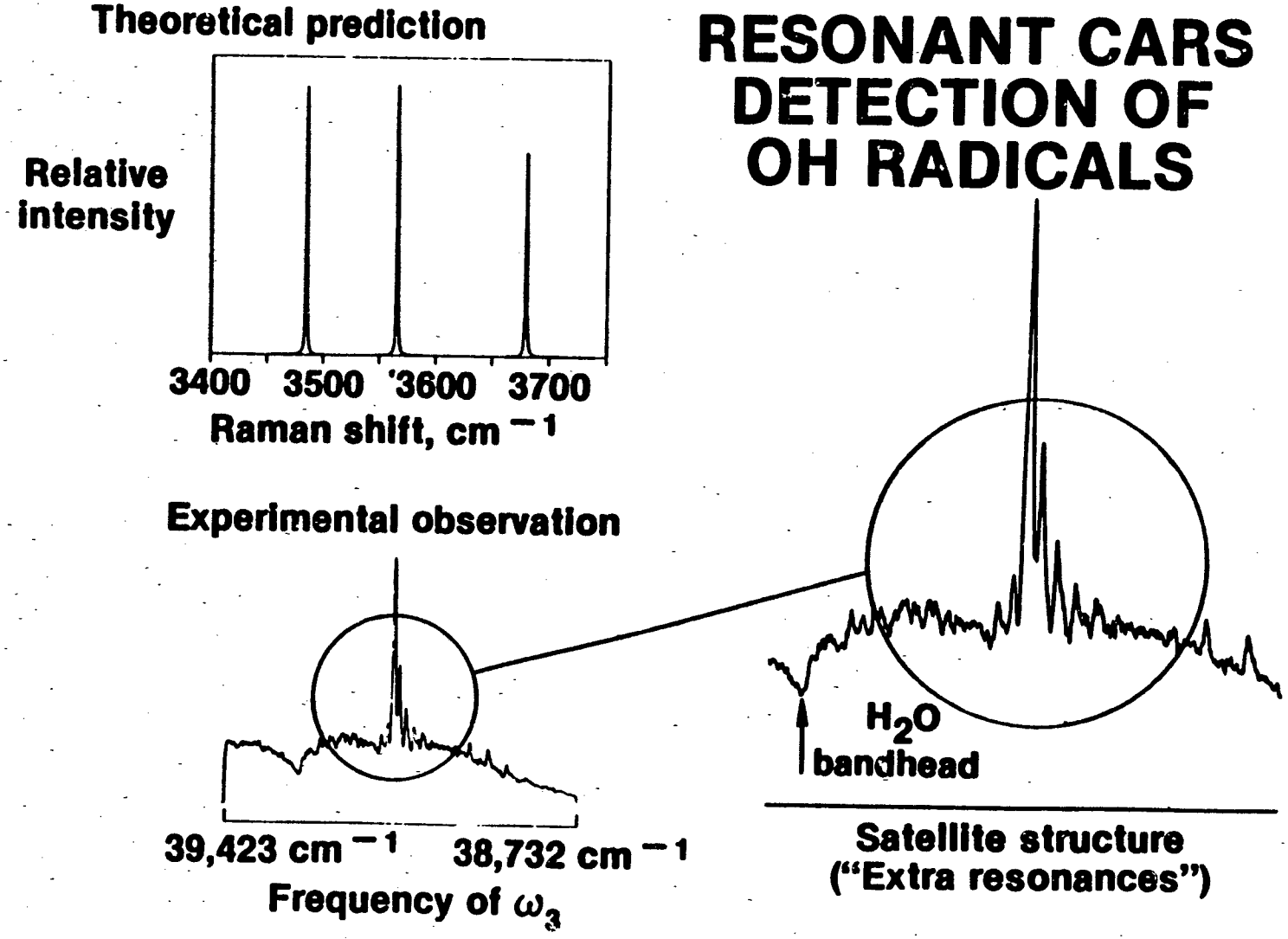

SPRAY CHARACTERIZATION USING PHASE ANGLE DETECTION

William D. Bachalo
Aerometrics, Inc.
P.O. Box 308
Mountain View, CA 94042

A new method with the potential for obtaining spray drop size and velocity measurements in sprays, two-phase flows, and eventually, in spray combustion is under investigation. The Phase/Doppler method is a unique method for obtaining drop size information wherein the measurements are obtained from the phase of the scattered light.

The theoretical description of the method was originally derived using a geometrical optics approach. This approximation provided an adequate description of the phenomena while remaining simple enough to understand the physics and the effects of the optical parameters. However, the exact Mie theory was used to verify these results and to investigate the possible effects of light scattered by the combined mechanisms of refraction and reflection. The Mie theory allowed the identification and avoidance of these regions. Calculations based on the simple geometrical optics approach were in excellent agreement with the experimental data for particles greater than 5 micrometers in diameter. Mie theory calculations demonstrated that particles as small as 1 micrometer can be measured.

The method , as illustrated in Figure 1, consists of an optical system which is the same as a LDV except that three detectors are located at selected spacings behind the receiver aperture. Droplets passing through the intersection of the two beams scatter light which produce an interference fringe pattern. The spacing of the fringes is directly proportional to the droplet diameter but also depends on the light wavelength, beam intersection angle, droplet refractive index (unless reflected light is measured), and the location of the receiver. Measurement of the spacing of the fringe pattern produced by the scattered light may be achieved by placing pairs of detectors at selected spacings in the fringe pattern or its image. As the fringes move past the detectors at the Doppler difference frequency, the detectors produce identical signals but with a phase shift proportional to the fringe spacing. The utilization of three detectors ensures that phase ambiguity does not occur, provides redundant measurements for signal validation and allows an expanded operating range while maintaining good sensitivity.

Experiments were conducted to disclose any practical limitations of the method. Monodisperse drop streams were used in conjunction with sprays in the optical path to assess the impact, if any, of random beam attenuations and distortion. Sprays typical of those found in gas turbine combustors were measured, Figure 2. The size distributions, size-velocity correlations, mean and rms velocities for each size class, and the time of arrival were obtained.

Each size distribution was normalized to account for the variation in sampling cross section with the drop size. Wherever possible, the results were compared to measurements performed with other methods. In all cases the results were very favorable.

Preliminary investigations have been conducted on the effects of turbulence-induced refractive index fluctuations produced by flames on the drop size measurements. Further research leading to measurements in spray flames will be conducted in the second year of the program.

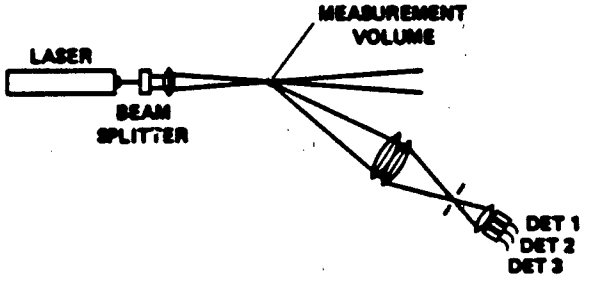

OPTICAL SYSTEM

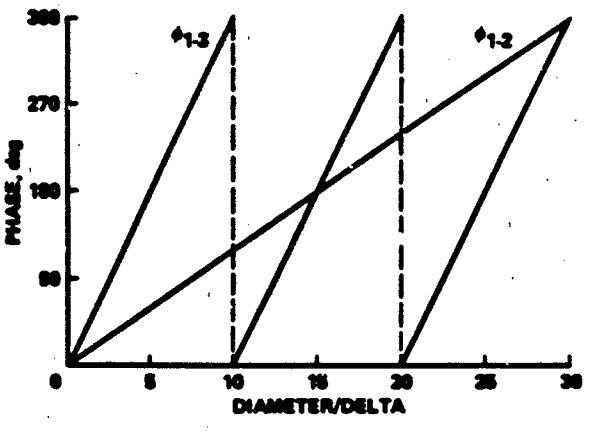

INSTRUMENT RESPONSE CURVES

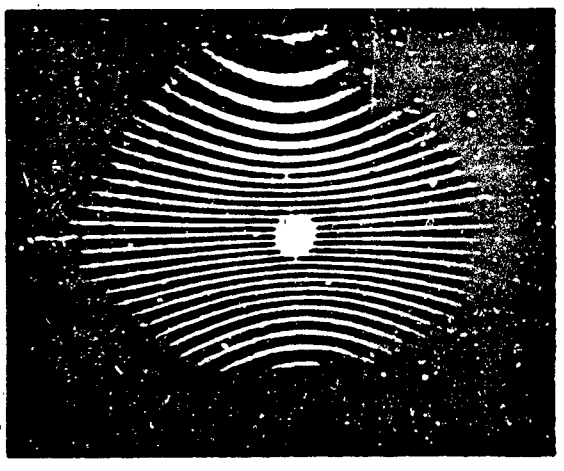

SCATTERED LIGHT INTERFERENCE PATTERN

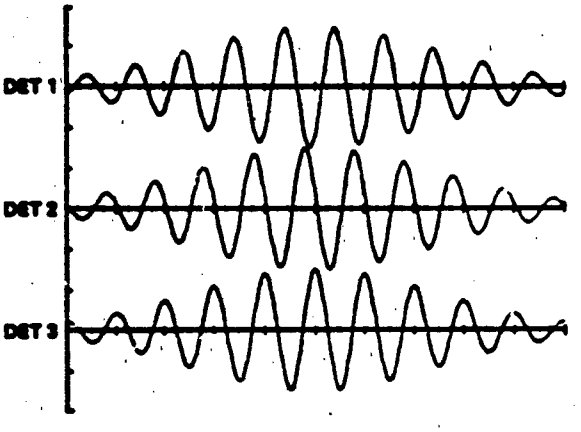

FILTERED DOPPLER BURST SIGNALS

Figure 1. Schematic of the Phase/Doppler Spray Analyzer Technique.

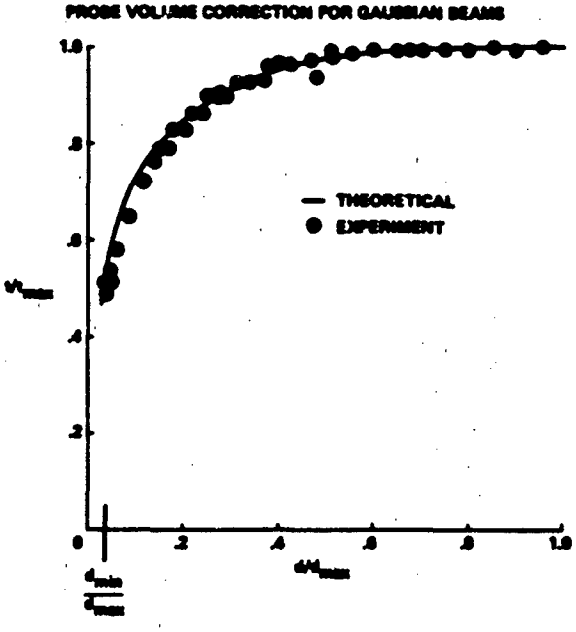

Figure 2a. Sample Volume Normalization

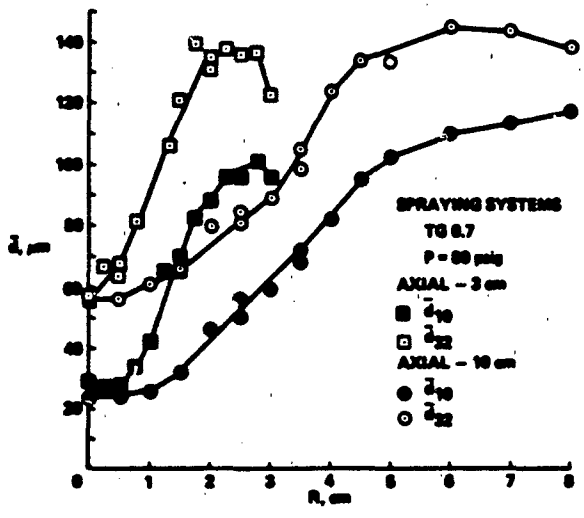

Figure 2b. Radial Mean Size Distributions

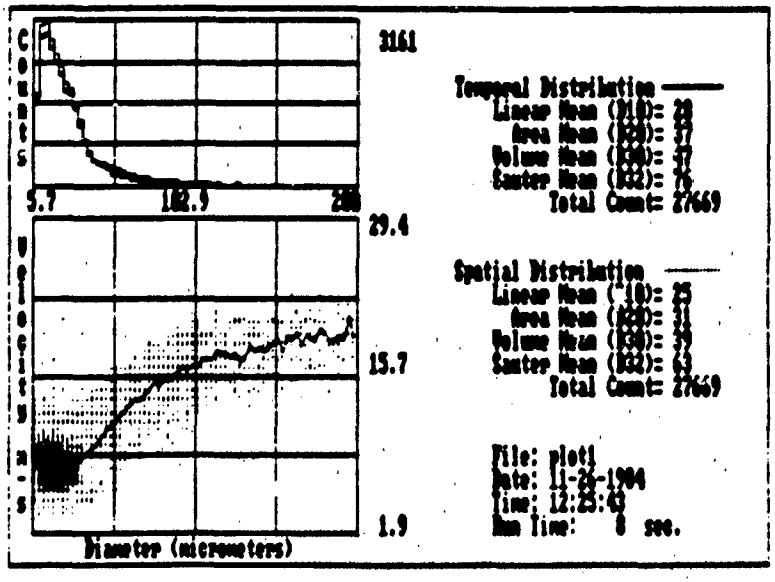

Figure 2c. Drop Size Distributions and Size-Velocity Correlations

Figure 2. Representative Experimental Data

LASER EMISSION AND COHERENT RAMAN SCATTERING FROM INDIVIDUAL FLOWING DROPLETS

Richard K. Chang, Marshall B. Long, and Roman Kuc
Yale University
Center for Laser Diagnostics
New Haven, Connecticut 06520

It may be possible to use the coherent but non-directional laser emission from individual particles as active markers for flow-field visualization and remote illumination. In particular, new applications may be viable with coherent emission droplets as velocimetry markers in otherwise optically dense two-phase flows and in overwhelmingly high elastic scattering environments such as near a solid boundary. Furthermore, determination of the chemical species of individual droplets appears to be possible with coherent Raman emission. New research has just been initiated on the nonlinear optical emission from water droplets and ethanol droplets with and without Rhodamine 6G or Courmarin dyes.

Laser emission from individual liquid ethanol droplets (radius ~30 μm and at room temperature) containing Rhodamine 6G at wavelengths commensurate with morphology-dependent resonances (MDRs) has been observed. For a conventional dye laser, optical feedback (i.e., higher Q) at selected wavelengths is provided by an external wavelength dispersive element. For a droplet dye laser, higher Q at selected wavelengths is provided by the MDRs associated with the liquid-air interface of the droplet. At these resonances, standing waves result from the total internal reflection at the liquid-air boundary of counterpropagating waves close to the circumference of the droplet (see Fig. 1). Since the fluorescence linewidth of Rhodamine 6G is homogeneously broadened, the emitted radiation will strongly favor those wavelengths which correspond to the MDRs. The laser emission was noted to consist of spectrally narrow peaks spanning the fluorescence gain profile. The output-vs-input intensity dependence was noted to be linear at low input power and was followed by an exponential growth, finally reaching a saturation region at higher power.

Stimulated Raman scattering (SRS) from individual H_2O or ethanol droplets at wavelengths commensurate with MDRs and the spontaneous Raman Stokes radiation has recently been observed. Two notable features in the SRS emission from the droplets are: (1) the occurrence of a series of spectrally narrow peaks that are nearly equally spaced in wavelength throughout the entire linewidth of the dominant spontaneous Raman vibrational modes (see Fig. 2); and (2) the input intensity required to achieve the SRS threshold for the droplet is an order of magnitude less than that for the corresponding bulk liquid with 2-4 cm path length. Both observations are consistent with MDRs resulting from the spherical liquid-air interface which forms an efficient optical cavity for the SRS. Investigations on the coherent anti-Stokes Raman scattering (CARS) from individual droplets are underway.

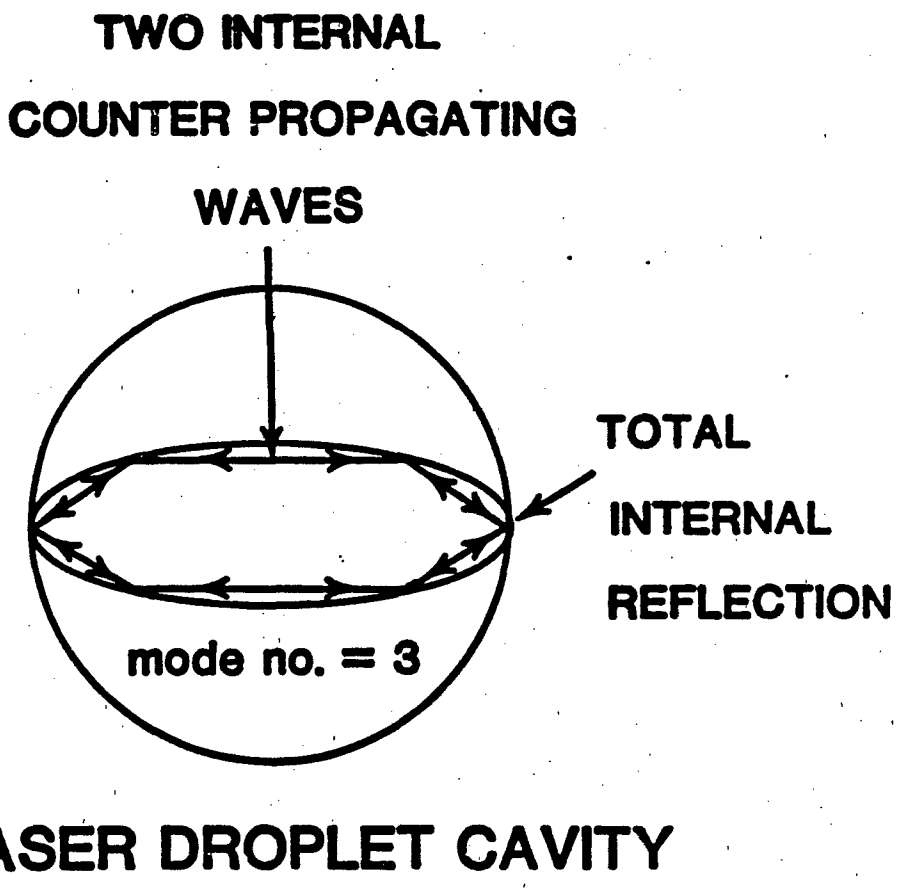

Figure 1. Optical wave structure within a droplet. Fluorescence radiation within the droplet undergoes total internal reflection at the liquid-gas interface. The droplet acts as an optical resonator for counterpropagating waves around the circumference.

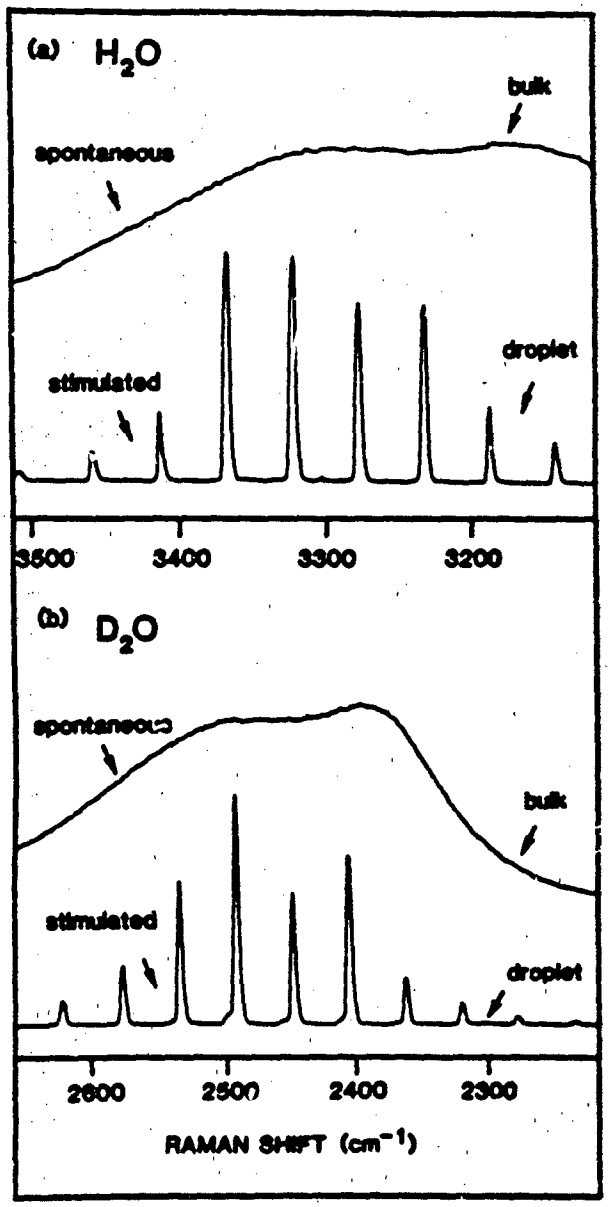

Figure 2. The cw spontaneous Raman scattering from bulk H_2O and D_2O in a cuvette is shown in the upper spectrum of (a) and (b), respectively. The discrete peaks in the lower spectra of (a) and (b) are from a single droplet using a single 10-nsec laser pulse. These regularly spaced SRS peaks correspond to MDRs.

SIZE AND SHAPE CHARACTERIZATION OF INDIVIDUAL FLOWING DROPLETS BY LASER LIGHT SCATTERING

Richard K. Chang, Boa-Teh Chu, and Marshall B. Long
Yale University
Center for Laser Diagnostics
New Haven, Connecticut 06520

In two-phase flows, the size and shape distribution of the fuel droplets affect combustion and their chemical by-products. The evaporation rate of a single droplet within a spray depends on the heat flux directed toward it and on its vapor environment. Both these quantities depend on the proximity of neighboring droplets and also on the collective evaporation and combustion properties of all the droplets. The temperature-dependent surface tension and the bulk viscosity of a single droplet affect the droplet shape as well as its shape oscillations as the droplets flow in a combustor and are acoustically perturbed.

We report a new technique for determining both the size changes and the shape distortions of individual droplets flowing in a linear stream. This technique is based on the "whispering gallery modes" or more accurately morphology-dependent resonances (MDRs) associated with microparticles having a rotational axis symmetry. For size and shape determination, we chose to measure the MDRs in the fluorescence spectra from ethanol droplets "tagged" with Rhodamine 6G dye. Highly monodisperse tagged ethanol droplets are generated by a modified Berglund-Liu vibrating orifice generator. The droplets have a radius in the 10-50 μm range with a monodispersity of one part in 10^4-10^5 and spacing within a linear stream of ∿100 μm.

The evaporation of droplets within a linear stream can be readily determined by measuring the wavelength shift of specific MDRs from successive droplets further downstream from the orifice, since the droplet decreases in size monotonically with time after exiting the orifice. Our results demonstrate that the wake of preceding droplets significantly decreases the evaporation rate of a droplet within the linear stream.

The surface tension and viscosity of an ethanol droplet flowing within a linear stream can be determined by measuring the wavelength oscillation of specific MDRs from successive droplets further downstream from a perturbation which can induce shape distortions. Figure 1 shows the experimental configuration. Shape perturbation at one location was initiated with two counterpropagating Ar^+ laser beams (514.5 nm, 8 mW each) impinging on a single tagged ethanol droplet. The subsequent shape distortion of droplets within the linear stream can be described by a quadrupole mode oscillation with an oscillation frequency $(f_2)^2 = 2\sigma/\pi^2\rho a^3$ and a damping constant $\tau_2 = a^2/5\nu$, where σ is the surface tension, ρ is the density, and ν is the kinematic viscosity. Figure 2 shows the MDRs in the fluorescence spectra from successive droplets downstream of the shape distorting perturbation. The MDRs exhibited a damped oscillation with a frequency f_2 and damping constant τ_2 for ethanol droplets. Our results compare well with electrodynamic calculations of the MDRs for equivolume droplets which oscillate between spheres and slightly oblate or slightly prolate spheroids.

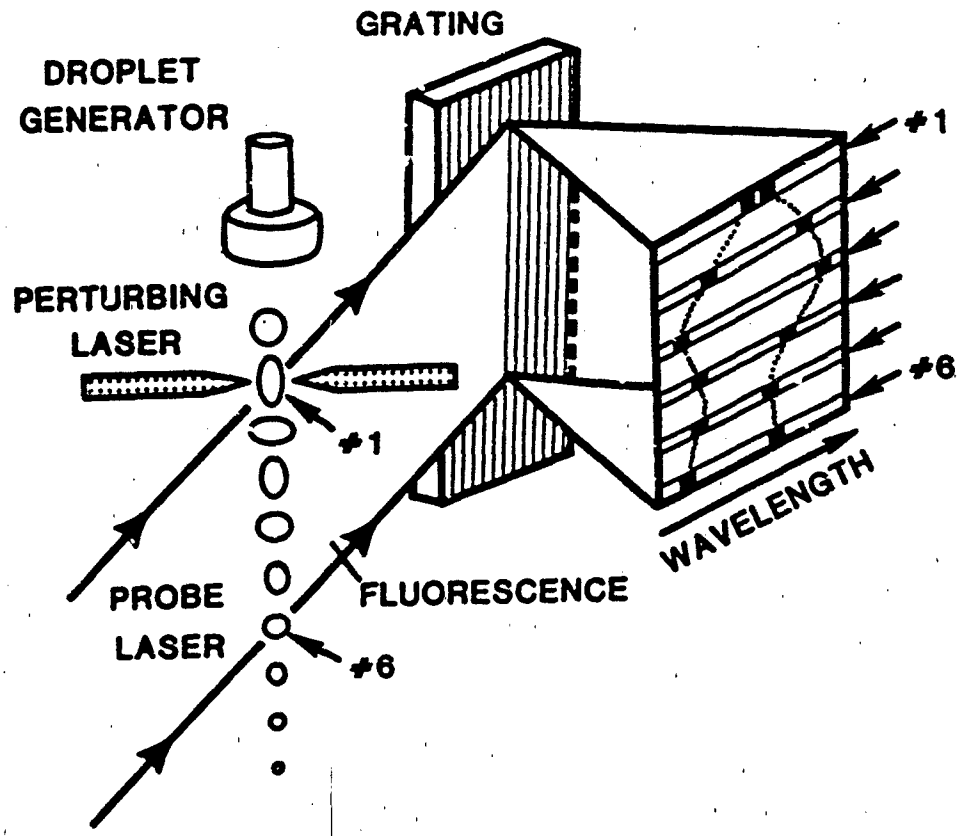

Figure 1. Schematic of the experimental arrangement for the laser-induced shape oscillations of flowing droplets. Two counterpropagating beams (Ar^+ laser, 514.5 nm) are focused on the absorbing dye-tagged ethanol droplet. A probe beam (pulsed N_2 laser) is focused into a sheet and induces fluorescence from the droplet. The dispersed fluorescence spectra highly monodisperse droplets in a linear stream are detected by a television camera.

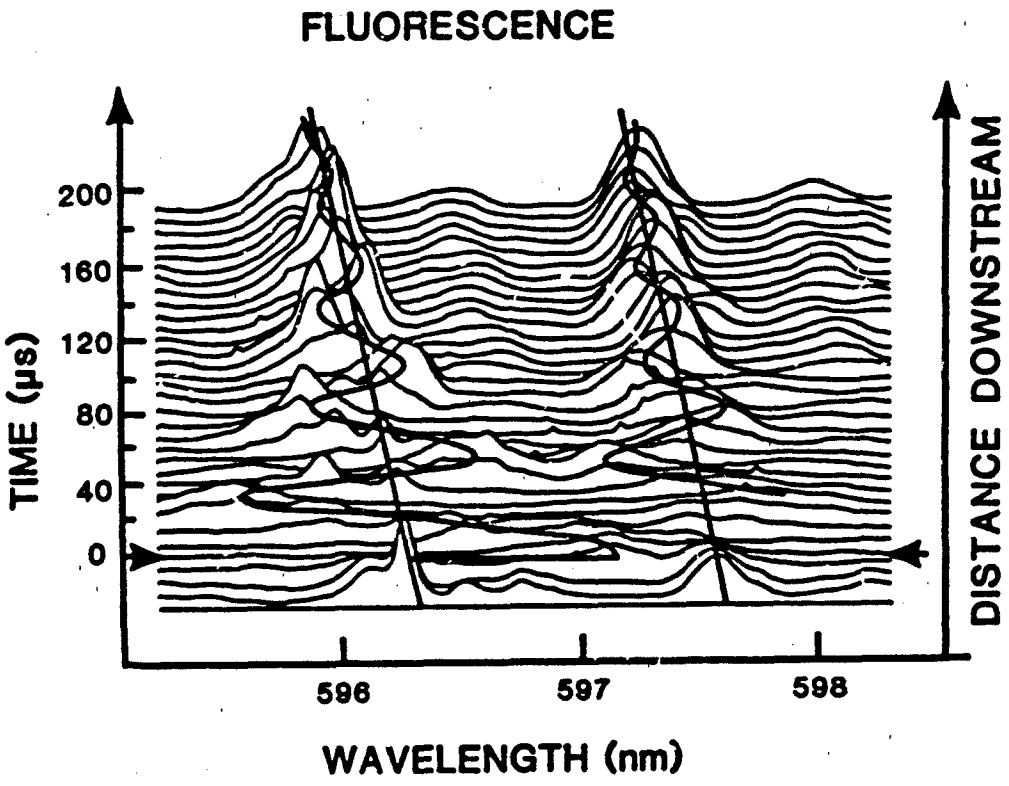

Figure 2. Fluorescence spectra from laser-perturbed droplets downstream from the orifice. Since the frequency of the droplet generation is known, the distance downstream is plotted as time delay after the Ar^+ laser perturbation defined as t = 0. Each droplet is perturbed by the Ar^+ laser beams at a location indicated by the two arrows. The subsequent freely damped oscillations of MDRs from droplets downstream yield a shape oscillation frequency and damping constant corresponding to a quadrupole resonance.

SPRAY CHARACTERIZATION WITH A NONINTRUSIVE OPTICAL SINGLE PARTICLE COUNTER

Cecil F. Hess
Spectron Development Laboratories, Inc.
3303 Harbor Boulevard, Suite G-3
Costa Mesa, CA 92626

The objective of this research program is to advance the understanding of droplet sizing technology in combustion environments using light scattering. The emphasis during this, the second year of this research program, has been in establishing what information of the scattered light is better suited to provide the size and velocity of droplets, which can then yield local mass flux measurements. The studies conducted indicate that the absolute intensity of the scattered light combined with the standard LDV will produce excellent results. This technique has been combined with auto calibrating algorithms to compensate for the loss of energy experienced when the laser beams or the scattered light travel through windows and other particles along the path. This is the basis of the IMAX technique. In such technique, two small laser beams of one color interfere in the center of a large beam of another color. The interference pattern produces the Doppler signal and also identifies the center of the large beam where the intensity is almost uniform.

An alternative and unique approach, referred to as P/MAX, is also under investigation. Here, instead of using laser beams with different colors, the P/MAX technique uses beams with polarizations normal to each other. This allows the use of low power single color lasers.

In order to perform mass flux measurements in addition to the size and velocity distributions, the active probe volume must be known. This probe volume is a function of particle size and several optical parameters. It is extremely important to understand and predict the probe volume, since it must be used to correct the number of events corresponding to the various size classes. These corrected counts will constitute the ordinate of the pdf of the size distribution. Figure 1 illustrates the probe volume configuration. Here, two lenses with focal lengths f_1 and f_2 image the probe volume on a pinhole of diameter D_p. The variation of the probe volume's nondimensional coordinate y' with particle size d' is shown on Figure 2. The experimental values were obtained by traversing a monodisperse string of droplets throughout the sensitive area. The effect of the probe volume on the size distribution is illustrated on Figures 3a and 3b. Figure 3a shows the raw counts obtained with two different size ranges. Figure 3b shows the counts corrected by probe volume. It can be observed that the size distributions obtained with the two size ranges produce the same result only after correcting the distributions by the probe volume. This test also demonstrates the instrument's self-consistency.

The Sauter Mean diameter (SMD) of the spray is plotted on Figure 4 as a function of radial position for two pressures. The trend shown is the expected one, namely, the SMD is small at the center of the spray and increases with radial position.

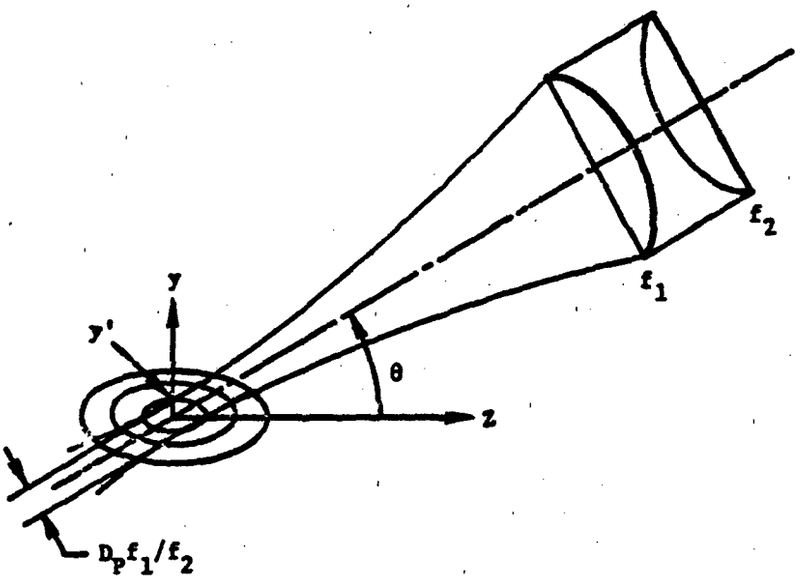

Figure 1. Schematic representation of a dual beam probe volume limited by a pinhole.

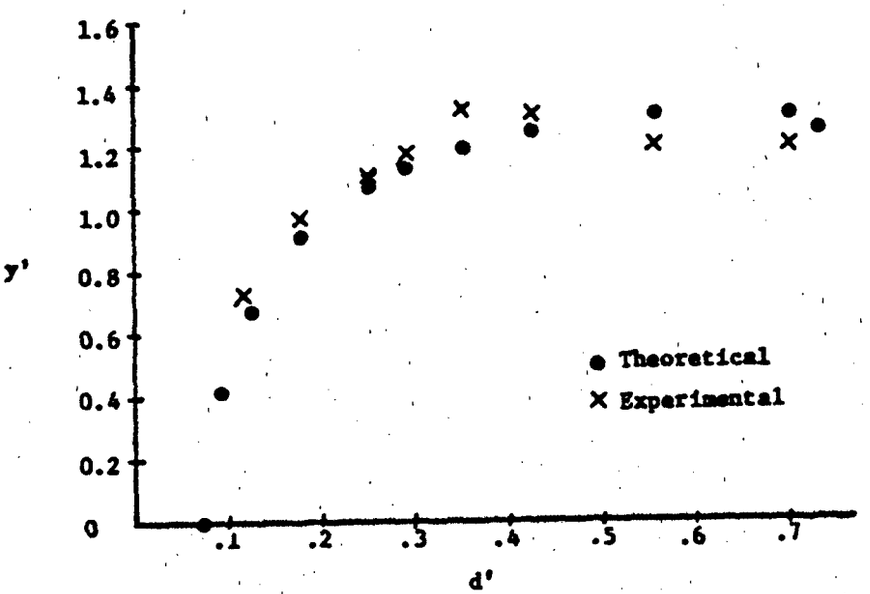

Figure 2. Experimental and theoretical variation of the probe volume coordinate y' with the nondimensional particle diameter d'.

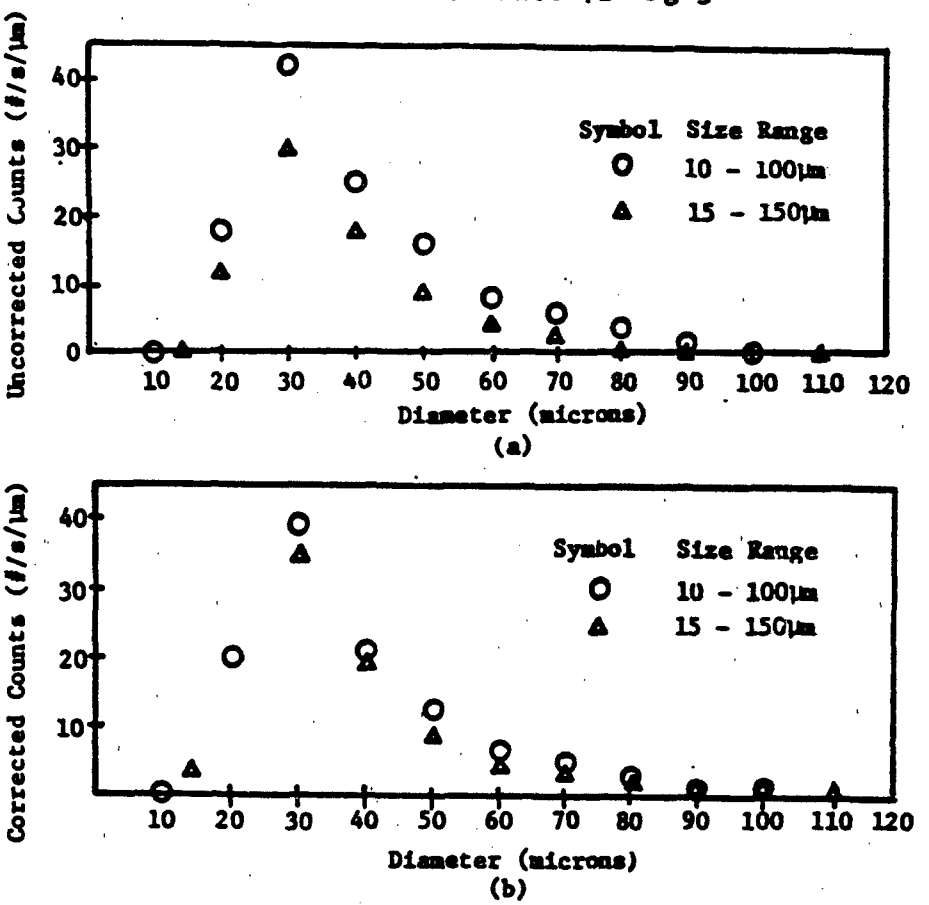

Figure 3. PIMAX measurements of a spray produced by a Parker Hannifin model 7 simplex nozzle using water at 60 psi, at a radial position = 0mm, and axial position = 50mm.

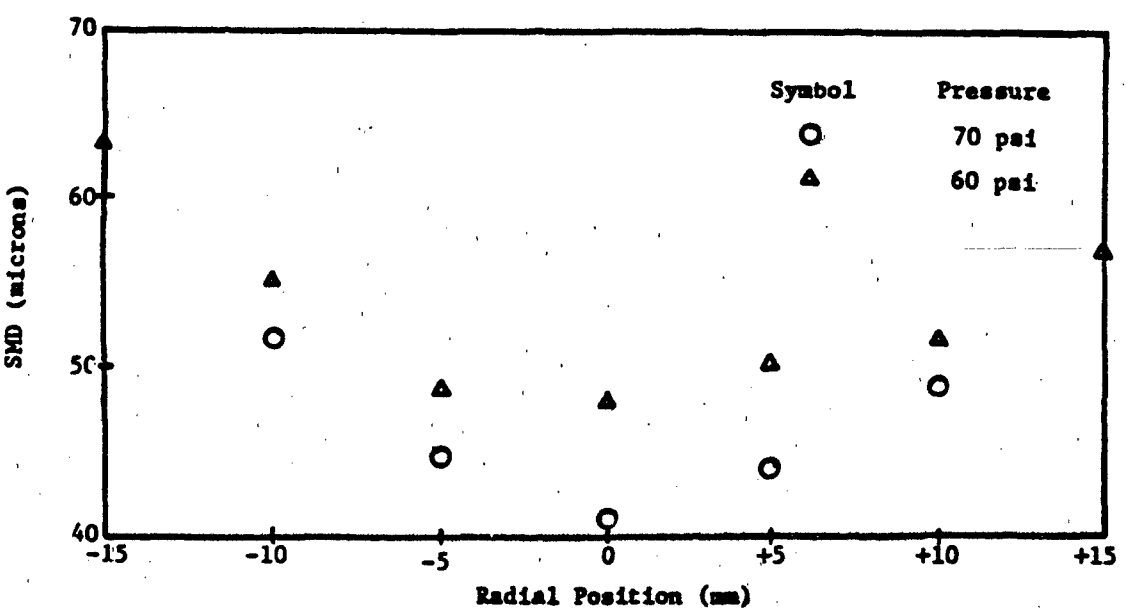

Figure 4. Variation of Sauter Mean diameter with pressure and radial position. Axial position = 50mm. Nozzle: Parker Hannifin Model 7 Simplex. Fluid: water.

INTELLIGENT LASER DIFFRACTION INSTRUMENTATION FOR PARTICLE SIZE ANALYSIS

E. Dan Hirleman and Joseph I. Koo
Arizona State University
Tempe, AZ 85287

Particle and droplet size distributions, being parameters of fundamental importance, should be priority measurement objectives for intelligent sensors in next-genetration propulsion systems. Unfortunately there are a number of problematic scientific issues limiting the development of laser light scattering particle sizing instruments capable of autonomous, self-diagnosing operation in hostile environments. Beam steering due to thermal gradients, multiple scattering from high number density aerosols, and contamination of windows and electro-optical components have been and will continue to be potentially catastrophic problems. The objective of this research effort is to contribute to the scientific knowledge base necessary to characterize and extend the applicability of laser diffraction instruments under these hostile conditions. Both the novel specific approaches discussed below and the emphasis on concepts relevant to intelligent instrumentation make this project unique.

The research is concentrated in three areas: development of rapid and robust computational algorithms for the laser diffraction inverse scattering problem; synergism of electro-optical detection strategies with the inverse scattering algorithms; and techniques for on-line calibration and performance evaluation particularly with respect to the potential detection and correction for multiple scattering effects. Figure 1 shows the laser diffraction system proposed here. The diffraction reference leg, the beam position detector, and a dynamically configurable ring detector array are novel concepts proposed to extend the standard configuration of laser, beam expander, transform lens, and fixed geometry detector. The modulated reference diffraction signature is carried through the particle field on the primary beam and separated after the detector using frequency-locked signal processing. Any deviation in the measured reference scattering pattern from the known reference pattern will directly indicate pertubations due to nonideal effects (e.g. multiple scattering) which will likewise have contaminated the particle field measurements. We envision an instrument which continuously performs self-calibration and diagnostics. Further, the intelligent sensor would continuously monitor the operating environment and reconfigure the detector geometry and inverse scattering algorithm to maintain operation near an optimal configuration. The importance of subtle changes in detection strategy are shown in Fig. 2 where the condition number (related to numerical stability) of the scattering matrix is plotted for two detector configurations. An intelligent instrument would use data such as Fig. 2 to determine an optimal detector geometry and the maximum resolution in the measured size distribution justified for a given operating environment.

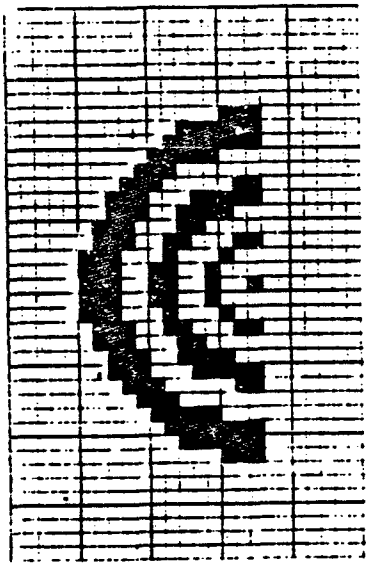

Figure 1a. Dynamically configurable ring detector.

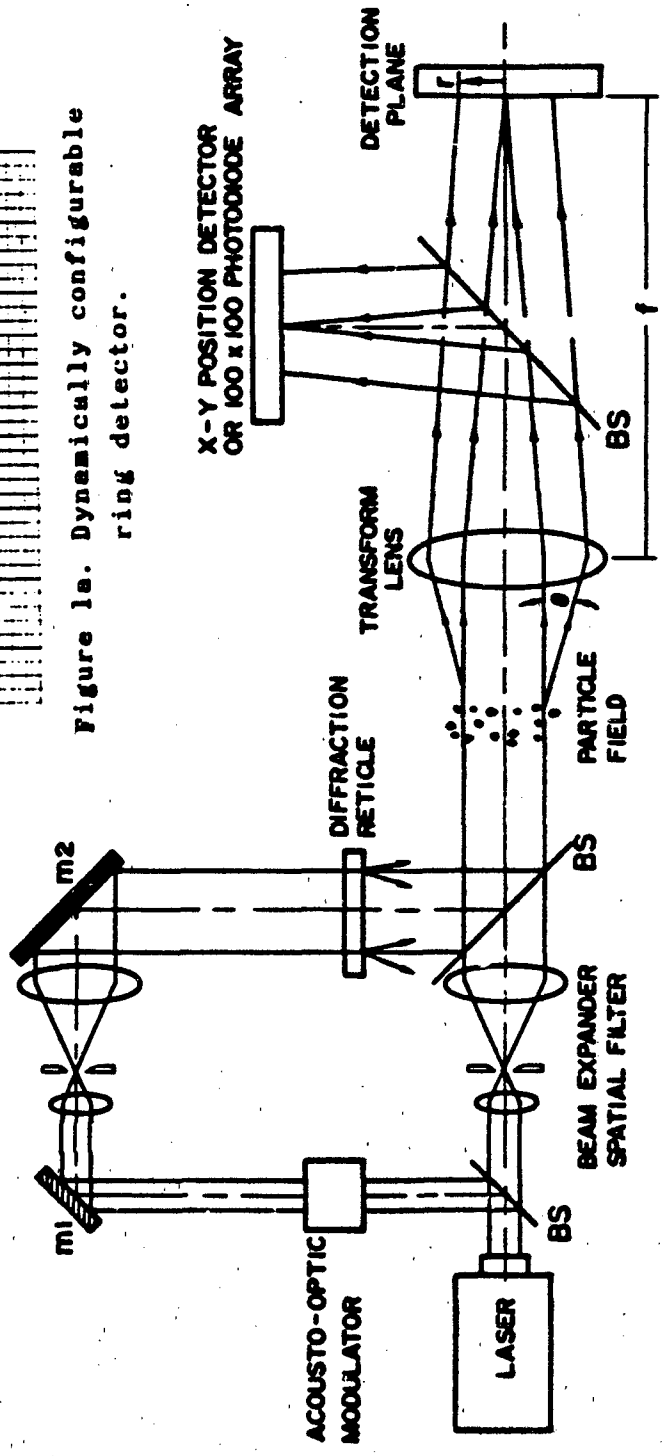

Figure 1. Schematic of intelligent laser diffraction particle sizing system.

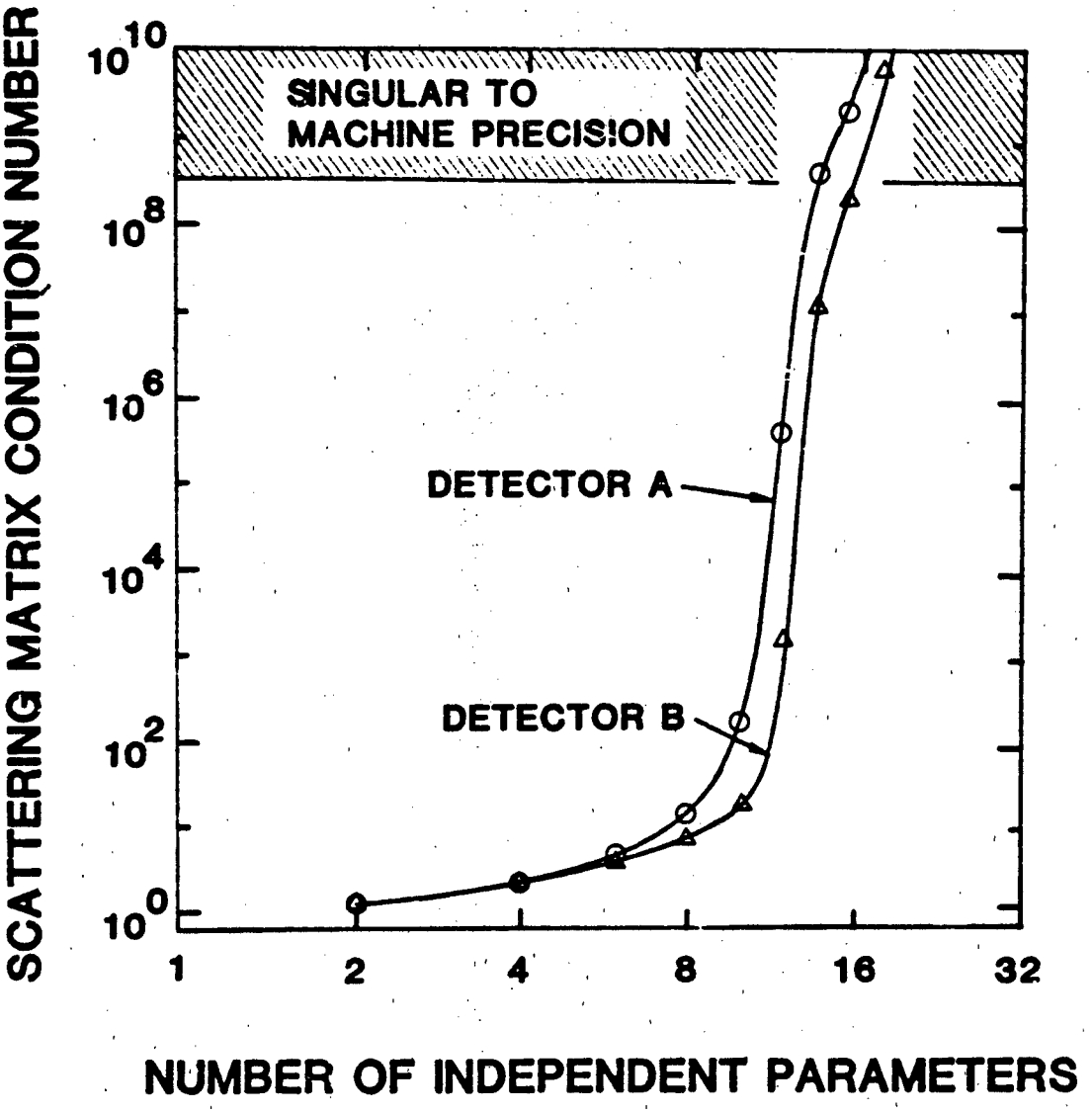

Figure 2. Condition number of the scattering matrix vs. the number of independent parameters (degrees of freedom) in the size distribution. Data for two detector geometries.

APPLICATION OF ATOMIC FLUORESCENCE TO MEASUREMENT OF COMBUSTION TEMPERATURES IN SOLID PROPELLANTS

Larry P. Goss and Arthur A. Smith
Systems Research Laboratories, Inc.
2800 Indian Ripple Road
Dayton, OH 45440-3696

The aim of this program is to obtain temperature data on the surface of a solid rocket propellant which can be related to the kinetics of the combustion process. Laser-induced-fluorescence (LIF) techniques are being used to measure the fluorescence spectrum and lifetime of an impurity introduced into the reacting material. Since spectra and lifetimes of selected impurities (rare-earth ions) have been shown by this research to be highly temperature sensitive over the range of interest (300-1050 K), it should be possible to obtain a temperature profile of the reacting surface of the propellant.

When two rare-earth-ion energy levels are separated by < 1000 cm^{-1}, the upper level typically will not fluoresce at low temperatures, the reason being that multi-phonon relaxation rates are extremely high (10^6/s) with small energy gaps since fewer phonons are required for quenching. At low temperatures no population build-up occurs in the upper energy level; therefore, no fluorescence is observed. As temperature increases, population buildup in the upper level increases and fluorescence increases relative to the lower energy level.

An example of this behavior is found in Dy^{+3}:LaF_3 (Fig. 1). Absorbed laser light excites Dy^{+3} in a high-energy level which radiatively and nonradiatively decays to the $F(^4F_{9/2})$ level. This level undergoes a fast thermal equilibrium which pumps a portion of its population into the nearby $G(^4I_{15/2})$ level. The fluorescence is then observed from both states. Notice the gradual build-up of the G-fluorescence line located at 4537 Å with temperature. The G level increases in intensity approximately 200 fold over a 973-K temperature range.

To understand the effect of temperature on the lifetimes of rare-earth transitions, one must examine the effect of temperature on the radiative and nonradiative relaxation rates which govern the observed lifetimes. The radiative probability includes both purely electronic and phonon-assisted transitions; the nonradiative probability includes relaxations by multi-phonon emission and effective energy-transfer rates arising from ion-ion interactions. The temperature dependence of the lifetime is solely determined by the temperature dependence of the nonradiative relaxation rate.

Nonradiative relaxation between J states can occur by the simultaneous emission of several phonons which are sufficient to conserve the energy of the transition. These multi-phonon processes arise from interaction of the rare-earth ion with the fluctuating crystalline electric field. Lattice vibrations are quantized as phonons having symmetry properties determined by the symmetry of the crystal and excitation energies determined by the masses of the constituent ions and the binding forces. Examples obtained in this program of the effect of temperature on the lifetime of a transition are shown in Fig. 2.

Phase I of this study has been successfully completed, and work on Phase II has been initiated. This phase includes extensive measurements to correlate the surface temperature measured using high-speed pyrometry and thermocouples with that measured using the fluorescence technique, for calibration purposes.

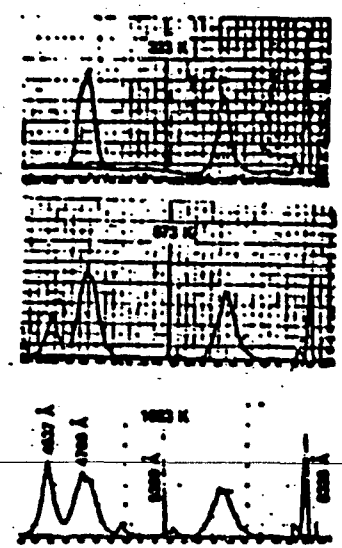

(a)

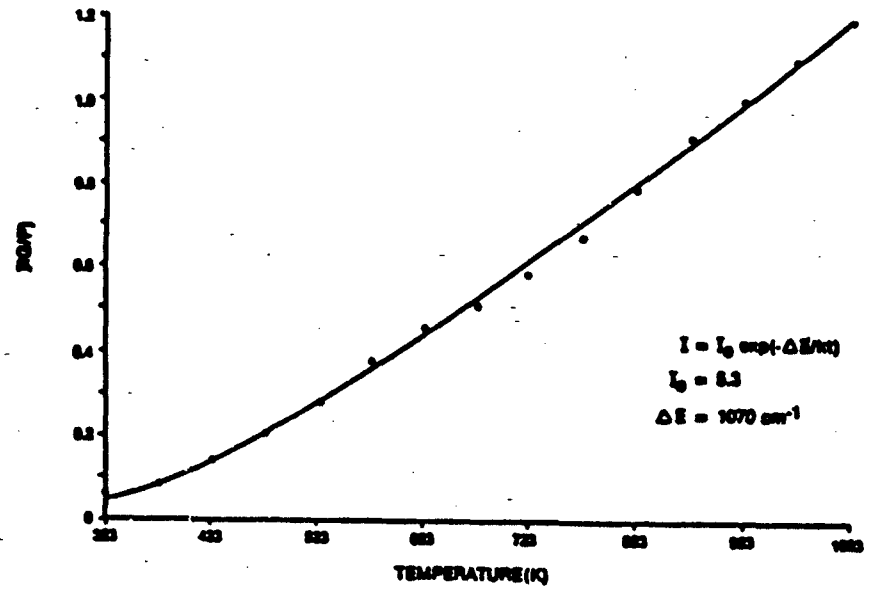

(b)

Figure 1. Temperature-Induced Spectral Variation of Dy^{+3}:LaF_3. (a) Experimentally Observed Variation of the G to F Fluorescence Levels with Temperature. (b) Plot of Intensity vs. Temperature Taken from Data in (a). Solid line represents fit to data assuming energy gap of 1070 cm^{-1}.

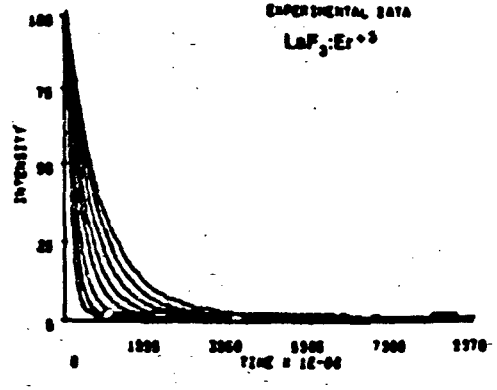

(a)

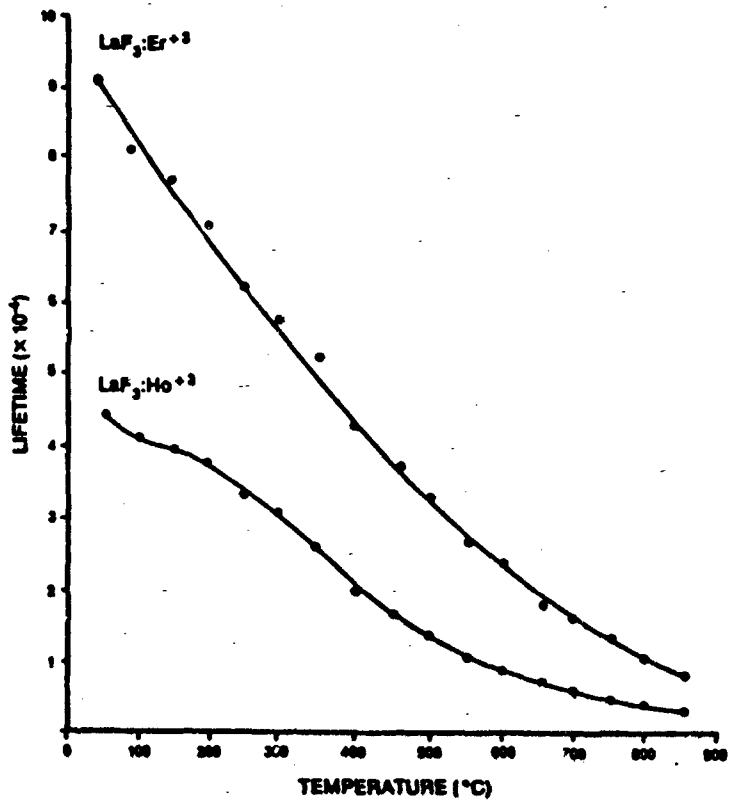

(b)

Figure 2. Temperature-Induced Lifetime Variation of Ho^{+3}:LaF_3 and Er^{+3}:LaF_3. (a) Fluorescent Decay from 100 to 800°C in 100-degree steps. (b) Lifetime Plot from Decay Data in (a).

REAL-TIME, TWO-DIMENSIONAL FUEL SPRAY VISUALIZATION

Lynn A. Melton
University of Texas
at Dallas
Richardson, TX 75080

James F. Verdieck
United Technologies
Research Center
East Hartford, CT 06108

Fuel spray properties are often very difficult to measure under realistic conditions. This research is part of a continuing effort to develop fluorescent additives which can be used to reveal spray properties such as simultaneous liquid/vapor concentrations, droplet temperature, and ambient oxygen pressure. These additives permit the use of laser-induced fluorescence in a planar sheet to determine the desired parameters non-intrusively, in real-time, from a selected plane in the evolving fuel spray.

Many previous studies of fuel sprays have relied on the determination of droplet size and number distibutions to analyze the sprays, whereas critical parameters such as vapor density and droplet temperature have been determined indirectly, or not at all. In contrast, our studies focus on the development of specific fluorescent additives which reveal directly the desired property from the fluorescence spectrum. Previous work at our laboratories has verified the use of such additives to provide simultaneous visualization of both liquid and vapor phases. The work described here is directed toward the development of fluorescent sensors for droplet temperature measurement.

Temperature sensor systems follow naturally from the vapor-liquid visualization studies, because both methods exploit the properties of organic exciplexes to interrogate properties of the spray. Figure 1 illustrates the essentials of exciplex formation and the subsequent two-color fluorescence. Because the equilibrium between the monomer and exciplex is temperature dependent, the ratio of the intensities of the emissions from E* and M* in the liquid phase provide a measure of temperature in the droplet. Thus, laboratory measurements of liquid phase fluorescence spectra as a function of temperature can provide a calibration curve for the intensity ratio, at specific wavelengths, versus temperature. This is shown schematically in Figure 2. In a spray experiment, if the emission from a particular spatial element were measured at these two wavelengths then the ratio would provide the droplet temperature from the calibration curve for the chosen set of additives, provided the vapor emission has been subtracted off. At present, several promising exciplex systems for use as optical thermometers are under development. One particular system appears especially exciting because the fluorescent emission changes from purple to yellow on going from room temperature to 75 degrees C. It is estimated that the determination of temperature can be obtained to a precision of a few degrees, provided the intensity ratio can be determined to about 1 percent accuracy.

REAL TIME, 2-D SPRAY/VAPOR MONITORING VIA EXCIPLEX FLUORESCENCE

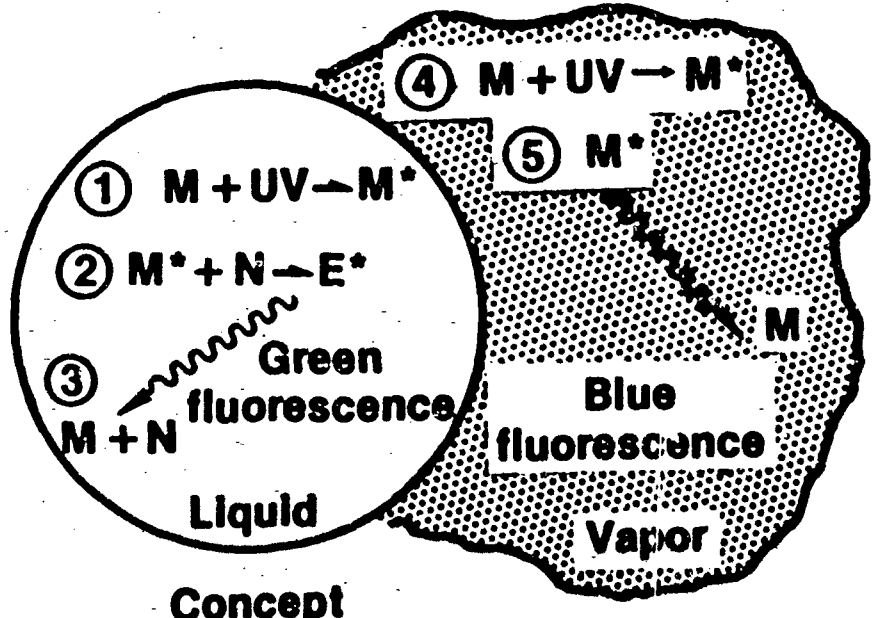

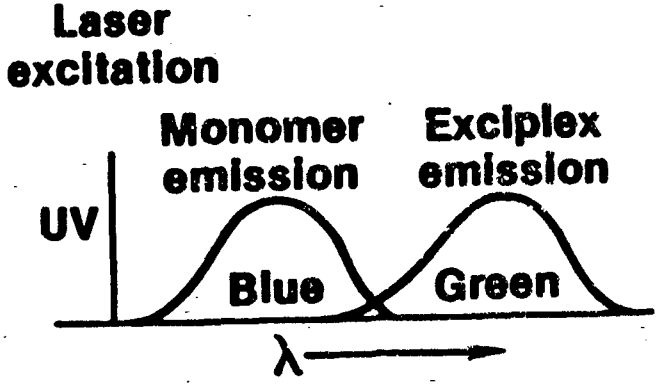

Concept

① , ④ Laser excitation of monomer in liquid or vapor

② Exciplex (excited complex) formation, liquid phase only

③ Exciplex fluorescence occurs in green

⑤ Monomer fluorescence occurs in blue

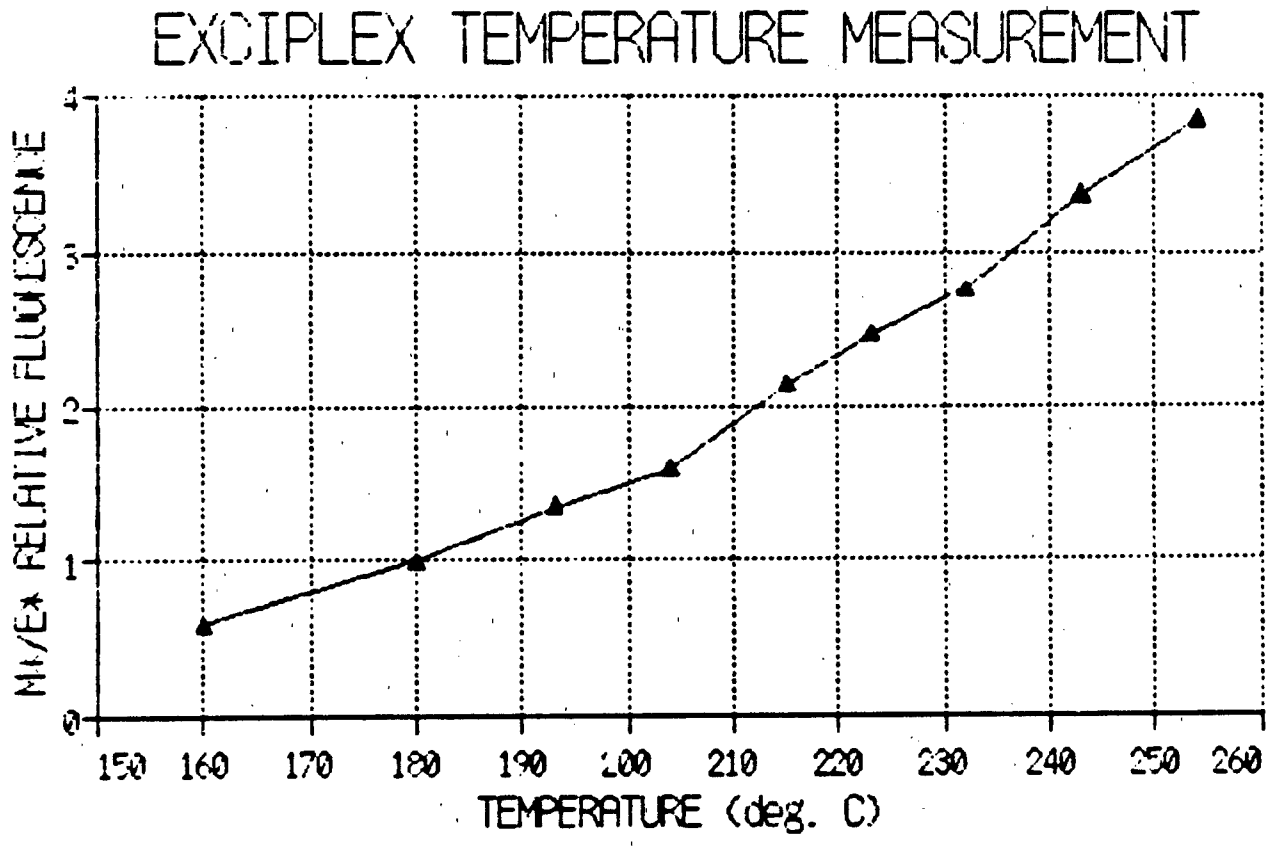

ACCOMPLISHMENTS

- Several exciplex systems have been examined as optical thermometers
- A preliminary calibration has been performed for the system--naphthalene/tetramethyl-p-phenylene diamine (shown in the graph above)
- The measurable temperature range can be modified by adjusting the concentration

SINGLE PARTICLE SIZING BY MEASUREMENT OF BROWNIAN MOTION

Alan C. Stanton and Wai K. Cheng*
Aerodyne Research, Inc., 45 Manning Road, Billerica, Massachusetts 01821

*also, Department of Mechanical Engineering
M.I.T, 77 Massachusetts Avenue, Cambridge, Massachusetts 02139

Few nonintrusive techniques are available for particle measurements in the submicron size range (<0.1 μm diameter), yet measurement of these particles is basic to an understanding of important processes in combustion, such as soot formation and oxidation. The objective of the present research is to investigate a new optical technique for the measurement of submicron particles, using a laser interferometric system to measure the Brownian motion of isolated particles in a gas stream. By measurement of the motion of many such particles, the size distribution may be obtained. This technique is unique in that it requires no a priori assumption on the particle size distribution, nor knowledge of the particle optical properties.

The experimental approach utilizes a laser interferometer system for measurement of a time-dependent signal sensitive to particle displacement. While the system is optically similar to the familiar Laser Doppler Velocimeter, important differences in its implementation form the basis of the present approach. To understand this approach, an appreciation of the chacteristic aspects of the Brownian motion of an isolated particle is required.

A representation of the motion of a 0.1 μm particle is shown in Figure 1. Random changes in particle velocity, of order 10^{-5} m s^{-1}, occur in characteristic times of 10^{-14} seconds due to collisions with gas molecules. With sufficient time resolution to measure instantaneous particle velocities, one would observe a Maxwellian velocity distribution. The characteristic time for the Maxwellian distribution to evolve is the relaxation time ($\approx 10^{-7}$ s as shown in Figure 1), which is a function of particle size and fluid properties. Because realizable sampling intervals are constrained to be much longer than the 10^{-14} s collision time, our strategy is to sample with an interval of $\sim 10^{-8}$ s, which is still fast compared to the relaxation time. Over this interval, the signal is a superposition of many random events, but its time dependence should exhibit statistical properties representative of the Brownian motion of a particle of a given size. The research effort this year is directed at demonstrating such correlations between signal statistics and particle size.

To understand the properties of the signal, we have simulated the Brownian motion sensor using a Monte Carlo technique. From analysis of simulated data, we have found the correlation shown in Figure 2. This plot shows a relationship between the mean time between signal extrema (derivative zero crossings) and a parameter, with dimensions of time, which is the square root of the product of the sampling interval and the particle relaxation time. The linearity of this plot shows that for fixed sampling intervals, the statistical property (the mean time between extrema) is proportional to the square root of the particle relaxation time. Thus, the relaxation time for Brownian motion of an individual particle may be determined from the statistics of the interference signal, and the particle size follows directly.

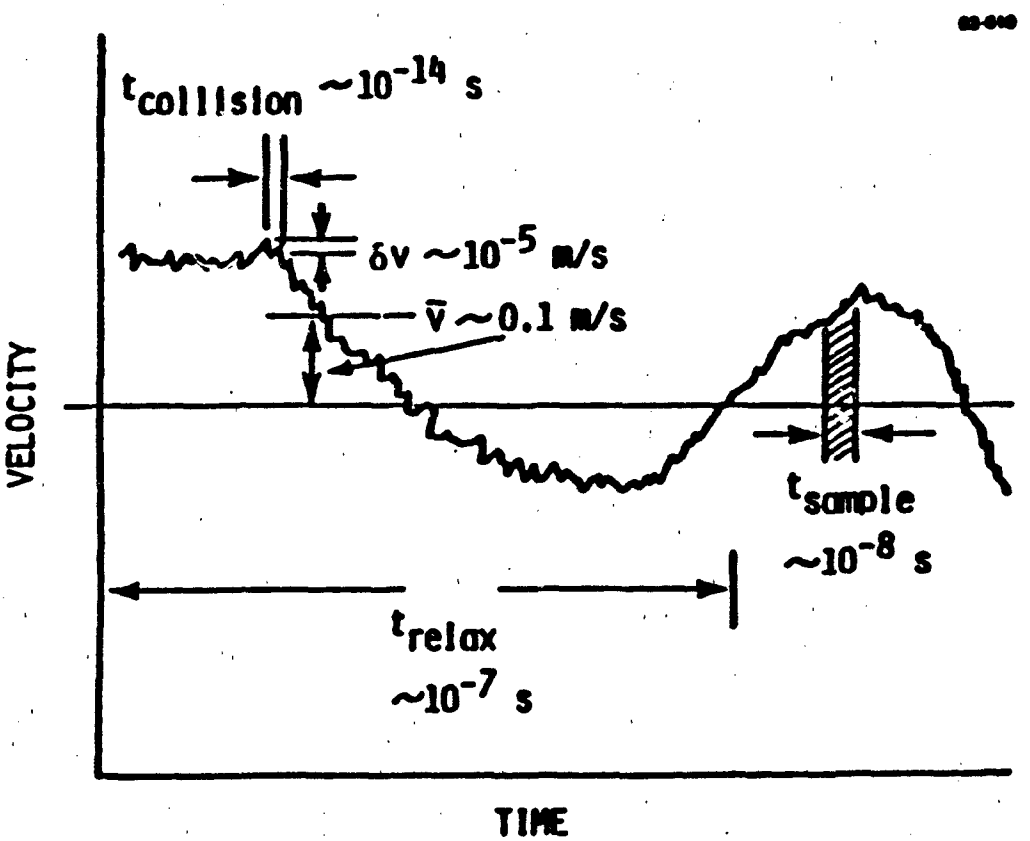

Figure 1. Time Dependent Motion of a 0.1 μm Diameter Particle in Air at 300 K and Atmospheric Pressure. The statistics of Brownian motion may be studied if measurements are made at sampling intervals shorter than the relaxation time.

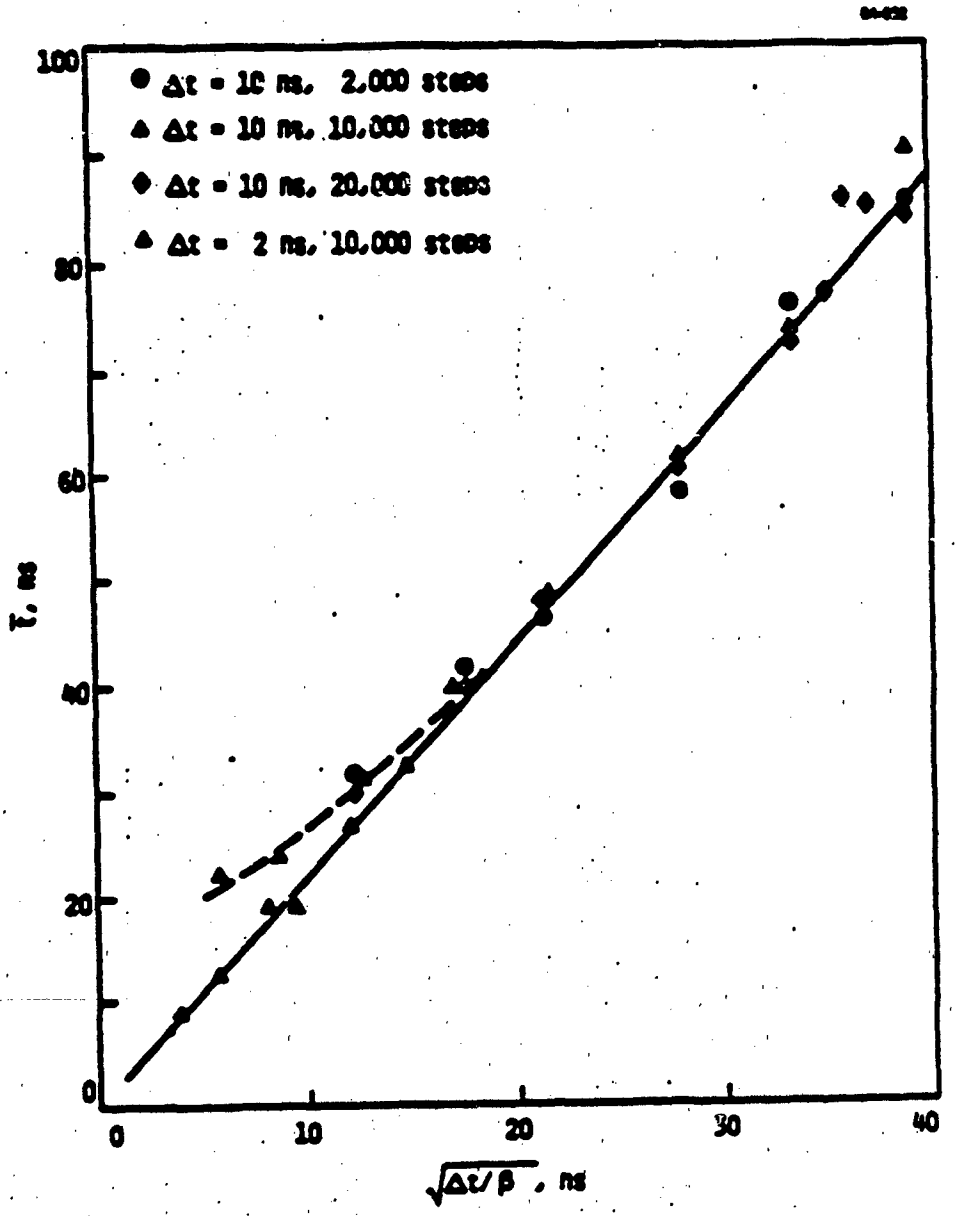

Figure 2. Correlation Between the Mean Time Between Signal Extrema ($\bar{t}$) and the Particle Relaxation Time, β^{-1}, Obtained from Analysis of Brownian Motion Sensor Signals Which Are Simulated Using a Monte Carlo Technique. The curvature occurs when the sampling interval Δt becomes comparable to the relaxation time.

PROPULSION RESEARCH GOALS

GENERAL GOALS: Research in support of rocket propulsion is directed at providing a fundamental basis for a new generation of propulsion concepts and improving the scientific understanding of phenomena associated with the generation of propulsive power. Research is needed from molecular to macroscopic scales in areas which include plasma acceleration, dynamics of rocket combustion, the behavior and synthesis of advanced energetic materials, characteristics of exhaust plume formation and radiation, and the dynamics of advanced propulsion concepts. Further knowledge is needed in these areas to meet mid-term and long-term Air Force technology goals related to improving performance, reliability, penetrability, and durability for Air Force mission applications involving space systems, ballistic missiles, and air launched missiles. However, specific provisions are also included for research directed toward scientific opportunities which cannot be related to particular mission areas at this time.

Future Air Force space missions for communications, surveillance, and weapons systems will require substantially higher power density and greatly improved propulsion for orbit raising. Research is expected to lead to improvements of 20% in propulsion efficiency with improved liquid and solid propellants and 100 to 400% with non-conventional systems such as electromagnetic plasma acceleration and energy beaming, magnetoplasmadynamics and nuclear power.

SPECIFIC GOALS:

The following topics summarize many of the current goals which are being addressed by the ongoing research programs.

Solid Propellant Mechanics To improve understanding of damage tolerant design for new materials. To investigate fatigue, damage propagation and detection, fracture, and effects of spectrum loading and sequencing. To extend the existing theories to three dimensions, including the interactions between viscoelastic behavior and damage, the micromechanics of propellant structure, and effects of temperature to obtain a approaches that can predict propellant stress-strain behavior from relatively simple tests. To establish an age-life model based on chemical reactions. To establish the relationship between carbon/carbon material processing variables and the kinetics of reaction of these materials with gases representative of rocket exhausts.

Noninterfering Diagnostic Techniques To achieve sensors which will enable the adaptive control and autonomous operation of high performance propulsion systems. To achieve diagnostic techniques for measuring the gas and gas-particle flow properties representative of rocket systems including plumes. To devise diagnostic techniques to obtain rapid and quantitative spatially and temporally resolved measurements of temperature, pressure, velocity, species concentrations and densities, and particle/droplet size and distribution in optically dense, high-temperature reacting, unsteady, turbulent flowing media. To establish techniques for obtaining rate date for energetic material being heated in excess of 10^5 K/s.

Exhaust Plumes To provide mechanistic basis for analyzing, interpreting, and altering plume radiance. Establish the influence of composition and flow environment on particle formation and growth mechanisms. To verify and improve predictive models for nucleation and condensation in multi-component, multi-phase systems. To determine reaction pathways and to obtain chemical rate data for combustion chamber, nozzle, and exhaust plume flows. To improve and devise diagnostic methodology for determining the spatial and temporal distribution of important species so that rate processes can be measured. To determine the mechanism of exhaust plume igntion in the presence of flame suppression additives.

Solid Propellants and Energetic Materials To control the behavior of energetic materials during combustion. To establish relationships between molecular structure, decomposition and combustion processes. To synthesize energetic ingredients leading to tough, high energy propellants with desireable properties which include low glass-transition temperatures, high thermochemical stability temperatures, high solid loadings, and smokelessness. To improve techniques to determine polymer properties.

Combustion and Reacting Flows To understand important bond rupture and heat release mechanisms so that research to modify burning rate and combustion efficiency can be directed at specific reaction sites. To explore methods for obtaining the key reaction parameters for energetic materials being heated at rates in excess of 10^4K/s. To determine the effects of acceleration-fields on propellant ballistics. To characterize the mechanisms leading to changes in solid propellant properties and burning modes that produce transition from normal deflagration to detonation of rocket motor grains. To increase the scope and usefulness of the JANAF Thermochemical Property Data.

Combustion Instability To improve analytical methods for interpreting, predicting, and avoiding instability behavior of solid motors through mechanistic understanding of contributions such as nozzle damping, acoustic erosivity, pressure coupling, vortex streaming, vortex sheading, distributed combustion, particle and structural damping, and high velocity effects. To acount for the more significant effects of 2-D and 3-D geometries. To defeat combustion instabiltiy by purposely dissipating acoustic energy in prescribed modes. To examine more direct means of measuring acoustic admittance. To conduct verification of new combustion response measurement techniques. To investigate methodologies for measuring the unsteady velocity, pressure, and temperature components in multi-dimensional unsteady reacting flows. To visualize nonsteady, multi-phase flow and condensed-phase breakup for the purpose of understanding the role of transient processes on acoustic energy gains or losses. To determine and characterize acoustic energy gains and losses in terms of flow field parameters. To understand contributions of heterogeneous structures in composite propellants.

Metal Combustion To characterize the basic mechanisms and chemistry involved in the formation of metal oxide particulates. To experimentally determine physical and chemical processes leading to the acceleration of metal droplet ignition and combustion. To explore methods of greatly reducing the size of metal oxide agglomerates entering nozzle convergent sections. To improve methods for simultaneously measuring temperature and concentration of

turbulent flame zones of multi-phase media so that conditions leading to metal com- bustion under solid propellant ram-rocket conditions (particularly high alti- tude) can be characterized. To assess the role of fluorine in the combustion of fluorinated metallic propellants and to determine mechanisms that affect oxide particle size.

Beamed Energy To quantify mechanisms of laser energy transfer to working fluids, to assess the barriers to optical access for energy transmission, and to establish approaches to plasma confinement. To enable consideration of candidate short wavelength energy beams with hydrogen; to determine if other working fluids and fuels offer promise.

Solar Thermal Propulsion Establish the mechanisms of solar radiation energy absorption under the desired thruster conditions.

Electromagnetic Acceleration To understand magnetoplasmadynamic processes for the purposes of establishing the conditions of sustained high energy density operation and to project upper limits of power density. To establish the mechanism leading to extended electrode life. To extend operational time of electrode and contact surfaces. To produce stable magnetoplasmadynamic flows for sustained high energy density operation. To produce conditions that vaporize and disperse metallic fuels being considered for use in low Earth orbits. To overcome cooling limitations on electrical propulsion systems operating continuously at megawatts power levels. To realize more weight efficient and less vulnerable heat rejection concepts for electrodes, chambers, and nozzles.

Ultra-High Energy Density To decrease the losses in thermionic flows. To explore novel approaches to high energy density storage. To devise means of accommodating plasma temperatures greatly in excess of material limits.

1985 AFOSR/AFRPL ROCKET RESEARCH MEETING
AUTHORS - ABSTRACTS and PRESENTATIONS

Anderson, W S 13
Andreshak, J L 7
Askins, R E 15
Bachalo, W D 69
Barbour, R A 55
Baum, J D 39
Becker, R J 55
Beckstead, M W 35
Becker, R J 31
Bedford, C D 6
Bischel, W K 61
Blackmer, A M 33
Blanks, J W 11
Boyer, C M 59
Branch, M C 18
Brill, T B 14
Brown, Robert S 33
Buswell, A T 55
Caledonia, G E 43
Campbell, D M 22, 23, 24
Canterberry, J B 11
Caveny, L H 38
Chang, F R 51, 52
Chang, I K 70, 71
Chanty, M 47
Chapman, R D 7
Chase, M W 25
Chen, F 34
Cheng, W K 76
Christe, K O 10
Chu, B T 71
Chung, T J 36
Cohen, N 26
Coolidge, M B 15
Coules, L M 43
Crowder, H 40
Daily, J W 62
Davis, J F 59
Dunlap, R 33
Edwards, T 22, 23
Elsch, J J 12
Eversole, J D 16
Exum, C R 63
Fisher, J L 51
Flanagan, J E 27
Frankel, M B 1
Frederick, R A Jr 32
Galle, J E 12
Gill, R J 28
Goss, L P, ...74
Graham, W H 11
Hanson, R K 64
Hart, D P 54
Hartwell, J A 4
Hedge, U G 34
Heimerdinger, D 47
Herrlinger, S P 7
Hersh, A S 37
Hesselink, L 65
Hess, C F 72
Hirleman E D 73
Hulsizer, S 22, 23
Jagoda, J I 20, 21
Jones, O C 57
Kaufman, M J, ...19
Keefer, D R 40
Kemp, N H 44
King, D Q 49
King, M K 29
Komar, J J 29
Koo, J I, ...73
Kozima, S 12
Krech, R H 43
Krier, H 42
Krueger, W A 51, 52
Kuo, K 70
Laird, J L 31
Lawless, J L 48
Levine, J N 39
Liu, C T 30
Long, M B 70, 71
Luehrmann, P F 31
Maciejewski, M 5
Marchand, S C 3
Martinez-Sanchez, M 47
Mazumder, J 42
McVey, J B 60
Melanson, D 47
Melton, L A 75
Merkle, C 41
Micci, M M 53
Miller, E 17
Mongeau, P P 54
Moriarty, R M 8
Morse, S D 9
Myrabo, L N 45
Nagurka, J I 66
Norwood, J 59
Olsen, D B 28
Osborne, J M 5
Osborn, J R 32
Oyumi, Y 14
Peters, C 40
Ramos, J I 66
Raun, R L 35
Reddy, D S 3
Rodgers, S L 15
Rosen, D I 43, 44
Sankar, S 34
Schaak, C J 10
Schaack, D F 56
Schackelford, S A 7, 15
Schmitt, R J 6
Schrade, H O 46
Seikel, G R 50
Shepard, I G 11
Shreeve, J M 2
Sirignano, W A 66
Smith, A A 74
Sommer, M T 67
Stanton, A C 76
Strahle, W C 20, 21
Suri, S C 3
Swithenbank, J 63
Talukder M A M 9
Thompson, W W 27
Trogler, William C 5
Trolinger, J D 56
Turchi, P J 59
Verdieck, J F 75
Verdieck, J F 68
Wayner, P C 58
Weaver, D P 22,23, 24
Weaver, D P 16
Weber, J F 1
Welle, R 40
Wenzel, K W 52
Wentberg, K 26
Willoughby, P G 33
Willer, R L 4
Woolery, D O 27
Yang, T F 51, 52
Zinn, B T 34

SPECIAL PRESENTATIONS AND OVERVIEWS:

Miller, R. S.	Mon	PM
Johnston, S.	Tues	PM
Hart, D. A.	Wed	AM
Weiss, R. R.	Wed	AM
Caveny, L. H.	Wed	AM
Roe, W. E.	Wed	AM
Hanson, R. K.	Wed	AM
Myrabo, L.	Wed	AM

END

FILMED

10-85

DTIC